

This work is protected by copyright and other intellectual property rights and duplication or sale of all or part is not permitted, except that material may be duplicated by you for research, private study, criticism/review or educational purposes. Electronic or print copies are for your own personal, non-commercial use and shall not be passed to any other individual. No quotation may be published without proper acknowledgement. For any other use, or to quote extensively from the work, permission must be obtained from the copyright holder/s.



**Non-anticoagulant glycosaminoglycan extracts isolated
from aquatic species inhibit BACE-1: a key drug target in
Alzheimer's Disease**

Thesis submitted in accordance with the requirements of Keele University for the
degree of Doctor in Philosophy

By

Courtney Jade Mycroft-West

July 2022

Abstract

Currently, only palliative drugs are available for the treatment of Alzheimer's disease, therefore there is an urgent need to develop therapeutics targeting the underlying aetiology of the disease. The clinical anticoagulant heparin has previously been reported to inhibit the primary neuronal β -secretase, BACE-1, which is responsible for the production of the widely regarded causative agent of Alzheimer's disease, amyloid peptides. Despite this, the utilisation of pharmaceutical heparin for the treatment of Alzheimer's disease has largely been precluded due to the potent anticoagulant activity displayed by this polysaccharide. This is primarily as a result of uncontrolled hemostasis being considered as a highly undesirable side-effect for Alzheimer's disease therapeutics. Furthermore, concerns regarding the use of heparin sources from mammalian species, primarily due to transmissible encephalopathies and religious beliefs, have hindered the deployment of heparin for alternative therapeutic applications. Glycosaminoglycans obtained from aquatic species have previously been shown to possess significantly attenuated anticoagulant activities, in comparison to mammalian heparin, while retaining a diverse array of additional biological activities. This is principally a result of the increased structural diversity displayed by glycosaminoglycans obtained from aquatic species in comparison to mammalian counterparts. Furthermore, the considerable amount of waste produced from the fishery and aquaculture industries offers a sustainable, financially viable alternative to mammalian derived glycosaminoglycan sources for potential therapeutic exploitation. Here several glycosaminoglycan extracts obtained from the tissue of aquatic species,

via proteolytic digestion, were observed to potently inhibit BACE-1, while being shown to displaying highly attenuated anticoagulant activities. The BACE-1 inhibitory activities of glycosaminoglycan extracts obtained from *Portunus pelagicus*, *Litopenaeus vannamei* and *Sardinia pilchardus*, were evaluated utilising a Förster resonance transfer assay and then subsequently compared to their respective anticoagulant activities (determined utilising the activated partial thromboplastin time assay). In comparison to mammalian heparin the glycosaminoglycan extracts obtained from *Portunus pelagicus*, *Litopenaeus vannamei* and *Sardinia pilchardus* exhibited increased therapeutic ratios of, 0.7, 22.7, 2.5-6.1 and 84.3, respectively. The extracts were evaluated for structure-function analysis utilising agarose gel electrophoresis, attenuated total reflectance Fourier transform infrared spectroscopy, circular dichroism spectroscopy, high pressure liquid chromatography disaccharide compositional analysis and nuclear magnetic resonance spectroscopy. Structural-function analysis indicated that the extent of 2-sulphated uronic acid residues, present within the extracts predominantly composed of heparan sulphate (*Portunus pelagicus*, *Litopenaeus vannamei*), may be indicative of increased BACE-1 inhibitory activity, with extracts containing higher levels of 2-sulphated uronic acid residues displaying increased BACE-1 inhibitory activity. Furthermore, extracts composed principally of chondroitin sulphate were also observed to inhibit BACE-1, although the potency of this action is likely dependent upon the fine structure of the polysaccharide. The interaction of glycosaminoglycans with BACE-1 was evaluated further through the use of circular dichroism spectroscopy and differential scanning fluorometry. This indicated that glycosaminoglycans inhibit BACE-1 via a mechanism that involves a conformational change, which likely renders the enzyme in an inactive conformation.

Acknowledgements

I would like to thank my supervisor Dr. Mark Skidmore for his constant guidance and counsel.

In addition, I would like to thank Keele University and Intellihep for their financial support. Thank you to the University of Liverpool, Universidade Federal de São Paulo, Manchester Institute of Biotechnology for the use of equipment throughout the project. In particular, I would like to thank Mr Anthony Devlin for his collaboration in the acquisition and analysis of the ATR-FTIR and CD spectra of glycosaminoglycans, including his contribution performing principal component analysis. I would also like to thank Dr. Marcelo Lima for his assistance in the analysis and acquisition of nuclear magnetic resonance spectra.

Furthermore, I would like to thank Ms. Patricia Proctor, Prof. Jeremy Turnbull, Prof. David Fernig, Dr Scott Guimond, Dr. Marissa Maciej-Hulme, Dr Joseph Holmen and Dr Gavin Millar for their assistance and guidance throughout this study.

Many thanks to all the members of staff at Keele University for their continuous support and encouragement throughout.

Finally, I would like to express considerable gratitude to my Family for their encouragement and support through this journey.

List of figures

Figure 1: Comparison of the structural features of heparan sulphate (HS) and heparin.	7
Figure 2: Biosynthesis of heparan sulphate (HS) and heparin.	13
Figure 3: Overview of the coagulation cascade.	16
Figure 4: Brain degeneration in Alzheimer's disease (AD).	20
Figure 5: APP processing.	23
Figure 6: BACE-1 structure.	34
Figure 7: Suggested models for the endogenous regulation of BACE-1 processing of APP by heparan sulphate proteoglycans.	37
Figure 8: BACE-1 inhibitory activity of size-defined unmodified PIMH.	38
Figure 9: Structure, IC ₅₀ values and anticoagulant activities of modified heparins.	40
Figure 10: Transport of LMWH derivatives across the blood-brain barrier (BBB).	41
Figure 11: BACE-1 fluorogenic peptide FRET assay schematic.	81
Figure 12: Typical differential scanning fluorimetry melt curve.	83
Figure 13: Crude glycosaminoglycan extraction process.	108
Figure 14: The electrophoretic mobility of 20 µg crude GAG extract obtained from <i>P. pelagicus</i> compared to <i>bona fide</i> glycosaminoglycans	109
Figure 15: ATR-FTIR spectra of glycosaminoglycans.	110
Figure 16: ATR-FTIR and CD spectra of crude <i>P. pelagicus</i> , coupled with PCA.	112
Figure 17: Circular dichroism spectra of glycosaminoglycans.	113
Figure 18: (A) ¹ H and (B) ¹ H- ¹³ C HSQC NMR spectra of crude <i>P. pelagicus</i> extract.	116

Figure 19: The electrophoretic mobility of 20 µg crude GAG extract obtained from <i>L. vannamei</i> compared to glycosaminoglycan standards _____	117
Figure 20: ATR-FTIR and CD spectra of crude <i>L. vannamei</i> extract, coupled with PCA. _____	118
Figure 21: (A) ^1H and (B) ^1H - ^{13}C HSQC NMR spectra of crude <i>L. vannamei</i> extract. _	119
Figure 22: The electrophoretic mobility of 20 µg crude GAG extract obtained from <i>S. pilchardus</i> compared to <i>bona fide</i> glycosaminoglycans _____	121
Figure 23: ATR-FTIR spectra and PCA of crude <i>S. pilchardus</i> extract. _____	122
Figure 24: (A) ^1H and (B) ^1H - ^{13}C HSQC NMR spectra of crude <i>S. pilchardus</i> extract. _	123
Figure 25: The electrophoretic mobility of 20 µg crude GAG extract obtained from <i>M. aeglefinus</i> compared to <i>bona fide</i> glycosaminoglycans. _____	124
Figure 26: ATR-FTIR and CD spectra of crude <i>M. aeglefinus</i> , coupled with PCA _____	125
Figure 27: (A) ^1H and (B) ^1H - ^{13}C HSQC NMR spectra of crude <i>M. aeglefinus</i> extract. 127	
Figure 28: The electrophoretic mobility of 20 µg crude GAG extract obtained from <i>M. merluccius</i> compared to <i>bona fide</i> glycosaminoglycans _____	128
Figure 29: ATR-FTIR and CD spectra of <i>M. merluccius</i> , coupled with PCA. _____	129
Figure 30: (A) ^1H and (B) ^1H - ^{13}C HSQC NMR spectra of crude <i>M. merluccius</i> extract. 132	
Figure 31: The electrophoretic mobility of 20 µg crude GAG extract obtained from <i>P. hypophthalmus</i> compared to <i>bona fide</i> glycosaminoglycans _____	133
Figure 32: ATR-FTIR and CD spectra of the crude <i>P. hypophthalmus</i> extract. _____	134
Figure 33: (A) ^1H and (B) ^1H - ^{13}C HSQC NMR spectra of crude <i>P. hypophthalmus</i> extract. _____	136
Figure 34: The electrophoretic mobility of 20 µg crude GAG extract obtained from <i>C. batrachus</i> compared to <i>bona fide</i> glycosaminoglycans _____	137

Figure 35: ATR-FTIR spectra of the crude <i>C. batrachus</i> extract. _____	138
Figure 36:(A) ^1H and (B) ^1H - ^{13}C HSQC NMR spectra of crude <i>C. batrachus</i> extract. _	139
Figure 37: The electrophoretic mobility of 20 μg crude GAG extract obtained from <i>O. gorbuscha</i> compared to <i>bona fide</i> glycosaminoglycans _____	141
Figure 38: ATR-FTIR and CD spectra of the crude <i>O. gorbuscha</i> extract. _____	142
Figure 39: (A) ^1H and (B) ^1H - ^{13}C HSQC NMR spectra of crude NMR <i>O. gorbuscha</i> extract. _____	143
Figure 40: Inhibition of human BACE-1 by heparin. _____	145
Figure 41: Inhibition of human BACE-1 by crude GAG extracts determined using FRET. _____	146
Figure 42: Inhibition of human BACE-1 by GAG standards determined using FRET. _	147
Figure 43: DEAE fractionation of crude GAG extracts. _____	149
Figure 44: Inhibition of human BACE-1 by fractionated GAG extracts determined using FRET. _____	151
Figure 45:Phylogenic tree of aquatic organisms utilised for GAG extraction. _____	154
Figure 46: Agarose gel electrophoresis of <i>P. pelagicus</i> F5. _____	180
Figure 47: ATR-FTIR spectra of <i>P. pelagicus</i> F5. _____	181
Figure 48: CD spectra of <i>P. pelagicus</i> F5. _____	182
Figure 49: UV-SAX HPLC disaccharide composition analysis performed on the bacterial lyase digest of PIMH in reference to the eight common Δ - disaccharide standards. 183	
Figure 50: UV-SAX HPLC disaccharide composition analysis performed on the bacterial lyase digest of HS in reference to the eight common Δ - disaccharide standards. _	184

Figure 51: UV-SAX HPLC disaccharide composition analysis performed on the bacterial lyase digest of <i>P. pelagicus</i> F5 in reference to the eight common Δ - disaccharide standards. _____	184
Figure 52: Nuclear magnetic resonance spectra of <i>P. pelagicus</i> F5. _____	186
Figure 53: Inhibition of human BACE-1 by heparin or <i>P. pelagicus</i> F5. _____	188
Figure 54: Inhibition of human BACE-1 by heparin or <i>P. pelagicus</i> F5. _____	189
Figure 55: The structural change of BACE-1 observed in the presence of heparin by CD spectroscopy. _____	191
Figure 56: The structural change of BACE-1 observed in the presence of <i>P. pelagicus</i> F5 by CD spectroscopy. _____	192
Figure 57: Differential scanning fluorimetry of BACE-1 in the presence of heparin or <i>P. pelagicus</i> F5. _____	194
Figure 58: anticoagulant activity of heparin and <i>P. pelagicus</i> F5. _____	195
Figure 59: Electrophoretic mobility of <i>L. vannamei</i> F4 and F5 compared that of <i>bone fide</i> glycosaminoglycans. _____	206
Figure 60: ATR-FTIR spectra of <i>L. vannamei</i> F4 and F5. _____	207
Figure 61: Principle component analysis Score Plot for PC1 vs. PC2 of the ATR-FTIR spectra <i>L. vannamei</i> F4 and F5 against a <i>bone fide</i> GAG library. _____	208
Figure 62. Circular dichroism spectra of <i>L. vannamei</i> F4 and F5. _____	209
Figure 63: Principle component analysis (PCA) score Plot for PC1 vs. PC2 of the circular dichroism spectra <i>L. vannamei</i> F4 and F5 against a <i>bone fide</i> GAG library. _____	210
Figure 64: UV-SAX HPLC disaccharide composition analysis was performed on the bacterial lyase digest of <i>L. vannamei</i> F5 _____	214

Figure 65: UV-SAX HPLC disaccharide composition analysis was performed on the bacterial lyase digest of <i>L. vannamei</i> F4	214
Figure 66: UV-SAX HPLC disaccharide composition analysis was performed on the ABC chondroitinase digest of <i>L. vannamei</i> F4	215
Figure 67: UV-SAX HPLC disaccharide composition analysis was performed on the ABC chondroitinase digest of <i>L. vannamei</i> F5	216
Figure 68: Nuclear magnetic resonance spectra of <i>L. vannamei</i> F4.	219
Figure 69: Nuclear magnetic resonance spectra of <i>L. vannamei</i> F5.	220
Figure 70: Inhibition of the human beta-secretase, BACE-1, <i>L. vannamei</i> F4 and F5 determined by FRET.	222
Figure 71: Inhibition of human BACE-1 by heparin, <i>L. vannamei</i> F4.	223
Figure 72: Inhibition of human BACE-1 by heparin, <i>L. vannamei</i> F5.	223
Figure 73: Anticoagulant activity of <i>L. vannamei</i> F4.	224
Figure 74: Anticoagulant activity of <i>L. vannamei</i> F5.	225
Figure 75: The secondary structural change of BACE-1 observed in the presence of heparin and <i>L. vannamei</i> F4.	226
Figure 76: Differential scanning fluorimetry of BACE-1 in the presence of heparin or <i>L. vannamei</i> F4.	227
Figure 77: Agarose gel electrophoresis of <i>S. pilchardus</i> F4 in 1-2-diaminopropane buffer.	238
Figure 78: ATR-FTIR spectrum of <i>S. pilchardus</i> F4.	239
Figure 79: Circular dichroism spectrum of <i>S. pilchardus</i> F4.	240
Figure 80: UV-SAX HPLC disaccharide composition analysis performed on the bacterial lyase digest products obtained from <i>S. pilchardus</i> F4	241

Figure 81:Nuclear magnetic resonance spectra for <i>S. pilchardus</i> F4. _____	243
Figure 82: Inhibition of human BACE-1 by <i>S. pilchardus</i> F4 or heparin as determined by FRET. _____	245
Figure 83: Inhibition of human BACE-1 by heparin or <i>S. pilchardus</i> F4. _____	245
Figure 84: Anticoagulation activity of <i>S. pilchardus</i> F4 in comparison to heparin. ____	246
Figure 85: The secondary structural change of BACE-1 observed in the presence of <i>S. pilchardus</i> F4. _____	247
Figure 86: Differential scanning fluorimetry of BACE-1 in the presence of <i>S. pilchardus</i> F4 or heparin. _____	248

List of tables

Table 1: Received composition and structure of the mammalian glycosaminoglycans.	4
Table 2: Preparation methods for low molecular weight heparins (LMWHs).	19
Table 3: Currently approved drugs for the treatment of Alzheimer's disease.	26
Table 4: Examples of small molecule BACE-1 inhibitors in clinical trials.	35
Table 5: Examples of HS/heparin like compounds extracted from aquatic species.	47
Table 6: Examples of GAG like compounds extracted from aquatic species possessing attenuated anticoagulant activities.	48
Table 7: Examples of CS like compounds extracted from aquatic species.	50
Table 8: Common glycosaminoglycan lyases utilised for analysis	62
Table 9: Δ -Disaccharides produced as a result of enzymatic degradation of glycosaminoglycans.	72
Table 10: $^1\text{H}/^{13}\text{C}$ NMR chemical shifts utilised for analysis of glucosaminoglycans.	77
Table 11: $^1\text{H}/^{13}\text{C}$ NMR chemical shifts utilised for analysis of galactosaminoglycans	78
Table 12. Yield of crude extracts.	107
Table 13: Example yields of GAG obtained from <i>clupeocephala</i> .	156
Table 14: Example yields of GAG obtained from <i>Crustacea</i>	157
Table 15: The prevalence of GAGs detected within each crude extract by agarose gel electrophoresis (AGE), ATR-FTIR, CD and NMR.	170
Table 16: Percentage BACE-1 inhibitory activities and approximate composition of crude GAG extracts.	171
Table 17: Percentage BACE-1 inhibition by fractionated GAG extracts determined using FRET.	175

Table 18: Corrected disaccharide composition analysis of <i>P. pelagicus</i> F5, heparin and HS. _____	185
Table 19: Corrected disaccharide composition analysis of <i>P. vannamei</i> F4, F5, heparin and HS. _____	212
Table 20: Corrected disaccharide composition analysis of <i>P. vannamei</i> F4, F5, CSA and CSC. _____	217
Table 21: Therapeutic ratio of <i>L. vannamei</i> F4 and F5 compared to heparin. _____	225
Table 22: Corrected disaccharide composition analysis of <i>S. pilchardus</i> F4, CSA and CSC. _____	242
Table 23: Approximate change in GAG composition following fractionation utilising DEAE-Sephacel anion exchange chromatography. _____	256
Table 24: Approximate GAG composition. Determined by HPLC disaccharide composition analysis and ^1H - ^{13}C NMR spectroscopy. _____	257
Table 25: Therapeutic ratio of fractionated extracts compared to heparin to heparin. _____	264

Glossary of terms

^1H - ^1H correlation spectroscopy; COSY

2-O-sulphotransferase; 2OST

3-O-sulphotransferases; 3OST

3'phosphoadenosine 5'phosphosulfate; PAPS

6-O-sulphotransferases; 6OST

Acetylglucosaminyltransferase-I; GlcNAcT-I

Alzheimer's disease; AD

Amyloid precursor protein; APP

Amyloid- β peptides; A β

Antithrombin binding site; AT binding site

Apolipoprotein E; APOE

APP intracellular cytoplasmic domain; AICD

Attenuated total reflectance Fourier transform infrared; ATR-FTIR

Blood brain barrier; BBB

Bovine lung heparin; BLH

Bovine spongiform encephalopathy; BSE

Cholinesterase inhibitors; CIs

Chondroitin sulphate A; CSA

Chondroitin sulphate C; CSC

Chondroitin sulphate; CS

Circular dichroism; CD

Creutzfeldt-Jakob disease; vCJD

D-galactosamine; GalN

D-glucosamine; GlcN

D-glucuronic acid; GlcA

Deep venous thrombosis; DVT

Dermatan sulphate; DS

Differential scanning fluorimetry; DSF

Ethylenediaminetetraacetic acid; EDTA

Exostosin like-genes; EXTL

Extracellular matrix; ECM

Factor; F

familial Alzheimer's disease; FAD

Föster resonance energy transfer; FRET

Fourier transform infrared spectroscopy; FTIR

Galactose; Gal

Galactosyltransferases-I; GalT-1

Galactosyltransferases-II; GalT-2

Glucuronyl C5-epimerase; Hsepi

Glucuronyltransferase-I; GlcAT-1

Glycosaminoglycans; GAGs

Glycosylphosphatidylinositol; GPI

Heparan Sulphate proteoglycans; HSPGs

Heparan sulphate; HS

Heparin cofactor II; HCII

Heparin-induced thrombocytopenia; HIT.

Heteronuclear multiple bond coherence; HMBC

Heteronuclear Single-Quantum Correlation; HSQC

Highly modified sulphated regions; NS domains

HS- β 1-4-glucuronyltransferase-II; HS-GlcAT-II

Hyaluronic acid; HA

Keratan sulphate; KS

L-iduronic acid; IdoA

Left- handed circularly polarised light LCP

Low molecular weight heparins; LMWHs

N-deacetylase/N-sulfotransferases; NDSTs

Neurofibrillary tangles; NFTs

Notch intracellular domain; NICD

Nuclear Magnetic Resonance; NMR

Nuclear Overhauser effect spectroscopy; NOESY

On principal component analysis; PCA

One-dimensional; 1D

Over transmissible spongiform encephalopathy's; TSEs

Over-sulphated chondroitin sulphate; OSCS

Partial thromboplastin time; aPTT

Porcine intestinal mucosa; PIMH

Porcine mucosal heparan sulphate; PMHS

Presilin-1; PSEN1

Presilin-2; PSEN2

Prion protein; PrP

Proteoglycans; PGs

Prothrombin time; PT

Prothrombin; FII

Prothrombinase complex; FVa

Right- handed circularly polarised light; RCP

Rotating frame Overhauser effect spectroscopy; ROESY

Serine; Ser

Strong anion-exchange high pressure liquid chromatography; SAX-HPLC

Thrombin; FIIa

Tissue factor; TF

Total correlation spectroscopy; TOCSY

Unfractionated heparin; UFH

uridine diphosphate-galactose; UDP

Uronic acid; UA

Xylose; Xyl

α 1-4-acetylglucosaminyltransferase-II; GlcNAcT-II

β -site amyloid precursor protein-cleaving enzyme 1; BACE-1

Table of contents

Abstract	i
Acknowledgements	iii
List of figures	v
List of tables	xi
Glossary of terms	xiii
Chapter 1: Introduction	1
1.1. Glycosaminoglycans and Proteoglycans	2
1.2. Heparin and Heparan Sulphate	5
1.2.1 Structure	5
1.2.2. Biosynthesis	8
1.3. The Coagulation Cascade	14
1.4. Clinical use of heparin	17
1.5. Alzheimer’s Disease	20
1.5.1 Pathophysiology of AD	20
1.5.2. Amyloid cascade hypothesis	21
1.5.3. Current treatments of AD	26
1.6. BACE-1	27
1.6.1. Validation of BACE-1 as a therapeutic target for AD	28
1.6.2. BACE-1 structure	32

1.6.3. BACE-1 Inhibitors in clinical trials	34
1.6.4. Glycosaminoglycans and glycosaminoglycan mimetics as BACE-1 inhibitors	36
1.7. Non-mammalian glycosaminoglycans GAGs as BACE1 inhibitors	42
Chapter 2: Methodology introduction	53
2.1. Isolation and purification of glycosaminoglycans	54
2.1.1. Tissue sourcing and pre-treatment	54
2.1.2. Release of GAGs chains from proteoglycans	56
2.1.3. Recovery and purification of crude glycosaminoglycans	58
2.1.4. Fractionation of glycosaminoglycans from crude extracts	60
2.2. Structural analysis of glycosaminoglycans	64
2.2.1. Agarose Electrophoresis	64
2.2.2. ATR-FTIR	65
2.2.3. Circular dichroism spectroscopy	68
2.2.4. SAX-HPLC glycosaminoglycan disaccharide composition analysis	71
2.2.5. Nuclear magnetic resonance	74
2.2.6. Principal component analysis	79
2.2.7. BACE-1 inhibitor screening utilising a fluorescent FRET peptide assay	80
2.2.8. Differential scanning fluorimetry	82
Chapter 3: Materials and Methods	84
3.1. Materials	85
3.2 Equipment and software	90

3.3 Methods	91
3.3.1 Extraction of glycosaminoglycans	91
3.3.2 Agarose Gel Electrophoresis of glycosaminoglycans	92
3.3.3 Attenuated Total Reflectance Fourier transform infrared spectroscopy (ATR-FTIR) coupled with principal component analysis (PCA)	93
3.3.4 Circular dichroism spectroscopy of glycosaminoglycans coupled with principal component analysis (PCA)	94
3.3.5 Nuclear Magnetic Resonance (NMR)	94
3.3.6 Beta secretase fluorescence resonance energy transfer (FRET) inhibition assay	95
3.3.7 DEAE-Sephacel anion-exchange chromatography	96
3.3.8 Constituent Δ -Disaccharide analysis of heparin/heparan sulphate polysaccharides	96
3.3.9 Constituent Δ -disaccharide analysis of chondroitin sulphate polysaccharides	98
3.3.10 Activated partial thromboplastin time (aPTT)	101
3.3.11 Prothrombin time (PT)	101
Chapter 4: Extraction and fractionation of glycosaminoglycans, possessing BACE-1 inhibitory activity, from aquatic species.	103
4.1 Introduction	104
4.1.2 Chapter aims	106
4.2 Results	106
4.2.1 Extraction of glycosaminoglycans from non-mammalian species.	106

4.2.1.1 <i>P. pelagicus</i>	109
3.2.1.2 <i>L. vannamei</i>	117
4.2.1.3 <i>S. pilchardus</i>	121
3.2.1.4. <i>M. aeglefinus</i>	124
3.2.1.5 <i>M. merluccius</i>	128
4.2.1.6 <i>P. hypophthalmus</i>	132
4.2.1.7 <i>C. batrachus</i>	136
4.2.1.8. <i>O. gorbuscha</i>	140
4.2.2 Screening of crude GAG extracts for BACE1 activities FRET.	145
4.2.3 DEAE anion exchange fractionation of crude GAG extracts and screening for BACE-1 inhibition.	148
4.3. Discussion	151
4.3.1 Extraction and analysis of crude glycosaminoglycans from aquatic species	151
4.3.2 Determination of BACE-1 inhibitory activity of crude glycosaminoglycans extracts from aquatic species.	172
4.3.3 Fractionation of glycosaminoglycans extracts from aquatic species with potent BACE-1 inhibitory activity.	174
Chapter 5: A glycosaminoglycan extract isolated from <i>Portunus pelagicus</i>, inhibits the Alzheimer's beta-secretase, BACE-1, with attenuated off target activities.	177
5.1. Introduction	178
5.1.2 Chapter aims	179
5.2 Results	180

5.2.1 Characterisation of the glycosaminoglycan extract from <i>Portunus pelagicus</i> , fraction 5.	180
5.2.2. <i>P. pelagicus</i> F5 inhibits the Alzheimer's Disease-Relevant β -Secretase	188
5.2.3 Heparin and <i>P. pelagicus</i> F5 induce a conformational change in the Alzheimer's Disease-Relevant β -Secretase.	190
5.2.4 Heparin and <i>P. pelagicus</i> F5 destabilise the Alzheimer's Disease-Relevant β - Secretase.	194
5.2.5. Attenuated Anticoagulant Activities of the <i>P. pelagicus</i> F5 extract	195
5.3. Discussion	196
Chapter 6: Glycosaminoglycan extracts with attenuated off target activities, isolated from <i>Litopenaeus vannamei</i>, inhibits the Alzheimer's beta-secretase, BACE1.	202
6.1 Introduction	203
6.1.2 Aims	205
6.2 Results	206
6.2.1 Characterisation of glycosaminoglycan extracts from <i>Litopenaeus vannamei</i>	206
6.2.2 <i>L. vannamei</i> F4 and F5 inhibits the Alzheimer's Disease-Relevant β - Secretase	221
6.2.3. Attenuated Anticoagulant Activities of the <i>L. vannamei</i> F4 and F5 extracts	224
6.2.4 Heparin and <i>L. vannamei</i> F4 induce a conformational change in the Alzheimer's Disease-Relevant β -Secretase.	226

6.2.4 Heparin and <i>L. vannamei</i> F4 destabilise the Alzheimer's Disease-Relevant β -Secretase.	227
6.3 Discussion	228
Chapter 7: Glycosaminoglycan extracts with attenuated off target activities, isolated from <i>Sardinia pilchardus</i>, inhibit the Alzheimer's beta-secretase, BACE1.	235
7.1 Introduction	236
7.1.2 Aims	237
7.2 Results	238
7.2.2 <i>S. pilchardus</i> F4 inhibits the Alzheimer's Disease-Relevant β -Secretase	244
7.2.3. Attenuated anticoagulant of the <i>S. pilchardus</i> F4 extract	245
7.2.4 Heparin and <i>S. pilchardus</i> F4 induce a conformational change in the Alzheimer's Disease-Relevant β -Secretase.	247
7.2.5 Heparin and <i>S. pilchardus</i> F4 destabilise the Alzheimer's Disease-Relevant β -Secretase.	248
7.3 Discussion	249
Chapter 8: Discussion and future directions	253
Chapter 9: References	266
Chapter 10: Appendix	292

Chapter 1: Introduction

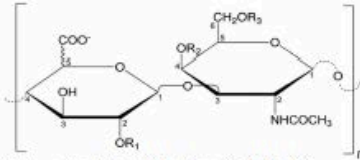
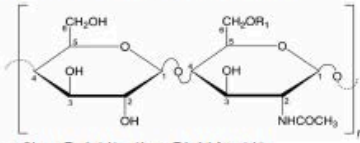
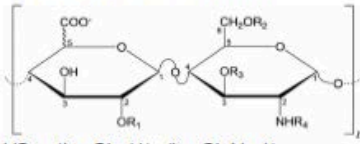
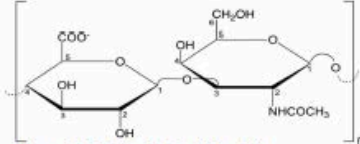
1.1. Glycosaminoglycans and Proteoglycans

Glycosaminoglycans (GAGs) are linear, unbranched, anionic heteropolysaccharides that can have molecular weights up to and in excess of 100 kDa (Gandhi and Mancera, 2008). They are comprised of disaccharide repeating regions in which one monosaccharide is either a uronic acid (UA; D-glucuronic acid, GlcA or L-iduronic acid, IdoA) or galactose (Gal) and the other an amino sugar (D-galactosamine, GalN or D-glucosamine, GlcN) (Gandhi and Mancera, 2008). Each monosaccharide in the repeating region may possess varying degrees of sulphation, contributing to the overall anionic properties of GAGs (Hook *et al.*, 1984). Furthermore, the geometry of the glycosidic linkage between disaccharide repeat regions can differ from an α or β configuration (Gandhi and Mancera, 2008). The structural differences between the disaccharide repeat regions gives rise to four main classes of GAGs: heparin/heparan sulphate (HS), chondroitin sulphate (CS)/dermatan sulphate (DS), keratan sulphate (KS), and hyaluronic acid (HA) (summarised in Table 1).

The galactosaminoglycans CS and DS are comprised of a D-acetylgalactosamine β 1 \rightarrow 3 linked to an uronic acid residue (GalNAc β 1 \rightarrow 3UA). The D-acetylgalactosamine monosaccharide can be variously O-sulphated at positions 4-O (chondroitin sulphate A) 6-O (chondroitin sulphate C). The uronic acid residue in CS is D-GlcA, distinguishing it from DS, which possesses L-IdoA, and both epimers can possess sulphate modifications at position 2-O. The disaccharide repeat region of CS/DS are in turn linked β 1 \rightarrow 4 to form an oligosaccharide (Prabhakar, Capila and Sasisekharan, 2009). Keratan sulphate also consists of D-Gal β 1 \rightarrow 4 however is linked to Gal rather than an uronic acid

(Ruoslahti, 1988). Furthermore, KS differs from CS/DS in that the glycosidic inter repeat consists of a β 1 \rightarrow 3 linkage and the D-Gal monosaccharide can only be 6-O-sulphated. Heparin/HS both contain D-GlcNAc α -1 \rightarrow 4 linked to an uronic acid. The D-GlcNAc monosaccharide can be modified by O-sulphation at positions 3-O, 6-O, and N-sulphation can occur following de-acetylation (Prabhakar, Capila and Sasisekharan, 2009). Sulphation can also occur at 2-O on IdoA and in rare cases GlcA (Hsieh *et al.*, 2016). There has also been evidence of the existence of free amino groups, however this may be artificial due to extraction processes (Yates and Rudd, 2016). Hyaluronic acid also consists of D-GlcNAc, however is non-sulphated and only contains D-glucuronic acid (GlcA). The possible modifications that can take place and structures of each GAG are demonstrated in Table 1. Referring to Table 1, it can be seen that HS/heparin is the most structurally diverse class of GAGs. If all the possible modifications that can occur are taken into account (including rare 2-O-sulphation on GlcA, 3-O-sulphation on GlcN and free amine groups, not shown in Table 1), there are potentially 48 different disaccharides that can occur along the HS/heparin chain (Turnbull, Powell and Guimond, 2001).

Table 1: Received composition and structure of the mammalian glycosaminoglycans. (Mycroft-West, Yates and Skidmore, 2018).

GAG	Major disaccharide repeating unit	Subunits	R ₁	R ₂	R ₃	R ₄
CS/DS	 <p>CS: →4) D-GlcA β(1-3) D-GalNAc β(1- DS: →4) L-Ido α(1-3) D-GalNAc β(1-</p>	CS-A	H	SO ₃ ⁻	H	N.A.
		CS-C	H	H	SO ₃ ⁻	N.A.
		CS-E	H	SO ₃ ⁻	SO ₃ ⁻	N.A.
		CS-D	SO ₃ ⁻	H	SO ₃ ⁻	N.A.
		DS (CS-B)*	SO ₃ ⁻	N.A.	N.A.	N.A.
Keratan sulfate II (KS)	 <p>→3) D-Gal β(1-4) D-GlcNAc β(1-</p>	KS-II*	SO ₃ ⁻	N.A.	N.A.	N.A.
Heparin/ HS	 <p>HS:→4) D-Glc β(1-4) D-GlcN α(1- Heparin:→4) L-Ido α(1-4) D-GlcN α(1</p>	HS*	H	H	H	COCH ₃
		Heparin*	SO ₃ ⁻	SO ₃ ⁻	SO ₃ ⁻ /H	SO ₃ ⁻
Hyaluronic acid (HA)	 <p>→4) D-GlcA β(1-3) GlcNAc β(1-</p>	N.A.	N.A.	N.A.	N.A.	N.A.

Abbreviations: GlcA, glucuronic acid; IdOA, iduronic acid; Gal, galactose; GalNAc, N-acetyl galactosamine; N.A., Not applicable.
*Structural representation of commonly occurring substitutions, rare variants have also been reported.

With the exception of HA, GAG chains are found covalently attached to a protein core forming the proteoglycan family (Schaefer and Schaefer, 2010). Proteoglycans (PGs) may contain one to >100 GAG chains and their protein core can range from 10 to >500 kDa (Prydz and Dalen, 2000). Proteoglycans are not limited to the attachment of one class of GAG, for instance aggrecan, syndecan and betaglycan can carry two types of side chains (Hardingham and Fosang, 1992); thus are termed hybrid PGs (Prydz and Dalen, 2000). For example, syndecan proteoglycans may have both CS and HS chains attached to their core protein (Iozzo and Schaefer, 2015). The attachment of a GAG chain to the protein core occurs through a specific tetrasaccharide moiety consisting of two Gal residues, a xylose (Xyl) residue and a GlcA residue (Prydz, 2015) (expanded upon in section 3.2). The GAG chain is extended from this tetrasacchride linker by the addition of disaccharide repeating regions (Table 1), this dictates the type of GAG synthesised. The tetrasaccharide region is attached to the protein core through an O-glycosidic link to a serine residue (GAG-GlcAGalGalXyl-O-CH₂-Ser) (Gandhi and Mancera, 2008). Keratan sulphate class 1 is an exception to this as it is linked to the protein core through a N-asparaginyl bond and HA, which is not synthesised on a protein core (Gandhi and Mancera, 2008).

1.2. Heparin and Heparan Sulphate

1.2.1 Structure

As mentioned, heparin and HS are the most structurally complex members of the GAG family (Gallagher and Walker, 1985). The primary HS/heparin chain produced during synthesis consists of the repeating disaccharide sequence, D-glucuronic acid β -1 \rightarrow 4 N-

acetylglucosamine α -1 \rightarrow 4 (GlcA β 1 \rightarrow 4GlcNA α -1 \rightarrow 4)_n (Gallagher and Walker, 1985). The microheterogeneity of HS and heparin arises from the variation in the chain modifications that may take place between each disaccharide repeat. The first of such modifications to take place is N-deacetylation/N-sulphation of the GlcNAc monosaccharides. Subsequent epimerization of GlcA, forming the C₅ epimer, IdoA may then take place. This may be followed by O sulphation at C₂ of the uronic and position C₆ and C₃ of glucosamine residues (Meneghetti *et al.*, 2015), Figure 1. 2-O sulphation of the uronic acid occurs predominantly at IdoA residues, however this is not always the case. During biosynthesis these modifications do not always run to completion therefore, there is potential for enormous diversity in the structure of a HS or heparin chain (Turnbull, Powell and Guimond, 2001).

Although HS and heparin are structurally related, heparin has been shown to differ in fine structure from mammalian forms of HS, for example extractions from human skin fibroblast and mouse bone marrow stromal cells (Gallagher and Walker, 1985). Heparin is exclusively synthesised within the secretory granules of mast cells, where it is formed upon a heparin proteoglycan, which consists of a unique protein core known as serglycin (Rabenstein, 2002). Although HS is also synthesised as a proteoglycan, it differs from heparin in that it is found on and/or secreted from almost all mammalian cells (*idem*). Furthermore, HS is not linked exclusively to one core protein, but forms several families of proteoglycans (HSPGs) with distinct core proteins. There are three main subfamilies of HS proteoglycans that are classified according to their mode of attachment to the cell membrane and the amino acid sequence of the core protein (*idem*). Firstly, there are four members of transmembrane HSPGs belonging to the

syndecan family. The second family of HSPGs are the glypicans, which contains six members and are attached to the cell membrane by a glycosylphosphatidylinositol (GPI) anchor (*idem*). Finally, HS proteoglycans can be secreted into the extracellular matrix (ECM), these HSPGs can also be classified according to their specific core protein (*idem*). Heparan sulphate is rarely found without association to a proteoglycan *in vivo*, in stark contrast to heparin (*idem*). The HS chains on HSPGs are also shorter and less abundant than on heparin proteoglycans (*idem*).

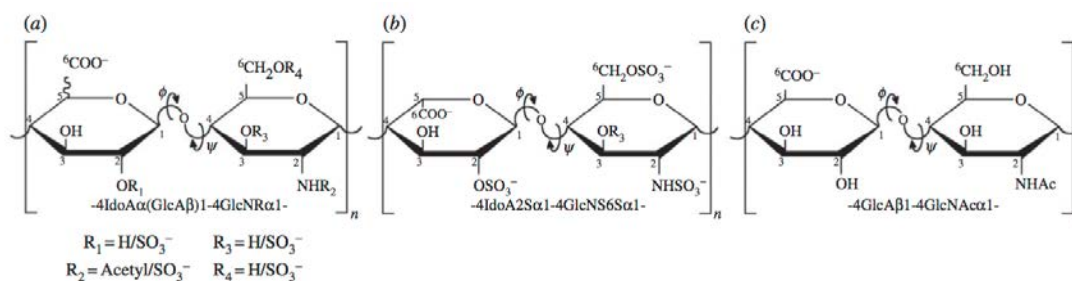


Figure 1: Comparison of the structural features of heparan sulphate (HS) and heparin. (A) possible modifications of the HS/heparin disaccharide, (B) the major disaccharide of heparin, accounting for 70-80% of the total chain, (C) the major disaccharide of HS (Menegetti et al., 2015).

The structural differences between HS and heparin are illustrated in Figure 1. Figure 1B demonstrates the trisulphated disaccharide motif that is the major product of near complete modification (with the exception of the rare 3-O-sulphate) during synthesis (L-IdoA(2S) α -1 \rightarrow 4D-N-GlcNS(6S)) (Gallagher and Walker, 1985). This trisulphated disaccharide, is the predominant constituent of heparin, making up approximately 70-80% of its chain (Meneghetti *et al.*, 2015). In contrast, approximately 40-60% of HS chains are composed of the primary product D-GlcA β 1 \rightarrow 4D-N-GlcNAc, Figure 1C. The D-GlcN in HS can be N-sulphated however, this is more infrequent than in heparin, where N-sulphation predominates. Epimerization to the C₅ epimer L-IdoA is also rarer in HS, in contrast to heparin in which this occurs frequently (Meneghetti *et al.*, 2015).

These structural differences lead heparin to higher levels of overall sulphation and hence more negative charge than HS. Furthermore, HS possesses a significantly higher mean molecular weight in comparison to heparin (Meneghetti *et al.*, 2015).

1.2.2. Biosynthesis

The biosynthesis of heparin and HS occurs predominantly within the Golgi apparatus by the action of several transmembrane enzymes (Kreuger and Kjellén, 2012). In the case of heparin, biosynthesis takes place exclusively in mast cells, whereas HS is synthesised by almost all mammalian cells (Sasisekharan and Venkataraman, 2000). Biosynthesis is initiated by the attachment of a tetrasaccharide linkage region (GlcA β 1-3-Gal β 1-3-Gal β 1-4-Xyl β 1-O-CH₂-Ser) to the proteoglycan core. After translation of the core protein, Xyl may be attached at Ser residues located within the sequence Ser-Gly-X-Gly (where X is any amino acid and Gly, glycine) (Garg, Linhardt and Hales, 2005). The addition of Xyl is catalysed by one of two xylosyltransferases (XylT1 or XylT2), Figure 2 (Kreuger and Kjellén, 2012). It should be noted that this form of O-glycosylation does not necessarily occur at all Ser residues within a core protein. After the addition of Xyl, galactosyltransferases-I (GalT-1) and galactosyltransferases-II (GalT-2) catalyse the attachment of two Gal residues respectively (Garg, Linhardt and Hales, 2005). Galactosyltransferases-I attaches a Gal residue to Xyl via a β 1-4 glycosidic linkage from uridine diphosphate-galactose (UDP-Gal), whereas galactosyltransferases-II catalyses the addition of a Gal residue to a β -linked Gal through a β 1-3 glycosidic linkage (*idem*). The synthesis of the linkage region is completed by the addition of GlcA. Glucuronic acid is attached to Gal through a β 1-3 glycosidic linkage by glucuronyltransferase-I (GlcAT-1)

forming the complete linkage tetrasaccharide (GlcA β 1-3-Gal β 1-3-Gal β 1-4-Xyl β 1 -O-CH₂-Ser), Figure 2.

After the formation of the linker tetrasaccharide, GlcNAc is subsequently attached thereby committing biosynthesis to heparin/HS (Turnbull, Powell and Guimond, 2001) as opposed to CS/DS. Transfer of GlcNAc from UDP-GlcNAc occurs at the non-reducing end of the linkage motif and is catalysed by member of the glycosyltransferase family, which possess acetylglucosaminyltransferase-I (GlcNAcT-I) activity (Kreuger and Kjellén, 2012). Glycosyltransferases are encoded for by the exostosin like-genes (EXTL) family, consisting of EXTL1, EXTL2, EXTL3 and EXTL4 (Garg, Linhardt and Hales, 2005). EXT2 and EXT3 have been shown to encode for GlcNAcT-I activity. Evidence suggests that EXT3 is the predominant gene responsible for the initiation of the synthesis of the disaccharide region (Kreuger and Kjellén, 2012) and has the highest catalytic efficiency for the transfer of GlcNAc to the linkage region (Garg, Linhardt and Hales, 2005). After attachment of the initial GlcNAc, the chain is elongated by the alternating addition of both GlcNAc and GlcA residues, from UDP-GlcNAc and UDP-GlcA respectively, Figure 2 (Turnbull, Powell and Guimond, 2001); chain elongation occurs by the action of HS-copolymerase complexes. The addition of GlcA and GlcNAc occurs through the action of HS- β 1-4-glucuronyltransferase-II (HS-GlcAT-II) and α 1-4-acetylglucosaminyltransferase-II (GlcNAcT-II), respectively. A HS-copolymerase complex consisting of EXTL1 and EXTL2 possesses both HS-GlcAT-II and GlcNAcT-II activity. However, complexes comprised of EXTL1 and EXTL3 is thought to only exhibit GlcNAcT-II activity (Garg, Linhardt and Hales, 2005). The product of chain elongation by

HS copolymerases is a primary HS/heparin chain consisting of (GlcA β 1 \rightarrow 4GlcNAc α -1 \rightarrow 4)_n (Turnbull, Powell and Guimond, 2001).

The primary HS or heparin chain may then undergo a series of modifications, the first being N-deacetylation, prior to N-sulfation of the GlcNAc residues. This occurs through the action of N-deacetylase/N-sulfotransferases (NDSTs). The N-deacetylase domain hydrolytically removes the acetyl group of GlcNAc. This hydrolysis is followed by the addition of a N-sulphate group from 3'phosphoadenosine 5'phosphosulfate (PAPS) to the unsubstituted position catalysed by the N-sulfotransferase domain of NDST (Garg, Linhardt and Hales, 2005), Figure 2. Four isozymes of the NDST family have been identified, each conferring different activities/specificities (*idem*). NDST-1 and NDST-2 have been shown to display higher activity for both N-deacetylase/N-sulfotransferases (*idem*). However, N-deacetylation/N-sulphation does not occur to completion along the heparin or HS chain. This results in a modified chain comprised of a variable domain structure of N-sulphated and N-acetylated regions (Kreuger and Kjellén, 2012). The N-sulphated and N-acetylated domains may be of variable lengths; this has been suggested to be dependent on the concentration of the sulphate donor PAPS (*idem*). N-deacetylation/N-sulphation of the primary sequence of HS or heparin is critical and essential for further downstream processing to take place (Garg, Linhardt and Hales, 2005). Therefore, it is this modification step that differentiates HS from heparin. Heparin displays a higher degree of modification in comparison to HS and this has been suggested to result from heparin requiring the NDST2 isozyme for biosynthesis, whereas HS does not (Kreuger and Kjellén, 2012).

Following N-deacetylation/N-sulphation, epimerization of the GlcA monosaccharide to IdoA can occur at C₅. This step is catalysed by heparin/HS glucuronyl C5-epimerase (Hsepi) (Garg, Linhardt and Hales, 2005), Figure 2. Although many GlcA residues are converted, this step also does not occur to completion (Kreuger and Kjellén, 2012). Evidence suggests that Hsepi acts on uronic acids on the non-reducing side of GlcNS and therefore occurs after N-deacetylation/N-sulphation (Garg, Linhardt and Hales, 2005). Regions containing N-sulphation and IdoA later result in the S-domains (Turnbull, Powell and Guimond, 2001). Once epimerization has occurred, the uronic acid residue in heparin and HS can subsequently undergo 2-O-sulphation. This process is catalysed by 2-O-sulphotransferase (2OST), which transfers a sulphate from PAPS onto the carbon atom present at position 2 of the uronic acid (Garg, Linhardt and Hales, 2005). To date, only one isoform of 2OST has been identified (Kreuger and Kjellén, 2012). Although 2-O sulphation of GlcA can occur, 2OST strongly favours the sulphation of IdoA (Garg, Linhardt and Hales, 2005). It has been proposed that this is due to 2OST interacting with Hsepi, as they have been shown to co-localize within the Golgi apparatus (Kreuger and Kjellén, 2012).

The final modifications, which may take place within the heparin/HS chain, are 6-O- and 3-O-sulphation. 6-O-sulphation can occur at position C-6 of either GlcNAc and/or GlcNS monosaccharaides and is catalysed by 6-O-sulphotransferases (6OST) (Garg, Linhardt and Hales, 2005), Figure 2. There are three isoforms of 6OST, which differ in their substrate specificities (Kreuger and Kjellén, 2012). 6OST has been reported to preferentially modify GlcNS residues flanked by 2-O-sulphated IdoA monosaccharaides (*idem*). 3-O-sulphation can occur at position C₃ of GlcN and is catalysed by 3-O-

sulphotransferases (3OST) (Garg, Linhardt and Hales, 2005). Seven isoforms of 3OST have been identified to-date; these have been shown to have distinct expression patterns (Kreuger and Kjellén, 2012). The expression of different isoforms maybe linked to the formation of specific HS motifs, which mediate protein ligand interactions (*idem*). An example of this is the importance of 3-O-sulphation in the formation of the antithrombin-binding pentasaccharide motif, discussed in section 4 and 4.1 (*idem*).

The modifications that occur during biosynthesis, give rise to the domain structure seen in HS. The predominant unsulphated D-glucuronic acid β 1 \rightarrow 4 D-N-acetylglucosamine disaccharide seen in HS constitutes the NA domains, whereas highly modified sulphated regions (NS domains) contain L-iduronic acid (2S) α -1 \rightarrow 4 D-N-sulfoglucosamine (6S). NA and NS domains are separated by NA/NS transition regions, which consist of partially modified disaccharides (Rabenstein, 2002). The domain structure is a predominant feature of HS chains opposed to heparin, which is comprised of mainly trisulphated disaccharide repeats, Figure 1B. The specific composition of the domains in HS is essential for their interaction with numerous proteins (Turnbull, Powell and Guimond, 2001). Although the disaccharide composition is an important feature in conferring HS-protein interactions, the sequence and domain structure must also be taken into account. A modification of particular importance is epimerization from D-glucuronic to L-iduronic acids, which imparts chain flexibility to HS (Meneghetti *et al.*, 2015). Therefore, the specific charge distribution and chain flexibility is an important feature to consider when defining HS-protein interactions (*idem*).

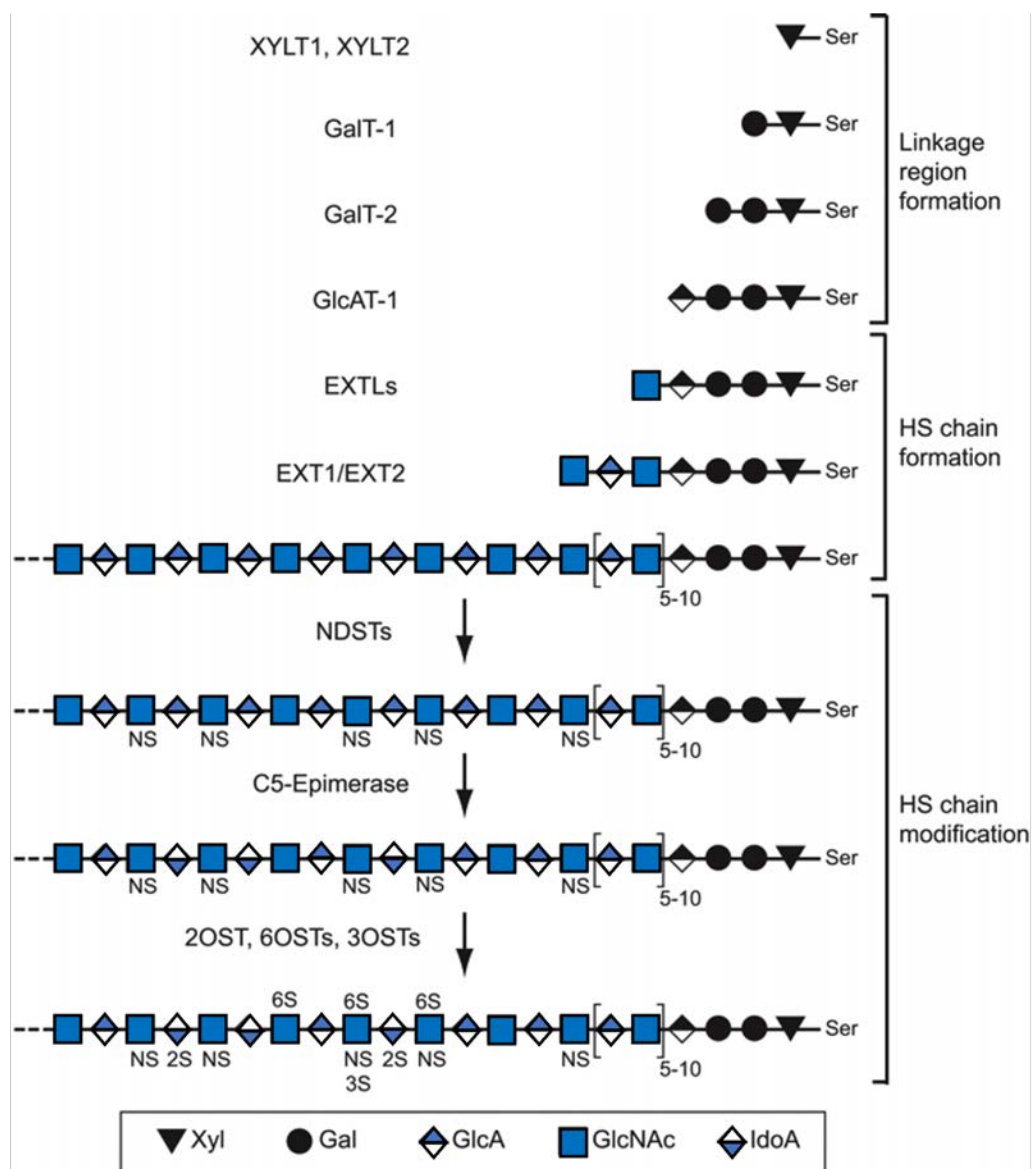


Figure 2: Biosynthesis of heparan sulphate (HS) and heparin. Illustration of the enzymes involved in each step of HS and heparin biosynthesis. During HS chain modification variable structures can be produced. The abbreviations used include: xylosyltransferase1 (XYLT1) xylosyltransferase 2 (XYLT2), galactosyltransferases-I (GalT-1), galactosyltransferases-II (GalT-2), glucuronyltransferase-I (GlcAT-1), exostosin like-genes (EXTLs), N-deacetylase/N-sulfotransferases (NDSTs), 2-O-sulphotransferase (2OST), 6-O-sulphotransferases (6OST), 3-O-sulphotransferases (3OST), N-sulphated (NS), glucuronic acid (GlcA), N-acetylated glucosamine (GlcNAc), iduronic acid (IdoA), serine (Ser), 6-O-sulphated (6S), 2-O-sulphated (2S), galactose (Gal), xylose (Xyl). Modified from (Kreuger and Kjellén, 2012).

1.3. The Coagulation Cascade

The maintenance of blood flow under normal physiological conditions and the ability to arrest bleeding upon vascular injury is known as haemostasis (Palta, Saroa and Palta, 2014). The haemostasis process encompasses both coagulation and platelet activation, which lead to the formation of a haemostatic plug at the site of vessel injury (Mackman, Tilley and Key, 2007). The cascade or waterfall model of coagulation was first described in the 1960s as a series of zymogen activation reactions (Versteeg *et al.*, 2013). The cascade model highlighted that the activation of a pre-cursor coagulation factor is required to propagate the activation of the downstream factor, in a stepwise manner (Adams and Bird, 2009). Coagulation factors are serine proteases that are cleaved to their activated states, usually in the presence of calcium ions. The coagulation cascade suggests that there are two pathways, the intrinsic and extrinsic pathways, which converge into a common pathway (Versteeg *et al.*, 2013) as depicted in Figure 3. These pathways differ in that the extrinsic pathway requires an external factor called tissue factor (TF) located in the extravascular tissue for activation. Whereas the components required for activation of the intrinsic pathway are located within the blood stream (*idem*). Although the current understanding of coagulation has advanced from this model, it is still used clinically to measure prothrombin time (PT) and activated partial thromboplastin time (aPTT) (Gailani and Renné, 2007), Figure 3. In-light of this, this model is still relevant for the scope of this work. For a current outline of the cell-based model of coagulation please refer to (Versteeg *et al.*, 2013).

The extrinsic pathway is triggered upon vascular damage, exposing subendothelial cells bearing TF to blood the component FVII (Monroe and Hoffman, 2009). Tissue Factor is a transmembrane glycoprotein, which is tightly associated with phospholipids in the cell membrane (Davie, Fujikawa and Kiesel, 1991). Tissue Factor becomes bound to FVII in the presence of calcium, converting the zymogen into the activated factor FVIIa via proteolysis (*idem*). The TF-FVIIa complex then catalyses the activation of FX to FXa, at this point the extrinsic and intrinsic pathway merge into the common pathway (Dahlbäck, 2000), Figure 3.

The intrinsic pathway (or contact activation pathway) is initiated when the plasma factor XII (FXII) is activated (FXIIa) upon contact with charged surfaces exposed through damage of the vessel wall. FXIIa activation is followed sequentially by the activation of FXI to FXIa and FIX to FIXa. The intrinsic pathway then converges with the extrinsic pathway upon activation of FX (Gailani and Renné, 2007).

The activation of factor FXa in the common pathway enables the formation of a phospholipid bound complex known as prothrombinase, in the presence of calcium ions (Davie, Fujikawa and Kiesel, 1991). The prothrombinase complex (FVa) functions to catalyses the activation of thrombin (FIIa) from prothrombin (FII) (Alquwaizani *et al.*, 2013). This occurs through the cleavage of prothrombin, releasing thrombin from the carboxyl-terminal. Thrombin is then able to potentiate the conversion of fibrinogen to fibrin and form a fibrin clot (Gailani and Renné, 2007). The activation of thrombin is the final proteolytic step of the coagulation cascade making the regulation of thrombin critical for maintaining homeostasis. Furthermore, thrombin is able to potentiate its

own formation, resulting in a positive feedback loop driving the formation of the fibrin clot (Li *et al.*, 2004) Figure 3.

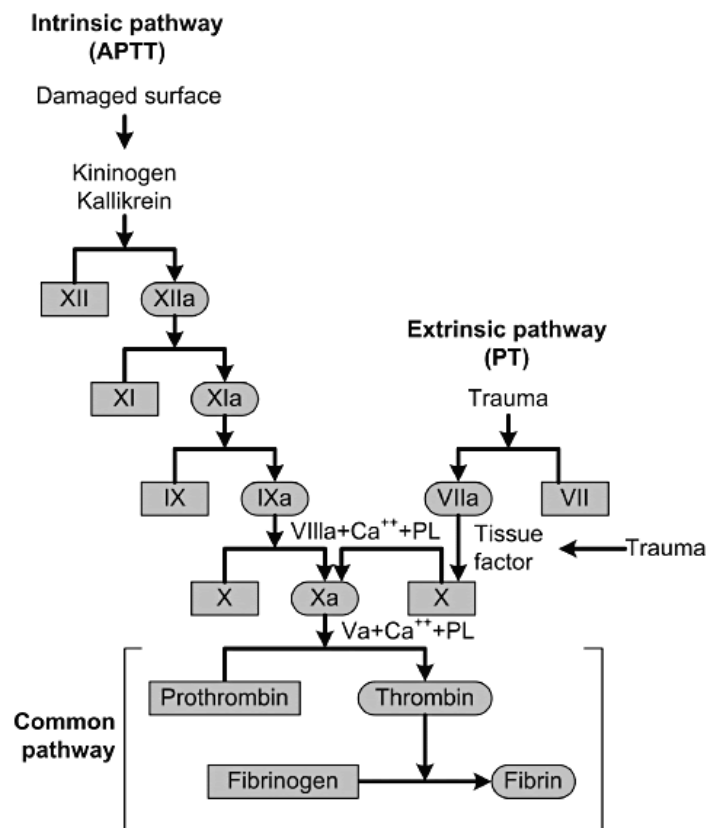


Figure 3: Overview of the coagulation cascade. Illustrating the intrinsic pathway (measures by aPTT) and the extrinsic pathway (measured by PT), converging on the common pathway (Adams and Bird, 2009).

The maintenance of homeostasis is dependent on the regulation of the coagulation cascade and restoration of normal blood flow. One of the primary regulators of coagulation is antithrombin, a member of the serpin family (serine proteinase inhibitors) (Li *et al.*, 2004). Other members include heparin cofactor II (HCII), protease nexin I, and protein C inhibitor. Serpins are poor inhibitors, until bound to heparin, which stimulates a conformational change in the serpin that facilitates protease-serpin binding and or exposes the active centre of the serpin to the protease. Heparin is able

to bind to antithrombin with high affinity for example through the pentasaccharide sequence [-4- α -D-GlcNS,6S (1-4) β -D-GlcA (1-4) α -D-GlcNS,3S,6S (1-4) α -L-IdoA2S (1-4) α -D-GlcNS,6S (1-)] known as the antithrombin binding site (AT binding site). This interaction mediates the inhibition of thrombin and activated FX (the point where the intrinsic and extrinsic pathways converge into the common pathway, Figure 3), halting the coagulation cascade. The binding of heparin to AT results in a conformational change enabling to AT to bind FXa with ~100 fold greater affinity (Olson and Chuang, 2002). The pentasaccharide sequence can also facilitate inhibition of thrombin by AT, however heparin chains must be greater than 18 disaccharide units in order to act as bridge between AT and thrombin (*idem*).

1.4. Clinical use of heparin

Heparin is most widely used as an anticoagulant owing to its ability to inactivate thrombin (FIIa) and activated factor X (FXa) in the coagulation cascade (Hirsh *et al.*, 2001). Preparations of full-length heparin, known as unfractionated heparin (UFH), have chain lengths varying from 2,000 - 40,000 Da (Lima *et al.*, 2011). Therefore, UFT is capable of binding both AT and thrombin with a 1:1 anti-FXa and anti-FIIa ratio (Hirsh *et al.*, 2001). Due to the structure of full-length heparin (see section 3.1), UFH preparations have a high variation in the charge density and disaccharide composition. Unfractionated heparin can therefore bind to a variety of proteins in plasma, endothelial cells, macrophages and platelets (Lima *et al.*, 2011). For the clinical use of UFH as an anticoagulant this is a disadvantage, as it leads to reduced bioavailability and unpredictable dose responses between patients (Hirsh *et al.*, 2001).

The disadvantages in the use of UFH led to the development of Low molecular weight heparins (LMWHs). Low molecular weight heparins (LMWHs) consist of smaller heparin chains produced through various methods such as chemical or enzymatic depolymerisation (Gray, Mulloy and Barrowcliffe, 2008). To be defined as a LMWH, 60% of the preparation must have a molecular weight below 8,000 Da (*idem*). Compared to UFH, LMWHs have a reduced ability to inactivate thrombin (FIIa) due to their reduced chain length (<18 disaccharides). However, LMWHs still contain the essential AT-binding domain for the inhibition of FXa. The anti-FXa to anti-FIIa ratios for LMWHs is between 2:1 and 4:1, depending on the molecular size (Hirsh *et al.*, 2001). The higher anti-FXa to anti-FIIa ratio observed in LMWHs is seen as an advantage for clinical use as it increases bioavailability due to decreased interactions with other serum proteins. Furthermore, LMWHs have a more predictable dose response due to their greater specificity for FXa compared to UFH (Linhardt and Sibel Gunay, 1999).

The differences between LMWHs occur due to the different methods in which they can be produced. One example is oxidative depolymerisation with hydrogen peroxide; this method relies on the generation of oxygen radicals from hydrogen peroxide in the presence of either a metal or alkali catalyst. The oxygen radicals are able to attack sensitive residues in the saccharide, such as unsubstituted residues at position C₂ and C₃. This produces the LMWHs ardeparin and parnaparin (*idem*), Table 2. A second method used to produce LMWHs is controlled oxidative depolymerisation through deamination. This process can be conducted using nitrous acid or another nitrosating reagent, for example isoamyl nitrate. Four LMWHs can be produced through this method; Certoparin, Dalteparin, Nadroparin and Reviparin, Table 2 (*idem*). The final

method by which LMWHs can be produced is β -eliminative cleavage, this can be conducted chemically and enzymatically. Enzymatic β -eliminative cleavage is carried out using heparin lyase 1 (heparinase), producing the LMWH tinzaparin. Chemical β -eliminative cleavage can be conducted using direct or indirect treatment with a base. Cleavage occurs specifically at IdoA monosaccharides independent of 2-O sulphation leaving an unsaturated uronic acid at the non-reducing terminus. This method is used to produce enoxaparin, Table 2 (*idem*).

Table 2: Preparation methods for low molecular weight heparins (LMWHs). Adapted from (Linhardt and Gunay, 1999).

LMWH	Preparation method
Ardeparin	Oxidative depolymerization with hydrogen peroxide
Parnaparin	Oxidative depolymerization with hydrogen peroxide
Certoparin	Deaminative cleavage with isoamyl nitrite
Dalteparin	Deaminative cleavage with nitrous acid
Enoxaparin	Chemical β -eliminative cleavage
Tinzaparin	β -eliminative cleavage by heparinase
Reviparin	Deaminative cleavage with nitrous acid
Nadroparin	Deaminative cleavage with nitrous acid

Currently the clinical use of LMWHs is exclusively used as an anticoagulant, for example in the treatment of deep venous thrombosis (DVT) (Lima *et al.*, 2011). However, recent studies have begun to uncover potential uses of modified LMWHs in the treatment of cancer, Alzheimer's disease (AD), inflammatory disorders such as asthma (Shastri *et al.*, 2015) and infectious diseases, for example malaria (Skidmore *et al.*, 2008).

It has been proposed that LMWHs can modulate various immune cells and pro-inflammatory cytokines. The widely used LMWH enoxaparin has been demonstrated to inhibit T-cell mediated release of multiple cytokines (IL-4, IL-5, IL-13 and TNF- α)(Shastri *et al.*, 2015). Among others the cytokines IL-4, IL-5, IL-13 and TNF- α have a critical role

in the response to allergens in asthma (Mahajan and Mehta, 2006), therefore the suppression of T-cells by LMWHs such as enoxaparin may be a promising therapeutic for asthma (Shastri *et al.*, 2015).

1.5. Alzheimer's Disease

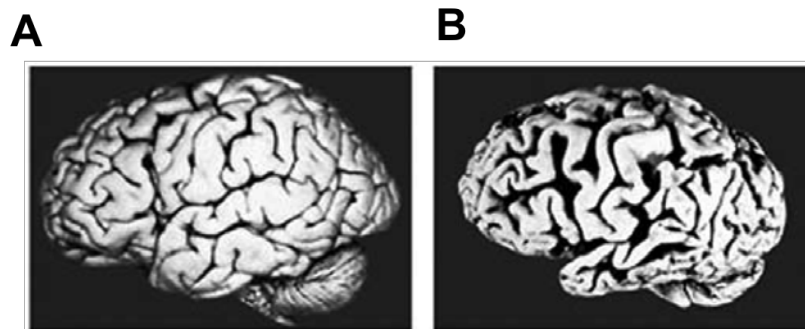


Figure 4: Brain degeneration in Alzheimer's disease (AD). AD results in cerebral atrophy in regions associated with learning and memory. Brain of a healthy person (**A**) compared with the brain of a patient with AD (**B**), shows shrinkage of gyri in the temporal and frontal lobes (Mattson, 2004)

Alzheimer's disease (AD) is a neurodegenerative disorder that leads to the progressive decline of memory and other cognitive functions within 3-9 years of diagnosis (Mattson, 2004; Querfurth and LaFerla, 2010). Alzheimer's Disease is also the leading cause of dementia in the elderly, accounting for 80% of cases worldwide (Kumar, Singh and Ekavali, 2015). The symptoms of AD are a consequence of gradual cerebral atrophy as a result of synaptic degeneration and neuronal death. Atrophy occurs in regions of the brain that are associated with memory and learning, for example the temporal and frontal lobes (Mattson, 2004). Figure 4B, shows the deterioration of an AD brain compared with that of a healthy individual, Figure 4A (*idem*). The majority of AD cases are sporadic (late onset) occurring over the age of 65 years (Liu *et al.*, 2013). However, a small percentage (~1%) of cases are early onset, developing before the age of 65.

These cases have been linked to autosomal dominant mutations and are referred to as familial Alzheimer's disease (FAD) (*idem*). The discovery of the genetic association of FAD has been significant in advancing the understanding of the aetiology of AD.

Alois Alzheimer first described two histological features of AD in 1907; the presence of extracellular β -amyloid plaques and neurofibrillary tangles (NFTs) (Karran, Mercken and Strooper, 2011). Since then, several hypotheses have been proposed aiming to explain the aetiology of AD including, the cholinergic hypothesis, the Amyloid cascade hypothesis, the tau hypothesis and the inflammation hypothesis (Kumar, Singh and Ekavali, 2015). Numerous studies have identified interactions between heparan sulphate/heparin and amyloid- β peptides ($A\beta$), the main constituent of β -amyloid plaques (Leveugle and Fillit, 1994; Zhang *et al.*, 2014). Heparan sulphate has also been shown to be an endogenous regulator of the β -site amyloid precursor protein-cleaving enzyme 1 (BACE-1), which is involved in the generation of $A\beta$ (Scholefield *et al.*, 2003). In-light of this evidence, this review will focus on the amyloid cascade hypothesis of AD, which postulates that the deposition of $A\beta$ within brain is a critical event in the aetiology of AD.

1.5.2. Amyloid cascade hypothesis

β -amyloid plaques are largely composed of aggregated deposits of $A\beta$ (Karran, Mercken and Strooper, 2011). $A\beta$ peptides are produced through the sequential cleavage of the type one transmembrane amyloid precursor protein (APP) in the amyloidogenic pathway. APP can be processed via two pathways, depending upon the site of primary cleavage, by either β -secretase (amyloidogenic pathway, Figure 5C) or α -secretase

(non-amyloidogenic pathway, Figure 5B) (Thinakaran and Koo, 2008). In the case of cleavage by β -secretase a soluble NH_2 -terminal fragment termed sAPP β is released from APP, leaving a membrane-associated COOH-terminal fragment, β -CTF (or C99) (*idem*). The predominant neuronal β -secretase is the aspartyl protease BACE-1 (*idem*)(discussed in 6.1). Cleavage by α -secretase in the non-amyloidogenic pathway occurs within the A β domain between residues Lys¹⁶ and Leu¹⁷. This liberates the peptide sAPP α from the NH_2 -terminal of APP and leaves α -CTF (C83) tethered to the membrane (*idem*) (Figure 5). sAPP α contains a fragment of the A β domain (Figure 5B); therefore, cleavage by α -secretase prevents the generation of intact A β (*idem*). Unlike the β -secretase site in the amyloidogenic pathway, it has been shown that several zinc metalloproteases can cleave APP at the α -secretase site, such as ADAM9, ADAM10, ADAM17 and TACE (Zhang *et al.*, 2011). The aspartyl protease, BACE-2 can also cleave at the α -secretase site (Thinakaran and Koo, 2008). The remaining membrane-bound C-terminal fragment (C99 or C83) then undergoes cleavage by γ -secretase. γ -secretase consists of four essential subunits, nicastrin, APh-1 and PEN-2 and a catalytic site comprised of Presilin-1 (PSEN1) or Presilin-2 (PSEN2), (*idem*). Cleavage by γ - releases either A β or p3, in the amyloidogenic or non-amyloidogenic pathways, respectively (*idem*), see Figure 5. A β is therefore secreted into the extracellular space where it can self-aggregate into β -amyloid plaques (Querfurth and LaFerla, 2010). This initially occurs through the formation of A β oligomers of 2-6 peptides, which then develop into fibrils and eventually β -amyloid plaques (*idem*). Cleavage by γ -secretase also liberates an APP intracellular cytoplasmic domain (AICD), in both pathways (Figure 5). AICD is involved in signalling transcription activation and is targeted to the nucleus after its release (*idem*).

The A β peptides produced in the amyloidogenic pathway of APP metabolism can be of variable lengths, between 36-43 amino acids (*idem*). This is due to γ -secretase having multiple cleavage sites within the transmembrane domain of β -CTF (*idem*). Monomers of A β 40 are the predominant species produced by γ -secretase. However, an imbalance favouring the production of A β 42 has been suggested to be an initiating factor in the development of AD. This is due to A β 42 having a higher propensity to oligomerize and form amyloid fibrils, than the shorter A β 40 (Walsh and Selkoe, 2007). Therefore, aberrant processing of APP, producing toxic A β plaques, makes the basis of the amyloid cascade hypothesis.

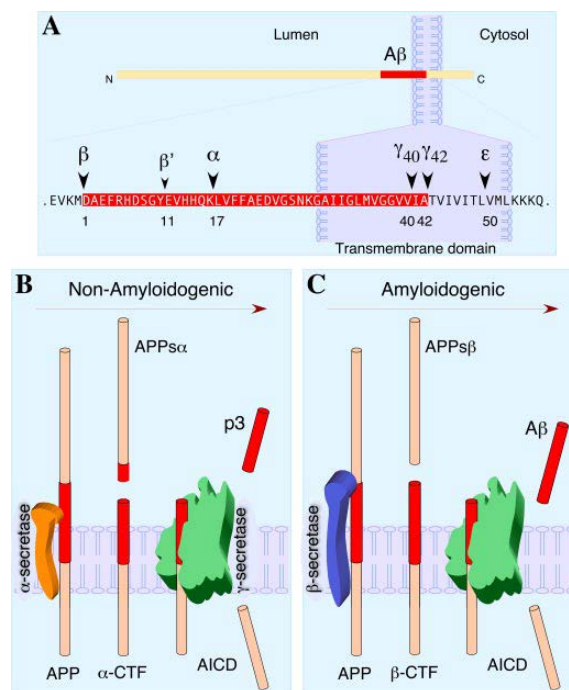


Figure 5: APP processing. (A) Structure of APP, with α , β and γ cleavage sites indicated. The A β domain is shown in red. (B) The non-amyloidogenic pathway of APP processing by α - and γ -secretase. α -secretase cleaves APP within the A β domain liberating sAPP α and preventing the generation of A β . γ -secretase then cleaves the membrane bound C-terminal, α CTF producing p3 and AICD. (C) The amyloidogenic pathway of APP processing by β - and γ -secretase. β -secretase cleaves APP liberating sAPP β . γ -secretase then cleaves the membrane bound C-terminal fragment, β -CTF generating A β and AICD (Thinakaran and Koo, 2008).

Evidence supporting this hypothesis initially came from the localization of the APP gene to chromosome 21 (*idem*). This was significant as Down's syndrome patients, caused by trisomy of chromosome 21, suffer from early onset AD; linking increased expression of APP and higher levels of A β to the early onset of AD (*idem*). Following this, several genetic studies have identified mutations with the APP gene, the first being a point mutation (C-T), causing an amino acid substitution (Val – Ile) within APP (Goate *et al.*, 1991). Since this discovery, 69 mutations in APP have been discovered that are causative of AD (Cruts, Theuns and Van Broeckhoven, 2012a)[date assessed 1/07/21]). Most of these mutations occur within close proximity to the β - or γ - secretase cleavage sites and therefore influence the proteolytic processing of APP (Zou *et al.*, 2014). For example, the Swedish mutation (Lys⁶⁷⁰→Asn and Met⁶⁷¹→Leu) (Yan and Vassar, 2014) which occurs directly upstream of the A β sequence increases the proficiency of β -secretase cleavage and production of A β (Zou *et al.*, 2014). Mutations that occur at the C-terminal end of the A β sequence, close to the γ - secretase cleavage site, cause an increase in the ratio of A β 42:A β 40 (*idem*). Mutations within the A β sequence have also been reported that do not affect the ratio of A β 42:A β 40 or total production, but do result in increased propensity for aggregation (*idem*). Mutations in the proteolytic enzymes involved in APP processing have also been reported, providing further support for this hypothesis. To date, approximately 326 mutations in PSEN1 and 68 in PSEN2 have been discovered (Cruts, Theuns and Van Broeckhoven, 2012b)[date assessed 1/07/21]). These subunits are the catalytic sites of γ - secretase; therefore mutations affect the cleavage of β -CTF shifting the production towards A β 42 rather than A β 40 (Zou *et al.*, 2014). These mutations provide evidence that the deposition of A β favouring the A β 42 species is sufficient to precipitate early onset AD, supporting the amyloid

cascade hypothesis. However, only ~1% of AD cases are linked to FAD, therefore other factors must contribute to the risk of developing late-onset AD.

In addition, the hyperphosphorylation of tau has been observed to occur in succession to deposition of A β in human stem-cell derived neuronal cultures obtained from AD subjects (Muratore *et al.*, 2014). Supporting that other AD related neuropathologies including NFTs, neuronal cell death, inflammation, vascular damage and neurochemical imbalances, consequently may be propagated due to excess accumulation of A β (*idem*). More recently experimental evidence has led to the proposal that an imbalance between A β peptide production and clearance, for example by microglia, is an influential factor in the pathogenesis of AD (Tan and Gleeson, 2019).

One further risk factor for AD is thought to be dependent on the protein apolipoprotein E (APOE) (Zou *et al.*, 2014). There are three common alleles of ApoE (ϵ 2, ϵ 3, ϵ 4), each of which confers a different susceptibility to the risk of developing AD. The possession of ϵ 4 can accelerate onset of AD, whereas ϵ 3 is considered neutral and ϵ 2 protective (Karran, Mercken and Strooper, 2011). Each allele codes for a different amino acid at either position 112 or 158 of the protein (Zou *et al.*, 2014), ϵ 2 (Cys112, Cys153), ϵ 3 (Cys112, Arg158) and ϵ 4 (Arg112, Arg158) (Liu *et al.*, 2013). The residue at position 112 has been suggested to be of importance due to it mediating the interaction between two lipid-binding domains of APOE. These are the low-density lipoprotein (LDL) receptor-binding site (residues 136-150) and a C-terminal major lipid-binding domain (residues ~240-270) (Mahley, Weisgraber and Huang, 2006). Studies have suggested that Arg112 present in APOE4 orientates Arg-61 in the N-terminal away from two alpha

helices, where it is positioned in the $\epsilon 2$ and $\epsilon 3$ variants. This shift allows Arg-61 to interact with a Glu-255 residue located in the C-terminal major lipid-binding domain to a greater extent (*idem*). This domain interaction has been shown to mediate several neuropathological effects, leading to the increased production of A β via enhanced proteolytic cleavage (*idem*). Inhibiting this interaction and reducing proteolytic cleavage of APP may provide a potential mechanism for decreasing the risk of AD development.

1.5.3. Current treatments of AD

There are currently five FDA approved drugs prescribed for the treatment AD, Memantine (Namenda), Donepezil (Aricept), Rivastigmine (Exelon), Galantamine (Razadyne) and the combined treatment of Donepezil and Memantine (Namenda) (Kumar, Singh and Ekavali, 2015), Table 3.

Table 3: Currently approved drugs for the treatment of Alzheimer's disease.

Drug name	Brand name	Disease Stage
Memantine	Namenda	Moderate to severe
Donepezil	Aricept	All stages
Rivastigmine	Exelon	All stages
Galantamine	Razadyne	Mild to moderate
Donepezil and Memantine	Namenda	Moderate to severe

Rivastigmine, Galantamine and donepezil are all cholinesterase inhibitors (CIs) (Casey, Antimisiaris and O'Brien, 2010). A fourth drug, tacrine also falls into this category however its use for treatment has been revoked due to serious side effects, such as liver toxicity (*idem*). Cholinesterase inhibitors (CIs) function to increase the bioavailability of acetylcholine, by increasing the concentration in the synaptic space. After release at the presynaptic neuron acetylcholine binds to postsynaptic cholinesterase receptors

initiating an action potential (*idem*). Cholinesterase inhibitors (CIs) act to block enzymatic degradation of acetylcholine, into acetyl CoA and choline by binding to the cholinesterase receptors in the postsynaptic membrane. Treatment with CIs may slightly improve the symptoms of AD or lead to their stabilization. (*idem*). Memantine is a NDMA antagonist that works to block the action of the excitatory neurotransmitter glutamate. Glutamate is thought to interfere with neurotransmission in the mid-late stages of AD and therefore contribute to neurodegeneration (*idem*).

Although these present AD treatments may reduce or stabilize the symptoms, improving the quality of life of patients, they do not alter the underlying pathologies or improve life span (*idem*). Therefore, treatment with CIs or NMDA antagonists is palliative and not curative or disease modifying. The lack of a disease modifying treatments available for AD has focused research into new treatments that can block the progression of the disease.

1.6. BACE-1

As mentioned in section 1.5.1, BACE-1 is the principle β -secretase responsible for the rate-limiting step in the amyloidogenic pathway of APP processing (Thinakaran and Koo, 2008). Although BACE-1 is expressed in nearly all cells, it is present to a higher extent and exhibits maximal activity in neuronal cells (Vassar, 2004). When synthesized, BACE-1 is a 501 amino acid transmembrane aspartic acid protease. After synthesis BACE-1 is subjected to several modifications for instance, glycosylation on four Asn residues and acetylation on seven Arg residues within the endoplasmic reticulum (Vassar and

Kandalepas, 2011). Further modifications take place within the Golgi compartment, including the addition of complex carbohydrates and removal of the prodomain of BACE-1 (*idem*). Another important modification of BACE-1 is the phosphorylation of Ser⁴⁹⁸, which is involved in the regulation of BACE-1 trafficking between the cell surface and endosomal compartments (*idem*). After these modification events have taken place, BACE-1 is primarily located within acidic (~pH 4.5) cellular environments such as endosomes and the Golgi apparatus (Yan and Vassar, 2014). Within these compartments, BACE-1 co-localises with APP and participates in its cleavage. BACE-1 trafficking between these sites and the cell surface is thought to be important in the regulation of APP cleavage (Shimizu *et al.*, 2008). On the cell surface, both BACE-1 and APP are located in lipid rafts and follow similar trafficking routes. It has been suggested that the neutral pH at the cell surface (pH 7.0) inactivates BACE-1 inhibiting APP processing. The decrease in pH upon trafficking to endosomal compartments is thought to result in the activation of BACE-1 and catalysis of APP (*idem*). Therefore, cleavage of APP and production of A β may occur predominately in endosomes and Golgi compartments (Zhang and Song, 2013). Inhibiting BACE-1 and cleavage of APP, either by direct binding or immobilization to the cell surface, is an important target for developing therapeutics for AD. Other potential targets include the other proteases involved in APP processing, γ -secretase and α -secretase.

1.6.1. Validation of BACE-1 as a therapeutic target for AD

β -secretase is responsible for the primary cleavage of APP in the amyloidogenic pathway and production of toxic A β fragments (see section 1.5.1). FAD mutations that

occur within APP have been shown to result in increased processing of APP by β -secretase compared to α -secretase. This results in increased production and deposition of toxic A β fragments (Yan and Vassar, 2014). Elevated BACE-1 activity and expression in brain regions affected by A β deposition has also been identified in sporadic cases of AD (Fukumoto *et al.*, 2002). After the identification of BACE-1, another aspartyl protease with 64% amino acid homology was discovered termed BACE-2 (Vassar and Kandalepas, 2011). Therefore, in order to validate BACE-1 as a therapeutic target for AD it was necessary to ascertain whether BACE-2 also possessed β -secretase activity. Although APP is a substrate for BACE-2, cleavage activity differs from BACE-1 occurring at sites within the A β domain (Cai *et al.*, 2001). This suggested that APP processing by BACE-2 would limit A β and therefore, be a poor β -secretase candidate. Furthermore, BACE-2 mRNA levels within the brain are relatively low compared to BACE-1; therefore it is unlikely to contribute to the production of cerebral A β (Vassar and Kandalepas, 2011). Initial studies also reported that the elimination of BACE-1 in knockout models eradicated β -secretase activity and the production of A β , without serious effects in physiology or behaviours in transgenic mice (Roberds *et al.*, 2001). Additionally, the reintroduction of BACE-1 to transgenic mice, through lentiviral delivery of BACE-1 RNAi, resulted in the restoration of the cognitive defects associated with amyloidosis (Vassar and Kandalepas, 2011). This evidence demonstrated that BACE-1 is the primary neuronal β -secretase and is a promising therapeutic target for the reduction of cerebral A β levels. Another important concern regarding inhibiting BACE-1 is the production of off-target toxicity as a result of the prevention of BACE-1 cleaving additional substrates. A proteomics screen has identified 68 potential BACE-1 substrates (Hemming *et al.*, 2009); therefore the effects of β -secretase on these substrates must also be taken into

account. More recently BACE-1 knockout models have identified that inhibition of the cleavage of the substrate neuregulin-1 causes a reduction in myelin sheath thickness of axons (Vassar and Kandalepas, 2011). This may be a concern for the development of BACE-1 inhibitors for the therapeutics of AD. However, it is unclear whether hypomyelination in these models are a result of the loss of BACE-1 activity in adults or during embryonic development (*idem*). Despite these possible side effects of BACE-1 inhibition, studies have indicated that partial inhibition of BACE-1 may effectively reduce A β deposition, limiting the potential for the development of side effects due (*idem*).

The other proteases involved in APP processing have also been described as potential targets for the development of therapeutics for AD. In the case of γ -secretase this is due to mutations within the catalytic domain (PSEN1 and PSEN2) being directly associated with the development of FAD. PSEN1 and PSEN2 knockouts have both been shown to eliminate γ -secretase activity, with PSEN1 models showing a reduction in A β production (De Strooper, Iwatsubo and Wolfe, 2012). The majority of FAD mutations within the presenilin's are associated with PSEN1, highlighting that γ -secretase inhibition is a potential target of drug development. However, numerous challenges were discovered to be associated with eliminating γ -secretase activity. In addition to APP, there have been over 50 different γ -secretase substrates identified, one of which is Notch1 (Jia, Deng and Qing, 2014). The cleavage of Notch1 by γ -secretase produces the Notch intracellular domain (NICD) (De Strooper *et al.*, 1999), which can then be translocated to the nucleus where it functions to regulate transcription of target genes. NICD is involved in the regulation of genes involved in cell development and differentiation

(Imbimbo *et al.*, 2007). Notch1 null mice have been shown to be embryonic lethal due to abnormal axial skeleton and spinal ganglia development (Wong *et al.*, 1997). These phenotypes are also seen in γ -secretase knockout models, which also exhibit defects in normal neurogenesis and neuronal survival (Shen *et al.*, 1997). Studies performing conditional presenilin knockouts in the forebrain demonstrated that a loss of activity enhances neurodegeneration. Therefore, evidence exists that a reduction in the activity of γ -secretase could result in further neurodegeneration independently of $A\beta$ production (Shen and Kelleher, 2007). Furthermore, the Notch1 has been linked to the differentiation of goblet cells and T- and B- cells; therefore, inhibition of γ -secretase has been linked to gastrointestinal bleeding and immunosuppression (Wolfe, 2012). These side effects make targeting γ -secretase a challenge for reducing the processing of APP and limiting $A\beta$.

As mentioned in section 1.5.1, α -secretase is responsible for cleaving APP in the non-amyloidogenic pathway preventing the possible production of $A\beta$. This is due to α -secretase cleaving APP at L688, which is located within the $A\beta$ domain (Macleod *et al.*, 2015). Therefore increasing the ratio of α -secretase processing, compared to β -secretase is also considered to be a target to reduce the formation of $A\beta$ and prevent AD (Jia, Deng and Qing, 2014). Overexpression of ADAM10 (a disintegrin and metalloproteases possessing α -secretase activity) has been shown to reduce $A\beta$ production and deposition in amyloid plaques (Postina *et al.*, 2004). Furthermore, it was reported that ADAM10 overexpression alleviated cognitive defects in transgenic mice (*idem*). This suggests that α -secretase may be a potential therapeutic target for AD, however potential side effects of over activation of ADAM10 and other disintegrin and

metalloproteases are not known. ADAM10 has over 30 identified substrates and is expressed in non-neuronal tissue, therefore over activation may produce unwanted side effects (Macleod *et al.*, 2015).

1.6.2. BACE-1 structure

BACE-1 has been crystallised with various inhibitors and in its active form (Hong *et al.*, 2000, 2002; Patel *et al.*, 2004; Turner *et al.*, 2005; Shimizu *et al.*, 2008). These studies revealed that BACE-1 is a transmembrane aspartic protease with a bilobal structure, Figure 6. The extracellular N-terminal domain and cytosolic C-terminal domain are separated by a substrate-binding cleft (Figure 6). A conserved Asp dyad, Asp32 and Asp228, is located in the N-terminal domain orientated towards the centre of the cleft, these residues participate in a hydrogen bond network that forms the catalytic site of BACE-1 (Hong *et al.*, 2000). Two water molecules, termed Wat1 and Wat2, mediate catalysis of the peptide substrate by the Asp dyad. Following substrate binding, Wat1 hydrogen bonds with the Asp dyad, enabling the nucleophilic attack of the scissile-bond carboxyl in the peptide substrate. This results in a geminal diol intermediate that is stabilized through the hydrogen bond network with the Asp dyad. Finally peptide bond (C-N) formation is catalysed through the transfer of a proton from Asp, resulting in an amino group on the N-terminal amino acid (Shimizu *et al.*, 2008). Crystal structures have observed a flexible antiparallel β -hairpin, described as a flap (residues 67-75), which partially covers the substrate-binding cleft containing the conserved Asp dyad. The flap is thought to participate in orientating the substrate for catalysis and controlling access

to the active site (*idem*). Therefore, conformational switching between active and inactive states is important to consider in the design of BACE-1 inhibitors.

The flap has been observed in multiple conformations in complex with inhibitors (Xu *et al.*, 2012) and at different pHs (Shimizu *et al.*, 2008). When complexed with the inhibitor OM99-2 the flap (residues 67-77) adopts a closed conformation compared to apo forms (*idem*), due to the formation hydrogen bonds between the inhibitor and BACE-1. Four hydrogen bonds are formed between the transition state isostere of OM99-2 and the Asp dyad of BACE-1. Additionally, ten hydrogen bonds are formed between the backbone of OM99-2 and the flap in BACE-1 (Hong *et al.*, 2000). These interactions resulted in the flap closing over the substrate binding cleft in BACE-1, identifying this as an important region for BACE-1 inhibitor design (Ghosh and Osswald, 2014).

Shimizu *et al.*, (2008) crystallised BACE-1 at pH 4.0, 4.5, 5.0 and 7.0. The optimum pH for BACE-1 activity has been determined to be pH 4.5, with no activity occurring less than pH 3.5 or greater than pH 5.5 (*idem*). Therefore, the crystal structure at pH 7.0 reflects BACE-1 in an inactive form (seen in blue, Figure 6). This indicated that the flap region of BACE-1 adopts a more open conformation at a catalytically active pH (*idem*) and was reported to be virtually identical to the inhibitor free apo structure crystallised by Patel *et al.*, (2004). Furthermore, a loop, termed the 10s loop, positioned around residue 328 is observed in a more open conformation in the active structures reported by Shimizu *et al.*, (2008) and Patel *et al.*, (2004). The open conformations reported of features in the active form of BACE-1 including the flap and the 10s loop, indicate that

BACE-1 has a large substrate-binding site in which entry is regulated by multiple residues.

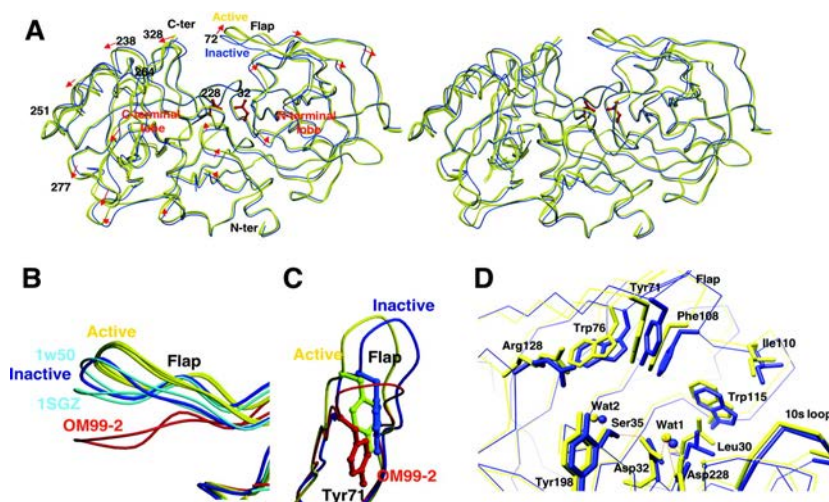


Figure 6: BACE-1 structure. (A) Superimposed image of BACE-1 at the inactive pH 7.0 (blue) and active structures (pH 4.0, 4.5, and 5.0). (B) Close up view of the superimposition of the flap (residues 60-75) in the inactive structure at pH 7.0 (blue), active structures (yellow), apo structure (light blue) and complexed with the inhibitor OM99-2 (red). (C) Front view of the flap. (D) Difference in location and the vicinity of the active cleft and flap between the active structure (yellow) and inactive structure (blue).

1.6.3. BACE-1 Inhibitors in clinical trials

The peptide-based, transition state analogue OM99-2 crystallised with BACE1 by Hong *et al.*, (2000) was one of the first generations of inhibitors. This peptide was designed based upon the observation that BACE-1 cleaves the Swedish mutation in APP, (Lys⁶⁷⁰→Asn and Met⁶⁷¹→Leu) 40 times faster than the normal variant due to increased affinity (Ghosh and Osswald, 2014). The replacement of the scissile bond with a non-hydrolysable analogue enabled the inhibition of BACE-1 and prevented cleavage of the peptide inhibitor (Vassar and Kandalepas, 2011).

These inhibitors showed potent inhibitory activity due to their ability to bind to the large open active site of BACE-1 (Vassar, 2014). Furthermore, crystallisation of these inhibitors with BACE-1 allowed for the elucidation of important structural regions. However, drug development based on these peptide transition state analogues has proved difficult due to unfavourable *in vivo* pharmaceutical properties, for example oral bioavailability, half-life and blood brain barrier (BBB) penetration (*idem*). Due to these requirements for BACE-1 inhibition, drug design has begun to focus on the development of small molecule inhibitors however, this has proved challenging due to the large hydrophobic substrate-binding cleft of BACE-1 (*idem*). In order to develop an efficient BACE-1 inhibitor for the therapeutics of AD, drug candidates must exhibit properties that enable both BBB penetration and have high affinity for the active site of BACE-1 (*idem*). An ideal BACE-1 inhibitor should have a molecular weight of less than 500 Da, be orally bioavailable and metabolically stable. Furthermore, potential inhibitors must be able to cross not only the BBB, but also both the plasma and intracellular membrane to gain access to the intracellular compartments where BACE-1 is active (Vassar and Kandalepas, 2011). Despite these challenges several pharmaceutical companies have developed BACE-1 inhibitors that have reached clinical trials, Table 4.

Table 4: Examples of small molecule BACE-1 inhibitors in clinical trials. * Indicates compounds which were removed from clinical trials (Vassar, 2014).

Company	Drug	Phase
AstraZeneca/Lilly	AZD3293	Phase 2/3
CoMentis	CTS-21166	Phase 1
Eisai/Biogen Idec	E2609	Phase 2
Janssen/Shionogi	-----	Phase 1
Lilly	LY2886721	Phase 2*
Merck	MK-8931	Phase 2/3
Novartis	-----	Phase 1
Pfizer	PF-05297909	Phase 1
Roche	RG7129	Phase 1*
Takeda	TAK-070	Phase 1
Vitaw/Boehringer Ingelheim	VTP-37948	Phase 1

1.6.4. Glycosaminoglycans and glycosaminoglycan mimetics as BACE-1 inhibitors

Work conducted by Scholefield *et al.*, (2003) demonstrated that endogenous HSPGs and BACE-1 co-localise on cell surfaces, in the Golgi complex and in endosomes where they interact to inhibit the cleavage of APP. It was demonstrated that bovine lung heparin (BLH) and porcine mucosal heparan sulphate (PMHS) could inhibit BACE-1 activity, both *in vitro* and *in vivo*; this suggested that HSPGs might regulate BACE-1 activity endogenously. Further confirmation was obtained using sodium chlorate treated cells (inhibits PAPS, and therefore sulphation during biosynthesis of HS/heparin), which displayed ~40% and ~20% increase in the amount of A β ₄₂ and A β ₄₀, respectively. This highlights that HSPGs modulate BACE-1, as abolishment of their interaction results in increased processing of APP. Furthermore, this effect was not demonstrated with α -secretase as the levels of sAAP α were unaffected, indicating that inhibition was specific to BACE-1.

Competitive binding assays revealed that the mechanism of interaction with HS was likely to occur within the active site of BACE-1, preventing access of the substrate APP. This was suggested to occur through HS binding to BACE-1, inducing an alteration to the conformation of the 'flap' that covers the active site (see section 6.1), (Figure 7). It was established that BLH and PMHS both showed greater inhibition with the use of full length APP, opposed to a peptide as a substrate for BACE-1 ($IC_{50} \approx 1-2 \mu\text{g}.\text{ml}^{-1}$; ~100 nM and $IC_{50} \approx \sim 5 \mu\text{g}.\text{ml}^{-1}$; ~200 nM, respectfully). This increased the maximum potential inhibition from ~60% to ~90-100% compared to the use of a peptide substrate. Heparan sulphate has previously been shown to bind to APP (Small *et al.*, 1994), leading

Scholefield and colleagues to postulate that binding to BACE-1 alone is not sufficient for maximal inhibition and that HS may act to sequester APP away from the active site of BACE-1 (Figure 7B). These two proposed mechanisms (Figure 7) indicate that it is likely membrane associated HSPG, e.g., syndecans or glypicans, are involved with the endogenous regulation of BACE-1. As both BACE-1 and APP are transmembrane proteins, syndecans or glypicans would be ideally positioned to interact and regulate their processing.

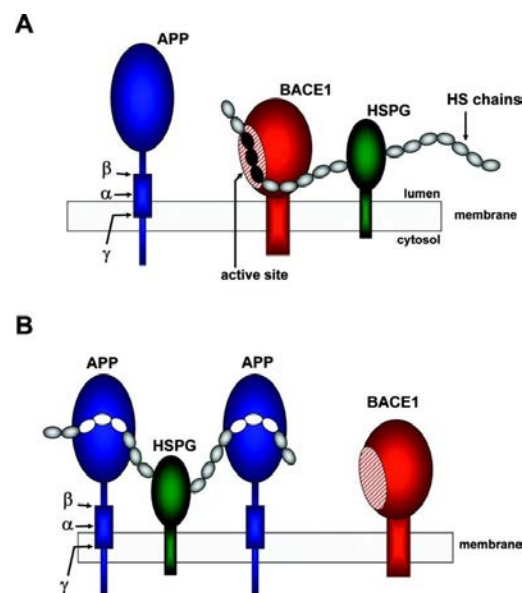


Figure 7: Suggested models for the endogenous regulation of BACE-1 processing of APP by heparan sulphate proteoglycans. (A) Direct inhibition of BACE-1, HS chains (grey) interact directly with BACE-1 (red), preventing APP (blue) entry into the active site. (B) Sequestration of APP, HS (white) binds APP (blue) sequestering it away from BACE-1 (red). (Scholefield et al., 2003)

Subsequently, Scholefield *et al.*, (2003) characterised the HS structural requirements which enable the interaction with, and regulation of BACE-1. Using oligosaccharides generated from bacterial lyase digestion, it was determined that inhibition was dependent on the saccharide size. Fragments with less than 10 monosaccharaides (10mers) displayed no inhibitory activity. An increase in inhibitory activity was observed

as chain length increased, with 24mers displaying the same inhibition as full-length heparin (Scholefield *et al.*, 2003). Similar results were obtained by Patey *et al.* (2006) (Figure 8) who also observed a minimum requirement for activity of 10 monosaccharide units (*idem*). However, inhibitory activity corresponding to that of full-length heparin was seen at a minimum of an 18 mer (*idem*). The relationship between saccharide size and inhibitory activity may also infer that both inhibition of BACE-1 and sequestration of APP occur concomitantly to regulate activity.

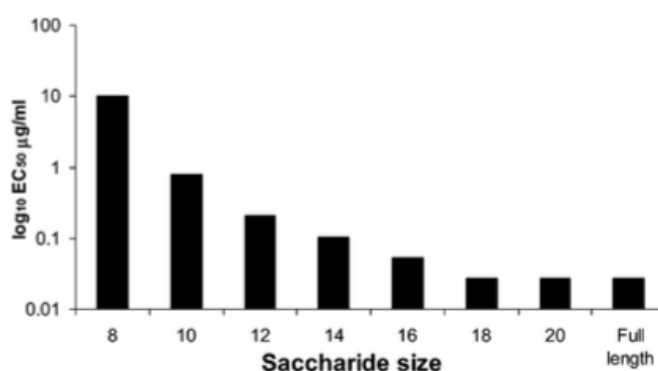


Figure 8: BACE-1 inhibitory activity of size-defined unmodified PIMH. A minimum of 10 monosaccharides was required for BACE-1 inhibition, with 18mers possessing equivalent inhibitory activity as full-length heparin (Patey *et al.*, 2006).

Using chemically modified heparins, Scholefield *et al.*, (2003) also determined that activity was dependent on 6-O sulphation; with removal yielding an 80% decrease in potency (Scholefield *et al.*, 2003). Furthermore, removal of 2-O sulfation resulted in decreased activity, however this was to a lesser extent than removal of 6-O sulphate groups. Partial sulphation at positions C₂ and C₆ were therefore found to enhance inhibitory activity of the heparin chain, however over sulphation resulted in a loss of activity. This indicated that potency is not directly correlated with sulphation level. Additionally, de-N-sulphation and re-N-acetylation resulted in an approximate five-fold

increase in potency. This was supported by Patey *et al.*, (2006) who also determined that N-sulphation or 2-O sulphation were not required for high levels of activity when 6-O sulphation was present.

The work conducted by Scholefield *et al.*, (2003) suggests that HS and heparin may have potential as therapeutic agents for AD. However, the potent anticoagulant activities of heparin and HS (discussed in section 4 and 4.1) which dictate their current clinical use, precludes their development for the treatment of AD. Therefore, it would be necessary to modify HS/heparin chains to remove the specific AT-binding pentasaccharide sequence that is responsible for their anti-coagulant properties. Patey *et al.*, (2006) identified that de-N-sulphation and re-N-acetylation of heparin chains resulted in the greatest interference with antithrombin/FXa, by approximately 3000-fold lower than unmodified heparin. A reduction in anticoagulant activity was also observed in saccharides with 2-O and 6-O de-sulphation, however this was to a lesser extent (approximately 200-fold compared to unmodified heparin). This is significant, as N-acetylation and 6-O de-sulphation have been shown to both increase inhibitory activity of BACE-1. Modified heparin chains possessing these substitutions possess a high therapeutic ratio, Figure 9 (Scholefield *et al.*, 2003; Patey *et al.*, 2006).

The identification that HS/heparin can be modified to remove anticoagulant activity and retain the ability to inhibit BACE-1 is fundamental for the use of these compounds as therapeutics for AD. Furthermore, the observation that a chain length of 10 monosaccharaides displays inhibitory activity limits other possible side effects of standard heparin therapeutics, such as heparin-induced thrombocytopenia (HIT). A

reduction in molecular weight and sulphation level has been shown to reduce HIT, which is a result of antibody production against heparin-platelet factor 4 complexes (Patey *et al.*, 2006).

$R_1 = \text{SO}_3^-/\text{H}, R_2 = \text{SO}_3^-/\text{H}, R_3 = \text{SO}_3^-/\text{H}/\text{COCH}_3$

compound	R ₁	R ₂	R ₃	IC ₅₀ (μg/mL)	R ² of IC ₅₀	ACA ^b	TR ^c
(1) PMIH	SO ₃ ⁻	SO ₃ ⁻	SO ₃ ⁻	0.028	0.998	100%	1
(2) <i>N</i> -acetyl	SO ₃ ⁻	SO ₃ ⁻	COCH ₃	0.031	0.995	0.03%	3136
(3) UA-2-OH	H	SO ₃ ⁻	SO ₃ ⁻	0.053	0.995	0.4%	147
(4) UA-2-OH, <i>N</i> -acetyl	H	SO ₃ ⁻	COCH ₃	0.091	0.999	0.03%	1092
(5) GlcN-6-OH	SO ₃ ⁻	H	SO ₃ ⁻	0.100	0.996	0.5%	61
(6) GlcN-6-OH, <i>N</i> -acetyl	SO ₃ ⁻	H	COCH ₃	0.410	0.995	0.03%	237
(7) UA-2-OH, GlcN-6-OH	H	H	SO ₃ ⁻	0.786	0.994	0.03%	123
(8) UA-2-OH, GlcN-6-OH, <i>N</i> -acetyl	H	H	COCH ₃	> 100	n/a	0.03%	1
(9) per-sulfated #	SO ₃ ⁻	SO ₃ ⁻	SO ₃ ⁻	0.053	0.998	35.0%	2
(10) APA ^d				n/a	n/a	n/a	n/a

Figure 9: Structure, IC₅₀ values and anticoagulant activities of modified heparins. Anticoagulant activities are expressed as a percentage of PIMH (defined as 100%). Substitution pattern is defined by R₁ R₂ R₃, corresponding to position-2 of iduronate, -6 of glucosamine, and -2 of glucosamine, respectively. The therapeutic ration was calculated from the IC₅₀ against BACE-1/anticoagulant activity (Patey *et al.*, 2006).

The major limiting factor for the development of therapeutics for AD seen with other BACE-1 inhibitors is their ability to cross the BBB while retaining their ability to bind to the large substrate cleft of BACE-1 (discussed in 6.3). LMWH have previously been shown to possess the ability to cross the BBB (Leveugle *et al.*, 1998), therefore may overcome this challenge of the development of BACE-1 inhibitors. Leveugle *et al.*, (1998) showed LMWH of up to 3 kDa (10-18 saccharide units) have the ability to cross the BBB, Figure 10. Therefore, the minimum of 10 monosaccharide units determined to

be required for BACE-1 activity falls within this range (Scholefield *et al.*, 2003; Patey *et al.*, 2006). This supports the use of modified LMWH as candidate pharmaceutical agents for AD as bioactive oligosaccharides possess suitable pharmacokinetics that permit enteral, intravenous, intramuscular and subcutaneous routes of administration.

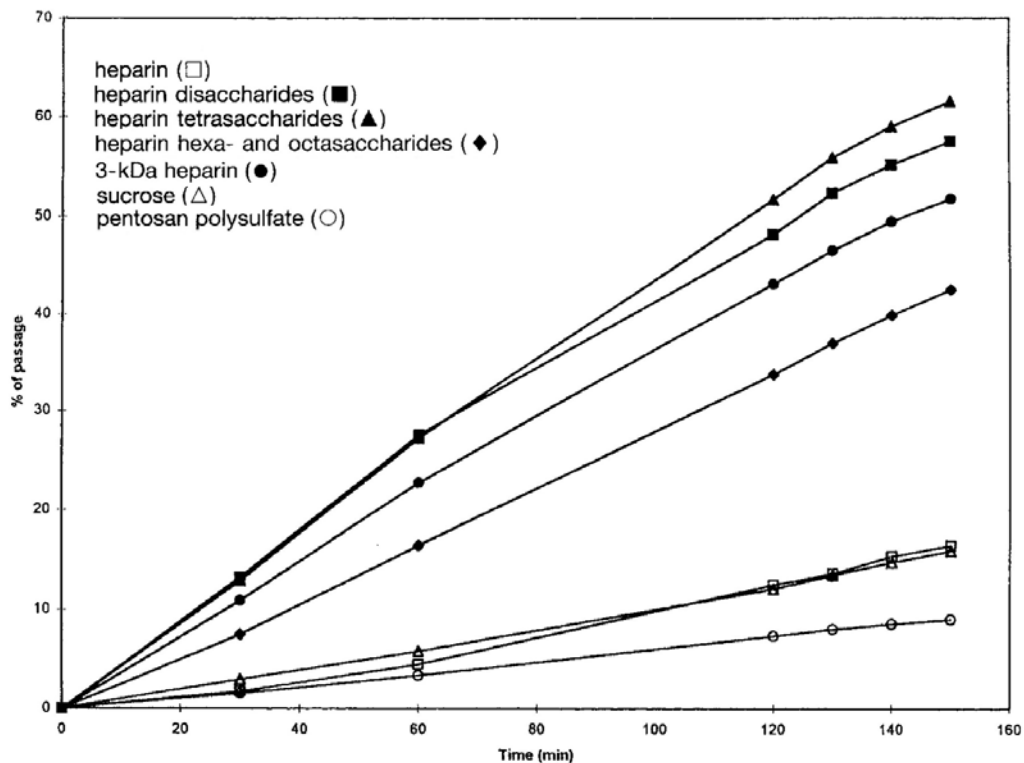


Figure 10: Transport of LMWH derivatives across the blood-brain barrier (BBB). Full length heparin did not penetrate the BBB, whereas LMWHs as large as 3 kDa showed BBB penetration (adapted from Leveugle *et al.*, 1998)

The pharmacological use of modified LMWH obtained from mammalian sources, for example bovine lung heparin (BLH), may in the future be limited due to recent concerns over transmissible spongiform encephalopathy's (TSEs) and religious restrictions. Additional concerns regarding heparin sourced from porcine origins, include diverting supplies from anticoagulant therapeutics, which are presently experiencing shortages due to high demand. Therefore, it would be beneficial to develop heparin and HS like

compounds derived from non-mammalian sources. Such compounds have been identified in marine species, which also exhibit naturally low anti-coagulant activities (Table 6). Therefore, further investigation into these compounds may provide a viable therapeutic for AD with minimal side effects.

1.7. Non-mammalian glycosaminoglycans GAGs as BACE1 inhibitors

The identification of the role of HSPGs as an endogenous regulator of BACE-1 by Scholefield *et al.*, (2003) highlighted a potential novel use for LMWHs in the treatment of AD. Heparin and LMWHs are currently widely used as anticoagulants and therefore, already extensively produced pharmaceuticals. However, their anticoagulant properties preclude the further use of LMWHs clinically for the treatment of conditions such as AD due to likely side effects they would produce. As discussed previously, the anticoagulant activities of heparins from mammalian sources have been attenuated through chemical modification (Scholefield *et al.*, 2003; Patey *et al.*, 2006). Although this increases the potential of the use LMWHs for other conditions besides antithrombotic agents, a further limitation is presented by their mammalian origin. This is due to concerns regarding contamination with pathogens, religious restrictions, safe manufacture of heparin for pharmaceutical use and increasing demand.

Heparin is currently one of the few drugs that cannot be effectively synthesised in full; as a result, it is obtained mainly from bovine lung (BLH) and porcine intestinal mucosa (PIMH) (Hedlund *et al.*, 2013). PIMH is currently the only FDA approved source of heparin, owing to concerns regarding bovine spongiform encephalopathy (BSE) from

BLH. BSE is a member of a class of degenerative neurological disorders known as tTSEs (Almond, 1998). Although the cause of TSEs is still debated, it is primarily thought to be due to the increased production of aberrant forms of the prion protein (PrP), which aggregate and cause neuronal dysfunction (Collins, Lawson and Masters, 2004). Generation of the abnormal form of PrP (PrP^{Sc}) is thought to be self-induced. Therefore, PrP^{Sc} can stimulate self-production through the conversion of the normal variant of PrP (PrP^C) (Almond, 1998) into the mutant PrP^{Sc} form. The ability of PrP^{Sc} to convert PrP^C can result in the transmission of abnormal prions to uninfected animals (*idem*). BSE transmission was only thought to occur within the bovine population, until the late 1980s when BSE was reported to have infected mice and cats (*idem*). This led to concerns over the possibility of transmission to humans, which was heightened with reports of a new variant of Creutzfeldt-Jakob disease (vCJD), a human form of TSE (*idem*). The possibility of transmission of TSEs from bovine sources led to the voluntarily removal of BLH production in Europe, USA and Japan. This resulted in PIMH being the only approved source of heparin in these countries. The quantity of PIMH required to meet current demand, which equates to 24 tones of heparin in the United States alone, led to increased importation of PIMH from China (Hedlund *et al.*, 2013). In 2007-2008 multiple reports arose concerning allergic-type reactions in patients administered with heparin obtained from Baxter Healthcare Corporation (*idem*). On the 28th February 2008 the FDA recalled all heparin supplied from Baxter after investigations of contamination that was traced back to suppliers in China. The FDA reported that heparin supplies from 12 Chinese companies had been adulterated with over-sulphated chondroitin sulphate (OSCS). CS can be readily obtained from animal cartilage and chemically modified to produce OSCS, which crudely mimics the anticoagulant activity

of heparin. This reduced the production costs of heparin pharmaceuticals, however when administered to patients provoked severe adverse immune responses. Since this discovery in 2008, the contamination of heparin supplies has resulted in over 200 deaths (*idem*). Due to the difficulty in regulating supplies from overseas and testing for contaminants, it would be beneficial to discover a source of heparin that is readily available and cheaper to produce. Furthermore, there are religious constraints with the use of bovine and porcine derived heparin, with some Hindus, Sikhs and Muslims not accepting their use (Eriksson, Burcharth and Rosenberg, 2013). These concerns have led the way for research into alternative, non-mammalian sources of heparin for the commercial market.

A promising non-mammalian source of pharmaceutical heparin comes from aquatic species. Numerous heparin and heparan sulphate like compounds have been identified belonging to phyla such as, Cnidaria, Crustacea, Tunicata and Mollusca (Table 5). These compounds are structurally related to heparin and HS in their disaccharide units (Figure 1). However, the percentage disaccharide composition varies according to the species from which they have been obtained (Pavão, 2014). Reports have also described varying anticoagulant activities between compounds extracted from different species, for example *Litopenaeus Vannamei* possess an equivalent aPTT of mammalian heparin (190 IU.mg⁻¹) (Brito *et al.*, 2014) whereas *Goniopsis Cruentata* has a five-fold reduction in activity (33 IU.mg⁻¹) (Andrade *et al.*, 2013). Furthermore, unique characteristics such as 2-O-sulphated GlcA residues (Gomes, 2010; Andrade *et al.*, 2013) have been identified in some of these marine compounds. Table 6 indicates several compounds isolated from different marine species which possess naturally reduced anticoagulant

activities and unique structural characteristics compared to mammalian heparin and HS. In addition, several aquatic species have also been identified which possess CS-like GAGs with increased structural diversity (Table 7). Polysaccharides analogous to GAGs, isolated from aquatic species therefore, offer rich, diverse structures, potentially exceeding the heterogeneity of their mammalian counterparts. These GAG-like compounds exhibit antiviral (Huang *et al.*, 2013), antiparasitic (Bastos *et al.*, 2014; Marques *et al.*, 2016; H. A. R. Suleria *et al.*, 2017) and anti-inflammatory properties (Brito *et al.*, 2008; Andrade *et al.*, 2013; Chavante *et al.*, 2014), while exhibiting low anticoagulant potential (*idem*) (Table 6). These unique polysaccharides offer largely unexplored areas of chemical space, hitherto inaccessible by chemical modifications and/or enzymatic synthesis, for the discovery of new pharmaceuticals. For example, chondroitin sulphates, specifically the E-unit, can be obtained from marine species in larger proportion's than mammalian sources and exhibit considerable highly favourable bioactivities. Unique substitutions, currently undiscovered in mammalian derived GAGs, such as those observed in FucCS isolated from sea cucumber species, possess favourable bioactivities. In addition, aquatic ecosystems display vastly augmented biodiversity compared with their terrestrial counterpart, with estimates between 33 and 66% of species yet to be discovered (Appeltans *et al.*, 2012; Suleria *et al.*, 2015), providing a rich resource for the discovery of novel GAG-like bioactive compounds. In comparison with GAGs from mammalian origins, aquatic sources offer the advantage of diminished off target effects such as potent anticoagulant activity. Chemically modified, low-sulphated mammalian derived heparin derivatives have been produced, which possess highly attenuated off-target effects, while retaining favourable bioactivities although limitations persist for heparin from mammalian origins. The abundance of

processed aquatic waste offers a valuable and emerging resource for the large-scale isolation of GAG-like polysaccharides with significant potential for future therapeutic application (Cahú *et al.*, 2012; Zhang, Xie and Linhardt, 2014; Suleria *et al.*, 2015, 2016; H. A. R. Suleria *et al.*, 2017; Hafiz Ansar Rasul Suleria, Addepalli, *et al.*, 2017; Hafiz Ansar Rasul Suleria, Masci, *et al.*, 2017); for example of which include those extracted from crustacean and mollusc by-products of the food industry such as shrimp heads and squid skin (Dietrich *et al.*, 1999; Cahú *et al.*, 2012; Suleria *et al.*, 2016; Cavalcante *et al.*, 2018). Consequently, raw material is easily obtainable, plentiful in supply, with favourable economic considerations and crucially, expanded chemical sequence space when compared with GAGs that are currently available for therapeutic development

Table 5: Examples of HS/heparin like compounds extracted from aquatic species.

Phylum/Subphylum	Species	Common name	Reference
Cnidaria	<i>Nematostella vectensis</i>	Starlet sea anemone	(Feta <i>et al.</i> , 2009)
Crustacea	<i>Goniopsis Cruentata</i> *		(Andrade <i>et al.</i> , 2013)
	<i>Litopenaeus Vannamei</i>		(Brito <i>et al.</i> , 2008, 2014)
	<i>Artemia franciscana</i>	San Francisco brine shrimp	(Chavante <i>et al.</i> , 2000)
	<i>Penaeus brasiliensis</i>	pinkspotted shrimp	(P. C. Dietrich <i>et al.</i> , 1999)
	<i>Homarus americanus</i> *	American lobster	(Hovingh and Linker, 1982)
Tunicata	<i>Styela plicata</i> *	Pleated Sea Squirt	(Cavalcante <i>et al.</i> , 2000)
Mollusca	<i>Anomalocardia brasiliiana</i>	Carib pointed-venus	(Nader, Ferreira and Paiva, 1984; Dietrich <i>et al.</i> , 1985, 1989; Pejler <i>et al.</i> , 1987)
	<i>Callista chione</i> *	Brown Venus	(Luppi, Cesaretti and Volpi, 2005)
	<i>Tivela mactroides</i>	Trigonal tivala	(Pejler <i>et al.</i> , 1987; Dietrich <i>et al.</i> , 1989)
	<i>nodipecten nodosus</i> *	Lions-paw Scallop	(Gomes, 2010)
	<i>Donax semistriatus</i>	Bean Clams	(Dietrich <i>et al.</i> , 1989)

Table 6: Examples of GAG like compounds extracted from aquatic species possessing attenuated anticoagulant activities.

Anticoagulant activity in comparison to mammalian heparin											
Thrombin inhibition (IIa)											
GAG	Source	Species	Average molecular weight (kDa)	aPTT (IU.mg ⁻¹)	HCII	Antithrombin (IC ₅₀) (μg.ml ⁻¹)	Factor Xa antithrombin	Bleeding effect (hemostasis) cut tail	Effect on thrombosis	Stimulation of heparan sulphate by endothelial cells	Reference
Hep/HS	Crab	<i>Goniopsis Cruentata</i>	19	33	12-fold reduction	Reduced	Reduced	Reduced	---	---	(Brito <i>et al.</i> , 2008; Andrade <i>et al.</i> , 2013)
Hep/HS	Pacific white shrimp	<i>Litopenaeus Vannamei</i>	36.5	Reduced	---	---	5 IU.mg ⁻¹	Negligible	---	Negligible	(Chavante <i>et al.</i> , 2014)
CS	Shrimp	<i>Litopenaeus Vannamei</i>	26	Negligible	80%	---	28%	Reduced	70% decrease in venous thrombus weight dose of 1.2 mg.kg ⁻¹	Equivalent	(Cavalcante <i>et al.</i> , 2018)
Hep/HS	Shrimp (crustacean)	<i>Artemia franciscana</i>	9.2	5.2	65.6 IU.mg ⁻¹	---	1.0 IU.mg ⁻¹	---	---	---	(Chavante <i>et al.</i> , 2000)
Hep/HS		<i>Styela plicata</i>	---	19	---	0.01	---	Negligible	---	---	(Cardilo-Reis, 2006)
Hep/HS		<i>Styela plicata</i> (whole body)	34	18	---	5.0	11 μg.ml ⁻¹	Negligible		---	(Santos <i>et al.</i> , 2007)

Hep/HS	Clam (mollusk)	<i>Callista chione</i>	11	97	---	---	52 IU.mg ⁻¹	---	---	---	(Luppi, Cesaretti and Volpi, 2005)
Hep/HS	Mollusk	<i>Nodipecten nodosus</i>	27 kDa	36	4 µg.ml ⁻¹	0.012	IC ₅₀ = 0.9 µg.ml ⁻¹	Negligible	1.0 mg.ml ⁻¹		((Gomes, 2010; Gomes <i>et al.</i> , 2015)

Table 7: Examples of CS like compounds extracted from aquatic species.

GAG	Source	Species	Molecular mass kDa	Non-sulphated (O unit) (%)	Disaccharide composition %						Other	References
					(A unit) (%)	(C-unit) (%)	(D unit) (%)	(E unit) (%)	(CSB) (%)	Trisulphated (%)		
CS	Pacific white shrimp	<i>Litopenaeus Vannamei</i>	26	N.D	N.D	N.D	N.D	N.D	N.D	N.D	GlcA(2,3)-GacNAc/GlcA(2,3)-GacNAc(6S)	(Cavalcante <i>et al.</i> , 2018)
CS	Monkish	-	48.7	12.9	51	28.2	1.3	6.3	0.4	>0.1	GlcA(2S)-GalNAc	(Maccari, Galeotti and Volpi, 2015)
CS	Cod	-	18.1	3.4	59.8	27.3	9.5	> 0.1	>0.1	>0.1	GlcA(2S)-GalNAc	(Maccari, Galeotti and Volpi, 2015)
CS	Spiny dogfish	-	13.4	7.4	25.3	55.7	10.5	0.8	0.3	>0.1	GlcA(2S)-GalNAc	(Maccari, Galeotti and Volpi, 2015)
CS	salmon	-	20.0	7.7	51.2	37.3	3.5	0.2	0.1	>0.1	GlcA(2S)-GalNAc	(Maccari, Galeotti and Volpi, 2015)
CS	tuna	-	32.9	1.6	63.2	28.3	4.6	1.1	1.2	>0.1	GlcA(2S)-GalNAc	(Maccari, Galeotti and Volpi, 2015)
CS	Chinese sturgeon	<i>Acipenser sinensis</i>	13.4	---	Detected	Detected	-	-	-	-	-	(Zhao <i>et al.</i> , 2013)

CS	Chinese sturgeon	<i>Acipenser sinensis</i>	37.5	~7%	~38	~55	-	-	-	-	-	(Maccari, Ferrarini and Volpi, 2010)
CS	Shark cartilage	-	>50	2.2	27.7	49.0	16.1	3.0	-	1.9	-	(Maccari, Ferrarini and Volpi, 2010)
CS/DS	Shortfin mako shark fins	<i>Isurus oxyrinchus</i>		2.2	28.4	17.5	6.7	3.8	12.4	-	-	(Higashi, Takeuchi, et al., 2015)
CS/DS	Silver chimaera fins	<i>Chimaera phantasma</i>		5.7	27.1	40.7	20.7	2.9	2.9	-	-	(Higashi, Okamoto, et al., 2015)
CS/DS	Smalltooth sand tiger fins	<i>Odontaspis ferox</i>		3.91	23.1	57.1	13.7	0.8	1.5	-	-	(Higashi, Takeuchi, et al., 2015)
CS/DS	Goblin shark fins	<i>Mitsukurina owstoni</i>		9.7	12.9	59.4	4.17	1.01	1.6	-	-	(Higashi, Takeuchi, et al., 2015)
CS/DS	Blue shark fins (without skin and cartilage)	<i>Prionace glauca</i>		10.6	30.8	13.4	2.9	1.8	6.9	-	-	(Higashi, Takeuchi, et al., 2015)
CS/DS	Blue shark fins (without skin)	<i>Prionace glauca</i>		0.9	25.2	52	18.4	3.5	---	-	-	(Higashi, Takeuchi, et al., 2015)
CS/DS	Birdbeak dogfish fins	<i>Deania calcea</i>		17.9	14.3	50.9	5.9	---	2.8	-	-	(Higashi, Takeuchi, et al., 2015)

CS/DS	Frilled shark fins	<i>Chlamydoselachus anguineus</i>	31.7	12.8	29.5	1.8	1.2	2.9	-	-	(Higashi, Takeuchi, et al., 2015)
CS/DS	Spotless smooth-hound	<i>Mustelus griseus</i>	6.3	29.6	32.5	18.8	2.6	2.4	-	-	(Higashi, Takeuchi, et al., 2015)
CS/DS	Cloudy catshark	<i>Scyliorhinus torazame</i>	9.1	22.3	41.8	13.7	3.0	3.4	-	-	(Higashi, Takeuchi, et al., 2015)
CS/DS	Kitefin shark fins	<i>Dalatias licha</i>	6.0	24.4	55.5	8.3	1.9	3.9	-	-	(Higashi, Takeuchi, et al., 2015)
CS/DS	Ray stingray fins	<i>Dasyatis akajei</i>	4.0	29.8	42.4	18.3	0.8	1.8	-	-	(Higashi, Takeuchi, et al., 2015)

Chapter 2: Methodology introduction

2.1. Isolation and purification of glycosaminoglycans

The isolation of GAGs from tissues in sufficient quantities for downstream applications exploits the chemical properties of this class of carbohydrates, for instance anionic charge, stability and molecular weight (van der Meer, Kellenbach and van den Bos, 2017). Generally, GAGs are found attached to a core protein in the form of PGs excreted into the ECM or attached to the cell membrane; with the exception of HA and chains liberated by endogenous endoglycosidic cleavage or proteolysis of PGs (Esko, 1993; Zhang, Zhang and Linhardt, 2010). In addition, PGs are also present within intracellular compartments such as endosomes, lysosomes and secretory granules (Zhang, Zhang and Linhardt, 2010). Therefore, in order to isolate solely GAGs chains the polysaccharide must be liberated from the protein core, subsequent to tissue homogenisation, before further purification can be conducted.

The typical extraction process for large scale isolation of GAGs is therefore, as follows; (1) sourcing and pre-treatment of tissue, (2) release of GAGs from constituent proteoglycans, (3) recovery and purification of crude GAG chains, and (4) fractionation of GAG sub-types based upon charge (Lima *et al.*, 2011; van der Meer, Kellenbach and van den Bos, 2017).

2.1.1. Tissue sourcing and pre-treatment

Where the downstream application of GAG extracts may involve a potential therapeutic, cosmetic or nutraceutical application, tissue should be obtained from a source meeting the requirements for human consumption (van der Meer, Kellenbach

and van den Bos, 2017). For instance, source tissue should be free from transmissible pathogens and medications such as antibiotics (*idem*). In relation to pharmaceutical heparin, the animal origin (porcine mucosa) is required to be clearly identified on individual preparations and is confirmed by PCR or immunological methods in order to mitigate the potential of BSE contaminants (Levieux, Rivera and Levieux, 2002; Ekins *et al.*, 2012; FDA, 2012). Many manufacturers also ensure full traceability, from farms, slaughterhouses and crude manufacturing facilities to analytical laboratories (van der Meer, Kellenbach and van den Bos, 2017).

Once obtained, the source tissue is washed in a cold salt solution and dissected prior to further processing (Zhang, Zhang and Linhardt, 2010; van der Meer, Kellenbach and van den Bos, 2017). If long term storage is required a preservative, for example an oxygen scavenger such as sodium bisulphate (1.5-2.5% w/w), calcium propionate or phenol, can be added to limit microbiological growth (van der Meer, Kellenbach and van den Bos, 2017). This is to prevent modification of the GAG chain as prolonged storage can result in de-sulphation (mainly glucosamine 6-O-desulphation) (Bianchini *et al.*, 1997; van der Meer, Kellenbach and van den Bos, 2017). Alternatively, tissue can be preserved by lyophilisation and subsequent homogenisation into a fine power (Zhang, Zhang and Linhardt, 2010).

Subsequently, tissue can be delipidated by incubation in an organic solvent such as acetone and/or sequential incubations with chloroform:methanol solutions (2:1→1:1→1:2; v/v), prior to drying in a fume hood overnight (Brito *et al.*, 2008; Nakano, Betti and Pietrasik, 2010; Zhang, Zhang and Linhardt, 2010; Chen *et al.*, 2011; Stelling *et al.*,

2019). The aforementioned delipidation in acetone can also be performed in concert with homogenisation of the dissected tissue, if no prior processing has been performed, and is commonly repeated two-three times (Brito *et al.*, 2008). In addition, delipidation can also be performed using diethyl ether-methanol (1:1), diethyl ether-ethanol (1:1) or petroleum ether (Nakano, Betti and Pietrasik, 2010). In the case of bone or shell tissue prior pre-treatment with EDTA, or an acid such as HCl, is required for decalcification following homogenisation into a powder (*idem*). The resulting dried, delipidated or decalcified tissue is then subjected to hydrolysis as outlined in section 2.1.2.

2.1.2. Release of GAGs chains from proteoglycans

With the exception of HA, GAGs are largely present as proteoglycans and therefore, must be liberated from their constituent core protein by hydrolysis prior to the isolation of free polysaccharide chains. This can be achieved through proteolytic digestion with non-specific proteases or by chemical means (Silva, 2006; van der Meer, Kellenbach and van den Bos, 2017). The resulting solubilised GAG chains can then be purified from other macromolecules present within the digested mixture as outlined in section 2.1.3.

Chemical hydrolysis can be conducted under alkaline conditions for instance using sodium borohydride or 1M NaOH at 4°C to remove GAG chains from core proteoglycans by β - elimination (Greiling, 1974; Conrad, 1995; van der Meer, Kellenbach and van den Bos, 2017). Under these conditions it is critical that high temperatures are avoided as the heparin chain may undergo modifications. For instance, at pH 11 base-catalysed

epoxide formation can lead to 2-O-desulphation of the uronic acid residue (van der Meer, Kellenbach and van den Bos, 2017). Additionally, a short peptide chain and tetrasaccharide linkage region will remain attached to the liberated GAG chain (Esko, 1993). Intact PGs and GAGs can also be extracted using 4M Guanidine hydrochloride at 4°C (Greiling, 1974; Esko, 1993; Nakano, Betti and Pietrasik, 2010; van der Meer, Kellenbach and van den Bos, 2017).

Proteolytic digestion can be conducted by autolysis (Nakano, Nakano and Sim, 1998; Cahú *et al.*, 2012) or the addition of non-specific proteases (Greiling, 1974; Silva, 2006; Nakano, Betti and Pietrasik, 2010; Zhang, Zhang and Linhardt, 2010; van der Meer, Kellenbach and van den Bos, 2017). Examples of exogenous non-specific proteases that have been utilised for GAG extraction include papain, trypsin, chymotrypsin, Pronase, or subtilisin proteases (*idem*). For exogenous enzymatic digestion the tissue is suspended in an appropriate buffer, with a pH of ~8 for subtilisin-type enzymes and heated to ~50-60 °C (Zhang, Zhang and Linhardt, 2010; van der Meer, Kellenbach and van den Bos, 2017). Typically, 0.2-2g/kg of enzyme is sufficient to achieve full digestion and substantially reduce the viscosity in 4-16 hours (*idem*). The resulting GAG chains produced by enzymatic hydrolysis will however also be linked to a small peptide in addition to the tetrasaccharide linkage region (Nakano, Betti and Pietrasik, 2010). Following digestion, the mixture is heated to denature the enzymes and filtered to remove debris prior to recovery of GAGs (van der Meer, Kellenbach and van den Bos, 2017).

2.1.3. Recovery and purification of crude glycosaminoglycans

The concentration of GAGs present in the hydrolysed tissue solution is low (~0.01% w/w) therefore GAGs must be concentrated prior to further purification (van der Meer, Kellenbach and van den Bos, 2017). Concentration of GAGs can be performed by precipitation using ammonium cations, organic solvents, or through the use of anion exchange resin (Silva, 2006; Nakano, Betti and Pietrasik, 2010; Zhang, Zhang and Linhardt, 2010; van der Meer, Kellenbach and van den Bos, 2017).

The strong anionic properties of GAG enable their purification directly from the hydrolysis extract utilizing anion-exchange chromatography. Ion-exchange resins utilised for this purpose include Dowex, ECTEOLA-cellulose, DEAE-cellulose, DEAE-Sephacel, Amberlite, Duolite and Lewatit (Silva, 2006; Nakano, Betti and Pietrasik, 2010; van der Meer, Kellenbach and van den Bos, 2017). These ion exchange resins can be applied directly to the hydrolysis extract and are large enough to facilitate their recovery by filtration, succeeding incubation for ~10-13 hours. During incubation with the ion-exchange resin the pH, temperature and salt concentration of the hydrolysis extract must be controlled to ensure minimal binding of weakly anionic contaminants (van der Meer, Kellenbach and van den Bos, 2017). Following agitation, the collected resin is subjected to a low NaCl wash prior to GAGs being eluted with a high concentration of NaCl (van der Meer, Kellenbach and van den Bos, 2017). The low NaCl wash functions to remove weakly bound material and eliminate any contaminants such as nucleic acids (*idem*). An advantage of the use of ion-exchange for the capture of GAGs is that the resin can be directly added to the hydrolysis extract and upon recovery can

be stored in sodium bisulphite prior to elution, this may be advantageous in the cases where transportation is required for further processing (*idem*).

In weakly acidic conditions hydrophobic primary amines, for example hexylamine, are positively charged and as such form insoluble complexes with highly charged GAGs (*idem*). The GAG-amine complexes can subsequently be collected as a precipitate following the addition of an organic solvent for example, methyl isobutyl ketone, as a result of the hydrophobicity of the primary amine (*idem*). Quaternary ammonium salts have also been identified that form insoluble complexes with GAGs, an example of which is cetylpyridinium chloride. The resulting precipitates can be collected by suspension in a 2M NaCl solution, followed by precipitation in an organic solvent (Silva, 2006; van der Meer, Kellenbach and van den Bos, 2017). In the case of precipitation using an organic solvent, such as ethanol or methanol, a relatively high GAG concentration is required (1-2%) for adequate recovery. Capture and elution of GAGs from anion exchange resin is therefore necessary prior to further purification using this method (Nakano, Betti and Pietrasik, 2010). For large scale GAG extraction (Kg tissue quantities) capture by ion-exchange is commonly utilised as a preliminary step, preceding further purification by precipitation using ammonium cations or organic solvents to obtain a crude GAG extract (van der Meer, Kellenbach and van den Bos, 2017).

2.1.4. Fractionation of glycosaminoglycans from crude extracts

Following the isolation of a crude extract several methods can be utilised to isolate distinct GAG sub-types, for instance fractionation using anion-exchange resin, sequential precipitation with organic solvents, and selective enzymatic or chemical degradation (Silva, 2006; Nakano, Betti and Pietrasik, 2010; Zhang, Zhang and Linhardt, 2010; van der Meer, Kellenbach and van den Bos, 2017). Prior to fractionation crude extracts are commonly dialysed against distilled H₂O, in order to remove contaminating salts, before being lyophilised and reconstituted in H₂O. The removal of contaminant salts is crucial to prevent interference with fractionation methods that are based upon the anionic properties of GAGs.

Anion exchange chromatography can also be employed for the fractionation of GAG-subtypes, in addition to recovery of crude GAGs extracts as described in section 2.1.3, due to their differing charge densities. Fractionation using this method principally utilises DEAE resin employing a NaCl gradient to differentially elute GAG sub-types based upon anionic charge (Silva, 2006; Nakano, Betti and Pietrasik, 2010; Zhang, Zhang and Linhardt, 2010). At low NaCl concentrations any remaining contaminants such as nucleic acids and glycoproteins, will be eluted, while GAGs will remain bound to the DEAE matrix (Silva, 2006). Sub-types of GAGs can then be fractionated based upon their charge density using an increasing NaCl gradient, with elution being positively correlated with anionic charge (*idem*). Separation of GAG sub-types by this method can be difficult in some cases due to the heterogeneity of GAGs and overlapping anionic charge densities (Silva, 2006; Nakano, Betti and Pietrasik, 2010).

Fractionation of GAG subtypes from crude extracts can also be conducted utilising organic solvents such as ethanol, methanol, propanol and acetone (Volpi, 1996b; Silva, 2006). In the case of ethanol, methanol and propanol, fractionation is conducted by the sequential addition of 0.1 volumes of solvent to a maximum of 2.0 volumes (*idem*). Following the addition of each 0.1 volume the solution is incubated at 4°C for >24 hours, after which the precipitate is collected by centrifugation (*idem*). The order of precipitation with increasing volumes of solvent generally, occurs from heparin → DS → CS, with heparin precipitating at ~ 1 volume (Volpi, 1996b; Silva, 2006; van der Meer, Kellenbach and van den Bos, 2017). Fractionation using this method can also be improved by the addition of a divalent cation, for example 2% NaCl, to the starting crude extract solution (Silva, 2006). Fractionation of GAG-subtypes can also be achieved using acetone following the general procedure outlined above, however precipitation occurs after the addition of differing volumes of acetone; heparin <0.6 volumes, DS at ~0.6-0.7 volumes and CS >0.7 volumes (Volpi, 1994; Silva, 2006). Fractionation utilising acetone has the advantage over other organic solvents as it does not require the addition of cations (*idem*).

Where fractionation of GAG sub-types using the aforementioned protocols has been ineffective, if necessary, selective enzymatic degradation can be employed by utilising polysaccharide lyases which act specifically upon glycosidic linkages through β -elimination (Silva, 2006; Zhang, Zhang and Linhardt, 2010). Polysaccharide lyases that act upon GAGs include, heparinases (also termed heparitinase; heparin/HS), chondroitinase (CS/DS and HA), and hyaluronate lyase (HA) (Table 8) (Nakano, Betti and Pietrasik, 2010; Zhang, Zhang and Linhardt, 2010).

Table 8: Common glycosaminoglycan lyases utilised for analysis (Zhang, Zhang and Linhardt, 2010). * Dependent on bacterial species source; ** weak activity.

Enzyme	Activity	Specificity
Chondroitin lyase ACI	CS/HA (endo)	$\rightarrow 3)\alpha$ -D-Gal/Glc**NAC NAC(4S/OH;6S/OH)(1 \rightarrow 4)- β -D-GlcA(1 \rightarrow
Chondroitin lyase ACII	CS/HA (exo)	$\rightarrow 3)\alpha$ -D-Gal/Glc**NAC NAC(4S/OH;6S/OH)(1 \rightarrow 4)- β -D-GlcA(1 \rightarrow
Chondroitin lyase ABC	CS/DS/HA (endo/exo*)	$\rightarrow 3)\alpha$ -D-Gal/Glc**NAC(4S/OH;6S/OH)(1 \rightarrow 4)UA (1 \rightarrow
Chondroitin lyase B	DS (endo)	$\rightarrow 3)\alpha$ -D-GalNAC(4S/OH;6S/OH)(1 \rightarrow 4)- α -L- Ido(2S/OH)(1 \rightarrow
Heparinase I (heparitinase III)	Heparin (endo)/HS domains	NS $\rightarrow 4)\alpha$ -D-GlcNS(6S/OH)(1 \rightarrow 4)- α -L- IdoA2S(1 \rightarrow
Heparinase II	Heparin/HS (endo)	$\rightarrow 4)\alpha$ -D-GlcN(S/Ac)(6S/OH)(1 \rightarrow 4)- α -L-IdoA/- β - D-GlcA(2S/OH)(1 \rightarrow
Heparinase III (heparitinase I)	HS (endo)	$\rightarrow 4)\alpha$ -D-GlcN(Ac/S)(OH/6S)(1 \rightarrow 4)- β -D-GlcA/- α -L-IdoA(2OH)
Hyaluronate lyase	HA (endo)	$\rightarrow 3)\alpha$ -D-GlcNAC(1 \rightarrow 4)- β -D-GlcA(1 \rightarrow
Hyaluronidase	HA/CS (endo)	$\rightarrow 3)\alpha$ -D-GlcNAC(1 \rightarrow 4)- β -D-GlcA(1 \rightarrow

Chondroitinase ABC will act upon all forms of CS, DS and HA, whereas chondroitinase AC will degrade sulphated and un-sulphated regions of CS and HA but not DS (*idem*). Digestion by chondroitinase ABC or AC results in cleavage of β (1 \rightarrow 4) glycosidic linkage, producing an unsaturated C4-C5 double bond in the uronic acid residue residing at the non-reducing end of the polysaccharide (*idem*). Chondroitinase AC I and ACII primarily degrade polysaccharide chains in an endolytic and exolytic manner, respectively while Chondroitinase ABC can possess either activity. Heparinase I (also known as heparitinase III) acts primarily upon heparin and to a limited extent upon the sulphated domains of HS due to specificity for N-sulphated glucosamine and 2-O-sulphated iduronic acid residues. Heparinase I will also act upon glucosamine residues bearing 6-O-

sulphation. In contrast, heparinase III principally cleaves between glucosamine residues possessing either N-sulphate or N-acetyl groups linked to glucuronic acid, therefore acts primarily upon HS. Heparinase III will cleave glucosamine residues containing 6-O-sulphation and also possess weak activity against iduronic acid containing disaccharides. Heparinase II will act upon disaccharides containing N-sulphated or N-acetylated glucosamine linked to either glucuronic acid or iduronic acid that bear variable levels of sulphation on either residue. Digestion by each heparitinase will also result in the production of an unsaturated C4-C5 double bond in the uronic acid residue residing at the non-reducing end of the polysaccharide. The broad substrate specificity of Heparinase II therefore enables the degradation of both heparin and HS. Depending on the desired type of GAG, the aforementioned enzymes can be used alone or in conjunction in order to selectively degrade the unwanted species present within a crude sample. Furthermore, the specificity of GAG lyases renders them valuable for structural analysis, as discussed in section 2.2 (*idem*).

In addition to selective enzymatic depolymerisation, N-sulphation of the glucosamine residue of HS and heparin makes these GAGs susceptible to nitrous acid degradation at pH 1.5 (room temperature). Depolymerisation utilising nitrous acid is specific for N-sulphated amino sugars and therefore can be utilised to distinguish between heparin/HS and CS/DS (*idem*).

2.2. Structural analysis of glycosaminoglycans

2.2.1. Agarose Electrophoresis

Agarose gel electrophoresis of GAGs can be employed to analyse the GAG composition of crude or fractionated extracts, requiring only μg levels of material (Volpi and Maccari, 2006). Gel electrophoresis of GAGs can be performed in either barium acetate or diamine buffers (for example 1,3-diaminopropane), where separation occurs based upon net anionic charge or the degree of affinity for diamine, respectively (Dietrich and Dietrich, 1976; Dietrich, McDuffie and Sampaio, 1977; Volpi and Maccari, 2006). In addition, discontinuous two-dimensional electrophoresis, utilising both buffer systems sequentially, can be employed to separate GAG sub-types and heparin into both slow-moving (low MW and charge) and fast-moving (high MW and charge) components (Dietrich, McDuffie and Sampaio, 1977; Volpi and Maccari, 2006).

Subsequent to performing agarose gel electrophoresis, gels can be stained to visualise the resolved GAGs based upon the metachromatic activity and anionic properties of these polysaccharides (Volpi and Maccari, 2006). Dyes previously used for the staining of GAGs post agarose electrophoresis include, toluidine blue, azure A, alcian blue, methylene blue and Stains-All with toluidine blue being the most common (Dietrich and Dietrich, 1976; Van de Lest *et al.*, 1994; Volpi and Maccari, 2006). Visualisation with toluidine blue alone can detect between $>0.1\text{--}1\ \mu\text{g}$ of GAG, however methods have been developed to improve detection limits by utilising a combination of dyes, for example toluidine blue/Stains-All (Volpi and Maccari, 2002, 2006). This method was able to detect $\sim 10\ \text{ng}$ of all GAG species, improving the detection limit by approximately 10-

fold (*idem*). Furthermore, the combined use toluidine blue and Stains-All enables the detection of HA without the need for alternative staining buffers, as is the case of toluidine blue alone (Volpi and Maccari, 2006). Staining with toluidine blue, either alone or in conjunction with Stains-All does, does however require precipitation of GAGs from the gel utilising cetylpyridinium chloride followed by fixation (drying) whereas other stains such as azure A do not require any pre-treatments (Dietrich and Dietrich, 1976; Dietrich, McDuffie and Sampaio, 1977; Van de Lest *et al.*, 1994; Volpi and Maccari, 2002). Staining using a combination of azure A/ammoniacal silver has also been observed to improve the detection limits of GAG by approximately 200-fold, however this method involves a greater number of steps (Van de Lest *et al.*, 1994; Volpi and Maccari, 2006).

Agarose gel electrophoresis can also be used in conjunction with enzymatic or chemical depolymerisation of GAGs, in order to support the composition, as both the degradation products and enzymes are not visualised (Volpi and Maccari, 2006). Furthermore, agarose gel electrophoresis can be utilised to monitor GAG-protein interactions as the degree of migration is influenced upon binding (Takahashi, Nader and Dietrich, 1981).

2.2.2. ATR-FTIR

Attenuated total reflectance Fourier transform infrared spectroscopy (ATR-FTIR) is an efficient label-free, non-destructive technique that can be employed to analyse a variety compounds in either liquid or solid states (Glassford, Byrne and Kazarian, 2013; Devlin, Mycroft-west, *et al.*, 2019). The majority of molecules absorb IR radiation within

the mid IR-region (between 4000 cm^{-1} and 400 cm^{-1}) as a result of molecular vibrations, for instance stretching, rocking, scissoring, twisting and wagging, that alter the dipole moment of the molecule. Where the frequency of the change in the dipole moment of the molecules functional groups corresponds to the frequency of the transmitted IR light, absorption occurs. This produces a characteristic IR spectrum for individual molecules that can be utilised for structural analysis of individual or mixtures of substances (Blum and John, 2012).

Fourier transform infrared spectroscopy (FTIR) utilises the principles of Fourier transforms and attenuated total reflectance to overcome the time-consuming nature of traditional infrared spectroscopy, where absorption of wavelengths of light were measured individually (Blum and John, 2012). Instead, ATR-FTIR utilises an interferometer, which enables the simultaneous recording of all wavelengths and a converts the resulting interferogram into a IR spectra using a Fourier transform (*idem*). Additionally, ATR is also commonly utilised in conjunction to FTIR to overcome the limitations of traditional transmission IR spectroscopy (*idem*). In the case of ATR, the IR incident light is directed at a crystal, for instance diamond, XnSe, silicone or germanium at an angle \geq the critical angle, leading to internal reflection and creation of an effervescent wave (Blum and John, 2012; Glassford, Byrne and Kazarian, 2013). When a sample is placed on the surface of the crystal the effervescent wave penetrates the sample, which absorbs the IR radiation, causing the wave to become attenuated. After multiple reflections the wave exists the crystal and is recorded (*idem*).

Infrared spectroscopy has been utilised extensively for the structural analysis of complex polysaccharides, such as GAGs. The complexity and number of vibrational modes that GAGs possess results in convoluted, but nevertheless characteristic, FTIR spectra which are influenced by the chemical composition, modifications, for instance sulphation, and the associated cation (Grant *et al.*, 1989; Devlin, Mycroft-West, *et al.*, 2019). As a result of this complexity the complete assignment of the FTIR spectra of GAGs is largely precluded, however efforts have been made to ascribe features associated with the major bands (Devlin, Mauri, *et al.*, 2019). For instance, bands observed at ~ 875 , ~ 800 and $\sim 820\text{ cm}^{-1}$ have been suggested to be attributed to C-H, 4S and 6S, respectively (Neely, 1957; Grant *et al.*, 1989, 1991; Devlin, Mauri, *et al.*, 2019). It has been proposed that this region can be used to discriminate between CS subtypes, based upon bands present at $\sim 820\text{ cm}^{-1}$ (6S) and 850 cm^{-1} (4S) in CSC and CSA respectively (Mainreck *et al.*, 2011). The band centred at $\sim 1248\text{ cm}^{-1}$ is also strongly associated with the presence and degree of sulphation, with HA exhibiting no peak in this region (*idem*) Similarly, the bands at ~ 1430 and 1635 cm^{-1} , associated with carbonyl group symmetric and asymmetric stretching respectively, are absent in the FTIR spectra of KS (Mainreck *et al.*, 2011; Devlin, Mauri, *et al.*, 2019). Bands in the region of $1200\text{--}900\text{ cm}^{-1}$ have also been assigned to C-O-C stretches of the glycosidic bond and the peak shoulder at 1559 cm^{-1} to C-N vibrations of the N-acetyl (amide group), both characteristic features of GAGs (Tipson, 1968; Grant *et al.*, 1991; Devlin, *et al.*, 2019).

Despite the complexity and extensive signal overlap observed for the FTIR spectra of GAGs, the presence of characteristic peaks signatures enables the differentiation of sub-types when coupled with multivariant analysis (Mainreck *et al.*, 2011; Devlin,

Mauri, *et al.*, 2019; Devlin, Mycroft-west, *et al.*, 2019). Furthermore, this method has been utilised to detect the species of origin of heparin preparations, the presence of contaminants such as OSCS and to characterise the GAG composition of crude samples (Devlin, Mauri, *et al.*, 2019; Devlin, Mycroft-West, *et al.*, 2019).

2.2.3. Circular dichroism spectroscopy

Circular dichroism (CD) spectroscopy measures the differential absorption of left- and right- handed circularly polarised (LCP and RCP, respectively) light, principally by asymmetric, chiral molecules. As circularly polarised light obeys Beer Lamber's Law, the difference in absorption of LCP and RCP light (ΔA) by a given chiral molecule is related to the difference between the extinction coefficient ($\Delta \epsilon$) for LCP and RCP light by; $\Delta A = A_l - A_r = \epsilon_l cl - \epsilon_r cl = \Delta \epsilon cl$, where c is defined as concentration in M, l path length in cm and $\Delta \epsilon$ molar CD in $M^{-1}.cm^{-1}$ (Johnson, 1988; Woody, 1996; Rudd, Yates and Hricovini, 2009). Circular dichroism can therefore be defined as; $\Delta \epsilon = \epsilon_l - \epsilon_r$ and is typically measured across a range of wavelengths, predominantly between $\lambda = 180 - 260\text{ nm}$ (*idem*).

As plane polarised light passes through an optically active solution the circular components are absorbed to different extents, due to differences in $\Delta \epsilon$, producing elliptically polarised light. Circular dichroism is therefore commonly reported in ellipticity, θ (deg) (Woody, 1996), which refers to the tangent of the ratio of the minor and major axis of the resultant ellipse (Figure –B) and is related to ΔA by; $\Delta A = \theta/32.98$ (Johnson, 1988; Woody, 1996). Furthermore, CD is commonly expressed as

molar ellipticity $[\theta]$ in order to account for path length (cm) and concentration (M);

$$[\theta] = \frac{100\theta}{c \cdot l}, \text{ where } [\theta] \text{ can be converted to } \Delta\epsilon; \Delta\epsilon = [\theta]/3298 \text{ (idem).}$$

Proteins are inherently chiral due to their constituent amino acids and contain several chromophores that can be detected utilising conventional CD spectrophotometers, for example amide groups (peptide bond) and aromatic side chains, which absorb at $\lambda = 190\text{-}240$ nm and $\lambda = 260\text{-}320$ nm, respectively. The asymmetric environment imparted by different protein secondary structures, such as α -helix and β -sheet, also gives rise to characteristic CD spectra as a result of influences on the peptide bond backbone (Johnson, 1988; Greenfield, 2006). A widely employed application of CD is the examination of protein conformation in solution; this enables the assessment of protein folding and thermal stability, when assessed over a range of temperatures. Changes in protein conformation as a result of ligand binding or alterations to the environment, such as pH and buffer composition, can also be monitored by CD (*idem*). In the case of proteins, CD is often reported in mean residue ellipticity, $[\theta]_{MR}$ by; $[\theta]_{MR} = \frac{100\theta}{c_{MR} \cdot l}$, which reports the molar ellipticity for individual amino acids in order to facilitate the comparison of proteins with vastly different molecular weights (Johnson, 1988; Woody, 1996).

In addition to proteins, CD can also be utilised to obtain structural information on many biomolecules, for example carbohydrates (Ranjbar and Gill, 2009). The hydroxyl and acetyl groups of carbohydrates possess CD bands <190 nm, as a result of high-energy transitions, which can be recorded by some modern instruments and by synchrotron

light sources (Rudd, Yates and Hricovini, 2009). In addition, common carbohydrate modifications such carboxyl and amide groups are attributed to CD bands at 200-240 nm and 180-200 nm due to $n \rightarrow \pi^*$ and $\pi \rightarrow \pi^*$ transitions respectively (Park and Chakrabarti, 1978). The carboxyl group present within the uronic acid residue of GAGs has been attributed to the CD band at ~210 nm, while the N-acetyl group (amide) is associated with bands at both ~210 and ~190 nm (Rudd, Yates and Hricovini, 2009). In addition, sulphate modifications and oxygen atoms present within hydroxyl groups, glycosidic linkages and within the pyranose ring, also contribute to the band at ~190 nm in the CD spectra of GAGs (*idem*). The influence on the 3-dimensional conformation of GAGs by the type of glycosidic linkage, epimerisation and presence of sulphate modifications gives rise to distinctive CD spectra for each GAG sub-type (Rudd, Yates and Hricovini, 2009; Stanley and Stalcup, 2011). For instance, heparin and HS both display a positive CD band <200 nm, while for other GAGs a negative CD band is observed in this region. This difference has been attributed the orientation of the glycosidic linkage; with HS/heparin possessing a 1-4 linkages as opposed to 1-3 (Stone, 1971; Park and Chakrabarti, 1978; Stanley and Stalcup, 2011). At wavelengths > 200 nm CD bands observed for GAGs are a result of overlapping transitions, largely proscribing assignment. It has however been reported that the magnitude and width of CD bands in this region varies between GAGs species as a result of epimerisation of the uronic acid residue and levels of sulphate modifications (T. R. Rudd *et al.*, 2007; Rudd, Skidmore, Guimond, Holman, *et al.*, 2009; Stanley and Stalcup, 2011). As a result of the varying abundance of these modifications and the difference in glycosidic linkage, distinctive CD spectrums are observed for each GAG sub-type (Rudd *et al.*, 2008; Rudd, Skidmore, Guimond, Holman, *et al.*, 2009; Rudd, Yates and Hricovini, 2009; Stanley and

Stalcup, 2011). Furthermore, the CD spectra of GAGs has also been demonstrated to be influenced by the associated cation, in particular Cu^{2+} (T. R. Rudd *et al.*, 2007; Rudd *et al.*, 2008; Rudd, Skidmore, Guimond, Holman, *et al.*, 2009; Stanley and Stalcup, 2011).

2.2.4. SAX-HPLC glycosaminoglycan disaccharide composition analysis

Strong anion-exchange high pressure liquid chromatography (SAX-HPLC) is commonly utilised to determine the percentage disaccharide composition of GAGs (Turnbull, 2001; Skidmore *et al.*, 2006). Firstly, GAG samples must undergo exhaustive degradation, this is primarily conducted by enzymatic degradation with the respective polysaccharide lyase as discussed in section 2.1.4 (*idem*). For heparin and HS samples digestion is primarily conducted with a mixture of heparitinase I, II and III in order to achieve maximal degradation of the polysaccharide chain. A sample may also be digested separately with individual heparinases in order to further resolve the fine domain structure of HS; based upon the specific enzymatic activities. In respect to CS, DS and HA, exhaustive digestion with chondroitinase ABC will result in near complete degradation of these polysaccharides. Selective digestion can also be performed utilising a chondroitinase with greater specificity for CS, DS or HA, respectively (Table 9).

Table 9: Δ -Disaccharides produced as a result of enzymatic degradation of glycosaminoglycans.

Standard reference	Heparin/HS disaccharides	CS/DS disaccharides	HA disaccharide
1	Δ -UA-GlcNAc	Δ -UA-GalNAc	Δ UA-(1 \rightarrow 3)-GlcNAc
2	Δ -UA-GlcNAc(6S)	Δ -UA-GalNAc(4S)	
3	Δ -UA-GlcNS	Δ -UA-GalNAc(6S)	
4	Δ -UA-GlcNS(6S)	Δ -UA-GalNAc(4S,6S)	
5	Δ -UA(2S)-GlcNS	Δ -UA(2S)-GalNAc(4S)	
6	Δ -UA(2S)-GlcNS(6S)	Δ -UA(2S)-GalNAc(6S)	
7	Δ -UA(2S)-GlcNAc	Δ -UA(2S)-GalNAc(4S,6S)	
8	Δ -UA(2S)-GlcNAc(6S)	Δ -UA(2S)-GalNAc	

All Δ -disaccharide standards, derived enzymatic degradation of each GAG subtype, can then be resolved using SAX-HPLC coupled with in line UV detection at $\lambda=223$ nm, which monitors the C4-C5 unsaturated bond introduced at the non-reducing end as a result of enzymatic cleavage (*idem*). Most commonly separation is achieved utilising the SAX Propac PA1 column, which has been reported to achieve superior resolution and repeatability of Δ -disaccharide in comparison to silica-based SAX columns (*idem*). Δ -disaccharide separation employing the Propac PA1 column is performed by injection at a flow rate of 1 mL.min⁻¹ onto a column preequilibrated in double-distilled H₂O at pH 3.5 (with HCl). Elution is then performed over ~45 minutes with a linear gradient of NaCl from 0-1 M (pH 3.5 with HCl) with in-line monitoring at $\lambda=223$ nm (*idem*). The resulting retention times of sample digestion products are then referenced to those of the appropriate commercially available Δ -disaccharide standards (or those purified using gel permeation chromatography) (Table 9; *idem*). It is of note that enzymatic cleavage of the glycosidic linkage abolishes the original identity of the uronic acid residue, rendering CS and DS disaccharides indistinguishable, whereas nitrous acid degradation of N-sulphate containing GAG leaves these residues intact. Separation of nitrous acid

degradation products is, however more difficult to achieve by SAX-HPLC and requires labelling of the resultant disaccharides with ^3H -borohydride to enable detection (*idem*). Separation of nitrous acid degradation products employing the SAX Propac PA1 column is achieved under the same conditions as for enzymatic derived Δ -disaccharide, however using a shallow NaCl gradient (0- 150 mM over 50 minutes succeeded by 150- 500 mM over 70 minutes) (*idem*).

Superior levels of detection of Δ -disaccharides to that of UV can also be achieved by SAX-HPLC utilising fluorescent detection post labelling. Subsequent to enzymatic digestion the resulting Δ -disaccharides can be labelled at newly generated reducing ends by reductive amination of the carbonyl group of the reducing end GlcNAc/NS, for example with 2-amino acridone (AMAC) (Kitagawa, Kinoshita and Sugahara, 1995; Skidmore *et al.*, 2006). Labelling procedures utilising AMAC are conducted under elevated temperatures in acidic conditions under which, HS/heparin is sensitive to de-N-sulphation (Skidmore *et al.*, 2006). Utilisation of the alternative fluorescent tag, 4,4-difluoro-5,7-dimethyl-4-bora-3a,4a-diaza-s-indacene- 3-propionic acid (BODIPY) hydrazide, enables labelling at the carbonyl group of the reducing end GlcAc/NS under lower temperatures, thus preventing possible de-N-sulphation (Skidmore *et al.*, 2006, 2010). Furthermore, labelling using BODIPY hydrazide enables separation using SAX HPLC without prior Δ -disaccharides or post column clean-up; as a result of the neural charge of BODIPY (*idem*). Disaccharide compositional analysis utilising the latter labelling methodology can improve detection limits by ~ 2000 -fold in comparison to UV detection, whereas for AMCA an ~ 10 -fold improved detection limit is obtained (Kitagawa, Kinoshita and Sugahara, 1995; Skidmore *et al.*, 2006, 2010).

2.2.5. Nuclear magnetic resonance

Nuclear magnetic resonance (NMR) is the principal method utilised for the structural elucidation of GAGs due to it being non-destructive and permitting the analysis of intact, un-labelled polysaccharides through ^1H , ^{13}C and ^{15}N isotopes (Li, Ly and Linhardt, 2012; Pomin, 2014; Song, Zhang and Linhardt, 2021). NMR spectroscopy of GAGs can be utilised to derive information regarding the percentage monosaccharide sequence, the level of impurities within a sample and to some extent for sequence analysis; in the case of oligosaccharides (*idem*). Ideally, NMR spectroscopy is performed upon mg quantities of extracts that are composed primarily of one class of GAG, with >80% purity and are performed utilising high field instruments (> 500 MHz), so that detailed structural information to be obtained (Li, Ly and Linhardt, 2012). Where a sample contains a mixture of GAGs, for instance a crude extract, accurate evaluation of the individual percentage monosaccharide sequence of each class is hindered due to low signal dispersion (*idem*). Despite this, sufficient resolution exists in order to obtain the overall GAG composition of crude extracts, as such NMR can also be utilised as an effective method for monitoring purification procedures.

One-dimensional (1D) proton (^1H) and carbon (^{13}C) NMR spectroscopy are the most basic approaches utilised for GAG analysis, with the former commonly used to obtain initial information regarding the class(es) of GAG present within a sample and the presence of contaminants (Li, Ly and Linhardt, 2012; Pomin, 2014; Song, Zhang and Linhardt, 2021). In the case of 1D ^1H NMR of GAGs resonances occur primarily within the window of 6.0 - 3.0 ppm, with the exception of acetyl groups at ~2.0 ppm (Pomin,

2014). Despite the low signal dispersion of signals between 6.0 - 3.0 ppm, which hinders full assignment of GAG based solely upon 1D-NMR, the identity of the GAG class can still easily be established by comparison of chemical shifts (*idem*). Principally, changes in the chemical environment as a result of de-shielding or shielding effects, results in downfield or upfield migration in the observed chemical shifts of the recorded nuclei. In the case of GAGs, this occurs a result of the monosaccharide composition (GlcA/IdoA or GalN/GlcN), anomericity of the glycosidic bond (α/β) and the position and extent of sulphation (O- and N-) (*idem*). As a result, the observed chemical shifts for each GAG class display distinct resonances, in particular for the acetyl group and protons bonded to anomeric carbons. For instance, the acetyl signal is observed at ~ 2.02 , ~ 2.04 , ~ 2.08 for CS, HS/heparin and DS, respectively (Pomin, 2014; Lauder, 2015). The proton bond to the anomeric carbon of GlcN also exhibits a signal downfield to that of Gal at $\sim 5.3 - 5.4$ ppm and $4.5 - 4.7$ ppm, respectively: the extent of deshelling is depending upon the presence and position of sulphate modifications (Table 10, Table 11). Furthermore, the resonance of the proton bonded to the anomeric carbon of the uronic acid residue exhibits a downfield shift in the case of IdoA compared to GlcA, which is also dependent upon sulphation and amino sugar (Table 10, Table 11). Typically, α -aromatic protons will exhibit resonances at $\sim 4.9 - \sim 5.5$ ppm compared to $\sim 4.4 - 5$ ppm for β - anomers, where resonances can be utilised to distinguish between CS, DS, heparin and HS (Pomin, 2014). In the case of distinguishing between DS and CS resolved signals attributed to the protons bonded to carbon 3 (U3) and 2 (U2) of the uronic acid can also be utilised, where the epimerised IdoA exhibits a downfield shift. This is most easily observed by comparing the ratio of U2 signals at ~ 3.37 ppm and 3.5 ppm for the un-epimerised and epimerised uronic acid, respectively (*idem*;Table 11). As such 1D, ^1H NMR spectroscopy

can clearly distinguish between each class of GAG, in particular when samples are >80% pure (*idem*). In some instances, the levels and positions of sulphate modifications within GAGs can also be tentatively determined depending on the purity of the sample (Table 10, Table 11). For instance, the presence of 2-O-sulphation of IdoA within heparin/HS results in a downfield shift in the resonance of the proton bonded to the anomeric carbon of IdoA to ~ 5.2 ppm from ~ 5.0 ppm (Table 10). Furthermore, the weaker deshielding effect of sulphation at position 6 of CS in comparison to sulphation at position 4 results in a reduction in downfield shift for the former modification; enabling the distinction of CSA and CSC type GAGs (Table 11). This is most clearly observed for the protons bonded to carbon 4 of Gal, which exhibit a resonance at ~ 4.7 ppm for GlcA-Gal4S and 4.2 ppm for GlcAGal6S (Table 11). Monodimensional ^{13}C NMR, despite possessing lower sensitivity, can also be utilised to further resolve the extent and positions of N-sulphate and O-sulphate modifications, due to the greater dispersion of chemical shifts resulting in a reduction in signal overlap (Li, Ly and Linhardt, 2012; Song, Zhang and Linhardt, 2021) (Table 10, Table 11).

In many cases, however 1D-NMR lacks sufficient resolution to fully characterise the monosaccharide composition of GAGs as a result of extensive signal overlap, particularly for heterogeneous mixtures. Where further characterisation is required multidimensional NMR methods can be employed, for instance HSQC, heteronuclear multiple bond coherence (HMBC), ^1H - ^1H correlation spectroscopy (COSY), total correlation spectroscopy (TOCSY), nuclear Overhauser effect spectroscopy (NOESY), rotating frame Overhauser effect spectroscopy (ROESY) (Li, Ly and Linhardt, 2012; Pomin, 2014; Song, Zhang and Linhardt, 2021).

Table 10: $^1\text{H}/^{13}\text{C}$ NMR chemical shifts utilised for analysis of glucosaminoglycans. * signals distinguishing between 6OH and 6S. ** Signals distinguishing between I2S and I2OH. *Signals distinguishing between NS and NAc. ****

Prevalent sequence	Glucosamine						Uronic acid					References
IdoA2S-GlcNS6S	A-1	A-2(NS)***	A-3	A-4	A-5	A-6(S) *	U-1**	U-2(S)	U-3	U-4	U-5	(Casu <i>et al.</i> , 1996; Yates <i>et al.</i> , 1996)
^1H	5.42	3.31	3.69	3.79	4.05	4.42+4.30	5.23	4.37	4.22	4.12	4.82	
^{13}C	99.5	60.7	72.5	78.8	72.0	69	102.1	78.9	72.1	79.0	72.3	
IdoA2S-GlcNAc6S	A-1	A-2(NAc) ***	A-3	A-4	A-5	A-6(S) *	U-1**	U-2(S)	U-3	U-4	U-5	(Yates <i>et al.</i> , 1996)
^1H	5.40	3.36	3.95	3.79	4.03	4.30-4.40	5.24	4.39	4.40	4.18	4.95	
^{13}C	93.7	57.1	70.9	78.2	72.0	68.8	101.3	75.3	65.4	73.0	69.8	
IdoA2S-GlcNS6OH	A-1	A-2(NS) ***	A-3	A-4	A-5	A-6*	U-1	U-2(S)	U-3	U-4	U-5	(Casu <i>et al.</i> , 1996; Yates <i>et al.</i> , 1996)
^1H	5.31	3.27	3.71	3.70	3.89	3.87	5.22	4.35	4.25	4.06	4.84	
^{13}C	100.0	60.8	72.4	80.5	73.8	62.6	102.0	77.6	70.7	78.7	71.4	
IdoA2OH-GlcNS6S	A-1	A-2(NS) ***	A-3	A-4	A-5	A-6(S) *	U-1**	U-2(OH)	U-3	U-4	U-5	(Casu <i>et al.</i> , 1996; Yates <i>et al.</i> , 1996)
^1H	5.38	3.24	3.65	3.71	4.02	4.36+4.23	5.04	3.78	4.12	4.08	4.84	
^{13}C	98.1	60.3	72.4	80.1	71.5	68.7	104.6	71.1	70.4	77.2	71.2	
IdoA2OH-GlcNAc6OH	A-1	A-2(NS) ***	A-3	A-4	A-5	A-6(S) *	U-1**	U-2(OH)	U-3	U-4	U-5	(Yates <i>et al.</i> , 1996)
^1H	5.40	3.29	3.70	3.70	3.91	3.84+3.90	4.89	3.79	3.96	4.14	4.72	
^{13}C	95.8	57.0	71.8	79.0	74.3	61.9	104.5	71.7	71.8	77.4	71.8	
GlcA2OH-GlcNAc6OH	A-1	A-2(Ac)***	A-3	A-4	A-5	A-6(OH) *	U-1**	U-2(OH)	U-3	U-4	U-5	(Casu <i>et al.</i> , 1994)
^1H	5.36	3.89	3.86	3.64	3.82	3.84	4.48	3.37	3.69	3.78	3.78	
^{13}C	99.6	56.1	73.5	81.1	72.0	62.2	105.2	76.3	78.9	79.1	79.1	
GlcA2S-GlcNS6S	A-1	A-2(NS)***	A-3	A-4	A-5	A-6(S) *	U-1**	U-2(S)	U-3	U-4	U-5	(Casu <i>et al.</i> , 1994)
^1H	5.44	n.d	n.d	n.d	n.d	n.d	4.74	4.14	3.98	3.85	3.88	
^{13}C	100.9	n.d	n.d	n.d	n.d	n.d	102.8	82.3	77.3	79.1	79.5	

Table 11: ¹H/¹³C NMR chemical shifts utilised for analysis of galactosaminoglycans *IdoA/ GlcA, ** 4S , 6S***

Prevalent sequence	Galactosamine						Uronic acid					References
GlcA-GalNAc6OH,4OH	Gal-1	Gal-2	Gal-3	Gal-4(OH) **	Gal-5	Gal-6(OH) ***	U-1*	U-2	U-3	U-4	U-5	
¹ H	4.56	4.04	3.88	4.13	3.74	3.78	4.61	3.42	3.68	3.84	4	
¹³ C	104.2	53.9	82.9	70.5	77.8	63.7	107.2	74.9	76.6	82.8	76.6	(Holme and Perlin, 1989; Mucci, Schenetti and Volpi, 2000; Pomin, 2014)
GlcA-GalNAc6S,4OH	Gal-1	Gal-2	Gal-3	Gal-4(OH) **	Gal-5	Gal-6(S)***	U-1*	U-2	U-3	U-4	U-5	
¹ H	4.58	4.06	3.88	4.22	4.01	4.26	4.53	3.39	3.62	3.77	3.72	
¹³ C	104.3	53.7	82.9	70.3	75.3	70.4	107.2	75.3	76.6	83.0	79.3	(Holme and Perlin, 1989; Mucci, Schenetti and Volpi, 2000; Pomin, 2014)
GlcA-GalNAc6OH,4S	Gal-1	Gal-2	Gal-3	Gal-4(S) **	Gal-5	Gal-6(OH)***	U-1 *	U-2	U-3	U-4	U-5	
¹ H	4.71	4.08	4.04	4.9	3.87	3.83	4.50	3.41	3.62	3.80	3.69	
¹³ C	103.8	54.4	78.5	79.4	77.5	63.9	106.6	75.2	76.5	83.4	79.6	(Holme and Perlin, 1989; Mucci, Schenetti and Volpi, 2000; Pomin, 2014)
IdoA-Gal	Gal-1	Gal-2	Gal-3	Gal-4	Gal-5	Gal-6	U-1 *	U-2	U-3	U-4	U-5	
¹ H	4.67-89	4.01-4.09	4.01-4.09	4.70	3.75-3.9	3.75-3.90	4.97	3.58	3.9	4.12	4.755	
¹³ C	104.70	54.90	78.19	78.87	77.42	63.81	105.6 6	71.99	73.59	82.50	72.11	(Holme and Perlin, 1989)

2.2.6. Principal component analysis

Principal component analysis is a multivariate statistical technique that is commonly employed to assist in the interpretation of large complex datasets by reducing the dimensionality, while retaining the information imparted by the variability amongst the data. Such information is expressed as new orthogonal variables termed principal components (PC), which can be utilised to objectively compare large datasets, when the values (eigenvalues) of these new variables are plotted against each other (Rudd, Skidmore, Guimond, Cosentino, *et al.*, 2009; Abdi and Williams, 2010; Jolliffe and Cadima, 2016). The PCs produced are constructed as linear combinations of the variables contained within the original dataset, with the first PC containing the factor with the greatest variance, followed by the second PC containing the second greatest variance and so on, for all the dimensions of the data. As such the lower order PCs correspond to the components of the original data set containing the greatest amount of information (or variance), while those of higher order (containing lower variance) are composed primarily of the noise and can be discarded. Typically, at the point in which the subsequent PC offers a minimal increase in variance, the latter PCs can be disregarded. Alternatively, the variance covered by each PC can be calculated as a percentage of the total variance and PCs covering ~90% of the variance are compared (Holland, 2019). In this way, PCA allows for the reduction in the dimensionality of the dataset while avoiding the loss of factors which account for to the greatest variance amongst the original dataset (Rudd, Skidmore, Guimond, Cosentino, *et al.*, 2009; Abdi and Williams, 2010; Jolliffe and Cadima, 2016; Holland, 2019).

The aim of PCA is therefore, to simplify complex datasets by extracting the variables containing the most important information, in the form of PCs, which can then be compared to determine similarities or differences among individual components of the dataset. This approach has been applied to deconvolute the complex spectra of GAGs produced from various spectroscopic techniques, for instance CD, NMR, ATR-FTIR and UV. For instance, the biological origin, level of purify and presence of contaminants in pharmaceutical heparin preparations has been determined using PCA coupled with the aforementioned spectroscopic techniques. Furthermore, the class of GAG and the associated cation can be determined by applying this methodology (Rudd *et al.*, 2007; Rudd *et al.*, 2008; Rudd, Skidmore, Guimond, Cosentino, *et al.*, 2009; Rudd, Skidmore, Guimond, Holman, *et al.*, 2009; Lima *et al.*, 2011; Devlin, Mauri, *et al.*, 2019; Devlin, Mycroft-west, *et al.*, 2019).

2.2.7. BACE-1 inhibitor screening utilising a fluorescent FRET peptide assay

Föster resonance energy transfer (FRET) is an optical phenomenon that occurs when the energy from an excited donor molecule is transferred in a radiationless manner to an acceptor, through dipole-dipole coupling, and results in the reduction of the donors fluorescent intensity (Sahoo, 2011; Algar *et al.*, 2019; Jones and Bradshaw, 2019). The transfer of energy is dependent upon the distance between the FRET pair (acceptor and donor), requiring a proximity of approximately 1-10 nm. In addition to proximity, in order for FRET to occur between a FRET pair there must be sufficient spectral overlap between the emission of the donor and the absorption (or excitation) of the acceptor molecule, where the degree of overlap is termed the spectral overlap integral (J) (Algar

et al., 2019). If compatible FRET pairs are selected, proximity is therefore the most critical parameter required for FRET to occur and can be determined by the Förster distance (R_0), which corresponds to the distance between the donor and acceptor molecules (R) at which energy transfer is 50% effective. The R_0 is dependent several factors including J , the quantum yield of the donor, the refractive index of the solution and the orientation of dipole transition moments of the acceptor and donor. Furthermore, R_0 can be utilised to determine R by measuring the efficiency of FRET (E_{FRET}), describing why FRET is often described as a molecular ruler (*idem*).

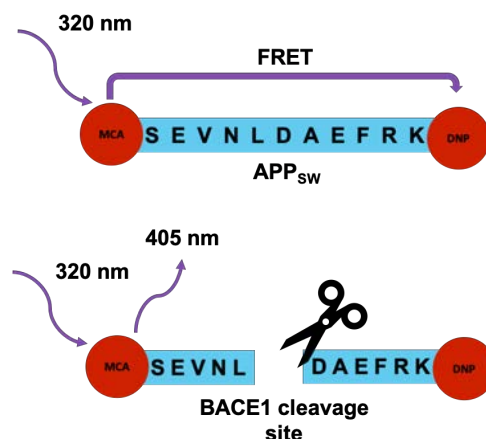


Figure 11: BACE-1 fluorogenic peptide FRET assay schematic. A fluorogenic peptide based upon the APP_{sw} mutation coupled to MCA (donor; $\lambda_{\text{ex}} = 320 \text{ nm}$, $\lambda_{\text{em}} = 405 \text{ nm}$) on the N-terminal and DNP (acceptor) on the C-terminal is utilised to monitor BACE1 activity. Cleavage of the fluorogenic peptide by BACE1 liberates quenching of MCA by DNP resulting in increased fluorescent emission ($\lambda_{\text{em}} = 405 \text{ nm}$).

When appropriate FRET-pairs are employed, consisting of different donor and acceptor molecules, the appearance or loss of FRET can also be utilised to determine the proximity of the pair by monitoring the fluorescent emission. This principal has been employed to monitor the cleavage of synthetic peptides, which have been conjugated to FRET pairs at the C and N terminal, by several proteases including BACE-1 (Wang *et al.*, 1993; Grüninger-Leitch *et al.*, 2002; Kennedy *et al.*, 2003; Scholefield *et al.*, 2003;

Beckman, Holsinger and Small, 2006; Patey *et al.*, 2006, 2008; Klaver *et al.*, 2010); Figure 11). Here, a synthetic fluorogenic peptide based upon the APP_{sw} mutation (MCA-SEVNLDAEFRK(DNP)RR-NH₂) has been employed, with the fluorophore 7-Methoxycoumarin-4-acetic acid (MCA) and quencher DNP, conjugated to the N- and C-terminus, respectively (Figure 11). Upon cleavage by BACE-1 between asparagine and leucin residues the N-terminal fragment containing MCA is liberated from DNP on the C-terminal and as a result is no longer in sufficient proximity for FRET to occur. As a consequence, upon excitation at $\lambda_{\text{ex}} = 320 \text{ nm}$, the fluorescent emission of MCA can be observed at $\lambda_{\text{em}} = 405 \text{ nm}$ (Figure 11). In the absence of BACE-1 cleavage, for instance in the case of inhibition, reduced fluorescence will be observed at $\lambda_{\text{em}} = 405 \text{ nm}$. This methodology has been employed previously to monitor BACE1 activity in the presence of GAGs (Beckman, Holsinger and Small, 2006; Klaver *et al.*, 2010). Furthermore, similar methodologies, utilising alternative FRET pairs have been employed to demonstrate the inhibition of BACE-1 by heparin and derivatives thereof (Scholefield *et al.*, 2003; Patey *et al.*, 2006, 2008).

2.2.8. Differential scanning fluorimetry

Differential scanning fluorimetry (DSF) enables the rapid measurement of protein thermal stability, utilising commonly available rt-PCR machines (Niesen, Berglund and Vedadi, 2007; Jeremy Johnson *et al.*, 2014). Monitoring of protein unfolding by DSF, as a function of a linear increase in temperature, utilises a hydrophobic fluorescent dye, most commonly Sypro orange (excitation wavelength of $\sim \lambda = 470 \text{ nm}$) (*idem*). Hydrophobic fluorescent dyes which, can be employed for DSF are largely quenched in aqueous environments, however upon protein denaturation an increase in

fluorescent emission is observed, which results from the exposure of hydrophobic regions present within the protein. The extent of protein unfolding can therefore be measured, and described graphically, as a function of fluorescence in the form of a melt curve (*idem*). From the resulting melt-curve the midpoint of the transition between the native folded protein conformation and the unfolded protein conformation can be determined (*idem*). This is the point at which the Gibbs free energy of unfolding (ΔG_u) is zero and is referred to as the melting point, T_m , (*idem*), see Figure 12.

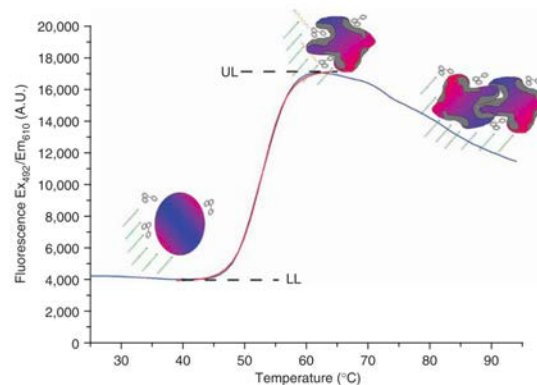


Figure 12: Typical differential scanning fluorimetry melt curve. Fluorescence intensity versus temperature for the unfolding of protein citrate synthase (purple) in the presence of SYPRO orange (white circles). Following protein unfolding, hydrophobic patches (gray) are exposed, resulting in an increase in fluorescent emission. Subsequent to the maximal peak intensity, a decrease in fluorescence is observed, due to protein aggregation. Lower fluorescence intensity, LL; upper level fluorescence intensity, UL. (Niesen, Berglund and Vedadi, 2007).

Previously, DSF has been utilised to determine interactions between proteins and ligands, for example for inhibitor screening, to establish alterations in the stability of protein variants and to optimise conditions for protein crystallography studies (Niesen, Berglund and Vedadi, 2007; Uniewicz *et al.*, 2010; Jeremy Johnson *et al.*, 2014; Vivoli *et al.*, 2014). Such applications of DSF are made viable through comparison of the T_m value of a given protein under contrasting conditions, for instance a change in T_m is observed in the presence of a binding ligand (*idem*).

Chapter 3: Materials and Methods

3.1. Materials

1,3-diaminopropane, 99%; VWR, Lutterworth, UK. Catalogue No. ACRO112352500.

10x PBS w/o Ca^{2+} and Mg^{2+} ; Sigma Aldrich, UK. Catalogue No. LZBE17-517Q.

Acetic acid, 99.5 %; Fisher Scientific, UK. Catalogue No. 10230753.

Acetone, 99.8%; VWR, Lutterworth, UK. Catalogue No. 20066.365.

Acetonitrile, HPLC grade; Fisher Scientific, UK. Catalogue No. 10407440.

Amberlite IRA-900; Fisher Scientific, UK. Catalogue No. 9050-97-9.

Applied Biosystems™ MicroAmp™ 96PCR Plate, 0.1mL; AB Biosystems, Warrington, UK. Catalogue No. 10670986.

BACE-1 Human Tag free; ACRO Biosystems, Newark, Delaware, USA. Catalogue No. BA1-H5213.

Bovine Serum Albumin, microbiological grade; Fisher Scientific, UK. Catalogue No. 12827172.

Calcium acetate; VWR, Lutterworth, UK. Catalogue No. 0225-500G.

Calcium chloride; Fisher Scientific, UK. Catalogue No. 10161800.

Centrifugal filter, 10 kDa; Vivaspın, Sartorius, Goettingen, Germany. Catalogue No. 10670333.

Chondroitin sulphate A, mw 10,000-30,000; Carbosynth, UK. Catalogue No. YC15288. Batch No. YC15288.1701.

Chondroitin sulphate C; Carbosynth, UK. Catalogue No. YC31458. Batch No. YC31458.1701.

Chondroitin sulphate disaccharide reference standard 1 Δ UA-GalNAc; Iduron, Manchester UK. Catalogue No. CD001.

Chondroitin sulphate disaccharide reference standard 2 Δ UA-GalNAc,4S; Iduron, Manchester UK. Catalogue No. CD002.

Chondroitin sulphate disaccharide reference standard 3 Δ UA-GalNAc,6S; Iduron, Manchester UK. Catalogue No. CD003.

Chondroitin sulphate disaccharide reference standard 4 Δ UA-GalNAc,4S,6S; Iduron, Manchester UK. Catalogue No. CD004.

Chondroitin sulphate disaccharide reference standard 5 Δ UA,2S-GalNAc,4S; Iduron, Manchester UK. Catalogue No. CD005.

Chondroitin sulphate disaccharide reference standard 6 Δ UA,2S-GalNAc,6S; Iduron, Manchester UK. Catalogue No. CD006.

Chondroitin sulphate disaccharide reference standard 7 Δ UA,2S-GalNAc,4S, 6S; Iduron, Manchester UK. Catalogue No. CD007.

Chondroitin sulphate disaccharide reference standard 8 Δ UA,2S-GalNAc; Iduron, Manchester UK. Catalogue No. CD008.

Chondroitinase ABC; Sigma, Dorset, UK. Catalogue No. C2905.

Clarias batrachus flesh and skin, Kim Son LTD

D-(+)-10-camphorsulfonic acid; Fisher Scientific, UK. Catalogue No. 10030610.

DEAE-Sephacel; BIO-RAD, UK. Catalogue No. 156-0020.

Dialysis membrane 3.5 kDa MWCO; BioDesignDialyse, Fisher Scientific, UK. Catalogue No. 12727496.

Dimethyl sulfoxide (DMSO) $\geq 99.9\%$; VWR, Lutterworth, UK. Catalogue No. N182-5X10ML.

Dimethyl sulfoxide; VWR, Lutterworth, UK. Catalogue No. 23500.260.

Ethanol, absolute. Fisher Scientific, UK. Catalogue No. E/0650DF/17.

Glycerol; Fisher Scientific, UK. Catalogue No. 10336040.

Heparinase enzymes I from the soil bacterium *Pedobacter heparinus*; Iduron, Alderley Edge, UK. Catalogue No. HEP-ENZ I.

Heparinase enzymes II from the soil bacterium *Pedobacter heparinus*; Iduron, Alderley Edge, UK. Catalogue No. HEP-ENZ II.

Heparinase enzymes III from the soil bacterium *Pedobacter heparinus*; Iduron, Alderley Edge, UK. Catalogue No. HEP-ENZ III.

Hexadecyltrimethylammonium bromide; Millipore, UK. Catalogue No. 8.14119.0100.

Hi-Res Standard Agarose; AGTC bioProducts, UK . Catalogue No. AGD1.

Hydrochloric acid extra pure 37%; Fisher Scientific, UK. Catalogue No. 10244100.

L-Glutamine 200mM; SLS, UK. Catalogue No. LZBE17-605E.

Litopenaeus vannamei flesh, MW Morrison Supermarkets PLC, UK

Melanogrammus aeglefinus head, Prime Seafoods LTD

Merluccius merluccius head, Prime Seafoods LTD

Methanol $\geq 98.5\%$; VWR, Lutterworth, UK. Catalogue No. 20903.368.

Non-sterile black 96 well flat-bottomed plates; Fisher Scientific, UK. Catalogue No. 11359163.

Novex™ Empty Gel Cassettes, Mini, 1.5 mm; Fisher Scientific, UK. Catalogue No. 11559156.

Oncorhynchus gorboscha flesh, Lidl Stiftung & Co. KG, UK

Pangasianodon hypophthalmus whole, Kim Son LTD

Pathromtin SL; Siemens, UK. Catalogue No. 10484200.

PCR Plate seals; Fisher Scientific, UK. Catalogue No. 11570274.

Phenol red; Fisher Scientific, UK. Catalogue No. 11317178.

Pierce graphite spin columns; Fisher Scientific, UK. Catalogue No. 10467734.

Pierce™ C18 spin columns; Fisher Scientific, UK. Catalogue No. 89870.

Porcine intestinal mucosa heparin, 193 IU mg⁻¹; Celsus, Cincinnati, OH, USA.

Catalogue No. 12150. Lot No. 11412.

Portunus pelagicus flesh, Tesco PLC, UK

ProPac PA-1 analytical column, 4 × 250 mm; ThermoFisher Scientific, Altrincham, UK.

Catalogue No. 039658. Lot No. 013-10-116.

Protease; Sigma Aldrich, UK. Catalogue No. P4860.

Quenched fluorogenic peptide substrate, MCA-SEVNLDAEFRK(DNP)RR-NH₂; R and D Systems, USA. Catalogue No. ES004.

Sardina pilchardus flesh, scale and skin, Tesco PLC, UK

Sodium acetate anhydrous; Fisher Scientific, UK. Catalogue No. 11434584.

Sodium chloride; Fisher Scientific, UK. Catalogue No. 10428420.

Sodium Hydroxide Solution 10M; Fisher Scientific, UK. Catalogue No. 10488790

Normal Human citrated plasma; Technoclone, Austria. Catalogue No. 3016137-004.

Sodium Phosphate Dibasic Fisher Scientific, UK. Catalogue No. 10182863.

Sodium Phosphate Monobasic Fisher Scientific, UK. Catalogue No. 10667823.

SphereClone analytical column, 4.6 x 250 mm; Phenomenex, Macclesfield, UK.

Catalogue No. 00G-4149-E0.

Sypro Orange, Invitrogen; Fisher Scientific, UK. Catalogue No. 10338542.

Syringe filtration, 0.2 µm; MiniSart, Sartorius, UK. Catalogue No. 10509821.

Syringe filtration, 0.45 µm; MiniSart, Sartorius, UK. Catalogue No. 10109180.

Thromborel S reagent; Siemens, Erlangen, Germany. Catalogue No. 10484202.

Toluidine blue; VWR, Lutterworth, UK. Catalogue No. E847-25G.

Trifluoroacetic Acid, 99+%; Fisher Scientific, UK. Catalogue No. 10112740.

Trimethylsilylpropanoic acid; Fisher Scientific, UK. Catalogue No. AC177390010.

Tris Base; Fisher Scientific, UK. Catalogue No. 10103203.

Triton™ X-100; Fisher Scientific, UK. Catalogue No. 10591461.

Trypan Blue 0.4% solution; SLS, UK. Catalogue No. LZ17-942E.

Trypsin/EDTA 10x; SLS, UK. Catalogue No. LZBE02-007E.

Unsaturated heparin disaccharide standard Δ UA-GlcNAc (IV-A); Iduron, Alderley Edge, UK. Catalogue No. HD006.

Unsaturated heparin disaccharide standard Δ UA-GlcNAc,6S (II-A); Iduron, Alderley Edge, UK. Catalogue No. HD008.

Unsaturated heparin disaccharide standard Δ UA-GlcNS (IV-S); Iduron, Alderley Edge, UK. Catalogue No. HD005.

Unsaturated heparin disaccharide standard Δ UA-GlcNS,6S (II-S); Iduron, Alderley Edge, UK. Catalogue No. HD004.

Unsaturated heparin disaccharide standard Δ UA,2S-GlcAc (III-A); Iduron, Alderley Edge, UK. Catalogue No. HD007.

Unsaturated heparin disaccharide standard Δ UA,2S-GlcNAc,6S (I-A); Iduron, Alderley Edge, UK. Catalogue No. HD003.

Unsaturated heparin disaccharide standard Δ UA,2S-GlcNS (III-S); Iduron, Alderley Edge, UK. Catalogue No. HD002.

Unsaturated heparin disaccharide standard Δ UA,2S-GlcNS,6S (I-S); Iduron, Alderley Edge, UK. Catalogue No. HD001.

Water, HPLC for Gradient Analysis; Fisher Scientific, UK. Catalogue No. 10449380.

3.2 Equipment and software

500 MHz Avance Neo spectrometer fitted with a 5-mm TXI Probe; Bruker, São Paulo, Brazil.

800 MHz AVANCE III spectrometer fitted with a TCI cryoprobe; Bruker, UK.

1. x 10 cm HPLC Column. GE Life Sciences, UK.

Step One Plus RT-PCR machine. Fisher, UK.

BeStSel analysis server; available at <https://bestsel.elte.hu/index.php> (Micsonai *et al.*, 2015).

GIMP software, v2.8; Berkeley, CA, USA.

Prism 7; GraphPad, San Diego, California, USA.

Jasco J1500 CD Machine. Jasco, UK. Catalogue No. J-1500.

MatLab software, R20018a; MathWorks, Cambridge, UK.

Brucker FTIR Alpha II Platinum FTIR with Diamond ATR; Bruker, UK. Catalogue No. 22017804.

PowerPac™; BIO-RAD, UK. Catalogue No. 1645050.

Quartz cuvette 0.2 mm path length; Hellma, Plainview, NY, USA.

Scanvac CoolSafe 55-4; SLS, UK, Catalogue No. FRE4500.

ImageJ I.X; available at <https://imagej.nih.gov/ij/> (Schneider, Rasband and Eliceiri, 2012).

RC 5C plus refrigerated centrifuge; Sorvall, UK.

Spectral Manager II software; Jasco, UK.

Tecan i-control software; Tecan, Switzerland.

Tecan Infinite M200 Multiwell plate reader. Tecan, Switzerland. Catalogue No. M200.

Omnicos software; ThermoFisher, UK.

Thrombotrack coagulation analyser; Axis Shield, UK.

TopSpin, 4.1.0; Bruker, UK.

X-Cell SureLock™ Mini-Cell Electrophoresis System; ThermoFisher, Altrincham, UK.

Vivibook Pro; Asus, Taiwan.

Rstudio, 1.4; Boston, Massachusetts, USA.

Coagulation cuvettes & ball bearings. Behnk Elektronik, Germany. Catalogue No. 050-220

HPLC Cecil 1100, with CE1200 wavelength monitor. Cecil, UK. Catalogue No. 1100.

Mnova, 14. 2.1; Mestrelab, Santiago de Compostela, SPAIN.

3.3. Methods

3.3.1. Extraction of glycosaminoglycans

The tissue obtained from various species were individually processed, commencing with delipidation via homogenisation with an excess of acetone. The resulting mixture was incubated for 24 hours at room temperature (*r.t*) and the defatted tissue was subsequently recovered by centrifugation for 10 minutes at 5670 g (*r.t*), before the remaining was acetone allowed to evaporate overnight. The tissue was then subjected to proteolytic digestion with Alcalase (17 U.Kg⁻¹ of dried tissue mass) in PBS, containing 1M NaCl and subsequently adjusted to pH 8.0 with NaOH containing, for 24 hours at 60°C under constant agitation. Proceeding digestion, the remaining debris were removed via centrifugation at 5670 x g for 10 minutes (*r.t.*), prior to the resulting supernatant being incubated with Amberlite IRA-900 ion-exchange resin (exchanged into the hydroxide counter ion form) for 24 hours under agitation (*r.t*). The resin was

recovered by filtration and washed successively with water (60°C) approximately 10 volumes and 1 M NaCl (*r.t*), or until the solution ran clear. Bound material was subsequently recovered through resuspension of the resin in 3 M NaCl for 24 hours under constant agitation (*r.t*). The resin was removed via filtration and crude GAGs were precipitated by the addition of ice-cold methanol (1:2 v/v) to the filtrate, followed by incubation for 48 hours at 4°C. The precipitate was collected by centrifugation at 4°C, 15,400 x g for 1 hour and the crude GAG extracts were re-suspended in distilled H₂O (dH₂O), prior to being dialysed against excessive changes of dH₂O (3.5 kDa MWCO membrane). The crude GAG extracts were then subjected to syringe filtration (0.45 µm) prior to lyophilisation and stored at 4°C until required.

3.3.2. Agarose Gel Electrophoresis of glycosaminoglycans

Agarose gel electrophoresis of GAGs (2-20 µg) was performed utilising 0.55% (w/v) agarose gels (80 × 80 x 1.5 mm) prepared in 1,3-diaminopropane-acetate buffer at pH 9.0. Electrophoresis was conducted for approximately 30 minutes in 0.5 M 1,3-diaminopropane-acetate buffer (pH 9.0), at a constant voltage of 150 V (~100 mA), employing a X-Cell SureLock™ Mini-Cell Electrophoresis System. Subsequently, gels were subjected to precipitation with 0.1% (w/v) cetyltrimethylammonium bromide solution for a minimum of 30 minutes and allowed to dry overnight. Staining was then achieved utilising acetic acid:ethanol:dH₂O (0.1:5:5 v/v) with 0.1% (w/v) toluidine blue, for approximately 1 hour prior to destaining in the same solution, with toluidine blue omitted, for 30 minutes. Images were acquired and processed with GIMP Software and ImageJ.

3.3.3. Attenuated Total Reflectance Fourier transform infrared spectroscopy (ATR-FTIR) coupled with principal component analysis (PCA)

Attenuated total reflectance Fourier transform infrared (ATR-FTIR) spectra of freeze-dried GAG samples were recorded using a Bruker Alpha II Platinum FTIR instrument fitted with a diamond ATR, in collaboration with Anthony Devlin. Spectra were recorded in the region of $4000 - 400 \text{ cm}^{-1}$ with a spectral resolution of 2 cm^{-1} . Sample spectra were acquired by 32 scans, over 5 repeats and were corrected for the pre-recorded background air spectrum utilizing Opus software (Bruker, UK). All further spectral correction and analysis was performed utilizing an Asus Vivibook Pro and R Studio by Anthony Devlin (Devlin et al., 2019). Spectra were baseline corrected (7th-order polynomial), normalised (between 0-1), and smoothed (Savitzky-Golay algorithm, 2nd degree polynomial, 21 neighbours); in order to negate for environmental fluctuations and variations in the quantity of the sample in contact with the ATR crystal. Spectral regions between $2000-2500 \text{ cm}^{-1}$, $<700 \text{ cm}^{-1}$ and $>3600 \text{ cm}^{-1}$ were removed prior to further processing in order to further mitigate the influence of environmental variations, for instance CO_2 and H_2O fluctuations, on principal component analysis (PCA). Subsequently second derivatives (Savitzky-Golay algorithm, 2nd degree polynomial, 41 neighbors) were plotted and PCA was performed on the corrected normalised matrix of intensities, employing singular value decomposition (mean-centered, base prcomp function).

3.3.4. Circular dichroism spectroscopy of glycosaminoglycans coupled with principal component analysis (PCA)

The circular dichroism (CD) spectra of GAG samples were recorded in HPLC grade H₂O (10 mg.mL⁻¹) between λ = 250-190 nm, 1 nm resolution (scan speed, 100 nm.min⁻¹) over 3 accumulations with a Jasco J-1500 spectrophotometer equipped with a quartz cuvette (0.2 mm pathlength). The spectrophotometer was pre-calibrated with 1 mg.mL⁻¹ (+)-10-camphorsulfonic acid in HPLC grade H₂O. A HPLC grade H₂O baseline was recorded prior to sample spectrum acquisition, employing identical settings, and subtracted from the sample spectra utilizing Spectral Manager II. Following acquisition spectra were normalised to 250 nm and subjected to PCA, employing singular value decomposition utilising R-studio (mean-centred, base prcomp function) on an Asus Vivibook Pro. All spectral acquisition and analysis was performed in collaboration with Anthony Devlin.

3.3.5. Nuclear Magnetic Resonance (NMR)

Nuclear Magnetic Resonance (NMR) experiments were performed upon GAG samples, which had been exchanged in D₂O (approximately 600 μ L, thrice) containing TMSP (0.003 % v/v). Spectra were recorded a Bruker 500 MHz Avance Neo spectrometer fitted with a 5-mm TXI Probe or a Bruker 800 MHz AVANCE III spectrometer fitted with a TCI cryoprobe (at 298 K or 343 K). In addition to 1-dimensional (¹H) spectra, ¹H–¹³C Heteronuclear Single-Quantum Correlation (HSQC) 2-dimensional spectra were collected using the standard pulse sequences available. Spectral processing and integrated was performed utilizing TopSpin and MestReNova.

3.3.6. Beta secretase fluorescence resonance energy transfer (FRET) inhibition assay

Compounds were assayed for inhibitory potential against recombinant human beta secretase (BACE-1; 0.3125 µg) utilizing a synthetic quenched fluorogenic peptide substrate based upon Swedish mutation of APP (APP_{sw}; MCA-SEVNLDAEFRK(DNP)RR-NH₂). The assay was conducted based upon a previously described system utilizing the principle of Förster resonance energy transfer (Schofield et al., 2003, Patey et al., 2006, Patey et al., 2008, Hadfield et al., 2018, Beckman et al., 2006, Kleva et al., 2010). Reactions were conducted at 37°C in 50 mM sodium acetate buffer pH 4.0 at final well volume of 100 µL. BACE-1 alone, or in the presence of GAGs, was incubated for 10 minutes at 37°C prior to addition of the substrate. Fluorescent emission was subsequently recorded at $\lambda_{\text{ex}} = 320 \text{ nm}$, $\lambda_{\text{em}} = 405 \text{ nm}$, over 90 minutes period using a Tecan Infinite® 200 Pro microplate reader. Control reaction wells omitting BACE-1 were also employed to ensure that decoupling of the fluorogenic peptide was not observed in the presences of GAGs. The relative change in fluorescence per minute (RFU.min⁻¹) was calculated in the linear range of the control containing BACE-1 alone, with normalised percentage inhibition subsequently, calculated from equation (1) and then fitted to a four-parameter logistics model using Prism 7 (% \pm SD, n = 3).

$$(1) \% \text{ Inhibition} = \left(\frac{(\bar{C}_+ - x_i)}{(\bar{C}_+ - \bar{C}_-)} \right) \times 100$$

Where, \bar{C}_+ and \bar{C}_- refer to the mean of the controls containing or omitting the enzyme, respectively and x_i is the i^{th} measurement in the presence of each test compound.

3.3.7. DEAE-Sephacel anion-exchange chromatography

Crude GAG extracts were re-suspended in 1 mL of HPLC-grade H₂O and injected onto a pre-packed DEAE-Sephacel column (1 x 10 cm) at a flow rate of 1 mL.min⁻¹, monitored by in-line UV detection at $\lambda = 232$ nm. Following the isocratic elution of unbound material, a stepwise NaCl gradient consisting of 0.25, 0.5, 0.8, 1 and 2 M NaCl was applied to the column at a flow rate of 1 mL.min⁻¹, producing in six fractions identified as F1-F6, respectively. The eluted fractions were dialysed extensively against HPLC grade H₂O (exchanged a minimum of 3 times per 24 hours), employing a 3.5 kDa MWCO membrane for 48 hours under constant agitation. The retentate was lyophilised and stored at 4°C prior to further processing.

3.3.8. Constituent Δ -Disaccharide analysis of heparin/heparan sulphate

polysaccharides

Porcine intestinal mucosa heparin, HS standards and fractionated GAG extracts were re-suspended in heparitinase lyase buffer (25 mM sodium acetate, 5 mM calcium acetate, pH 7) prior to being subjected to exhaustive enzymatic degradation at 37°C by the consecutive addition of heparinase I, III and II (2.5 mIU) at 2-hour intervals. Succeeding this, a cocktail of heparinase I, III and II (2.5 mIU) was applied to the sample, followed by a further incubation overnight at 37°C in order to ensure maximal polysaccharide degradation. Heparitinase enzymes were subsequently denatured at 95°C for 5 minutes and the samples were allowed to cool before being stored at 4°C

Chromatographic separation of the heparitinase digested samples (50 μg) was performed using high performance anion exchange chromatography (HPAEC). Samples were made up to 1 mL in HPLC-grade H_2O (pH 7.4) prior to being injected onto a ProPac PA-1 analytical column (4 \times 250 mm), which had been pre-equilibrated in HPLC-grade H_2O (pH 7.4), at a flow rate of 1 $\text{mL}\cdot\text{min}^{-1}$. The column was held under isocratic flow for 10 minutes, preceding to the elution of Δ -disaccharides by the application of a linear gradient of NaCl (from 0 to 2 M in HPLC-grade H_2O , pH 7.4) over 60 minutes. Elution was monitored by in-line UV detection at $\lambda_{\text{abs}} = 232 \text{ nm}$ via the unsaturated C=C bond, introduced as a result of heparinase digestion, between C₄ and C₅ of the uronic acid residues. Retention times were compared to those of commercially available Δ -disaccharide reference standards (2 μg), encompassing the 8 most common standards found in Hp and HS. The column was washed extensively with 2 M NaCl and HPLC-grade H_2O prior to use and between runs. Heparinase digestion and chromatographic separation of fractionated GAG extracts were performed with matched heparin and HS controls (with known Δ -disaccharides compositions) in order to ensure that a lack of enzymatic degradation products was not a result of defective enzymatic activity.

Where necessary, resultant Δ -disaccharides were purified from heparinase enzymes and contaminating buffer salts utilising C18 and graphite spin columns. Denatured heparinase enzymes were firstly bound to a pre-activated C18 spin column (50% methanol (aq.) followed by HPLC-grade H_2O) and the newly generated Δ -disaccharides were collected following sequential column washes with HPLC-grade H_2O . The Δ -disaccharide samples were then desalted by immobilisation upon a graphite spin column (pre-washed with 80% acetonitrile, 0.5% (aq.) trifluoroacetic acid and HPLC-

grade H₂O). Contaminating buffer salts were subsequently removed by extensive washes of HPLC-grade H₂O prior to elution of Δ -disaccharides with 40% acetonitrile, 0.5% trifluoroacetic acid (aq.). The graphite spin column eluate was subjected to serial lyophilisation prior to further processing in order to remove remaining volatile contaminants.

3.3.9. Constituent Δ -disaccharide analysis of chondroitin sulphate polysaccharides

Chondroitin sulphate A, CSC and fractionated GAG extracts (50 μ g) were subjected to exhaustive enzymatic digestion with chondroitinase ABC (2.5 mIU) in 50 mM Tris-HCl, 60 mM sodium acetate, 0.02% w/v BSA, pH 8.0 at 37 °C for 4 hours. Subsequently, an additional 2.5 mIU of chondroitinase ABC was added to the samples. Following further incubation being at 37 °C overnight, the samples were heated to 95°C for 5 minutes in order to denature the chondroitinase ABC. Samples were subsequently stored at 4°C until required.

Chromatographic separation of the chondroitinase ABC digested samples (50 μ g) was performed using high performance anion exchange chromatography (HPAEC). Samples were made up to 1 mL in HPLC-grade H₂O (pH 3.5) prior being injected onto a SphereClone analytical column (4.6 x 250 mm), which had been pre-equilibrated in HPLC-grade H₂O, at a flow rate of 1 mL.min⁻¹. The column was held under isocratic flow for 10 minutes, prior to initiating a linear gradient of NaCl (from 0 to 2 M in HPLC-grade H₂O, pH 3.5) over 60 minutes. Elution of the Δ -disaccharide was monitored by in-line UV detection at $\lambda_{\text{abs}} = 232$ nm via the unsaturated C=C bond between C₄ and C₅ of the

uronic acid residues, introduced as a consequence of heparinase digestion. Authentic, commercially available Δ -disaccharide standards, encompassing the 4 most common standards found in CS and DS, were employed as a mixture (2 μ g each) and served as chromatographic references with the elution times cross-references with GAG samples. The column was washed extensively with 2 M NaCl (in HPLC-grade H₂O, pH 3.5) and HPLC-grade H₂O (pH 3.5) prior to use and between runs. Chondroitinase ABC digestion and chromatographic separation of fractionated GAG extracts were performed with matched CSA and CSC controls (with known Δ -disaccharides compositions) in order to ensure that a lack of detectable enzymatic degradation products was not a result of defective enzymatic activity.

3.3.10. Influence of GAG binding on the secondary structure of human BACE1, determined by circular dichroism spectroscopy

The circular dichroism spectrum of 6.12 μ M (9 μ g) native, human BACE-1 was recorded in 50 mM sodium acetate (pH 4.0), alone or in the presence of GAG samples (4.5 – 36 μ g), utilising a J-1500 Jasco CD spectrometer equipped with a 0.2 mm path length quartz cuvette and Spectral Manager II software. Spectra were recorded at a scan speed of 100 nm.min⁻¹, over λ = 190 – 320 nm with 1 nm resolution and are presented as the mean of five independent scans, corrected for background buffer absorbance (50 mM sodium acetate, pH 4.0). Prior to spectral acquisition, human BACE-1 was buffer exchanged thrice, employing a 10 kDa centrifugal filter at 12,000g, in order to remove commercially supplied buffer. To ensure the observed change in the CD spectrum of BACE-1 in the presence of GAG samples was not simply a result of the addition of the polysaccharide

alone, which are known to possess CD spectra at high concentrations (T. R. Rudd *et al.*, 2007; Rudd, Skidmore, Guimond, Holman, *et al.*, 2009), control spectra were subtracted prior to analysis using Spectral Manager II software. In addition, the theoretical summative CD spectra, of human BACE-1 and GAG alone, was confirmed to differ from the observed experimental CD spectra. This indicates that the observed change in the CD spectra of BACE-1 alone or in the presence of GAG ligands is a result of a conformational upon binding. Subsequently, secondary structure prediction was performed utilizing the BeStSel analysis server on the unsmoothed data (Micsonai *et al.*, 2015) between $\lambda = 190\text{-}260$ nm. Data was then presented as the smoothed spectrum, employing a 2nd order polynomial to 9 neighbours (Savitzky-Golay algorithm), using Prism 7.

3.3.11. Investigating the thermal Stability of Human BACE-1 in the presence of GAGs with differential scanning fluorimetry

Differential scanning fluorimetry (DSF) was carried out employing the method described by Uniewicz *et al.* (2010) based on a modification to the original method of Niesen *et al.* (2007). Human BACE-1 (1 μg) was subjected to DSF utilising 96-well qPCR plates, in the presence of Sypro Orange (20 X) and 50 mM sodium acetate, pH 4.0, with a final well volume of 40 μl . Where necessary, GAG samples were incorporated to a maximal concentration of 200 $\mu\text{g.mL}^{-1}$. In addition, controls containing GAG alone were assayed to ensure any recorded increase in fluorescence was not a result of interactions of the polysaccharide and Sypro Orange. An AB Biosystems StepOne plus qPCR machine, with the TAMRA filter set deployed, was used to carry out melt curve experiments, with an

initial incubation phase of 2 min at 25°C, which increased successively every 30s by 0.5°C, to a final temperature of 90°C. Data analysis was completed using Prism 7 with the first derivative plots smoothed to 21 neighbours, using a 2nd order polynomial (Savitzky-Golay algorithm). The peak of the first derivatives (yielding T_{ms}) was determined using MatLab software. Data are presented with the relevant GAG controls subtracted.

3.3.12. Activated partial thromboplastin time (aPTT)

Three-fold serially diluted crude GAG extracts (25 μ l) were incubated for 2 mins at 37°C with normal human citrated plasma (50 μ l) and Pathromtin SL reagent (50 μ l), prior to the addition of 50 mM calcium chloride (25 μ l). The time taken for clot formations to occur was recorded using a Thrombotrak Solo coagulometer, with an upper limit of 2 minutes imposed (representing 100% inhibition of clotting). HPLC-grade H₂O (exhibiting a normal aPTT clotting time of approximately 30-40 seconds) and sodium porcine mucosal heparin (193 IU.mg⁻¹) were employed as controls. The EC₅₀ values of all test and control samples were determined, following normalisation (0-100 % response), using a four-parameter non-linear regression model fitted with Prism 7.

3.3.13. Prothrombin time (PT)

Three-fold serially diluted GAG samples (50 μ L) or HPLC grade H₂O were incubated for 1 minute at 37°C with normal human citrated plasma (50 μ L), prior to the addition of Thromborel S reagent (50 μ L). The time taken for clot formation to occur was recorded

using a Thrombotrak Solo coagulometer, with an upper limit of 2 minutes was imposed, (representing 100% inhibition of clotting). A HPLC-grade H₂O control was employed, representing 0% inhibition of clotting (normal PT clotting time of approximately, 13 – 14 seconds), in addition to porcine mucosal heparin (193 IU.mg⁻¹). The EC₅₀ values of all test and control samples were determined following normalisation (0-100 % response), using a four-parameter non-linear regression model fitted with Prism 7.

**Chapter 4: Extraction and fractionation of glycosaminoglycans,
possessing BACE-1 inhibitory activity, from aquatic species.**

4.1. Introduction

In order to examine the BACE-1 inhibitory activity of GAGs obtained from aquatic species it is first necessary to extract and purify GAGs in sufficient quantities to conduct structural and bioactivity analysis. For the purpose of structure-function analysis it is critical that the extraction process does not introduce artefacts for instance, depolymerization or de-sulphation of the GAG chain and that sufficient yields are produced to enable structural analysis, which may require mg quantities of purified material (van der Meer, Kellenbach and van den Bos, 2017). In addition, if downstream a potential therapeutic or commercial application is desired, it is critical that the process is robust, scalable and reproducible. Several protocols have been developed to achieve this goal many of which have been directed towards the isolation of heparin; owing to the potent anticoagulant activities and clinical use of heparin. Such protocols have also been adapted in the search for alternative non-mammalian sources of potent heparin-like anticoagulants and in the discovery of non-anticoagulant GAGs with potential alternative therapeutic or commercial applications (Greiling, 1974; Esko, 1993; Nakano, Betti and Pietrasik, 2010; Zhang, Zhang and Linhardt, 2010; van der Meer, Kellenbach and van den Bos, 2017), see section 2.1. In addition, extraction and purification protocols have also been developed for the small-scale isolation of GAGs from tissue specimens and cell cultures for structural analysis (Guimond *et al.*, 2009).

Owing to the complexity and heterogeneity of GAGs, extraction and subsequent purification of individual species is challenging. For instance, in the case of pharmaceutical grade heparin, preparations are often composed of approximately 10%

DS (Guerrini, Bisio and Torri, 2001; Lima *et al.*, 2011). In 2008, the heparin contamination crisis highlighted the difficulty in monitoring pharmaceutical heparin, where samples adulterated with over-sulphated CS, entered the clinical market (Guerrini *et al.*, 2008). Furthermore, several non-GAG contaminants, such as phosphates, ethylenediaminetetraacetic acid (EDTA) and histamine, have been identified within commercial heparin preparations (McGeown, Martin and Neill, 1955; Casu *et al.*, 1987; Hermann, Frank and Ring, 1994; Pan *et al.*, 2010; Lima *et al.*, 2011). The presence the aforementioned contaminants have previously been associated with adverse clinical outcomes, therefore the extraction and purification of GAGs for therapeutic applications must be strictly monitored to ensure product safety. In addition, concerns regarding transmissible spongiform encephalopathies have resulted in the removal of heparin sourced from bovine species from the market (Levieux, Rivera and Levieux, 2001; Lima *et al.*, 2011). It is therefore, reasoned that GAG extracts intended for therapeutic purposes should identified as free from transmissible pathogens. Several techniques have therefore been developed to improve the monitoring and detection of contaminant species within heparin preparations, for instance, polymerase chain reaction, immunogenic assays and spectroscopic techniques, such as and infrared, ultraviolet circular dichroism and nuclear magnetic resonance (Levieux, Rivera and Levieux, 2001; Liverani, Mascellani and Spelta, 2009; Rudd, Skidmore, Guimond, Cosentino, *et al.*, 2009; Rudd, Skidmore, Guimond, Holman, *et al.*, 2009; Rudd, Yates and Hricovini, 2009; Keire *et al.*, 2010; Pan *et al.*, 2010; Lima *et al.*, 2011; Devlin, Mauri, *et al.*, 2019; Devlin, Mycroft-west, *et al.*, 2019). In particular spectroscopic techniques offer robust, time effective and sensitive methods for monitoring heparin preparations for contaminant species. As such, several

spectroscopic techniques have been utilised to monitor the extraction of GAG from non-mammalian sources, in addition to assessing the purify of the resulting extracts, see section 2.2.

4.1.2. Chapter aims

The aims of this chapter are to extract GAGs from a variety of non-mammalian, aquatic species, and establish their constituent GAG carbohydrate profiles. Subsequent to the successful extraction and characterisation of the crude GAGs, BACE-1 inhibitory activity assays will be established using a fluorescent, peptide-based, FRET assay (section 3.1.4). The crude extracts will be further fractionated in order to isolate components that possess high BACE-1 inhibitory activity.

4.2. Results

4.2.1. Extraction of glycosaminoglycans from non-mammalian species.

Glycosaminoglycans extracts were obtained from the tissue of ten non-mammalian aquatic species, which met the aforementioned criteria; *P. pelagicus*, *L. opalescens*, *M. merluccius*, *C. batrachus*, *G. morhua*, *M. aeglefinus*, *O. gorbuscha*, *P. hypophthalmus*, *S. pilchardus* and *L. vannamei* (Table 12), utilising the process summarised in Figure 13.

Briefly, tissue was delipidated by homogenisation and incubation with an excess of acetone, prior to being recollected via centrifugation. The remaining tissue was left to dry and subsequently subjected to proteolytic digestion for 24 hours to release GAG chains from their constituent proteoglycans, prior the removal of debris by

centrifugation. The collected supernatant was subjected to batch strong anion exchange chromatography utilising Amberlite IRA-900 resin (hydroxide counter ion form) to capture and partially purify GAGs from other macromolecules present within the supernatant of the digestion product. Crude glycosaminoglycans were then eluted from the Amberlite IRA-900 resin with 3M NaCl, which had previously received excessive washes with dH₂O (60°C) and 1M NaCl (r.t), to remove weakly bound material. Crude GAGs extracts were then precipitated from the eluate by the addition of an equal volume of methanol (v/v; -20°C). Precipitates were finally collected by centrifugation, resuspended in dH₂O and dialyzed against dH₂O in order to remove contaminating salts, prior to lyophilisation. The yield of the crude extracts obtained were between ~10-20 mg.Kg⁻¹ of the original wet tissue (summarised in Table 12).

Table 12. Yield of crude extracts.

Species	Common name	Initial tissue weight (Kg)	Crude extract (mg)	mg.Kg ⁻¹
<i>P. pelagicus</i>	Atlantic pilchard	2	31	13
<i>M. merluccius</i>	Pink salmon	11	189	17
<i>C. batrachus</i>	Whiteleg	7	110	15
	Shrimp			
<i>M. aeglefinus</i>	Blue Crab	8	147	18
<i>O. gorbuscha</i>	European Hake	3	24	7
<i>P. hypophthalmus</i>	Walking Catfish	7	128	19
<i>S. pilchardus</i>	Haddock	3	63	19
<i>L. vannamei</i>	Iridescent shark	3	41	12
	catfish			

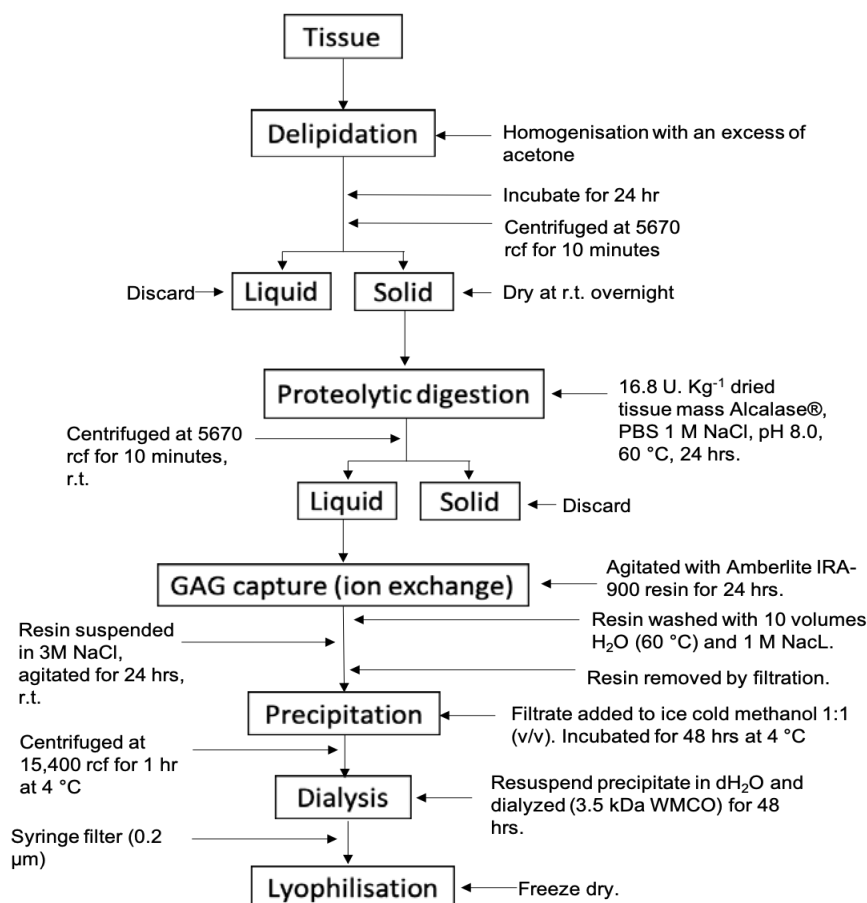


Figure 13: Crude glycosaminoglycan extraction process. Tissue was homogenised with an excess of acetone, incubated at r.t. for 24 hours prior to centrifugation at 5670 rcf for 10 minutes. The delipidated tissue was dried at r.t overnight and subsequently digested with a non-specific protease (PBS 1M NaCl, pH 8.0 at 60°C for 24 hrs) to liberate glycosaminoglycan chains. Glycosaminoglycans were then captured utilizing Amberlite IRA- 900 anion exchange resin under agitation for 24 hrs. The resin was then washes with 10 volumes of H₂O at 60°C followed by 10 volumes of 1M NaCl. Finally bound material was eluted with 3M NaCl and precipitated with ice cold methanol (1:1 v/v) for 48 hrs at 4 °C. Precipitated material was collected via centrifugation at 15,400 rcf for 1 hr at 4°C, resuspended

To determine the presence of GAGs within each crude extract, samples were initially subjected to agarose gel electrophoresis in 1,3-diaminopropane buffer (pH 9.0) and the migration of the constituents compared to that of known heparin, HS, CS and DS standards. To further assess the GAG composition within each crude extract, samples were subjected to ATR-FTIR and circular dichroism spectroscopy, coupled with PCA. The presence of GAGs and the approximate percentage of each sub-type, within each extract was finally estimated utilising ¹H and ¹H-¹³C NMR spectroscopy.

4.2.1.1. *P. pelagicus*

When subjected to agarose gel electrophoresis the crude extract obtained from *P. pelagicus* was observed to have a similar electrophoretic mobility to mammalian HS/heparin, with no bands corresponding to either monosulphated CS (CSA/CSC), disulphated CS (CSD) or dermatan sulphate (DS) (Figure 14). This suggests that the crude *P. pelagicus* extract contains GAGs, which are primarily HS/heparin like in nature.

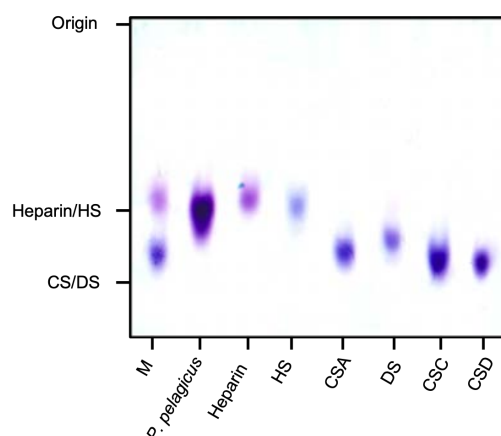


Figure 14:The electrophoretic mobility of 20 µg crude GAG extract obtained from *P. pelagicus* compared to bona fide glycosaminoglycans; heparin, heparan sulphate (HS), dermatan sulphate (DS) and chondroitin sulphate A, C and D (CSA, CSC and CSD, respectively), using agarose gel electrophoresis in 50 mM 1,3-diaminopropane buffer. M = mixture of CSA and heparin.

spectroscopy was employed. The ATR-FTIR spectra of the crude *P. pelagicus* extract contained several features representative of GAGs, with peaks corresponding to S=O, symmetric carbonyl stretching and asymmetric stretching at $\sim 1248\text{ cm}^{-1}$, 1430 cm^{-1} and 1635 cm^{-1} , respectively (Figure 15, Figure 16)(Mainreck *et al.*, 2011; Devlin, Mauri, *et al.*, 2019; Devlin, Mycroft-West, *et al.*, 2019). The peak shoulder observed at 1559 cm^{-1} has also previously been assigned to coupled C-N vibrations of N-acetyl (amide) groups, a characteristic feature of GAGs (*idem*).

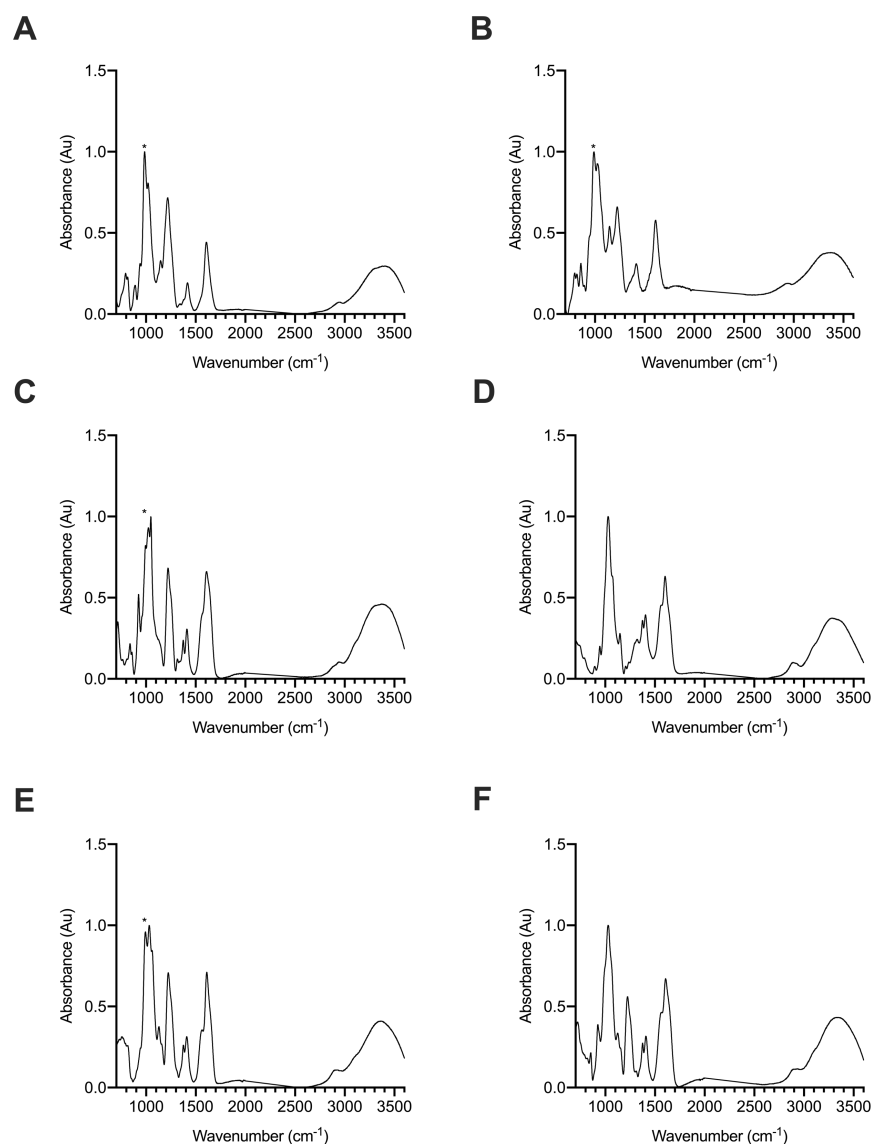


Figure 15: ATR-FTIR spectra of glycosaminoglycans. (A) heparin, (B) HS, (C) DS, (D) HA, (E) CSC, (F) CSA. * Peak at 990 cm^{-1} .

Notably, the ATR-FTIR spectra of HS exhibits a peak at 990 cm^{-1} with a peak shoulder at 1025 cm^{-1} . This is the reverse in the ATR-FTIR spectra of CS, where the main peak occurs at 1025 cm^{-1} and the peak shoulder at 990 cm^{-1} (Figure 15). Bands in the region of 1200-900 cm^{-1} have previously been assigned to the C-O-C glycosidic bond stretches (Tipson, 1968; Grant et al., 1991; Devlin et al., 2019), therefore the differences observed between CS and HS in this region could be attributed to differences in glycosidic bond linkages between these GAGs.

The crude extract obtained from *P. pelagicus* contained a split peak at 990 cm⁻¹ and 1025 cm⁻¹, with the former peak being more prominent. This could suggest that the crude *P. pelagicus* extract contains a higher proportion of HS than CS. There are also differences in the intensities of peaks at ~1450 cm⁻¹ and 1600 cm⁻¹ between HS and CS samples (Figure 15), with *P. pelagicus* crude extract more closely resembling HS in these regions (Figure 16). The peak shoulder present at ~1370 cm⁻¹ has also been suggested to be indicative of a HS/CS mixture, indicating that the crude *P. pelagicus* sample may contain a mixture of these GAGs (Devlin, Mycroft-West, *et al.*, 2019). The differences between the spectra in the region of >3000 cm⁻¹ (OH stretch region) are associated with the changeable moisture levels introduced during sample acquisition and not likely to result from underlying structural differences.

As previously mentioned, it is not currently possible to provide complete assignment of the ATR-FTIR spectra of GAGs. Therefore, the ATR-FTIR spectra of the *P. pelagicus* crude extract was subjected to post-acquisition multivariate analysis against a library of known GAGs comprising 185 heparins, 31 HS, 44 CSs and DSs, 11 HAs and 6 OSCs, using PCA (Devlin, Mycroft-West, *et al.*, 2019); Figure 16C).

Post-acquisition PCA of the ATR-FTIR spectral library of GAGs distinctly separates each sub-type, with HA, HS and heparin (glucosaminoglycans) residing in the top left portion of the plot. Within this region heparin, HS and HA are further separated along both principal components (PC1 and PC2), with HA residing at the uppermost position as opposed to heparin which resides at the lowest point. Heparan sulphate is variably distributed between these points, possibly owing to separation based upon degree of

sulphation (DoS; (Devlin, Mycroft-West, *et al.*, 2019). The galactosaminoglycans, CS and DS, are separated into a distinct region, residing towards the bottom right portion of the plot, with PC2 further separating CS from DS (Figure 16C).

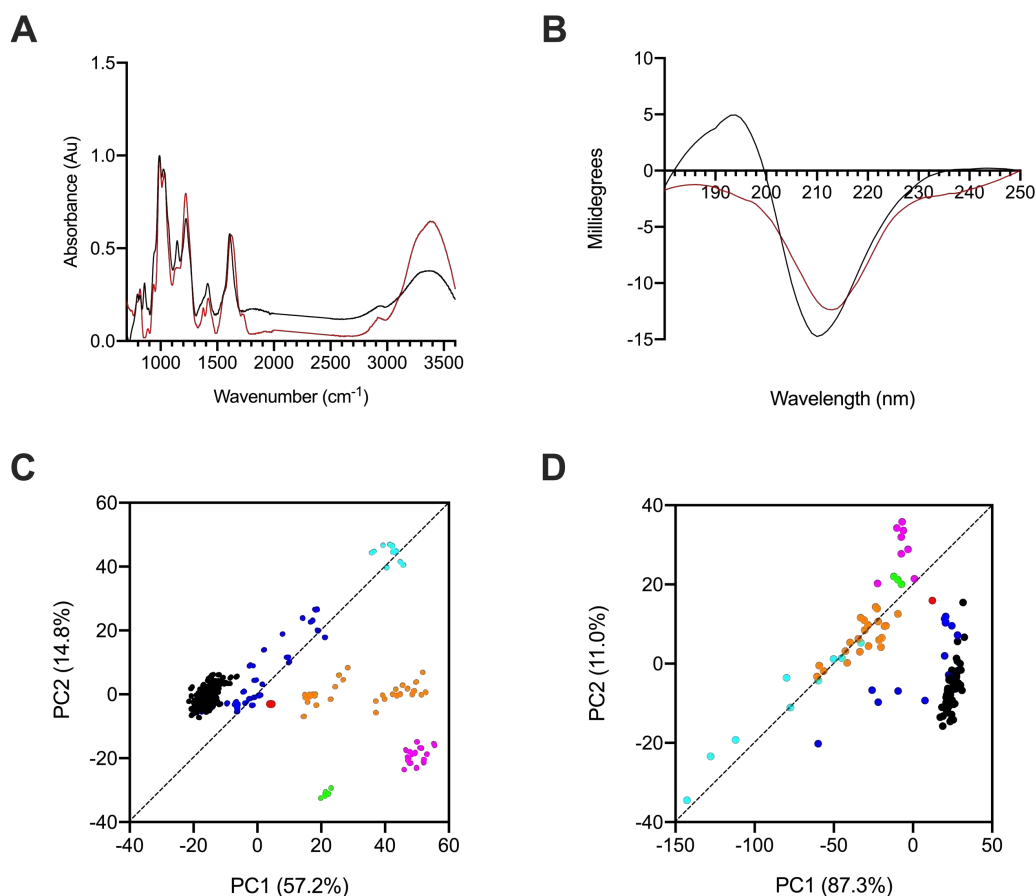


Figure 16: ATR-FTIR and CD spectra of crude *P. pelagicus*, coupled with PCA. (A) ATR-FTIR and **(B)** circular dichroism spectra of crude *P. pelagicus* extract (red) and HS (black). **(C)** Principal component analysis (PCA) score plot for PC1 vs. PC2 of A and **(D)** of B against a bone fide GAG library. Heparin, black; HS, blue; CS, orange; DS, magenta; HA, cyan; over-sulphated CS, green; crude *P. pelagicus*

Comparison of the crude *P. pelagicus* extract against the same GAG library located the sample within the region containing mammalian HS. Principle component 1 which converts 57.2% separates the *P. pelagicus* crude extract slightly towards the region containing CS as opposed to heparin. This region has previously been identified with heparin samples containing CS contaminants (Devlin, Mycroft-West, *et al.*, 2019).

Principle component 2, covering 14.8% of the variance, located the crude *P. pelagicus* towards heparin and HS samples containing a greater DoS.

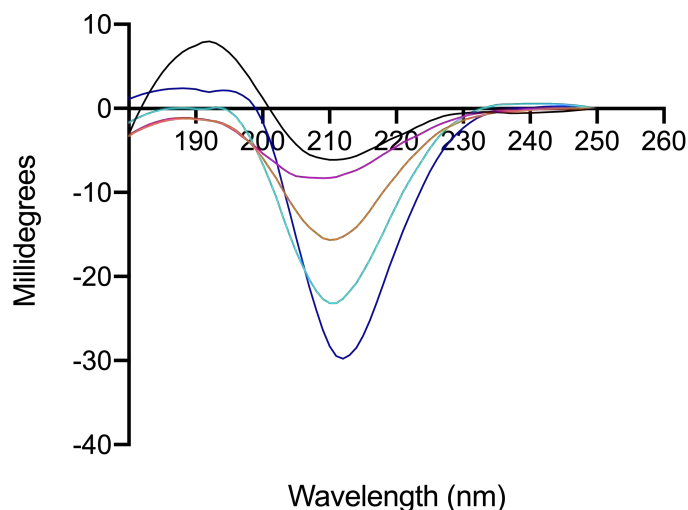


Figure 17: Circular dichroism spectra of glycosaminoglycans. Heparin, black; DS, magenta; CS, orange; HA, cyan; HS, blue.

The circular dichroism spectra of GAGs are sensitive to uronic acid conformation (Rudd, Skidmore, Guimond, Holman, *et al.*, 2009), glycosidic linkage and levels of sulphate modifications (Stone, 1971). Glycosaminoglycans therefore, exhibit distinct CD spectra, which can be used to differentiate between subtypes. Furthermore, PCA has previously been employed to further discriminate between different GAGs based upon CD spectral analysis (Rudd *et al.*, 2008; Rudd, Skidmore, Guimond, Cosentino, *et al.*, 2009; Rudd, Skidmore, Guimond, Holman, *et al.*, 2009). The CD spectra of all GAGs exhibited a negative band at ~210 nm, albeit with differing intensities: HS>HA>CS>DS>heparin as previously reported (Figure 17) (T. R. Rudd *et al.*, 2007; Rudd *et al.*, 2008; Rudd, Skidmore, Guimond, Cosentino, *et al.*, 2009; Stanley and Stalcup, 2011). A slight redshift was also observed for heparin and HS in comparison to other GAGs. A second band was observed at ~190 nm, which in the case of heparin and HS was positive, whereas for CS,

DS and HA this band was negative. This is also in agreement with the literature, which assigns the contrasting signs of ellipticity to differences in glycosidic linkage and sulphation levels (Rudd, Yates and Hricovini, 2009). The CD spectra of the crude *P. pelagicus* extract exhibited a negative band at ~212 nm and 190 nm, suggesting that the crude extract contains a larger proportion of CS/DS than indicated by FTIR spectroscopy (Figure 16).

Post-acquisition PCA was further employed to compare the CD spectrum of the crude *P. pelagicus* with that of known GAGs. Principal component analysis separated each GAG into discrete regions with heparin and HS residing within the bottom portion of the plot and the remaining GAGs separating towards the middle to-top portion of the plot. Comparison of PC1 and PC2 (converging 98.3 % of the variance) separated the crude *P. pelagicus* extract within the regions associated with heparin/HS and CS/DS (Figure 16). This supports that the crude extract may contain a larger proportion of CS/DS than initially indicated by FTIR and agarose gel electrophoresis.

1D ^1H and 2D ^1H - ^{13}C HSQC NMR was then employed to confirm the GAG composition of the crude *P. pelagicus* extract (Figure 18). The presence of both CS, DS and heparin/HS within the crude extract can be demonstrated by the respective resonances at 2.02 ppm, 2.06 ppm and 2.04 ppm in the ^1H spectra (Figure 18, Table 10, Table 11). The ^1H signals between 5.4 -5.3 ppm corresponds to the anomeric proton of glucosamine (Figure 18, Table 10). In addition, the peak observed at 3.28 ppm and 5.2ppm corresponds to position 2 of NS-glucosamine (A2) and the ^1H bonded to the anomeric carbon of IdoA at ~5.2 ppm (I1) further confirming the presence of HS/heparin within

the crude sample (Figure 18, Table 10). Peaks corresponding to CS can also be observed at ~3.4 ppm, ~4.5 ppm and ~4.6, which can be tentatively assigned to U2, Gal1 and U1, respectively; due to overlapping resonances at 4.5 ppm with the ^1H of the anomeric carbon of GlcA in HS (Table 11, Figure 18). Integration of the A2 and N-acetyl peaks from the ^1H spectra peak indicates that the crude sample contains ~70% HS/heparin, which contains >50% N-sulphate modification, ~30% CS and <1% DS. This is supported by the lower intensity of the signals associated with CS and DS within the ^1H spectra (Figure 18).

As a result of the overlapping resonances of both CS and HS further characterisation based the ^1H spectrum was precluded. ^1H - ^{13}C HSQC NMR was therefore utilised to resolve some of the overlapping signals and confirm assignments made by ^1H -NMR. Integration of the N-acetyl and A2 signals from the ^1H - ^{13}C HSQC indicated that the crude *P. pelagicus* sample was composed of ~60% HS/heparin and 40% CS. Integration of the N-Acetyl and A2 signals attributed to HS indicated that ~66% of the HS component is N-sulphated. In addition, the signals attributed to position 6 of galactosamine and glucosamine could be detected at ~4.2-4.3/68-67 and 3.8-3.77/62-61 ppm, corresponding to 6S or 6OH, respectively (Figure 18). This indicates the presence of 6-sulphation on both the CS and HS/heparin components of the extract. No signals attributable to anomeric region were detected due to the low resolution of the spectra.

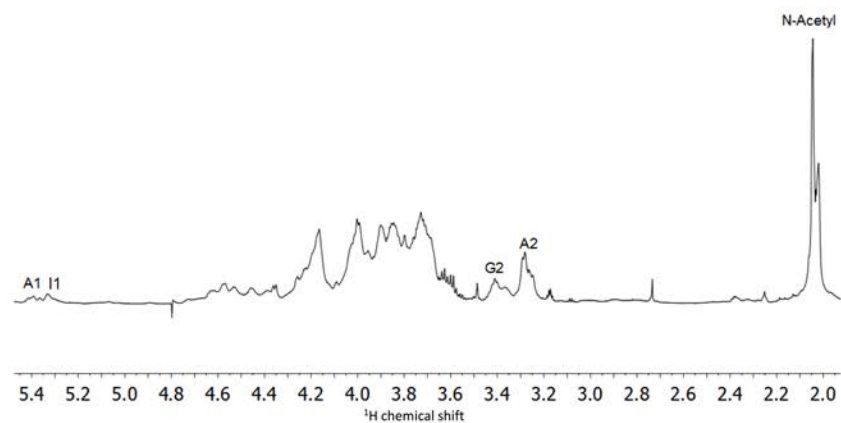
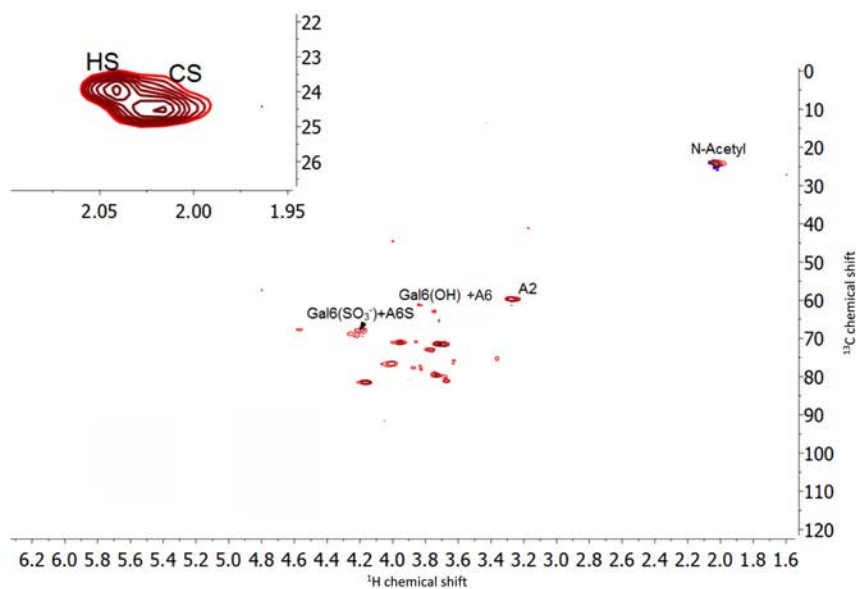
A**B**

Figure 18: (A) ^1H and (B) ^1H - ^{13}C HSQC NMR spectra of crude *P. pelagicus* extract. Major signals associated with HS and CS are indicated. Spectral integration was performed using labelled signals. Key: galactosamine, Gal; glucosamine, A; glucuronic acid, G; iduronic acid, I. Spectra recorded at 298K.

3.2.1.2. *L. vannamei*

When subjected to agarose gel electrophoresis the crude extract obtained from *L. vannamei* separated into two distinct bands, with the major component corresponding to the migration distance of HS/heparin standards. The minor band exhibited the closest electrophoretic mobility to CS standards, however with slightly increase migration (Figure 19). This suggests that the crude *L. vannamei* extract contains a mixture of GAGs with the major component being HS/heparin like in nature.

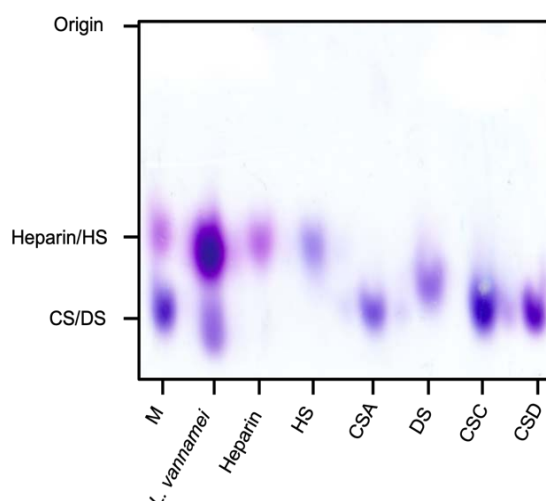


Figure 19:The electrophoretic mobility of 20 μ g crude GAG extract obtained from *L. vannamei* compared to glycosaminoglycan standards; heparin, heparan sulphate (HS), dermatan sulphate (DS) and chondroitin sulphate A, C and D (CSA, CSC and CSD, respectively), using agarose gel electrophoresis in 50 mM 1,3-diaminopropane buffer. M = mixture of CSA and heparin.

The ATR-FTIR spectra of the crude *L. vannamei* extract also contained peaks corresponding to S=O, amine, symmetric carbonyl stretching and asymmetric stretching at 1230 cm^{-1} , 1559 cm^{-1} , 1430 cm^{-1} and 1635 cm^{-1} , respectively (Figure 20, Figure 15)(Mainreck *et al.*, 2011; Devlin, Mycroft-West, *et al.*, 2019). Indicating the presence of sulphated, uronic acid containing GAGs within the sample. Additionally, the crude *L.*

vannamei extract contained a split peak at 990 cm^{-1} and 1025 cm^{-1} , with the latter being more prominent. This could suggest the crude *L. vannamei* extract contains a higher proportion of CS than originally indicated by agarose gel electrophoresis, however the extract more closely resembles HS than CS at $\sim 1450\text{ cm}^{-1}$ and 1600 cm^{-1} (Figure 20).

The ATR-FTIR spectra of the crude *L. vannamei* extract was subjected to PCA against the previously described library of GAGs. Comparison of PC1 and PC2, covering $\sim 72\%$ of the variance, located the crude *L. vannamei* extract close to the region containing mammalian HS. Principle component 1, which covers $\sim 57\%$ of the variance separates the crude extract slightly towards the region containing CS/HS as opposed to heparin

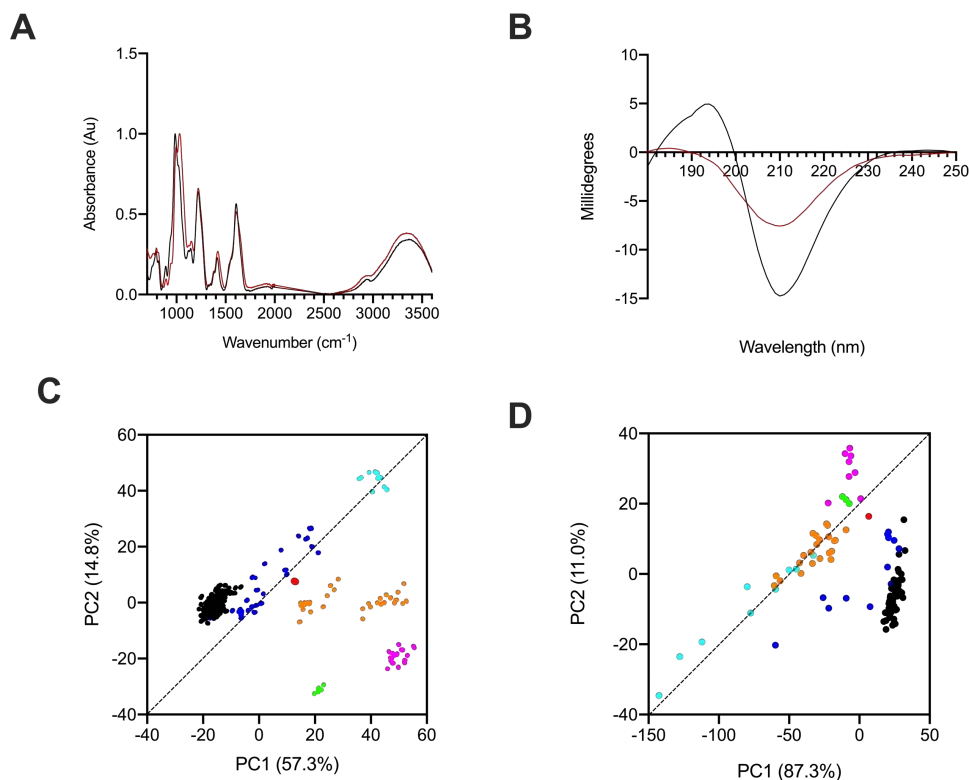


Figure 20: ATR-FTIR and CD spectra of crude *L. vannamei* extract, coupled with PCA. (A) ATR-FTIR and (B) circular dichroism spectra of crude *L. vannamei* extract (red) and HS (black). (C) Principal component analysis (PCA) score plot for PC1 vs. PC2 of A and (D) of B against a bone fide GAG library. Heparin, black; HS, blue; CS, orange; DS, magenta; HA, cyan; over-sulphated CS, green; crude *L. vannamei* extract, red.

(Figure 20). The ATR-FTIR spectra of the crude *L. vannamei* therefore supports that the extract is composed of a mixture of HS and CS.

The CD spectra of the crude *L. vannamei* extract exhibited a negative band at ~ 210 nm and a minor positive band at 190 nm, features widely attributed to the CD spectra of heparin and HS (Figure 20). Post-acquisition PCA of the crude *L. vannamei* CD spectra located the extract between the CS and HS regions, again suggesting that the sample contains a mixture of these GAGs (Figure 20).

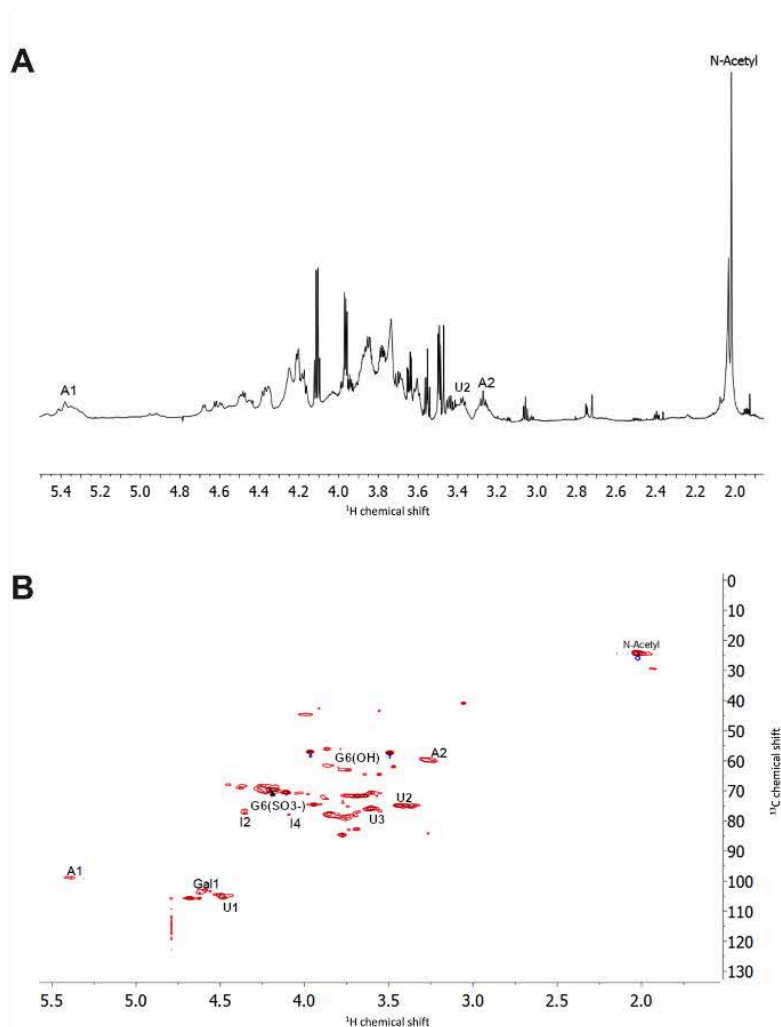


Figure 21: (A) ^1H and (B) ^1H - ^{13}C HSQC NMR spectra of crude *L. vannamei* extract. Major signals associated with HS and CS are indicated. Spectral integration was performed on the HSQC using labelled signals. Key: galactosamine, Gal; glucosamine, A; glucuronic acid, U; iduronic acid, I; galactosamine and glucosamine, G. Spectra recorded at 298K.

^1H and ^1H - ^{13}C HSQC NMR was employed to confirm the GAG composition of the *L. vannamei* extract. The presence of both CS, and heparin/HS within the crude extract can be demonstrated by the respective resonances at 2.02 ppm and 2.04 ppm (Figure 21). A small proportion of DS can also be detected at 2.08 ppm in the ^1H spectrum (Figure 21). The signals at 5.4 – 5.3 ppm, corresponding to the anomeric proton of glucosamine, are present in the ^1H NMR spectrum of the crude *L. vannamei* extract, indicating the presence of HS/heparin. Furthermore, the signal corresponding to position 2 of NS glucosamine (A2) is present, supporting the presence of HS/heparin within the crude *L. vannamei* sample. Integration of the A2 and N-acetyl peaks in the ^1H spectra suggests that the sample is composed of ~66% HS, ~30% CS and <5% DS (Figure 21). While some signals were resolved in the ^1H spectrum, attributable to glucosamine and glucuronic acid, the overlapping resonances associated with different GAGs classes prevents further characterisation based upon the ^1H spectrum. ^1H - ^{13}C HSQC NMR was therefore utilised to resolve overlapping signals and to further corroborate the GAG composition (Figure 21). The integration of N-acetyl and A2 signals of the ^1H - ^{13}C HSQC spectra revealed that the extract is composed of approximately 53% CS, 47% HS/Heparin and <5% DS, with the HS component being ~65% N-sulphated. It should be noted that the ^1H - ^{13}C HSQC spectral resolution was poor likely affecting the accuracy of the integrals. The ^1H - ^{13}C HSQC spectra resolved signals that can be tentatively attributed to IdoA at ~4.4-77.5 ppm (I2), 4.1/78 ppm (I4) and ~4.8/71 ppm (I5), potentially indicating the presence of epimerised uronic acid residues. In addition, the presence of signals attributed to glucuronic acid were observed, for instance the anomeric carbon at ~4.5/105 ppm. The presence of signals attributed to the anomeric carbon of both galactosamine and glucosamine were also detected at ~4.6/104 ppm and ~5.4/100

ppm, respectively. In addition, the signals attributed to position 6 of galactosamine and glucosamine were observed at $\sim 4.2\text{--}4.3/68\text{--}67$ and $3.8\text{--}3.77/62\text{--}61$ ppm, corresponding to 6S or 6OH. The poor spectra resolution prevented integration of the $\text{Gal6}(\text{SO}_3^-)$ and $\text{Gal6}(\text{OH})$ signals however the signal indicates suggests that both CS and HS components contain significant levels of 6S. Therefore, both ^1H and $^1\text{H}\text{--}^{13}\text{C}$ NMR spectroscopy indicate that the crude *L. vannamei* is composed of a mixture of CS and HS with significant sulphate modifications within both components.

4.2.1.3. *S. pilchardus*

When subjected to agarose gel electrophoresis the crude extract obtained from *S. pilchardus* was observed to have similar electrophoretic mobility to CS and DS. Minimal material present within the crude compound was found to possess similar electrophoretic mobility to HS/heparin (Figure 22). This suggest that the crude *S. pilchardus* extract is composed largely of galactosaminoglycans.

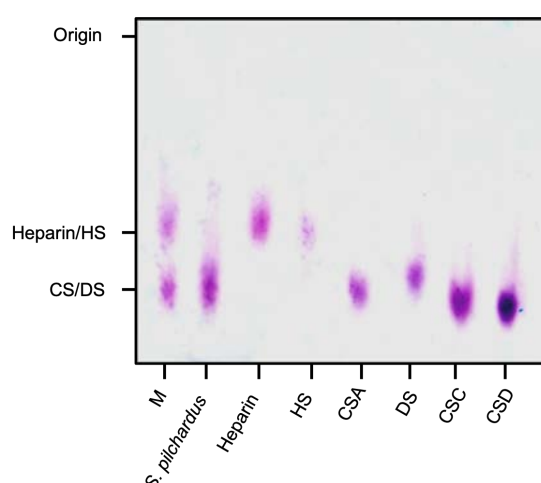


Figure 22:The electrophoretic mobility of 20 μg crude GAG extract obtained from *S. pilchardus* compared to bona fide glycosaminoglycans; heparin, heparan sulphate (HS), dermatan sulphate (DS) and chondroitin sulphate A, C and D (CSA, CSC and CSD, respectively), using agarose gel electrophoresis in 50 mM 1,3-diaminopropane buffer. M = mixture of CSA and heparin. Spectra recorded at 298K.

To further confirm the presence of GAGs within the crude *S. pilchardus* extract ATR-FTIR spectroscopy was employed. The ATR-FTIR spectra crude *S. pilchardus* also contained peaks corresponding to S=O, amide, symmetric carbonyl stretching and asymmetric stretching at 1230 cm^{-1} , 1559 cm^{-1} , 1430 cm^{-1} and 1635 cm^{-1} , respectively (Figure 23)(Mainreck *et al.*, 2011; Devlin, Mycroft-West, *et al.*, 2019). Furthermore, a band can be observed at $\sim 820 \text{ cm}^{-1}$ of greater intensity than at 850 cm^{-1} , which may be indicative of the presence of 6-O-sulphated CS (CSC; *idem*). This supports that the extract is composed of sulphated, uronic acid containing GAGs. Additionally, the *S. pilchardus* extract contained a split peak at 990 cm^{-1} and 1025 cm^{-1} , with the latter being more prominent, supporting that the extract is predominantly composed of CS. This was also confirmed by post-acquisition PCA analysis of the ATR-FTIR spectra of the crude *S. pilchardus* extract, which located the sample in the region corresponding to CS, when comparing PC1 and PC2 (covering $\sim 72\%$ of the variance; Figure 23).

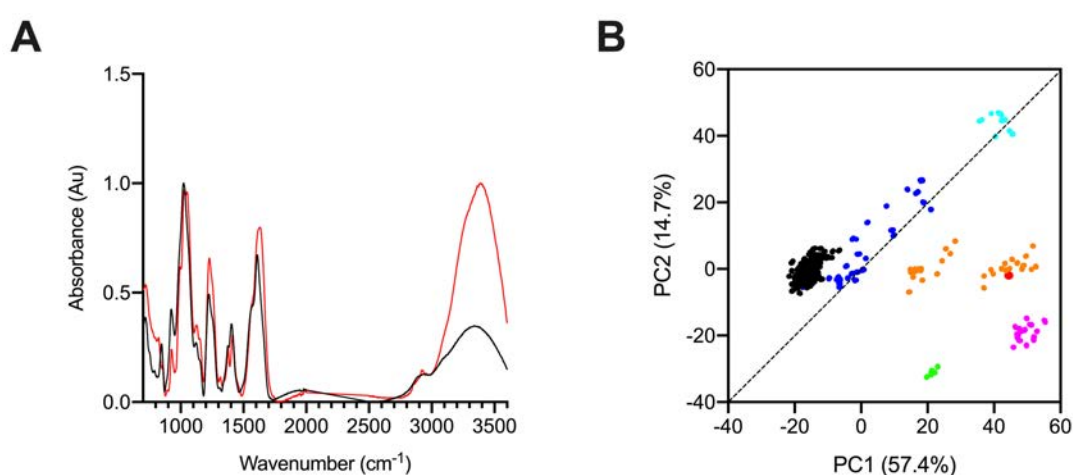


Figure 23: ATR-FTIR spectra and PCA of crude *S. pilchardus* extract. (A) ATR-FTIR spectra of crude *S. pilchardus* extract (red) and CS (black). (B) Principal component analysis (PCA) score plot for PC1 vs. PC2 of A. Heparin, black; HS, blue; CS, orange; DS, magenta; HA, cyan; over-sulphated CS, green; crude *S. pilchardus* extract, red.

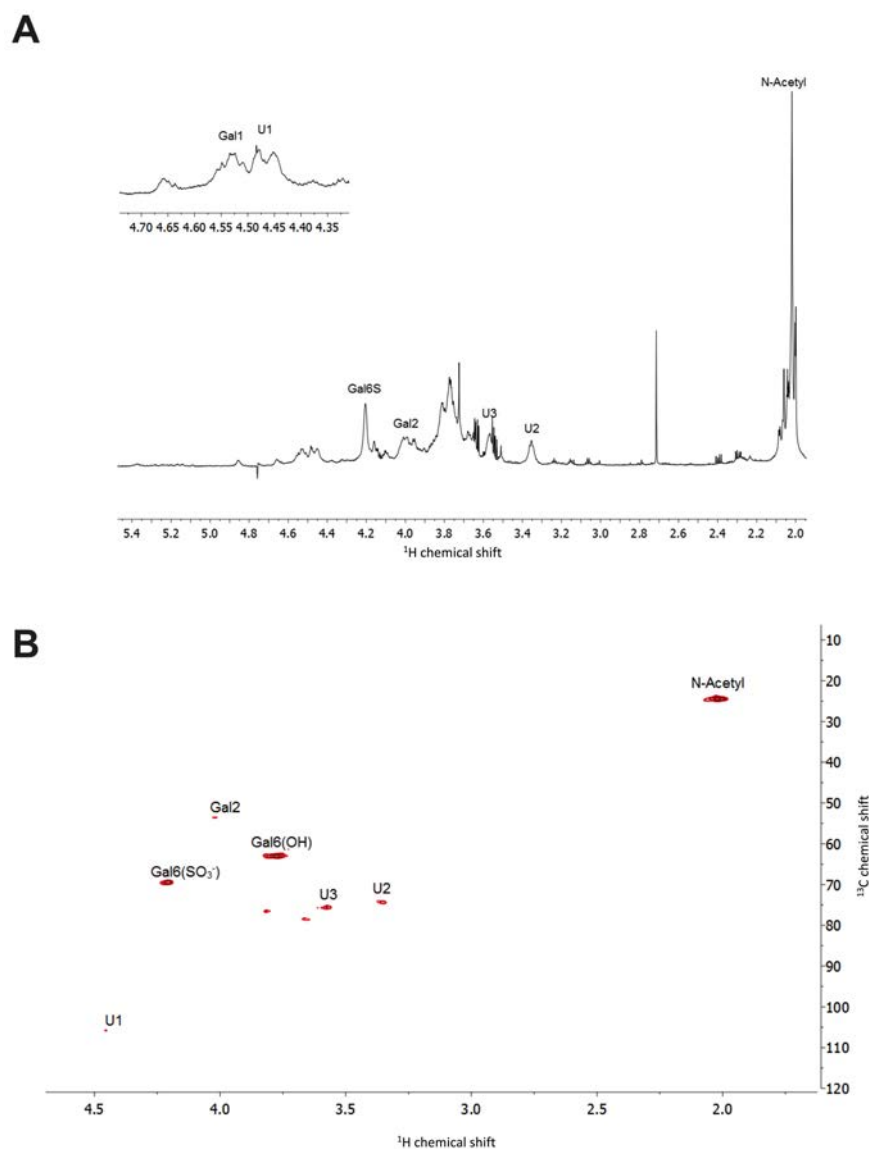


Figure 24: (A) ^1H and (B) ^1H - ^{13}C HSQC NMR spectra of crude *S. pilchardus* extract. Major signals associated with HS and CS are indicated. Spectral integration was performed on the HSQC using labelled signals. Key: galactosamine; Gal, uronic acid; U.

^1H and ^1H - ^{13}C HSQC NMR was employed to confirm the GAG composition of the crude *S. pilchardus* sample. ^1H NMR indicated that the crude sample is composed primarily of CS with a small proportion of heparin/HS and DS, with resonances at 2.02, 2.04 and 2.06 ppm, respectively (Figure 24). Integration of the N-Acetyl signals indicated that the sample is composed of 78% CS, 10% HS and 12% DS. This is confirmed by detection of signals corresponding to the anomeric protons of galactosamine and glucuronic acid at

~4.58 ppm and 4.48 ppm (indicated as Gal1 and U1; Figure 24), and presence of minor anomeric protons corresponding to glucosamine and iduronic acid (at ~5.4 and 5.2 ppm). Additionally, the signal at 4.2 ppm corresponding to position 4 of Gal(4OH) and can be indicative of 6-sulphation, supporting that the CS component of the *S. pilchardus* extract contains primarily CSC units as opposed to CSA. A signal corresponding to 4 sulphated Gal can also be observed at ~4.9 ppm, however this is less intense than that of the signal corresponding to Gal(4OH). ^1H - ^{13}C HSQC NMR (Figure 24) was used to further resolve overlapping signals and confirm the primary composition of the *S. pilchardus* extract. Integration of N-acetyl signals indicated confirmed that crude extract is primarily composed of CS at > 75%. Furthermore, integration of Gal(6S) and Gal6(OH) signals indicated that extract contains ~34% CSC units. No signals attributed to Gal4S were detected, however it is of note that the signal corresponding to this sulphation site occurs within the region of H₂O suppression.

3.2.1.4. *M. aeglefinus*

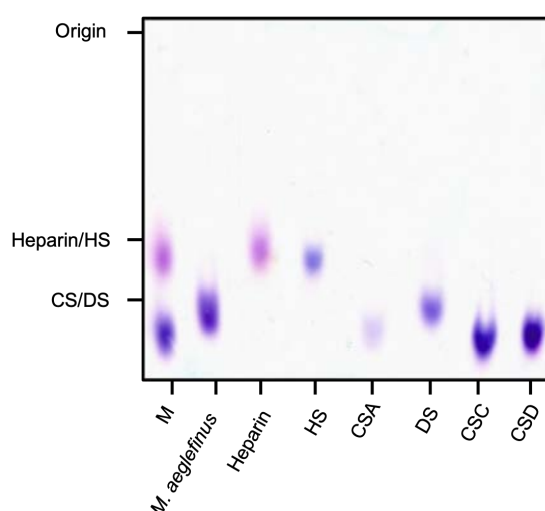


Figure 25: The electrophoretic mobility of 20 µg crude GAG extract obtained from *M. aeglefinus* compared to bona fide glycosaminoglycans; heparin, heparan sulphate (HS), dermatan sulphate (DS) and chondroitin sulphate A, C and D (CSA, CSC and CSD, respectively), using agarose gel electrophoresis in 50 mM 1,3-diaminopropane buffer. M = mixture of CSA and heparin.

When subjected to agarose gel electrophoresis the crude extract obtained from *M. aeglefinus* was observed to have a similar electrophoretic mobility to DS/CS, with the migration distance being closer to that of DS (Figure 25). No bands corresponding to HS/heparin were detected, suggesting that the crude *M. aeglefinus* sample is composed primarily of galactosaminoglycans.

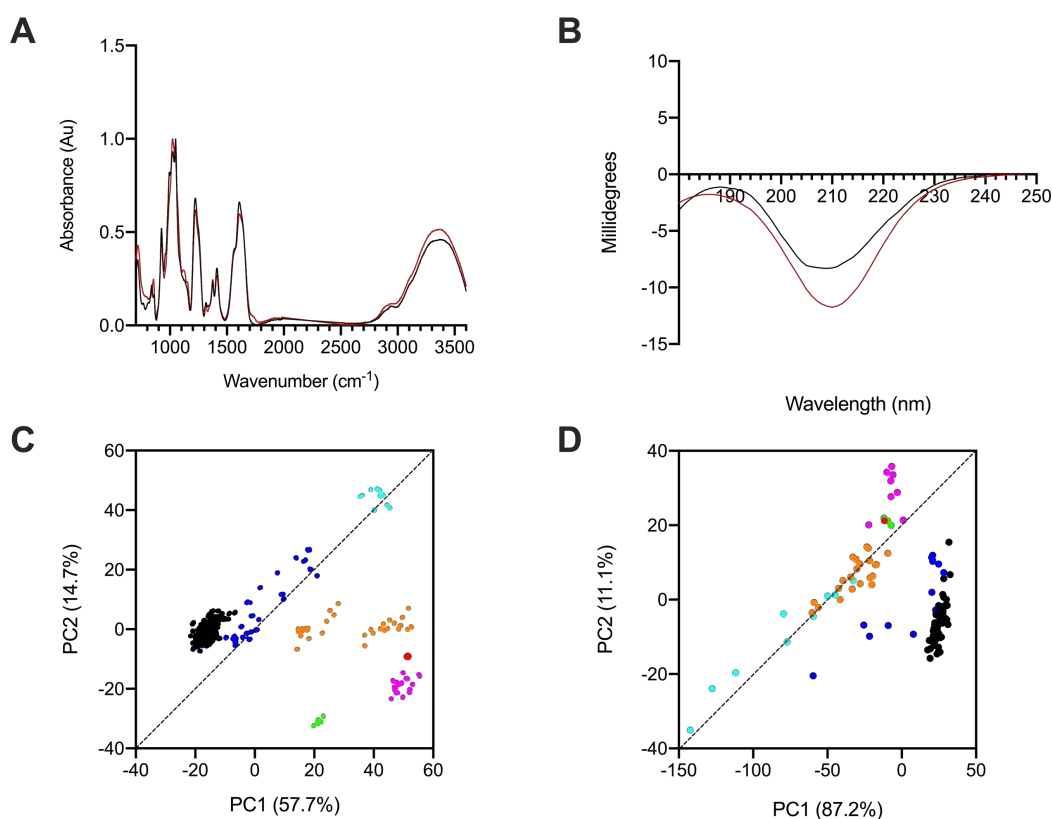


Figure 26: ATR-FTIR and CD spectra of crude *M. aeglefinus*, coupled with PCA (A) ATR-FTIR and (B) circular dichroism spectra of crude *M. aeglefinus* extract (red) and DS (black). (C) Principal component analysis (PCA) score plot for PC1 vs. PC2 of A and (D) of B against a bone fide GAG library. Heparin, black; HS, blue; CS, orange; DS, magenta; HA, cyan; over-sulphated CS, green; crude *M. aeglefinus*

To further elucidate the GAG composition of the crude *M. aeglefinus* extract ATR-FTIR spectroscopy was employed. The common peaks attributed to sulphated uronic acid containing GAGs were also observed within the ATR-FTIR spectra of the crude *M. aeglefinus* extract, for example at 1230 cm⁻¹, 1430 cm⁻¹, 1635 cm⁻¹ and a peak shoulder at 1559 cm⁻¹ (Figure 26). A broad peak can also be observed centred at 1025 cm⁻¹ with

minor shoulders at $\sim 990\text{cm}^{-1}$ and 1045 cm^{-1} . This can also be observed in the ATR-FTIR spectra of DS, albeit to a greater extent (Figure 15, Figure 26), with the latter peak being absent in both CS and HS/heparin samples (Figure 15). Furthermore, peaks at $\sim 1450\text{ cm}^{-1}$ and 1600 cm^{-1} within the crude *M. aeglefinus* ATR-FTIR spectra more closely resemble CS/DS than HS/heparin. This may suggest that the crude *M. aeglefinus* extract is composed of a mixture of CS and DS (Figure 26). This is supported by post acquisition PCA of the crude *M. aeglefinus* ATR-FTIR spectra against the previously described GAG library, where comparison of PC1 and PC2, covering $\sim 72\%$ of the variance, located the extract between the regions associated with CS and DS (Figure 26).

The CD spectra of the crude *M. aeglefinus* extract contained two negative bands at 210 nm and 190 nm. This is in line with the CD spectral features of both CS and DS, however the intensity of the negative band at 210 nm within the CD spectra of the crude *M. aeglefinus* more closely resembles that of DS (Figure 26). In accordance with this PCA analysis of the crude *M. aeglefinus* extract against a library of GAGs located the sample within the region associated with DS and OSCS, when PC1 and PC2 were compared (covering 98% of the variance) (Figure 26).

^1H - and ^1H - ^{13}C HSQC NMR was employed to further elucidate the GAG composition of the crude *M. aeglefinus* extract (Figure 27). ^1H NMR indicated that the crude extract was primarily composed of CS with the major acetyl signal occurring at $\sim 2.02\text{ ppm}$. Several peaks of lesser intensity were also observed between 2.04 - 2.09 ppm, which could be attributed to DS and HS/heparin. Additionally, signals corresponding to U2 and U3 of GlcA were also detected at $\sim 3.3\text{ ppm}$ and 3.5 ppm , respectively. Furthermore, the

signal corresponding the Gal and GlcA anomers can be observed at ~4.5 ppm and 4.6 ppm, respectively, with only minimal signals present at resonances > 5.0 ppm. Comparison of the resonances associated with 4-suphated Gal indicates this modification is largely absent as a signal can be seen only at 4.2 ppm as opposed to ~4.8 ppm: corresponding to Gal4(OH) and Gal4(S), respectively. The signal at 4.2 ppm can also be attributed to Gal6S, therefore CSC units may be present within the crude *M. aeglefinus* extract (Figure 27).

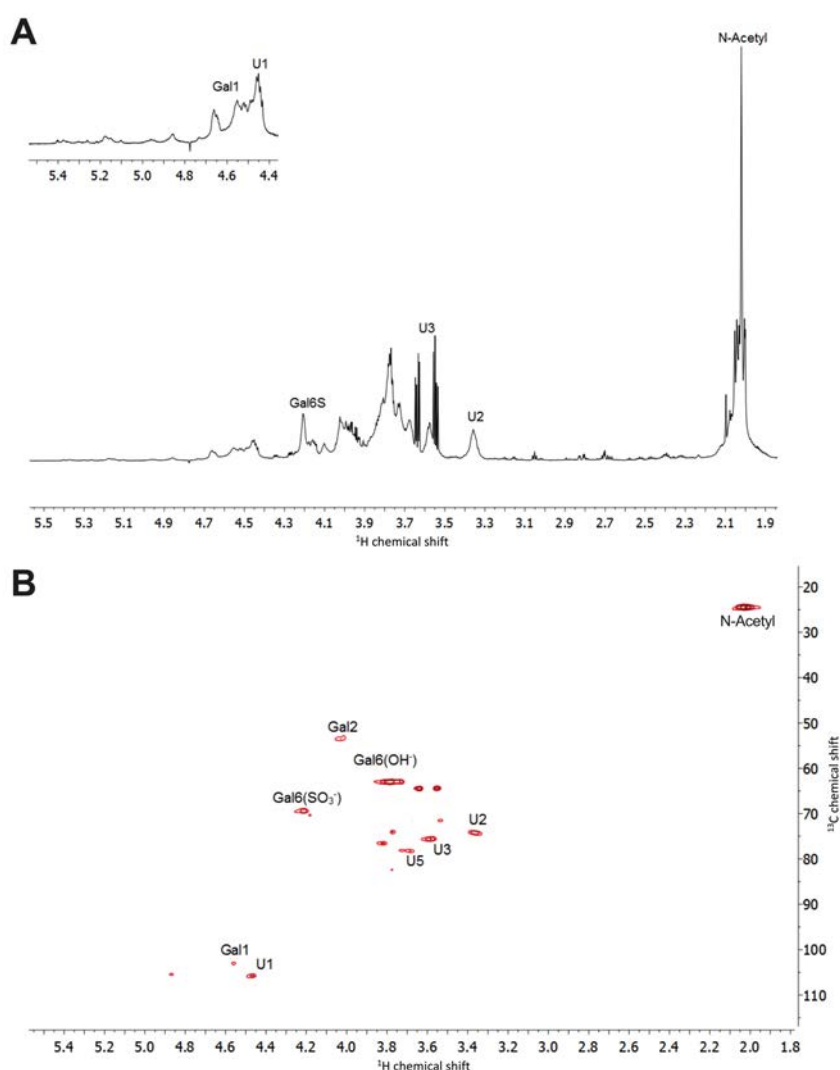


Figure 27: (A) ^1H and (B) ^1H - ^{13}C HSQC NMR spectra of crude *M. aeglefinus* extract. Major signals associated with CS are indicated. Spectral integration was performed on the HSQC using labelled signals. Key: galactosamine; Gal, uronic acid; U. Spectra recorded at 298K.

^1H - ^{13}C HSQC NMR was used to resolve overlapping signals and to further determine saccharide composition estimates using peak volume integration. The integration of N-acetyl signals was prohibited as a result of the low spectral resolution. Anomeric peaks corresponding to GlcA-Gal (4.4-4.6/103-107 ppm), an additional peak can be observed downfield at $\sim 4.9/105$ ppm, which could be attributed to IdoA-Gal. No signals attributed to heparin/HS were observed and as a result this GAG is likely present at concentrations $<5\%$ of the total sample. As a result, integration of the ^1H NMR spectra was performed, assigning the peaks in the region of 2.06 ppm to DS, providing an estimated composition of 58% CS, 42% DS. In regard to the modifications present on the CS component, no peaks were detected attributable to 4-O-sulphation at $\sim 4.9/79$ ppm. Furthermore, integration of the signals corresponding to Gal6S and GalOH indicated that the sample contains $\sim 71\%$ unsulphated CS (Figure 27). Therefore, the crude *M. aeglefinus* is primarily composed of a low sulphated CS.

3.2.1.5. *M. merluccius*

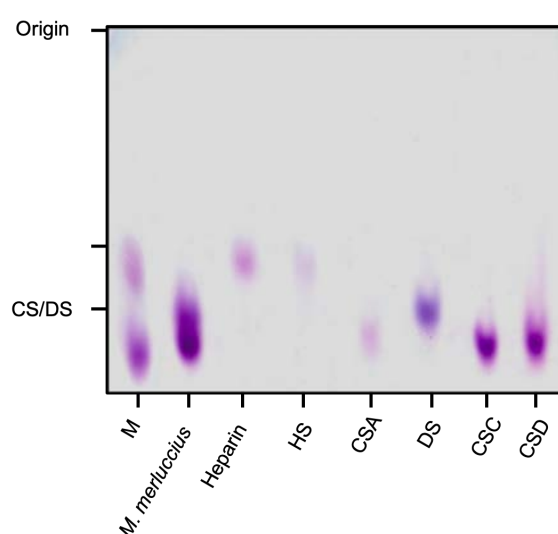


Figure 28: The electrophoretic mobility of 20 μg crude GAG extract obtained from *M. merluccius* compared to bona fide glycosaminoglycans; heparin, heparan sulphate (HS), dermatan sulphate (DS) and chondroitin sulphate A, C and D (CSA, CSC and CSD, respectively), using agarose gel electrophoresis in 50 mM 1,3-diaminopropane buffer. M = mixture of CSA and heparin.

When subjected to agarose gel electrophoresis the crude extract obtained from *M. merluccius* was observed to have similar electrophoretic mobility to CS/DS, with no bands corresponding to either HS or heparin (Figure 28). This suggests that the crude *M. merluccius* extract contains a mixture of galactosaminoglycans.

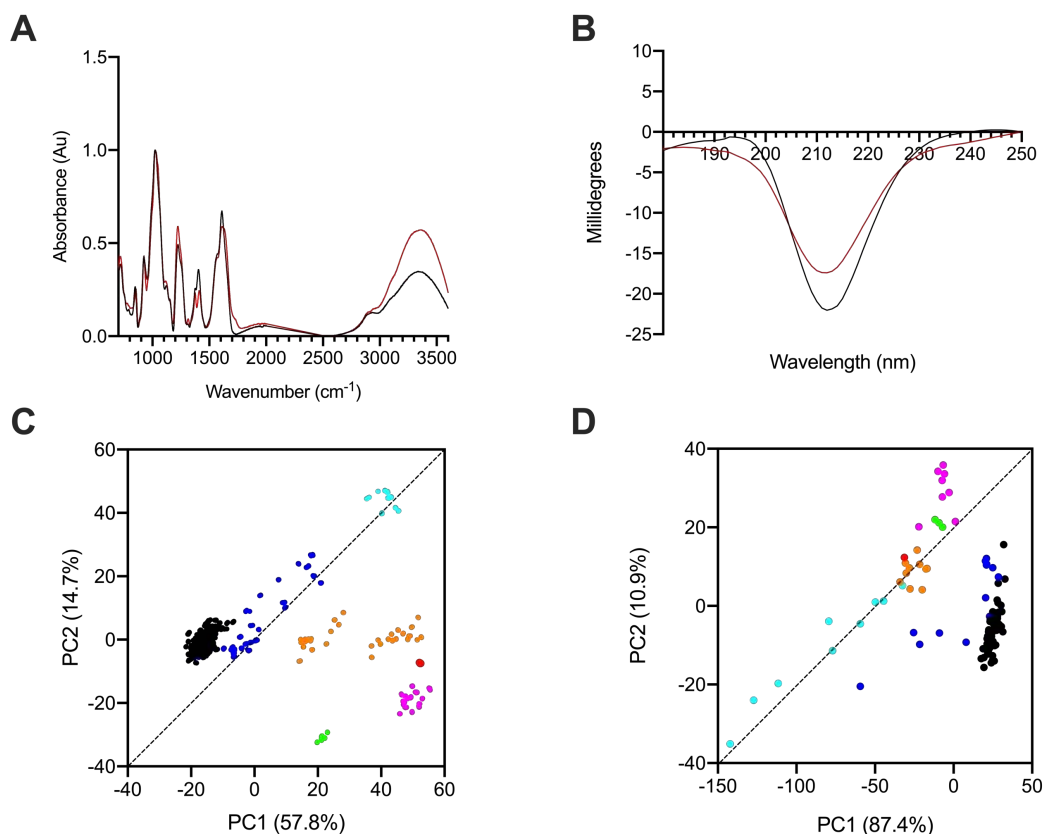


Figure 29: ATR-FTIR and CD spectra of *M. merluccius*, coupled with PCA. (A) ATR-FTIR and (B) circular dichroism spectra of crude *M. merluccius* extract (red) and CS (black). (C) Principal component analysis (PCA) score plot for PC1 vs. PC2 of A and (D) of B against a bone fide GAG library. Heparin, black; HS, blue; CS, orange; DS, magenta; HA, cyan; over-sulphated CS, green; crude *M. merluccius*

The presence of GAGs within the crude *M. merluccius* extract was further confirmed by ATR-FTIR and CD spectroscopy coupled with PCA. The ATR-FTIR spectra of the crude *M. merluccius* extract contained several features representative of sulphated uronic acid containing GAGs, for instance S=O, symmetric carbonyl stretching and asymmetric stretching and C-N vibrations at 1230 cm⁻¹, 1430 cm⁻¹, 1635 cm⁻¹ and 1559 cm⁻¹,

respectively (Figure 29). The crude extract obtained from *M. merluccius* also contained a peak 1025 cm^{-1} , suggesting that the crude *M. merluccius* extract contains primarily CS. The differences in the intensities of peaks at 1450 cm^{-1} and 1600 cm^{-1} also more closely resemble CS in the crude *M. merluccius* spectra, further supporting that the extract is composed of CS. A peak can also be observed at 850 cm^{-1} which has been suggested to be indicative of CSA (Mainreck *et al.*, 2011), however this peak is also present within the FTIR spectra of DS and HS (Figure 29, Figure 15).

The ATR-FTIR spectra of the crude *M. merluccius* extract was then subjected to PCA against the previously described library of GAGs (Figure 29). Comparison of PC1 and PC2, covering ~73% of the variance, separated the crude *M. merluccius* extract between the regions associated with CS and DS, supporting that the sample contains a mixture of galactosaminoglycans (Figure 29).

The CD spectra of the crude *M. merluccius* extract exhibited a negative band at ~212 nm and negative ellipticity in the region of 190 nm, further supporting that the extract is primarily composed of galactosaminoglycans (Figure 29). Post-acquisition PCA of the CD spectra of *M. merluccius* indicated that the sample separated within the CS region, when PC1 and PC2 were compared (covering ~98% of the variance), suggesting that the sample contains predominantly CS.

Finally, ^1H - and ^1H - ^{13}C HSQC NMR was employed to confirm the GAG composition of the crude *M. merluccius* extract (Figure 30). ^1H -NMR indicated that the crude extract was primarily composed of CS, with a small component of HS/heparin and DS, indicated by

signals corresponding to acetyl groups at 2.02, 2.04 and 2.08 ppm, respectively. Integration of the N-acetyl peak performed on the ^1H spectra indicated that the crude extract is composed of approximately ~63% CS, ~25% HS/heparin, ~12% DS. Signals corresponding to CS can be observed within the ^1H spectra, for instance position 2 and 3 of GlcA at ~3.2 and ~3.5 ppm, respectively. Furthermore, signals attributed to the anomeric carbons occur between 4.4 and 4.6 ppm and therefore, corresponds to CS. A low intensity peak can also be observed at ~5.1 ppm, which may correspond to the anomeric carbon of IdoA in DS or HS/heparin (Table 10, Table 11). Furthermore, comparisons of the signals attributed to position 4 of Gal bearing 4-O-sulphate modifications at ~4.9 ppm or 4-OH at ~4.2 ppm, indicate minor amounts of CSA units. The overlapping resonance at 4.2 ppm with position 6 of 6-O-sulphated Gal, may however indicate the presence of some CSC units (Table 11). ^1H - ^{13}C HSQC NMR was used to resolve overlapping signals and to further determine saccharide composition (Figure 30). Integration of the acetyl peak on the ^1H - ^{13}C HSQC was prohibited by the poor spectral resolution. Despite this the intensity of signals within the aromatic region at ~4.5/103 ppm and ~4.4/106 ppm corresponding to CS, support that this is the major GAG component of the crude *M. merluccius* extract. Integration of the signals corresponding to Gal6S and GalOH indicated that the sample contains ~75 % unsulphated CS, therefore the crude *M. merluccius* extract primarily contains unsulphated CS.

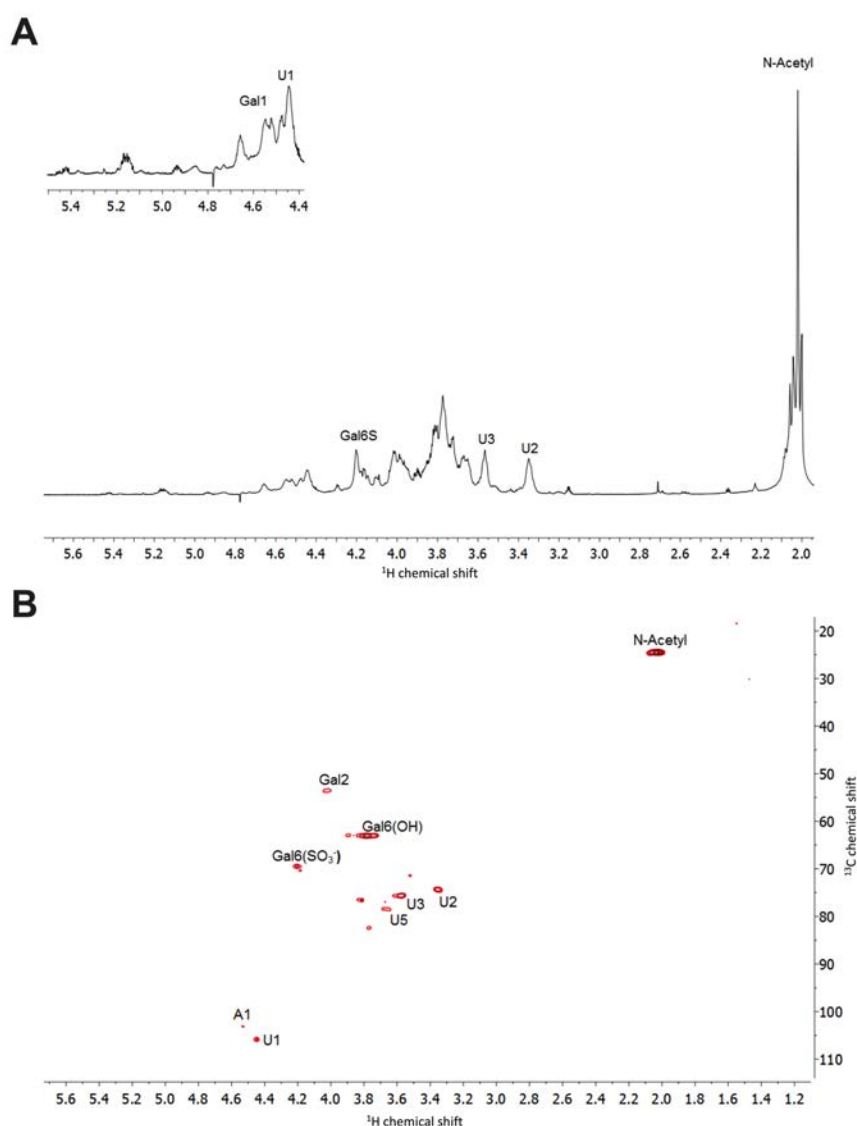


Figure 30: (A) ^1H and (B) ^1H - ^{13}C HSQC NMR spectra of crude *M. merluccius* extract. Major signals associated with CS are indicated. Spectral integration was performed on the HSQC using labelled signals. Key: galactosamine; Gal, uronic acid; U. Spectra recorded at 298K.

4.2.1.6. *P. hypophthalmus*

When subjected to agarose gel electrophoresis the crude extract obtained from *P. hypophthalmus* separated into one band with a migration distance corresponding to that of DS. No bands were present within the sample that possessed a similar electrophoretic mobility to either CS, HS or heparin standards, suggesting that the crude *P. hypophthalmus* sample is composed primarily of DS (Figure 31).

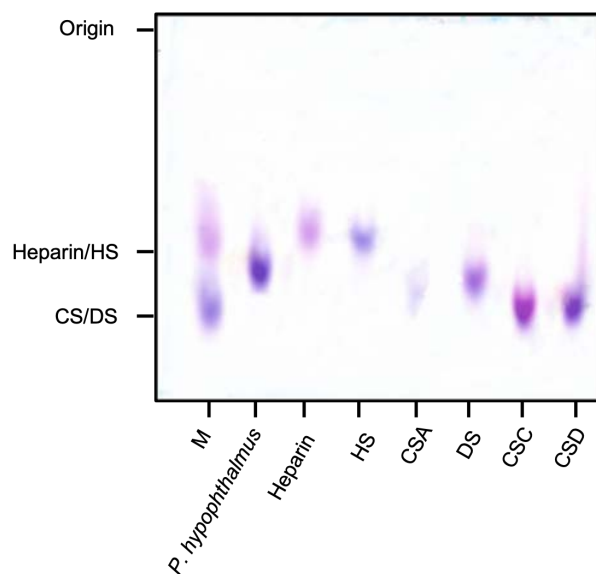


Figure 31: The electrophoretic mobility of 20 µg crude GAG extract obtained from *P. hypophthalmus* compared to bona fide glycosaminoglycans; heparin, heparan sulphate (HS), dermatan sulphate (DS) and chondroitin sulphate A, C and D (CSA, CSC and CSD, respectively), using agarose gel electrophoresis in 50 mM 1,3-diaminopropane buffer. M = mixture of CSA and heparin.

The ATR-FTIR spectra of the crude *P. hypophthalmus* extract contained peaks associated with sulphated uronic acid containing GAGs at 1230 cm⁻¹, 1430 cm⁻¹, 1635 cm⁻¹ and a peak shoulder at 1559 cm⁻¹ (Mainreck *et al.*, 2011; Devlin, Mycroft-West, *et al.*, 2019). A split peak was also observed at 1025 cm⁻¹ and 1045 cm⁻¹, with the latter being observed solely in DS (Figure 15, Figure 32). Furthermore, the peaks observed at ~1450 cm⁻¹ and ~1600 cm⁻¹ more closely resemble CS/DS than HS/heparin. A peak can also be observed at ~850 cm⁻¹, which is also present in DS samples (Figure 32). This suggests that the *P. hypophthalmus* extract is primarily composed of DS. Supporting this, when the ATR-FTIR spectra of crude *P. hypophthalmus* was subjected to post acquisition PCA against the previously described GAG library the sample located within the region corresponding to DS, when PC1 and PC2 were compared (covering ~72% of the variance) (Figure 36C).

The CD spectra of the crude *P. hypophthalmus* extract exhibited a negative band at ~210 nm, with no positive band being observed at ~190 nm. Furthermore, the intensity of the negative band at ~210 nm, more closely resembled that of DS than CS. When the CD spectra of the crude *P. hypophthalmus* was subjected to PCA against a library of GAGs the sample located within the region containing DS, when PC1 and PC2 were compared (covering 98% of the variance)(Figure 32). This further supports that the crude *P. hypophthalmus* extract is primarily composed of DS.

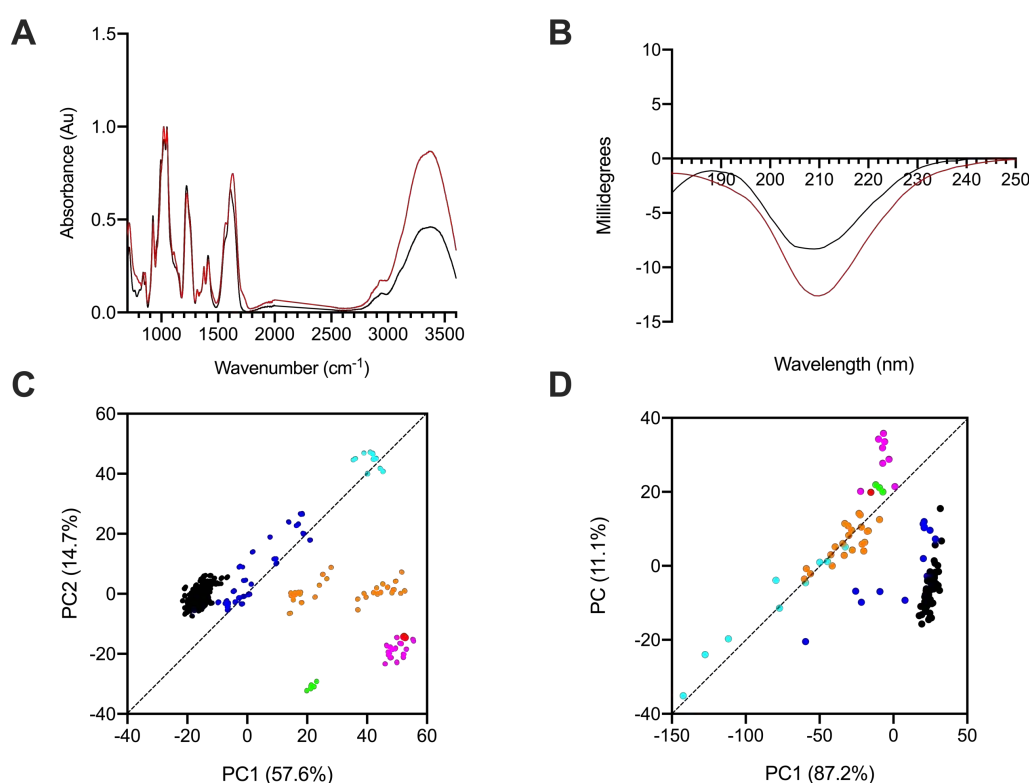


Figure 32: ATR-FTIR and CD spectra of the crude *P. hypophthalmus* extract. (A) ATR-FTIR and (B) circular dichroism spectra of crude *P. hypophthalmus* extract (red) and DS (black). (C) Principal component analysis (PCA) score plot for PC1 vs. PC2 of A and (D) of B against a bone fide GAG library. Heparin, black; HS, blue; CS, orange; DS, magenta; HA, cyan; over-sulphated CS, green; crude *P. hypophthalmus*

To corroborate that the crude *P. hypophthalmus* is primarily composed of DS ^1H - and ^1H - ^{13}C HSQC NMR was employed (Figure 33). Integration of the N-acetyl signals on the ^1H -NMR at ~ 2.08 , ~ 2.04 and ~ 2.02 ppm indicated that the sample was composed of $\sim 60\%$ DS, $\sim 30\%$ CS and $\sim 10\%$ HS. This is supported by the presence of peaks corresponding to position 2 of the uronic acid of both DS and CS at ~ 3.5 and ~ 3.3 ppm, with the latter signal being relatively low in intensity. Furthermore, this can also be observed for peaks corresponding to the anomeric carbon of the uronic acid residue at ~ 4.9 and 4.5 ppm for CS and DS respectively (Figure 33, Table 11). ^1H - ^{13}C HSQC NMR was utilised to further resolve the overlapping signals and to confirm the GAG composition of the crude *P. hypophthalmus* extract. The acetyl signal was broad centring at ~ 2.08 ppm, supporting that the extract is composed primarily of a mixture of DS and CS. The low spectral resolution did however preclude peak volume integration. Additionally, a signal was observed at $\sim 4.9/105$ ppm supporting the assignment made by ^1H -NMR of the anomeric carbon of IdoA in DS. No peak was observed at $\sim 4.5/107$ ppm again supporting that the extract is primarily composed of DS. The peak corresponding to position 2 of IdoA in DS was also present at $\sim 3.5/72$ ppm within the ^1H - ^{13}C HSQC spectra. Furthermore, only signals corresponding to unsulphated position 6 of Gal were observed, which is common for DS samples, and indicates this modification is largely absent (Table 10).

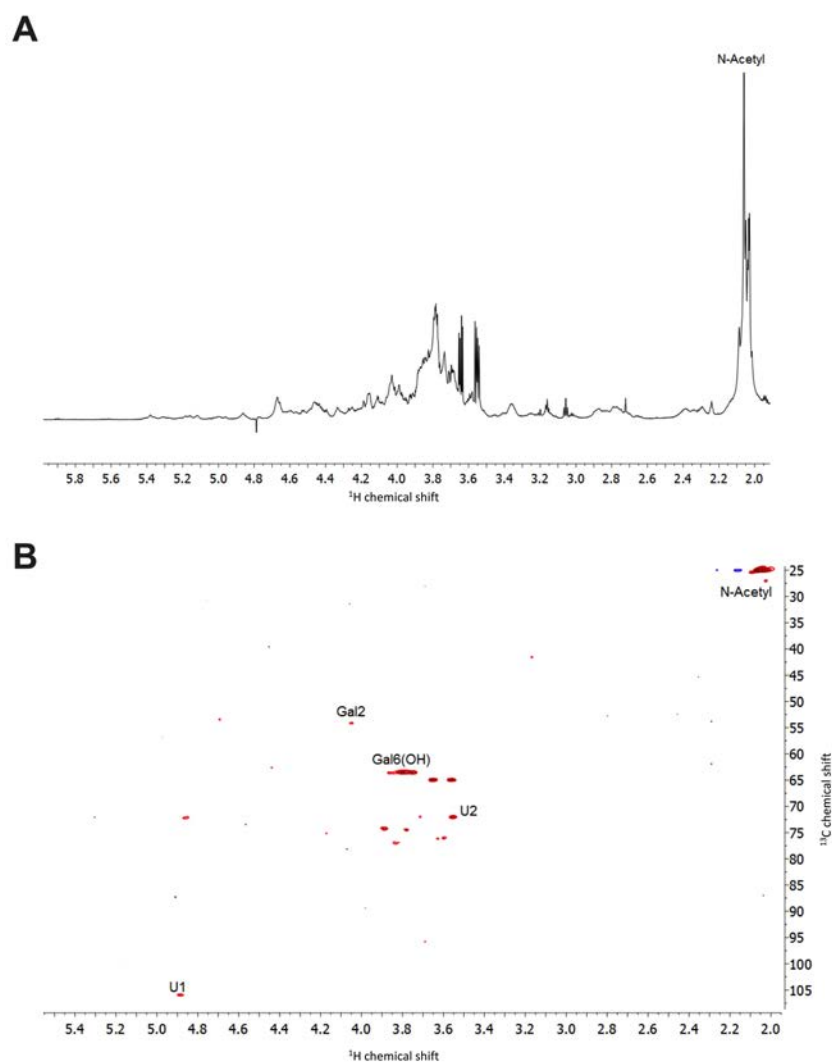


Figure 33: (A) ^1H and (B) ^1H - ^{13}C HSQC NMR spectra of crude *P. hypophthalmus* extract. Major signals associated with DS are indicated. Spectral integration was performed on the HSQC using labelled signals. Key: galactosamine; Gal, uronic acid; U.

4.2.1.7. *C. batrachus*

When subjected to agarose gel electrophoresis the crude extract obtained from *C. batrachus* separated into one band with similar electrophoretic mobility to CS and DS. No bands were observed with a migration distance corresponding to heparin/HS. This

therefore, suggests that the extract obtained from *C. batrachus* is primarily composed of galactosaminoglycans (Figure 34).

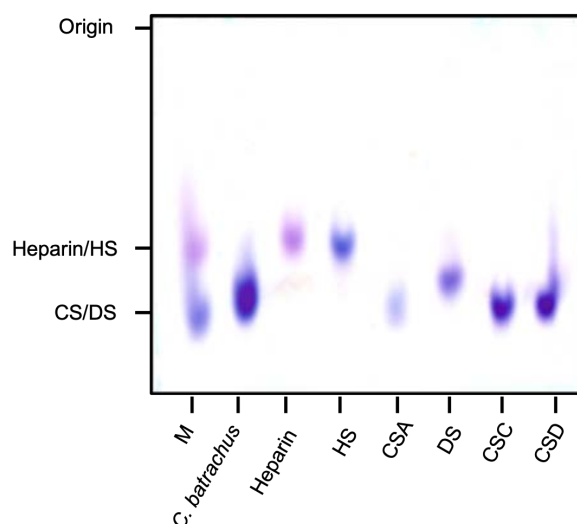


Figure 34: The electrophoretic mobility of 20 µg crude GAG extract obtained from *C. batrachus* compared to bona fide glycosaminoglycans; heparin, heparan sulphate (HS), dermatan sulphate (DS) and chondroitin sulphate A, C and D (CSA, CSC and CSD, respectively), using agarose gel electrophoresis in 50 mM 1,3-diaminopropane buffer. M = mixture of CSA and heparin.

To further resolve the GAG composition of the crude *O. batrachus* extract, ATR-FTIR and CD spectroscopy was employed. The ATR-FTIR spectra of the crude *C. batrachus* sample contained peaks at 1230 cm^{-1} , 1430 cm^{-1} , 1635 cm^{-1} and a peak shoulder at 1559 cm^{-1} , which are characteristic peaks of sulphated uronic acid containing GAGs (Mainreck *et al.*, 2011; Devlin, Mycroft-West, *et al.*, 2019). A peak centred at $\sim 1025\text{ cm}^{-1}$, containing a peak shoulder at 990 cm^{-1} , was also observed. No peak was observed at $\sim 1045\text{ cm}^{-1}$, suggesting that the extract is primarily composed of CS. The peaks present at $\sim 1450\text{ cm}^{-1}$ and 1600 cm^{-1} however more closely resemble that of DS than CS, with a split peak being present in the former region (Figure 35, Figure 15). A peak can also be observed at 850 cm^{-1} which is common to both CSA and DS samples.

When the ATR-FTIR spectra of the crude *C. batrachus* extract was subjected to post-acquisition PCA against the previously described GAG library, PC1 (covering 57.5 % of the variance) separated the sample towards the region containing CS, DS and HA. When comparing PC1 and PC2, covering 72% of the variance, the crude *C. batrachus* sample separated within the CS region (Figure 35). This suggests that the crude *C. batrachus* extract is primarily composed of CS.

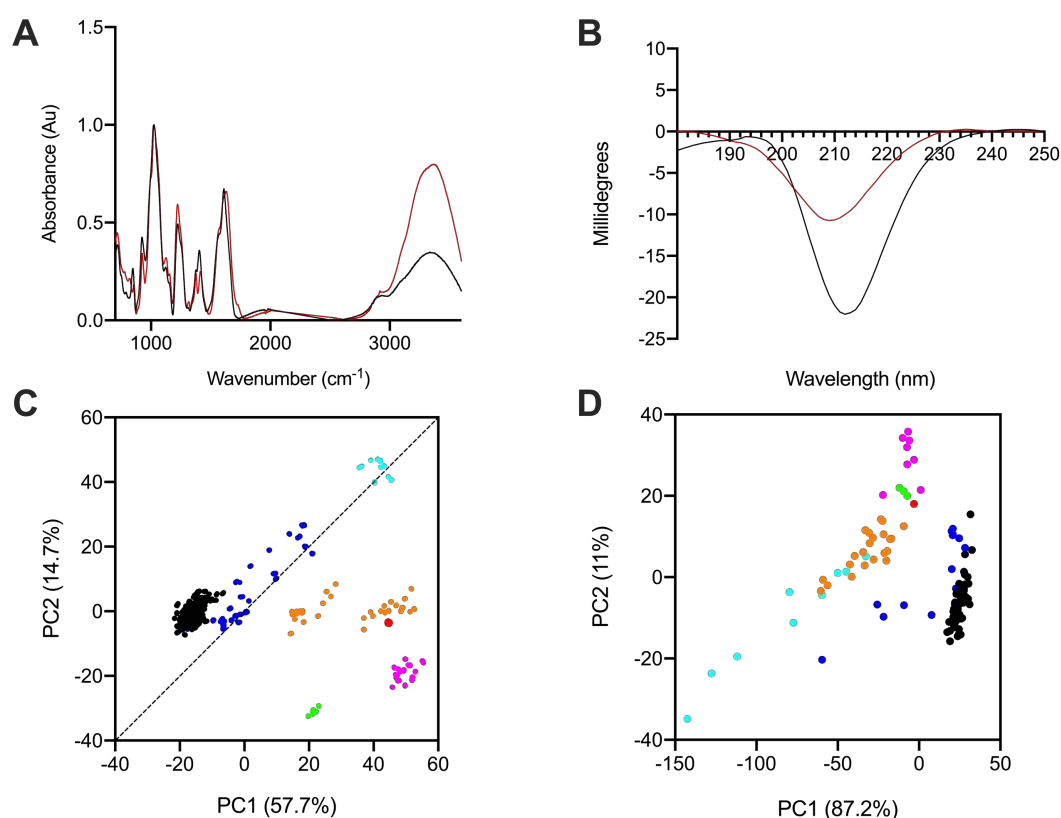


Figure 35: ATR-FTIR spectra of the crude *C. batrachus* extract. (A) ATR-FTIR and (B) circular dichroism spectra of crude *C. batrachus* extract (red) and CS (black). (C) Principal component analysis (PCA) score plot for PC1 vs. PC2 of A and (D) of B against a bone fide GAG library. Heparin, black; HS, blue; CS, orange; DS, magenta; HA, cyan; over-sulphated CS, green; crude *C. batrachus*.

The CD spectra of the crude *C. batrachus* extract exhibited a negative band at ~ 210 nm, with no positive band observed at ~ 190 nm, supporting that the extract is primarily

composed of CS/DS. The intensity of the negative band at ~210 nm however more closely resembled that of DS than CS. The CD spectra of the crude *C. batrachus* sample was subjected to PCA against a library of GAGs to further, which separated the sample towards the region containing DS when PC1 and PC2 were compared (covering ~98% of the variance) (Figure 35).

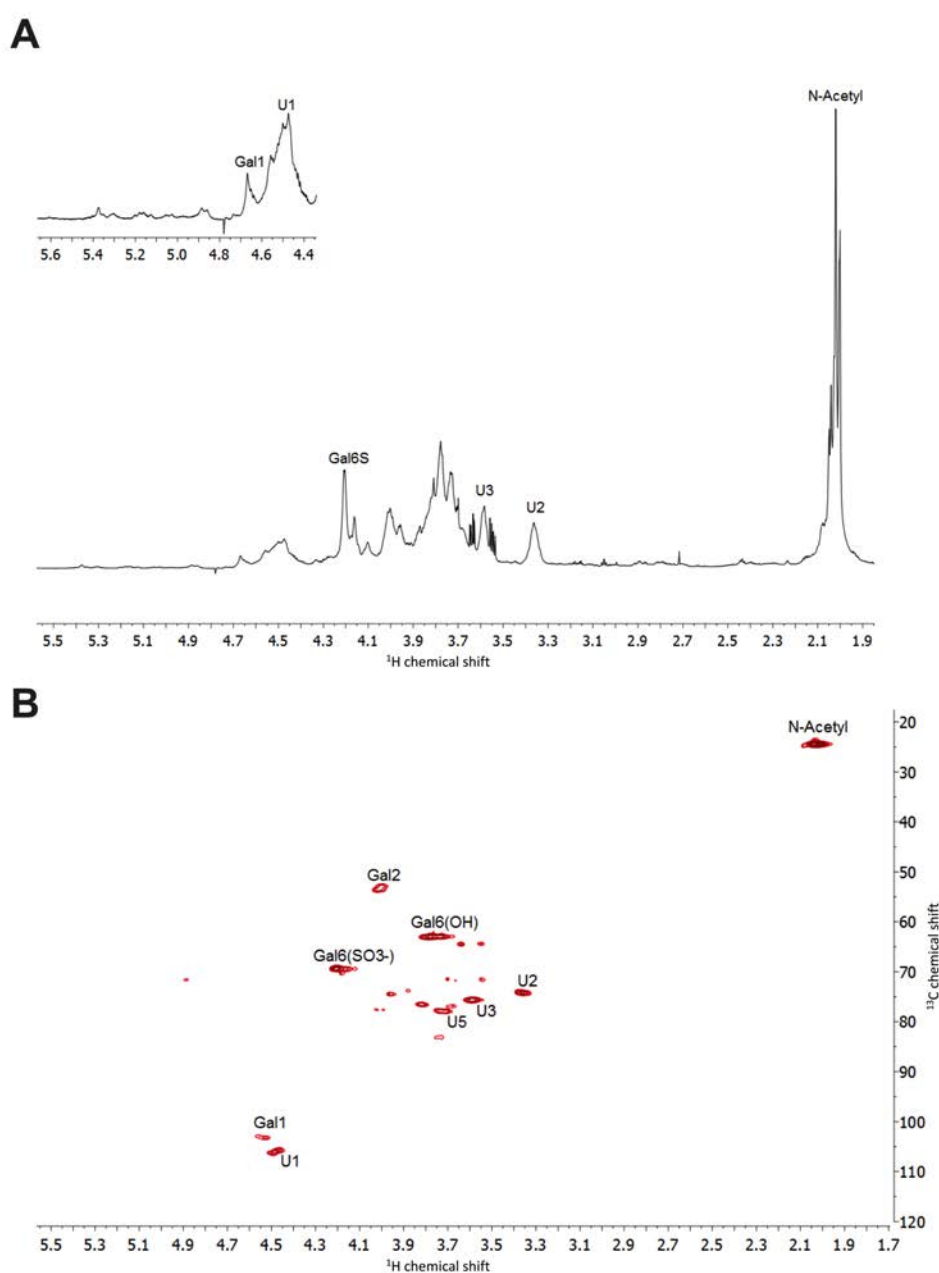


Figure 36:(A) ^1H and (B) ^1H - ^{13}C HSQC NMR spectra of crude *C. batrachus* extract. Major signals associated with CS are indicated. Spectral integration was performed on the HSQC using labelled signals. Key: galactosamine; Gal, uronic acid; U.

^1H - and ^1H - ^{13}C HSQC NMR was employed to further confirm the GAG composition of the crude *C. batrachus* extract (Figure 36). ^1H NMR indicated that the crude extract was primarily composed of CS (~90) with a small component of DS and HS/heparin (<5%), at 2.02, 2.04 and 2.08 ppm respectively (Table 10, Table 11). This is supported by the intensity of peaks corresponding to the anomeric protons of Gal and GlcA at ~4.7 and ~4.4 ppm, respectively (Table 11). In contrast the anomeric signals corresponding to IdoA and GlcN in HS/heparin between 5.3-5.5 ppm are low in intensity (Table 10). Additionally, the resonance attributed to IdoA in DS at ~4.9 ppm is low in intensity (Table 11). The signals corresponding to position 2 and 3 of GlcA in CS can also clearly be observed at ~3.4 and ~3.6 ppm, respectively. This supports that the crude *O. batrachus* extract is primarily composed of CS. The signal observed at ~4.2 ppm, corresponding to Gal6S4OH, also indicates that the extract is primarily unsulphated at position 4 and may contain sulphate modifications at position 6 of the Gal residue (Table 11). ^1H - ^{13}C HSQC NMR was used to resolve overlapping signals and to further determine saccharide composition. Peak volume integration of the N-acetyl peak was performed indicating that the crude extract is composed of primarily of ~90% CS, <5% HS and DS. Furthermore, only signals attributed to the anomeric carbons of Gal and GlcA were detected at 4.5-4.7/10-107 ppm. Peak volume integration of the signals corresponding to Gal6S and GalOH indicated that the sample contains ~ 60 % unsulphated CS (Figure 36).

4.2.1.8. *O. gorboscha*

When subjected to agarose gel electrophoresis the crude extract obtained from *O. gorboscha* separated into one band which possessed similar electrophoretic mobility to

CS and DS standards. No bands were present with migration distances corresponding to heparin/HS. This suggests that the crude extract obtained from *O. gorbuscha* contains predominantly galactosaminoglycans (Figure 37).

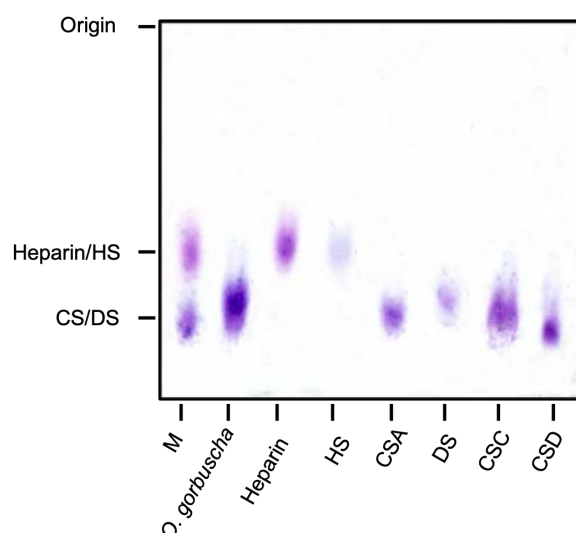


Figure 37: The electrophoretic mobility of 20 µg crude GAG extract obtained from *O. gorbuscha* compared to bona fide glycosaminoglycans; heparin, heparan sulphate (HS), dermatan sulphate (DS) and chondroitin sulphate A, C and D (CSA, CSC and CSD, respectively), using agarose gel electrophoresis in 50 mM 1,3-diaminopropane buffer. M = mixture of CSA and heparin.

To further elucidate the GAG composition of the crude *O. gorbuscha* extract ATR-FTIR and CD spectroscopy was employed (Figure 38). The ATR-FTIR spectra of the crude *O. gorbuscha* extract contained several peaks that are associated with sulphated uronic acid containing GAGs, for instance 1230 cm^{-1} , 1430 cm^{-1} , 1635 cm^{-1} and a peak shoulder at 1559 cm^{-1} (Mainreck *et al.*, 2011; Devlin, Mycroft-West, *et al.*, 2019). A peak was also observed at $\sim 1025\text{ cm}^{-1}$ which is indicative of CS. Furthermore, peaks in the region of $\sim 1450 - 1600\text{ cm}^{-1}$ more closely resembled those of CS/DS than HS/heparin. A peak can also be observed at $\sim 850\text{ cm}^{-1}$, which has been suggested to be indicative of CSA units (Mainreck *et al.*, 2011), within the spectra of the crude *O. gorbuscha* extract (Figure 38). This peak can however be observed in the ATR-FTIR spectra of DS and HS (Figure 15).

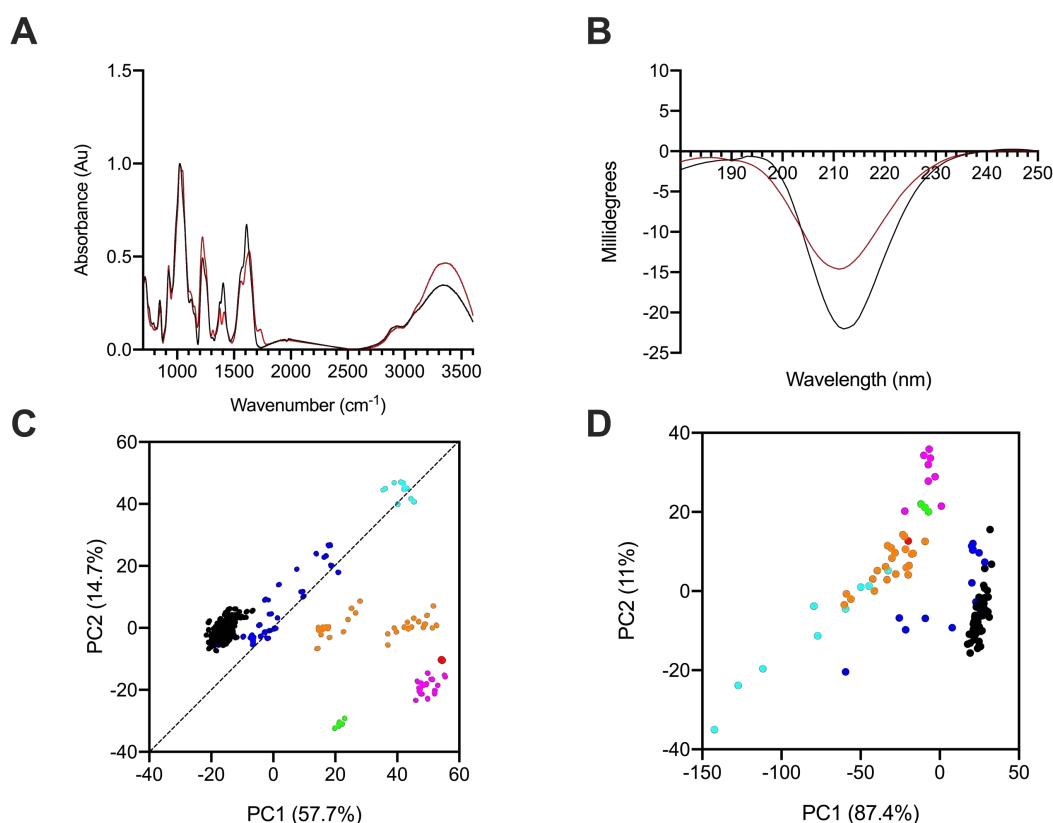


Figure 38: ATR-FTIR and CD spectra of the crude *O. gorbuscha* extract. (A) ATR-FTIR and (B) circular dichroism spectra of crude *O. gorbuscha* extract (red) and CS (black). (C) Principal component analysis (PCA) score plot for PC1 vs. PC2 of A and (D) of B against a bone fide GAG library. Heparin, black; HS, blue; CS, orange; DS, magenta; HA, cyan; over-sulphated CS, green; crude *O. gorbuscha*.

When the ATR-FTIR spectra of the crude *O. gorbuscha* extract was subjected to post-acquisition PCA against the previously described GAG library, the sample located between the regions containing CS and DS, when PC1 and PC2 were compared (covering ~72 % of the variance; Figure 38). This suggests that the crude *O. gorbuscha* extract is composed of a mixture of CS and DS. The CD spectra of the crude *O. gorbuscha* extract exhibited a negative band at ~210 and no positive band was observed at ~190 nm, supporting that the extract is primarily composed of CS/DS (Figure 38). When subjected to PCA against a library of GAGs, the crude *O. gorbuscha* sample located within the region containing CS and slightly towards the region containing DS, when PC1 and PC2

were compared, covering ~98% of the total variance (Figure 38). This supports that the crude *O. gorbuscha* is composed of a mixture of CS and DS.

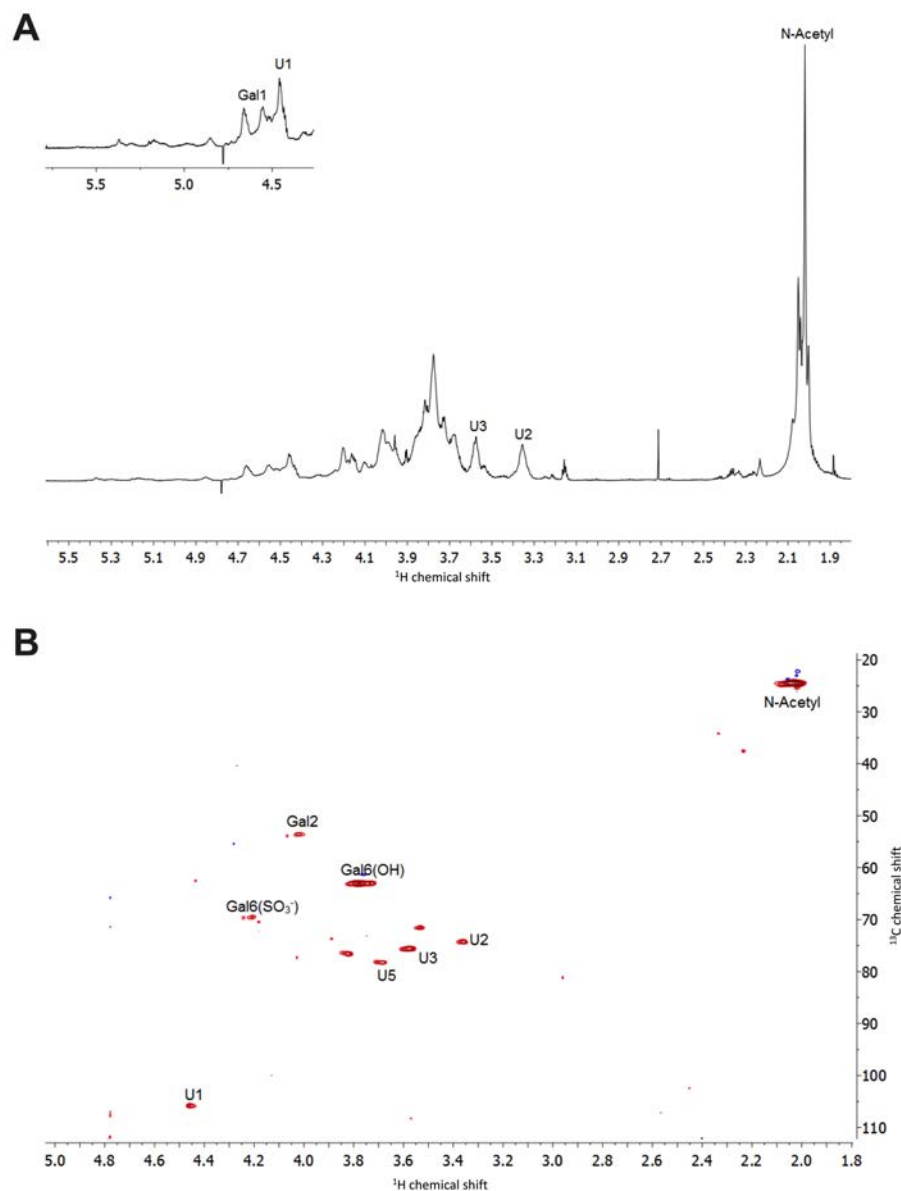


Figure 39: (A) ^1H and (B) ^1H - ^{13}C HSQC NMR spectra of crude NMR *O. gorbuscha* extract. Major signals associated with CS are indicated. Spectral integration was performed on the HSQC using labelled signals. Key: galactosamine; Gal, uronic acid; U.

^1H - and ^1H - ^{13}C HSQC NMR was employed to confirm the GAG composition of the crude *O. gorbuscha* extract. ^1H NMR indicated that the crude extract was composed of CS (~60%), HS (~20%) and DS (~10%) with resonances corresponding to the acetyl region

at ~2.02, ~ 2.04 and ~2.08 ppm respectively (Table 10, Table 11). Signals corresponding to the anomeric protons of Gal and GlcA can be observed with relatively high intensities at ~4.5 ppm and 4.4 ppm (Table 11, Figure 39). This is in contrast to the anomeric signals associated to DS and HS >5 ppm (Figure 39, Table 10, Table 11). Furthermore, resonances attributed to position 2 and 3 of GlcA in CS can clearly be observed at ~3.4ppm and 3.6 ppm, respectively (Table 11, Figure 39). A minor signal attributable to position 2 of IdoA in DS can also be observed at ~3.5 ppm. ^1H - ^{13}C HSQC NMR was used to resolve overlapping signals and to further determine the composition of the crude *O. gorbuscha* extract. Only anomeric signals attributable to CS were observed in the region of 4.5-4.7/103-107 ppm, supporting that CS is the primary GAG component within the crude *O. gorbuscha* extract. Integration of the signals corresponding to Gal6S and GalOH indicate that the sample contains ~85 % unsulphated CS (Figure 39).

4.2.2. Screening of crude GAG extracts for BACE1 activities FRET.

Following the isolation of crude GAG extracts from a variety of non-mammalian species, BACE-1 inhibitory activity was evaluated, in comparison to heparin (porcine origin), utilising the previously described fluorogenic peptide FRET APP_{SW} peptide assay (Figure 40; (Scholefield *et al.*, 2003; Beckman, Holsinger and Small, 2006; Patey *et al.*, 2006; Klaver *et al.*, 2010). Heparin exhibited an IC₅₀ of 2.4 $\mu\text{g.mL}^{-1}$ ($R^2 = 0.9$) at pH 4.0, with maximal inhibition occurring at concentrations above 5 $\mu\text{g.mL}^{-1}$ (~92%).

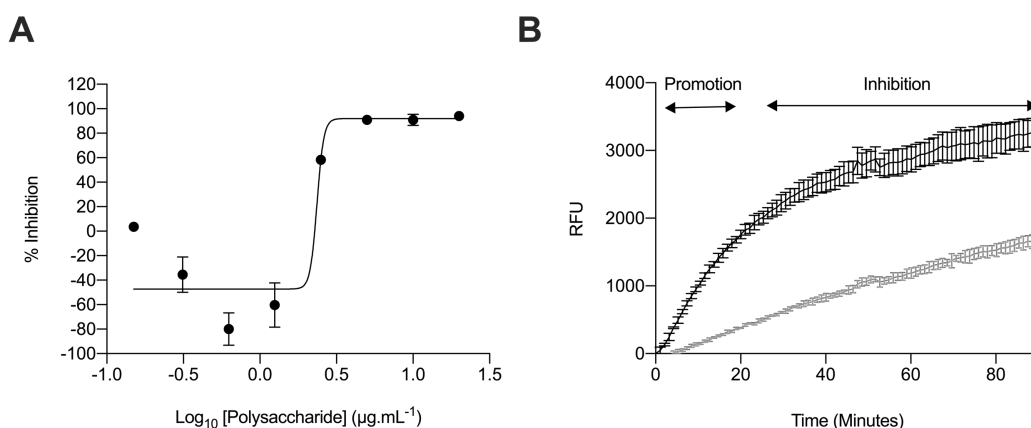


Figure 40: Inhibition of human BACE1 by heparin. (A) Dose response of heparin as determined using FRET; IC₅₀ = 2.4 $\mu\text{g.mL}^{-1}$ ($R^2 = 0.9$). (B) Time-course of BACE1 activity alone (grey) or in the presence of 625 ng.mL⁻¹ heparin (black). (n = 3, \pm SD).

In the presence of low concentrations of heparin (1250.0-312.5 ng.mL⁻¹; maximum negative BACE-1 inhibition = 80% at 625 ng.mL⁻¹) promotion of BACE-1 activity was observed, with percent activity returning to that of the negative control values at concentrations lower than 312.5 ng.mL⁻¹. This indicates that both inhibitory and stimulatory effects are dose dependent (Figure 40). By monitoring the time course increase in fluorescence, generated as a result of peptide cleavage, an initial period of

BACE-1 activation could be observed in the presence of heparin at concentrations between 1250.0-312.5 ng.mL⁻¹ in contrast to negative controls (Figure 40, Appendix 1). This stimulatory period was subsequently followed by a reduction in the rate of peptide cleavage at time points >20 minutes, indicating a second phase of enzyme inhibition (Figure 40, Appendix 1).

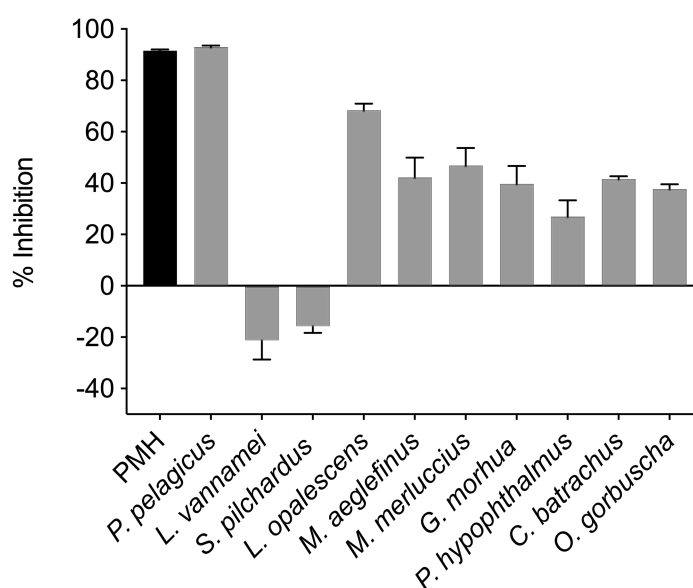


Figure 41: Inhibition of human BACE-1 by crude GAG extracts determined using FRET. (n = 3, \pm SD).

Following the establishment of the assay crude GAG extracts were screened for their ability to inhibit BACE-1 at 5 μ g.mL⁻¹; the concentration at which heparin exhibited maximal inhibitory activity (Figure 40, Figure 41). The crude extract obtained from *P. pelagicus*, composed of ~70% heparin/HS and 30% CS, exhibited the greatest BACE-1 inhibitory activity and was comparable to that of PMH at ~93% (Figure 41). The extract obtained from *C. batrachus*, containing >90% CS, was observed to possess a BACE-1 inhibitory activity of ~42% (Figure 41). This is in contrast to previous reports that CS possesses minimal BACE-1 inhibitory activity (Scholefield *et al.*, 2003). As a result, the

inhibitory activity of galactosaminoglycan standards against BACE-1 was assessed in comparison to heparin, under matched conditions (Figure 42). Under the conditions utilised in the present study all GAG were observed to possess BACE-1 inhibitory activity of > 50% when tested at 5 $\mu\text{g.mL}^{-1}$ (Figure 42).

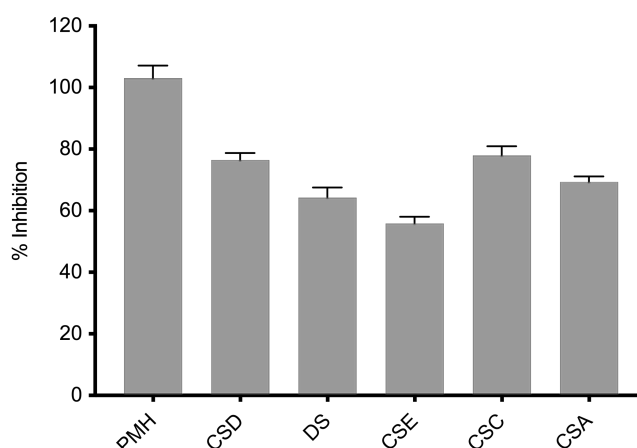


Figure 42: Inhibition of human BACE-1 by GAG standards determined using FRET. (n = 3, \pm SD).

The final extracts obtained were primarily composed of a mixture of GAG, albeit to different extents. The major GAG component of the extracts obtained from *M. merluccius*, *G. morhua*, *O. gorbuscha* and *S. pilchardus* was CS. These extracts possessed BACE-1 inhibitory activities of 49%, 40%, 38% and -16%, respectively. The extract obtained from *P. hypothalamus*, which primarily contained DS, exhibited BACE-1 inhibitory activity at ~28% (Figure 41). Finally, the extract obtained from *L. vannamei*, was composed of ~60% HS and 40% CS and exhibited a BACE-1 inhibitory activity of -21% (Figure 41).

4.2.3. DEAE anion exchange fractionation of crude GAG extracts and screening for BACE-1 inhibition.

Following establishing that the crude GAG extracts possessed BACE-1 inhibitory activities, the extracts were purified further by DEAE-Sephacel anion exchange chromatography utilising a stepwise sodium chloride gradient, with the aim of isolating the active components. Fractionation resulted in the collection of 6 fractions corresponding to 0 M, 0.25 M, 0.5 M, 0.8 M, 1M and 2M NaCl, (F1-6, respectively; Figure 43). Each fraction was then re-assayed for BACE-1 inhibitory activity in order to determine whether purification resulted increased activity (Figure 44).

Fractionation of the crude GAG extract obtained from *P. pelagicus* resulted in one primary fraction, eluted with 1 M NaCl, which exhibited a BACE-1 inhibitory activity of 96% (F5; Figure 43). Fractionation of the crude *P. pelagicus* therefore, resulted in a 3% increase in BACE-1 inhibitory activity. The crude extract obtained from *L. vannamei* was separated into two primary fractions, eluted with 0.8 M and 1 M NaCl (F4 and F5, respectively; (Figure 43). *L. vannamei* F4 and F5 was found to possess a BACE-1 inhibitory activity of 91% and 71%, respectively (Figure 44). Fractionation, therefore resulted in an increase in BACE-1 activity by 112% (F4) and 92% (F5). The *L. vannamei* fraction eluted with 0.5 M NaCl (F3) possessed a BACE-1 inhibitory activity of 6% (Figure 44), indicating that the eluants with lower affinity for DEAE-Sephacel, within the crude *L. vannamei* extract, possessed minimal BACE-1 inhibitory activity. The crude extract obtained from *S. pilchardus* was fractionated into one primary sample, eluted with 0.8

M NaCl (F4), which possessed 75% BACE-1 inhibitory activity (Figure 43, Figure 44). *S. pilchardus* F4, therefore displayed an ~ 91% increase in activity following fractionation.

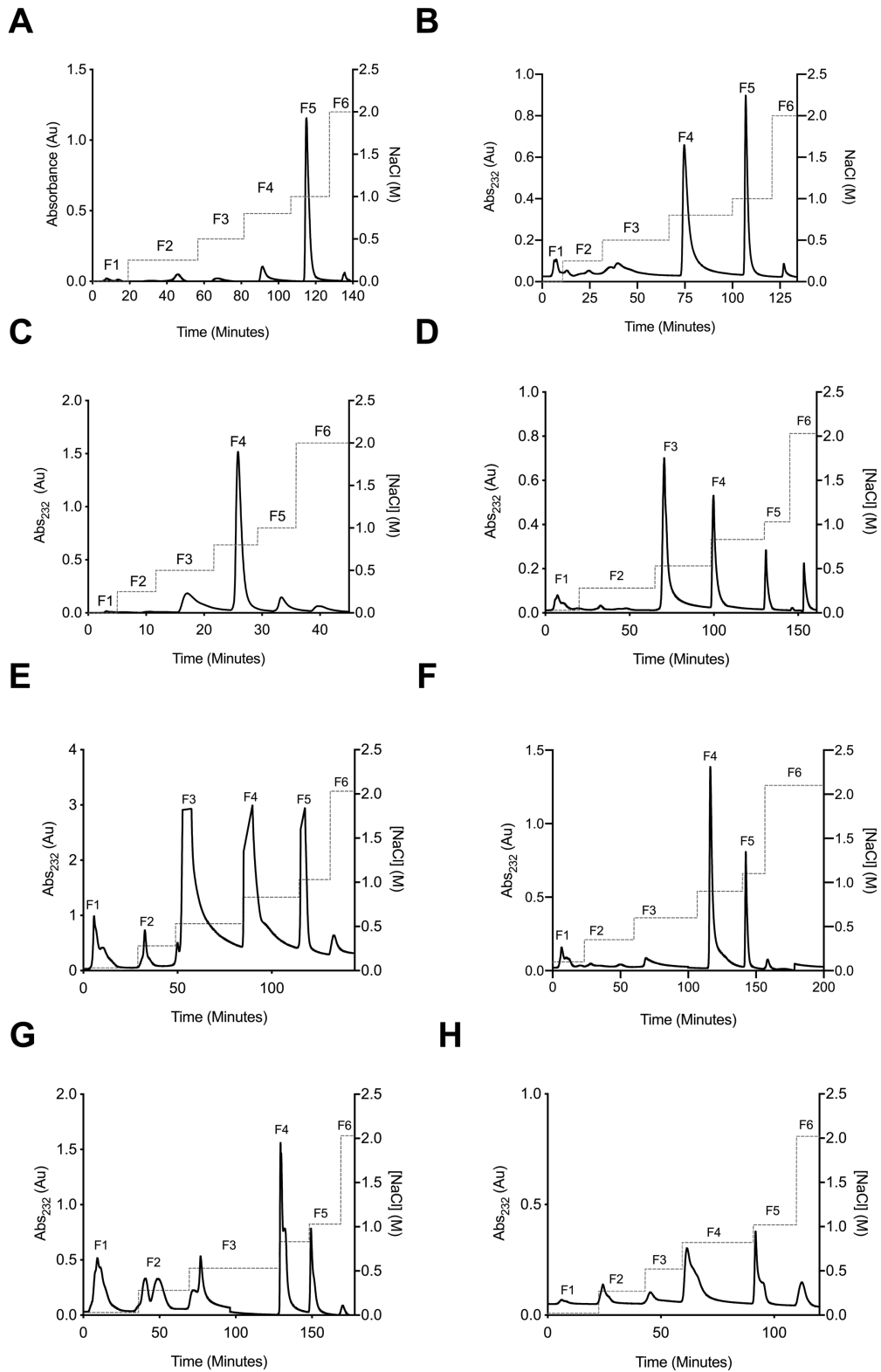


Figure 43: DEAE fractionation of crude GAG extracts. Fractions 1-6 (F1-6; $\lambda_{\text{Abs}} = 232 \text{ nm}$, solid line) were eluted using a stepwise NaCl gradient with HPAEC (dashed line). (A) *P. pelagicus*, (B) *L. vannamei*, (C) *S. pilchardus*, (D) *M. aeglefinus*, (E) *M. merluccius*, (F) *P. hypophthalmus*, (G) *C. batrachus*, (H) *O. gorbuscha*.

activity, respectively (Figure 43, Figure 44). Fractionation of the crude *M. aeglefinus* extract therefore resulted in an increase in BACE-1 activity of 19% (F3), 18% (F4), 26% (F5). The extract obtained from *M. merluccius* was also separated into three fractions, which were eluted with 0.5 M (F3), 0.8 M (F4) and 1 M (F5) NaCl respectively. The fractions possessed a BACE-1 inhibitory activity of 60% (F3), 55% (F4) and 45% (F5), resulting in an increase of 11%, 6%, -4%, respectively (Figure 43, Figure 44).

The extract obtained from *P. hypophthalmus* was separated into two fractions, which were eluted at 0.8 and 1 M NaCl (F4 and F5, respectively). *P. hypophthalmus* F4 and F5 both exhibited a BACE-1 inhibition of 45%. Thereby the BACE-1 inhibition of *P. hypophthalmus* increased by 17% following fractionation (Figure 43, Figure 44).

The extract obtained from *C. batrachus* separated into three fractions, which were eluted at 0.5, 0.8 and 1 M NaCl (corresponding to F3, F4 and F5, respectively). *C. batrachus* fraction F3, F4 and F5 possessed BACE-1 inhibitory activity of 50%, 40%, and 64% respectively. Thereby exhibiting an Increases in BACE-1 inhibition of 8% (F3), -2% (F4) and 8%. (F5), in comparison to the crude *C. batrachus* sample (Figure 43, Figure 44).

The extract obtained from *O. gorboscha* was separated into two components, with the eluted fraction occurring at 0.8 M and 1 M NaCl, corresponding to F4 and F5, respectively. The BACE-1 inhibitory activity of F4 was -5 % and 20% for F5. This therefore, resulted in loss of activity from the crude sample. (Figure 43, Figure 44).

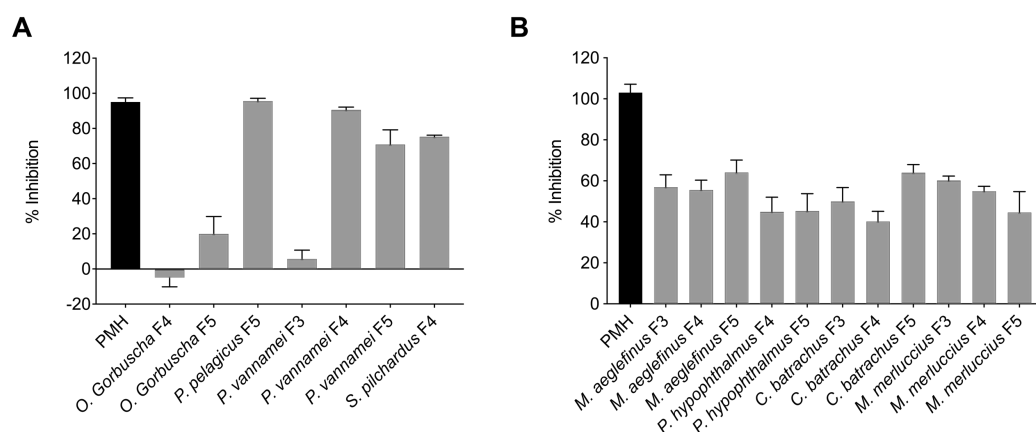


Figure 44: Inhibition of human BACE1 by fractionated GAG extracts determined using FRET. (n = 3, \pm SD).

4.3. Discussion

4.3.1 Extraction and analysis of crude glycosaminoglycans from aquatic species

Eight aquatic species were selected based upon the ability to source large quantities of tissue from the food industry, these included *P. pelagicus*, *M. merluccius*, *C. batrachus*, *G. morhua*, *M. aeglefinus*, *O. gorboscha*, *P. hypophthalmus*, *S. pilchardus* and *L. vannamei* (Table 12). This was with the aim of isolating GAGs from aquatic species which are either farmed for consumption, or in which waste tissue can be collected as a by-product of industrial food processing. Following extraction, the crude extracts were characterised in order to determine the GAGs composition and to evaluate the BACE-1 inhibitory activity of the resulting samples. Furthermore, the analytical techniques; agarose gel electrophoresis, ATR-FTIR and CD, were compared to the gold standard, NMR spectroscopy, in order to assess their applicability for the analysis of crude GAG samples.

Following obtaining tissue from sources meeting the standards for human consumption, the tissue was processed immediately after receipt, in order to avoid modifications of the GAG chains, which can occur following long-term storage, and in order to avoid lengthy lyophilisation times (Bianchini *et al.*, 1997; Zhang, Zhang and Linhardt, 2010; van der Meer, Kellenbach and van den Bos, 2017). Processing was initiated by dissecting the tissue prior to delipidation in acetone in concert with mechanical homogenisation. Acetone was selected for delipidation due to the ease of use and reduced toxicity compared to alternative procedures, such as those utilising chloroform (Nakano, Betti and Pietrasik, 2010; Zhang, Zhang and Linhardt, 2010; Chen *et al.*, 2011; Stelling *et al.*, 2019). Where tissue was sourced containing bone no prior de-calcification pre-treatment was performed, therefore any liberated GAGs were likely a product solely of the skin, muscle, or connective tissue. In addition, minimal digestion of bone tissue was observed following subsequent processing procedures. Following delipidation, the tissue was recollected, and excess acetone was allowed to evaporate, succeeding this GAG were hydrolysed from core proteins utilising proteolytic digestion with a non-specific protease. Enzymatic hydrolysis was again selected as a result of increased simplicity and reduced toxicity in comparison to chemical methodologies, in particular where large quantities of tissue material are being processed. Furthermore, chemical hydrolysis has been demonstrated to induce de-sulphation of the uronic acid residue, when the reaction temperature and pH are not adequately controlled ((van der Meer, Kellenbach and van den Bos, 2017). The non-specific protease selected for enzymatic hydrolysis, Alcalase, is an alkaline serine endopeptidase obtained from *Bacillus licheniformis*, which possesses broad specificity (Tacias-Pascacio *et al.*, 2020). Alcalase has been demonstrated to possess greater enzymatic activity than other

commercial proteases which have previously been utilised for GAG extraction, for instance papain, trypsin and chymotrypsin (*idem*). Moreover, the optimum conditions for Alcalase are stated to be between pH 7-8.5 at 70°C, however full activity has been demonstrated at room temperature in the pH range of 5-11 and therefore rigorous monitoring of the reaction conditions is not required (*idem*). Furthermore, Alcalase has been demonstrated to be stable in the presence of organic solvents, which is advantageous as digestion was conducted subsequent to acetone delipidation and activity was therefore less likely to be affected by trace amounts of solvent (*idem*). For all ten tissue samples full digestion with Alcalase at 60°C pH 8.0 (PBS, containing 1M NaCl) occurred within 24 hours, with the exception of bone material that was present within the sample. Proceeding digestion, the remaining debris was removed by centrifugation and Amberlite IRA-900 strong anion exchange resin (exchanged into the hydroxide counter ion form) was added directly to the supernatant in order to capture the liberated GAG chains. Amberlite IRA-900 was selected based upon the previous literature (Brito *et al.*, 2008; Saravanan and Shanmugam, 2010; van der Meer, Kellenbach and van den Bos, 2017), furthermore the resin diameter allowed for easy recovery from the supernatant following incubation. Subsequently, the bound material was eluted with 3M NaCl following extensive washing of the resin with dH₂O (60°C) and 1M NaCl, to remove weakly bound anionic contaminants such as nucleic acids. Crude extracts were then purified further by precipitation with ice cold methanol, added directly to the eluant (1:1 v/v) which had not been subjected to any prior pre-treatment. Succeeding precipitation, the crude extracts were collected via centrifugation and dialysed against dH₂O (MWCO 8 kDa), prior to lyophilisation. Subsequently the crude extracts were reconstituted in dH₂O, subjected to analysis to determine the presence

of GAGs within the sample by various techniques and evaluated for BACE-1 inhibitory activity.

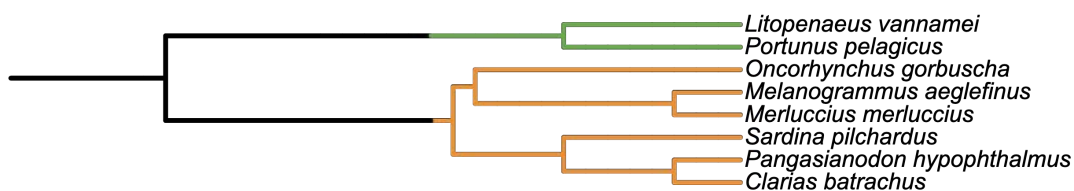


Figure 45: Phylogenetic tree of aquatic organisms utilised for GAG extraction. Green; organisms belonging to the crustacea genus, orange; organisms belonging to the clupeocephala genus.

All crude extracts yielded between $\sim 10\text{--}20 \text{ mg.kg}^{-1}$ of the original wet tissue weight. With the exception of *P. pelagicus* and *L. vannamei*, which belong to the genus Crustacea, the remaining species belong to the genus clupeocephala (bony fishes) (Figure 45). The highest yields were obtained from clupeocephala samples where the skin and/or the organisms head had also been processed, in contrast to solely the meat and connective tissue. This included crude extracts obtained from *M. merluccius* (head), *C. batrachus* (whole), *M. aeglefinus* (head), *P. hypophthalmus* (skin and flesh) and *S. pilchardus* (skin, scale and flesh) with yields of 16.6, 15.0, 18.0, 18.8 and 18.5 mg.kg^{-1} , respectively. In contrast the lowest yield was obtained from *O. gorboscha* flesh, where the skin had been removed, at 8.6 mg.kg^{-1} ; nearly half of that obtained from the aforementioned clupeocephala samples. This may suggest that a greater yield of GAG can be obtained from regions of clupeocephala which are not utilised for foodstuff, supporting that waste products of the aquaculture and fishery industries may provide a valuable source of GAGs. In support of this, Raghuraman (2013) and Gomes and Dietrich (1982) also isolated GAGs in greater yields from the heads of mackerel and catfish (*Pseudoplatystoma fasciatum*) respectively, in comparison to flesh samples

(Gomes and Dietrich, 1982; Raghuraman, 2013). As a result of the interest in obtaining GAGs from waste products, investigations have primarily been conducted to identify the yield and composition of GAGs from the inedible portions of commonly farmed aquatic species. Arima *et al.*, (2013) compared the yield of crude GAG extracts obtained from the inedible regions of several clupeocephala and identified that the skin of *Trachurus japonicus* (Japanese Jack mackerel) contained a three-fold greater yield than head region at 7.0 mg.g⁻¹. Furthermore, a two-fold increase in GAG yield was observed for the skin of *Bothrocara hollandi* (Eelpout) and *Careproctus rastrinus* (rough snailfish) compared to the head region (7.4 mg.g⁻¹ and 15.7 mg.g⁻¹, respectively). In contrast the same study observed a greater yield of GAGs in the head region of *Lycodes nakamurae* (Eelpout at 4.8 mg.g⁻¹), *Icelus toyamensis* (Eelpout at 0.8 mg.g⁻¹) and *Sebastolobus macrochir* (broadbanded thornyhead at 9 mg.g⁻¹). Gomes and Dietrich (1982) also achieved a higher yield of GAG from the head of *P. fasciatum* in contrast to the skin at 0.6 mg.g⁻¹, however the region identified to contain the greatest yield of GAGs was the gills (1.7 mg.g⁻¹). Examples of the yields previously reported for the anatomical regions of clupeocephala which are regarded as waste can be seen in Table 13; between approximately 2.2 and 0.005 mg.g⁻¹. The yields obtained of crude GAGs from clupeocephala in the current study are aligned with those at the lower end reported in the literature, however it is important to note that the yields presented in Table 13 are reported as a fraction of dry tissue weight, in contrast to the original wet starting tissue mass. This may therefore, account for the lower yield of GAGs obtained in the current work. Furthermore, variations in the yields obtained may be accounted for by differences in the extraction procedure and purity of the GAG extract.

Table 13: Example yields of GAG obtained from clupeocephala. * Per dry tissue weight.

Species	Common name	Anatomical region	Yield (mg.g ⁻¹)*	Reference
<i>Trachurus japonicus</i>	Japanese jack mackerel	head	1.87	(Arima <i>et al.</i> , 2013)
<i>Scomber scombrus</i>	Atlantic mackerel	skin	7.01	(Arima <i>et al.</i> , 2013)
	Pacific bluefin	Head	2.89	(Arima <i>et al.</i> , 2013)
	tuna	Stomach	1.87	(Arima <i>et al.</i> , 2013)
<i>Thunnus orientalis</i>		Intestines	0.42	(Arima <i>et al.</i> , 2013)
		Atrium	11.64	(Arima <i>et al.</i> , 2013)
		Gill	8.85	(Arima <i>et al.</i> , 2013)
<i>Nemipterus virgatus</i>	Golden threadfin bream	Skin and spine	0.32	(Arima <i>et al.</i> , 2013)
<i>Oreochromis niloticus</i>	Nile tilapia	Scale	3.9	(Arima <i>et al.</i> , 2013)
<i>Bothrocara hollandi</i>	Eelpout	Head	4.3	(Arima <i>et al.</i> , 2013)
		Skin	8.5	(Arima <i>et al.</i> , 2013)
<i>Lycodes nakamurae</i>	Eelpout	Head	4.8	(Arima <i>et al.</i> , 2013)
		Spine	0.4	(Arima <i>et al.</i> , 2013)
		skin	0.1	(Arima <i>et al.</i> , 2013)
<i>Icelus toyamensis</i>	Eelpout	Head	0.8	(Arima <i>et al.</i> , 2013)
		Skin	0.2	(Arima <i>et al.</i> , 2013)
<i>Sebastolobus macrochir</i>	Broadbanded thornyhead	Head	9.0	(Arima <i>et al.</i> , 2013)
	Rough snailfish	Skin with spine	0.6	(Arima <i>et al.</i> , 2013)
<i>Careproctus rastrinus</i>		Head	7.4	(Arima <i>et al.</i> , 2013)
		Spine	0.5	(Arima <i>et al.</i> , 2013)
		Skin	15.7	(Arima <i>et al.</i> , 2013)
		Fin	7.4	(Arima <i>et al.</i> , 2013)
<i>Limanda aspera</i>	Yellowfin sole	Spine	4.0	(Arima <i>et al.</i> , 2013)
		Dorsal fin	22.3	(Arima <i>et al.</i> , 2013)
		Tail fin	7.0	(Arima <i>et al.</i> , 2013)
<i>Thunnus thynnus</i>	Atlantic blue fin tuna	Skin	12.8	(Krichen <i>et al.</i> , 2018)
	Tuna	Bones	0.0023	(Maccari, Galeotti and Volpi, 2015)
	Dogfish	Bones	0.028	(Maccari, Galeotti and Volpi, 2015)
	Salmon	Bones	0.01	(Maccari, Galeotti and Volpi, 2015)
	Monkfish	Bones	0.034	(Maccari, Galeotti and Volpi, 2015)
	Cod	Bones	0.001	(Maccari, Galeotti and Volpi, 2015)
<i>Labeo rohita</i>	Rohu	Head	0.005	(Gavva <i>et al.</i> , 2020)
<i>Piaractus brachypomus</i>	Pacu	Head	0.004	(Gavva <i>et al.</i> , 2020)
	Catfish	Head	0.7	(Gomes and Dietrich, 1982)
		Skin	0.09	(Gomes and Dietrich, 1982)
<i>Pseudoplantystoma fasciatum</i>		Ileum	0.1	(Gomes and Dietrich, 1982)
		Liver	0.05	(Gomes and Dietrich, 1982)
		Gills	1.7	(Gomes and Dietrich, 1982)

The crude extracts obtained from the meat and connective tissue of the crustaceans, *P. pelagicus* and *L. vannamei* yielded 13.0 and 12.1 mg.kg⁻¹. Previous yields of crude GAG extracts obtained from shrimp heads have been reported up to 86.6 mg.kg⁻¹ (Table 14), ~ 7 fold greater than that obtained from *L.vannamei* in the present work, which utilised the edible muscle within the tail and abdomen (Table 14), The discrepancy between yields may be therefore be accounted for by the region of the organism utilised, with the cephalothorax of the shrimp containing a higher proportion of GAGs. This is supported by work by the same group who observed a lower yield of GAG extracts when the whole shrimp was processed, when equivalent extraction methodology was utilised (Nader *et al.*, 1983). Having said this minor improvements in the extraction protocol not reported and the purity of the GAG extract are also likely to contribute to the observed increased yield.

Table 14: Example yields of GAG obtained from Crustacea *yield per dry tissue weight or ** starting tissue weight; † yield of crude extract.

Species	Common name	Anatomical region	Yield (mg.g ⁻¹)	Reference
<i>Macrobrachium acanthurus</i>	Cinnamon river shrimp	Whole (without exoskeleton)	0.4-0.6*	Nader <i>et al.</i> , 1983
<i>Penaeus brasiliensis</i>	spotted pink shrimp	Whole (without exoskeleton)	0.8*	Nader <i>et al.</i> , 1983
		Heads	32.5x10 ^{3**}	Dietrich <i>et al.</i> , 1999
<i>Penaeus sp.</i>	Shrimp	Whole (without exoskeleton)	1.3*	Nader <i>et al.</i> , 1983
<i>litopenaeus vannamei</i>	Whiteleg shrimp		86.6x10 ^{3**†}	Cavalcante <i>et al.</i> , 2018
		Heads	70.8x10 ^{3**†}	Brito <i>et al.</i> , 2008
			79x10 ^{3*}	Cahu <i>et al.</i> , 2012

Overall, this indicates that the anatomical region possessing the greatest yield of GAGs differs between species, in particular for clupeocephala, in which the head, gills, fins or

skin are all regions that have been reported to contain the largest GAG content (Table 13). Whereas for the crustaceans, belonging to *Penaeus sp.*, the cephalothorax appears to contain a higher proportion of GAGs. Further investigations comparing the GAG yield and composition, between each anatomical region under equivalent conditions, should therefore be conducted for each species studied within the current work in order to determine the region in which the greatest GAG yield can be obtained. Furthermore, this would allow the determination of the region which possesses the highest yield of bioactive GAG, akin to pharmaceutical heparin preparations obtained from porcine intestinal mucosa. In addition, as the yields of crude extracts reported in the current work are largely lower than those in the literature, future studies should also be undertaken to optimise extraction protocols. This may include, increasing the number of acetone delipidation steps performed and comparing the use of chloroform:methanol solutions for delipidation. Moreover, the enzyme utilised for hydrolysis should be compared, along with the addition of decalcification utilising EDTA, the quantity and type of anion exchange resin utilised and precipitation of crude extracts with primary amines or organic solvents (Greiling, 1974; Silva, 2006; Zhang, Zhang and Linhardt, 2010; Nakano, Betti and Pietrasik, 2012; van der Meer, Kellenbach and van den Bos, 2017; Talmoudi, Ghariani and Sadok, 2020).

Subsequent to the extraction of crude samples from all eight species, the presence of GAGs was determined by agarose gel electrophoresis in 1-2- diaminopropane buffer followed by staining by toluidine blue. This methodology, albeit with minor modifications, has been utilised extensively to identify the presence of GAG within crude extracts and offers the advantage of other techniques in that a crude estimation

of the extract composition can be evaluated based upon electrophoretic migration (Medeiros *et al.*, 2000; Talmoudi, Ghariani and Sadok, 2020). In order to confirm that the primary components of the crude extracts, several spectroscopic techniques were subsequently employed. Initially, ATR-FTIR was utilised as this technique is label-free, non-destructive and requires minimal sample quantity or preparation time (Glassford, Byrne and Kazarian, 2013; Devlin, Mycroft-West, *et al.*, 2019). Furthermore, FTIR has utilised extensively in the structural elucidation of glycosaminoglycan extracts obtained from aquatic species (Garnjanagoonchorn, Wongekalak and Engkagul, 2007; Ben Mansour *et al.*, 2009; Karimzadeh, 2018; Krichen *et al.*, 2018; Talmoudi, Ghariani and Sadok, 2020) and when coupled with PCA has enabled the discrimination between classes of GAG, species of origin of heparin preparations and the presence of contaminants (Devlin, Mauri, *et al.*, 2019; Devlin, Mycroft-West, *et al.*, 2019). In addition to ATR-FTIR, CD spectroscopy combined with PCA has also been demonstrated to distinguish between galactosaminoglycan sub-types (CSA, CSC and DS), presumably as a result of the influence of modifications to the conformation and environment of the uronic acid residue (Rudd, Skidmore, Guimond, Cosentino, *et al.*, 2009; Rudd, Yates and Hricovini, 2009). Again CD, requires μg quantities of sample, can be obtained in a short timeframe and is technically undemanding. These techniques, therefore offer several advantages over NMR spectroscopy, which requires greater technical knowledge, considerably more sample and access to high resolution spectrometers, which may be cost prohibitive in particular for the analysis of crude sample preparations. In light of this, the effectiveness of agarose gel electrophoresis and ATR-FTIR and CD spectroscopy combined with PCA, for the estimation of crude GAG composition, was assessed in comparison to ^1H and ^1H - ^{13}C HSQC NMR spectroscopy.

This enabled the accuracy of the aforementioned techniques for the analysis of crude GAG samples to be evaluated.

Commonly metachromatic techniques, such as the carbazole, alcian blue and dimethylethylene blue (DMMB) assays, are employed to detect the presence of GAGs within crude extracts. The carbazole assay is based upon the reaction of uronic acid with carbazole reagent, which results in a coloured complex that can be measured at 525 nm and therefore, enables an estimation of total GAGs present within a sample (Muir, 1962; Talmoudi, Ghariani and Sadok, 2020). There are however, several drawbacks to the carbazole assay, for example KS cannot be detected and the presence of salts and/or other carbohydrates can lead to an over estimation of total GAG content (Frazier *et al.*, 2008; Talmoudi, Ghariani and Sadok, 2020). Similarly, the alcian blue and DMMB assays act to detect the presence of GAG based upon interaction with the respective dyes. Alcian blue is a tetravalent cation containing Cu^{2+} which interacts with sulphate groups of GAGs at low pH enabling their detection at 605 or 620 nm: following precipitation of the complexes with 0.4 M guanidine-HCl, removal of excess dye with DMSO and complex disassociation in 4 M guanidine-HCl. Dimethylethylene blue is a thiazine dye, which undergoes a metachromatic shift at 530nm in the presence of GAGs, which can subsequently be utilised to determine the presence of these carbohydrates in solution (Templeton, 1988). The alcian blue assay offers the advantage over DMMB in that it is not affected by contaminants such as proteins or nucleic acids, however it cannot detect the presence of HA or unsulphated GAGs (Frazier *et al.*, 2008; Talmoudi, Ghariani and Sadok, 2020). Furthermore, such metachromatic techniques only enable the estimation of total GAG content. Therefore, despite the increased simplicity of these methods,

when compared to agarose gel electrophoresis, the later method was selected to in order establish an estimate the presence and composition of GAGs within the crude extracts. Utilising this method galactosaminoglycans and glucosaminoglycans standards could clearly be distinguished as separate bands, with the latter possessing greater electrophoretic mobility. No separation was observed between HS and heparin or CS and DS standards when they were ran as a mixture, therefore largely precluding the accurate determination of GAG-subtype based upon this method. Furthermore, HA is not stained under the conditions utilised in this study (Volpi and Maccari, 2002). Another drawback of agarose gel electrophoresis (1,2- diaminopropane buffer) coupled with staining with toluidine blue is that DNA contaminants, which are also stained by toluidine blue, possess similar electrophoretic mobility to HS. DNA and HS can, however, often be distinguished based upon their metachromatic properties following staining, appearing light blue or dark blue/purple, respectively. Despite these drawbacks dark purple/blue bands corresponding to either CS/DS or heparin/HS were identified in all eight crude samples, albeit to different extents, enabling the estimation of the GAG composition of each sample. The crude samples obtained from clupeocephala all displayed primary bands corresponding to CS/DS whereas those isolated from Crustacea displayed primary bands corresponding HS/heparin (Table 15). This is in accordance with the literature, whereby the primary GAG species identified from clupeocephala and crustacea are CS/DS or heparin HS, respectively (Table 5, Table 7). Furthermore, CS/DS or heparin/HS could be observed with detection limits of species comprising ~10% of the total sample composition (~ 2 μ g), with the exception of the crude sample obtained from *P. pelagicus*.

In order to overcome the limitations of agarose electrophoresis, under the methodology employed in this work, several potential adaptations could be employed. Firstly, in order to further increase the resolution between HS and heparin or CS and DS a stacking gel could be employed utilising a low concentration of agarose in the absence of 1-2-diaminopropane, with the aim of concentrating the samples prior to separation. Furthermore, the optimum concentration of 1-2-diaminopropane (in both the running buffer and gel) and the percentage of agarose could be determined under the electrophoretic system employed in this study. Alternatively, the gel length and running time could be optimised in order to further improve the resolution. Previous studies have also utilised discontinuous buffer systems, employing 0.04 M barium acetate pH4.0 preceded by 0.05 M 1-2-diaminopropane pH9.0, in order to separate heparin from HS (Bianchini *et al.*, 1997; Medeiros *et al.*, 2000). Therefore, in order to further evaluate the GAG composition of the extracts isolated in the present work a discontinuous buffer system could have been utilised. Moreover, in order to overcome the absence of staining of HA by toluidine blue, a further staining step could be employed using Stains-All (Volpi and Maccari, 2002, 2006; Talmoudi, Ghariani and Sadok, 2020). This two-step staining method has also been demonstrated to increase the level of detection by approximately 10-fold, which may enable the detection of minor GAG components of the extracts that were not detected by agarose gel electrophoresis (*idem*).

Additional electrophoretic techniques, such those employing cellulose acetate and nitrocellulose, have also been established in order to resolve, heparin, HS, CS, DS, HA and KS (Cappelletti, Del Rosso and Chiarugi, 1979; Schuchman and Desnick, 1981; Volpi

and Maccari, 2006). All major GAG classes were separated by cellulose acetate electrophoresis performed discontinuously in barium acetate, followed by the same buffer with the addition of ethanol and stained with alcian blue (Cappelletti, Del Rosso and Chiarugi, 1979). This method exploits the differential binding of GAGs to barium acetate in addition to their sensitivity to being precipitated by organic solvents. Despite the resolution achieved by this method a major drawback is the requirement of several consecutive steps and sensitivity to the electrophoretic system utilised (*idem*). A further technique utilising cellulose acetate, performed in a buffer system comprised of EDTA and lithium chloride, followed by staining with alcian blue, has also been described to separate all major GAG species; this method is advantageous as it avoids the need of successive electrophoretic steps (Schuchman and Desnick, 1981). Electrophoresis employing nitrocellulose, performed in barium acetate and subsequently stained with Azur A, has also been reported to separate CS, DS, heparin (slow moving and fast-moving components) and KS. This methodology, however cannot separate HA from DS (Volpi, 1996a). In order to ascertain the GAG composition of the crude extracts obtained in this work, cellulose acetate electrophoresis performed in EDTA and lithium chloride could be compared to the aforementioned discontinuous agarose gel electrophoresis methodology, with successive staining with toluidine blue and Stains All (Schuchman and Desnick, 1981; Bianchini *et al.*, 1997; Volpi and Maccari, 2002). This would enable the determination of the optimum electrophoretic technique, which enables the separation of all major GAG species, in the lowest time, with minimum complexity and to the greatest degree of sensitivity.

Following estimating the GAG composition utilising agarose gel electrophoresis, ATR-FTIR spectroscopy was employed. The ATR-FTIR spectra of all eight crude extracts were characteristic of sulphated GAGs, with peaks corresponding to S=O and C-N vibrations of N-acetyl groups at $\sim 1248\text{ cm}^{-1}$ and 1559 cm^{-1} , respectively. In addition, peaks at 1430 cm^{-1} and 1635 cm^{-1} , which correspond to asymmetric and symmetric carbonyl stretching, were observed in all crude samples indicating the presence of uronic acid residues (Mainreck *et al.*, 2011; Devlin, Mauri, *et al.*, 2019; Devlin, Mycroft-West, *et al.*, 2019; Mauri *et al.*, 2019). This further corroborated that the crude extracts are primarily composed of sulphated GAGs, containing uronic acid and amino sugar residues (CS, DS, HS and heparin). The relative intensity of the peaks present at 990 cm^{-1} and 1025 cm^{-1} could also largely be utilized to estimate whether the major GAG component was CS, DS or HS/heparin like in nature. Heparin/HS standards exhibited a peak of greater intensity at 990 cm^{-1} in contrast to 1025 cm^{-1} , whereas the reverse was true for CS/DS samples. In addition, the FTIR spectra of DS standards exhibited an additional peak centering at 1045 cm^{-1} . In the case of the crude extract obtained from *P. pelagicus* the intensity of the peak present at 990 cm^{-1} was greater than that at 1025 cm^{-1} . The major GAG composition of the extract obtained from *P. pelagicus* was determined to be primarily HS/heparin by all other methods utilized for characterization in this study, supporting that the peak at 990 cm^{-1} is indicative of HS/heparin (Table 15). In contrast the extract obtained from *L. vannamei*, which was determined to be primarily HS/heparin by all other methods, exhibited split peak in the region of $990\text{-}1045\text{ cm}^{-1}$, with the peak observed 1025 cm^{-1} being greater in intensity (Table 15). $^1\text{H}\text{-}^{13}\text{C}$ HSQC NMR analysis of the crude *L. vannamei* indicated low proportion of epimerisation to IdoA units, despite the presence of relatively intense signals attributed GlcNAc/S, likely

indicating that the glucosaminoglycan present in this sample is primarily HS like. The relative intensity of the peak at 990 cm^{-1} , in contrast to 1025 cm^{-1} , was observed to be greater in the ATR-FTIR spectra of heparin standards in comparison to HS. As peaks in the region of $900\text{--}1200\text{ cm}^{-1}$ have previously been attributed to C-O-C stretches of the glycosidic bond (Tipson, 1968; Grant *et al.*, 1991; Devlin, Mauri, *et al.*, 2019), the level of epimerisation to IdoA, and the resulting influence on the anomericity of the linkage ($\beta \rightarrow \alpha$), could account for the relative increase in the intensity of the peak observed at 990 cm^{-1} in heparin. As the crude *L. vannamei* sample likely lacks extensive uronic acid epimerisation this could account for why the primary peak in the region of $990\text{--}1045$ occurs at 1025 cm^{-1} despite this extract being primarily composed of HS. Furthermore, the crude *L. vannamei* samples is composed of a mixture of CS and HS, therefore this likely also influences the overall observed peak intensity. With the exception of the crude *L. vannamei* sample, where the major peak occurred at 1025 cm^{-1} the primary GAG component of each extract was determined to be CS like by all other methods utilized for characterization in this study (Table 15). Furthermore, in the case of the crude extract from *P. hypothalamus*, which was determined to be primarily comprised of DS, the peak with the highest intensity in the region of $990\text{--}1045\text{ cm}^{-1}$ was the latter wavenumber. This may suggest that the peak at 1045 cm^{-1} is indicative of epimerisation of the uronic acid in galactosaminoglycans. The region between $990\text{--}1045\text{ cm}^{-1}$ may therefore, be utilized to estimate the prevalence each GAGs within a sample and extent of epimerisation. Previously, the presence of peaks at 820 cm^{-1} and 850 cm^{-1} have been suggested to be indicative of CSC and CSA, respectively (Mainreck *et al.*, 2011). This was also observed for CSC and CSA standards in the current work, however peaks were also observed at 820 cm^{-1} and 850 cm^{-1} in the ATR-FTIR spectra of

HS/heparin and DS standards, respectively. This suggests that peaks at 820 cm^{-1} and 850 cm^{-1} are may be indicative of sulphation at position 6 or 4, regardless of the underlying GAG backbone. All of the crude GAG extracts exhibited peaks at both 820 cm^{-1} and 850 cm^{-1} , with the exception of *O. gorbuscha* and *M. merluccius*, in which a peak was observed solely at the latter wavenumber. Based upon the ATR-FTIR spectra this suggests that the crude extracts obtained from *O. gorbuscha* and *M. merluccius* lack sulphation at position 6 of the amino sugar, whereas all other crude samples possess a mixture of sulphation patterns, albeit to different extents. This was partially supported by ^1H - ^{13}C NMR, which indicated that the extracts obtained from *O. gorbuscha* and *M. merluccius* contain the highest level of 6OH, at ~ 85 and $\sim 75\%$, respectively. This, therefore supports that the peaks at 820 cm^{-1} and 850 cm^{-1} may be indicative of the level of 4S or 6S modifications present within the GAG. It is however important to note that signals corresponding to sulphation at position 4 were not detected in the NMR spectrum as a result of overlapping resonances with H_2O . Therefore, further correlation analysis should be conducted in conjunction with NMR spectroscopy (performed at $\sim 333\text{K}$), utilizing GAGs with known total sulphate compositions, in order to support this claim. As further assignments of the GAG composition based solely upon the ATR-FTIR is prohibited due to the complexity and extensive signal overlap, post-acquisition PCA was employed as previously described (Devlin, Mauri, *et al.*, 2019; Devlin, Mycroft-West, *et al.*, 2019). By employing PCA against a library of GAG standards, the primary component of each extract could easily be established, by comparison of PC1 and PC2. Where the crude extracts contained a mixture of GAGs, the extent of separation between regions corresponding to each GAG standard allowed for qualitative estimation of the samples composition. For instance, the crude extract isolated from *P.*

pelagicus was found to be composed of ~ 70% HS and 30% CS by NMR spectroscopy, whereas the extract obtained from *L. vannamei* determined to be ~ 60% HS and 30% CS. Both samples located towards the region associated with HS/heparin, however the latter samples was separated further towards the CS region across PC1. For the extracts obtained from clupeocephala, which were primarily composed of CS and DS (Table 16, Table 15) the extent of separation between the regions associated with CS and DS was also indicative of the extent of either component within the sample. For instance, the extracts obtained from *C. batrachus* and *S. pilchardus* containing ~90% and 78% CS, respectively were located within the CS cluster. Whereas the extract obtained from *P. hypophthalmus* (composed of 60% DS) was located with the DS region. All other clupeocephala extracts were located between these regions, with the extent of separation towards CS or DS, across PC2, indicating which of the respective components is present to the greatest extent within the sample. Therefore, while ATR-FTIR coupled with PCA cannot provide a quantitative estimation of the overall GAG composition within each extract, akin to that which can be obtained from NMR, the former technique could be utilised to provide an accurate estimation of the composition of each sample qualitatively.

Circular dichroism coupled with PCA has also been utilized to distinguish between GAG sub-types primarily based upon the sensitivity of this technique to the conformation and environment of the uronic acid residue (Stone, 1971; Rudd, Skidmore, Guimond, Cosentino, *et al.*, 2009). Heparin and HS standards could be clearly distinguished from other GAG classes by the presence of a positive CD band at ~190 nm, with the former being of greater intensity. This is in agreement with previous reports and has attributed

to the orientation of the glycosidic linkage, extent of epimerisation and presence of sulphate modifications (Stone, 1971; Park and Chakrabarti, 1978; Rudd, Yates and Hricovini, 2009; Stanley and Stalcup, 2011). Furthermore, all standard GAGs exhibited a negative CD band at ~210 nm, albeit with differing intensities: HS>HA>CS>DS>heparin. The difference in intensity of the negative CD band at ~210 nm has also been suggested to result from the level of epimerisation of the uronic acid residue and extent of sulphate modifications (Rudd, Skidmore, Guimond, Cosentino, *et al.*, 2009; Stanley and Stalcup, 2011). With the exception of the extract obtained from *L. vannamei*, which possessed a minor positive CD band at ~190 nm, all crude extracts exhibited a negative CD band at both ~190 nm and ~210 nm. Therefore, all eight crude extracts exhibited CD spectra characteristic of GAGs. Due to the broad CD spectral features of CD, which are a summation of the samples total composition, elucidation of the structural characteristics of the sample is largely prohibited based solely upon individual spectra. As a result, post-acquisition multivariate analysis against a library of standards is often employed to enable further characterization. For instance, many databases are widely available which permit the determination of protein secondary structure based upon their CD spectra. Here PCA, was able to clearly distinguish between all GAG classes analyzed, including CS, DS, HS, heparin and HA when PC1 and PC2 were compared. Furthermore, when the CD spectra of the crude GAG extracts were subjected to PCA against the same library of standards the primary GAG components of each sample could be established. For instance, the extract obtained from *P. pelagicus* was located within the region associated with HS, however PC1 separated the sample marginally towards the region containing CS. The *P. pelagicus* extract was subsequently determined to be composed of ~70% HS and 30% CS by ¹H NMR spectroscopy, therefore

confirming the results obtained following PCA of the CD spectrum. Alike to PCA of the ATR-FTIR spectrum, analysis of the CD spectra of *L. vannamei* also located within the region containing HS, however PC1 separated this sample further towards CS, indicating that this sample likely contains a greater amount of this GAG than the extract obtained from *P. pelagicus*. This was again confirmed by ^1H NMR spectroscopy which indicated that the *L. vannamei* sample contained ~60% HS and ~40% CS. The extracts obtained from clupeocephala, which were primarily composed of CS and DS (Table 15, Table 16), all separated between the regions associated with CS and DS. With the exception of the extract obtained from *C. batrachus*, the extent of separation between these regions was indicative of the level of CS and DS present within the sample, as confirmed by NMR spectroscopy (Table 15, Table 16). This discrepancy may be a result of underestimation of the percentage of DS present within the *C. batrachus* by integration of the ^1H NMR spectrum. All other clupeocephala extracts which were found to contain predominantly CS were located within the CS and DS region, with the extent of separation towards the latter region by PC2 correlating with the increasing concentration of DS within the sample. Therefore, alike to ATR-FTIR, CD can be utilised to provide a qualitative estimation of the composition of each sample, albeit with less sensitivity, when coupled with PCA.

Table 15: The prevalence of GAGs detected within each crude extract by agarose gel electrophoresis (AGE), ATR-FTIR, CD and NMR. +; detected, ++; estimated predominant component.

Species	AGE			ATR-FTIR			CD			NMR		
	HS	CS	DS	HS	CS	DS	HS	CS	DS	HS	CS	DS
<i>P. pelagicus</i>	++			++	+		++	+	+	++	+	+
<i>L. vannamei</i>	++	+	+	++	+		++	+	+	++	+	+
<i>S. pilchardus</i>		++	+		++					+	++	+
<i>M. aeglefinus</i>		+	+		+	+		+	+	+	+	+
<i>M. merluccius</i>		+	+		++	+		++	+	+	++	+
<i>P. hypophthalmus</i>		+	++			++		+	++	+	+	++
<i>C. batrachus</i>		+	+		++	+		+	+	+	++	+
<i>O. gorbuscha</i>		+	+		+	+		++	+	+	++	+

In conclusion all of the techniques employed enabled an estimation of the major GAG components to be determined to a good degree of accuracy, with each technique identifying the identical primary component within each crude sample; *P. pelagicus* (HS), *L. vannamei* (HS), *S. pilchardus* (CS) *M. merluccius* (CS), *C. batrachus* (CS), *M. aeglefinus* (CS), *O. gorbuscha* (CS) and *P. hypophthalmus* (DS) (Table 15). Furthermore, components that were present at approximately >20% were detected by ATR-FTIR and CD spectroscopy coupled with PCA, for example CS present in *P. pelagicus* and *L. vannamei* (Table 15, Table 16). Additional minor components (approximately <20%) were identified within all samples by NMR spectroscopy (Table 15, Table 16). Despite this agarose gel electrophoresis is a useful low-cost method for the estimation of GAG composition, within crude samples, which does not require access to specialist equipment. Furthermore, detection limits and resolution between GAGs could be increased by the use of discontinuous buffer systems and additional staining steps. ATR-

FTIR and CS spectroscopy, although requiring more specialised equipment, displayed a greater level of sensitivity for the elucidation GAG components within the crude samples, in particular when utilised in conjunction with PCA. ATR-FTIR, was however found to be superior to CD, as the latter technique was less sensitive for discriminating between galactosaminoglycans. Furthermore, ATR-FTIR offers the advantage of low-cost portable equipment, minimal sample preparation time and estimation of degree and positions of sulphate modifications. ATR-FTIR for the analysis of crude GAG samples is also advantageous over NMR spectroscopy as a result of the latter technique requiring substantial spectral acquisition time, greater costs and the requirement of large amounts of sample. In addition, the presence of contaminants within crude samples can greatly affect the observed chemical shifts making NMR spectrum analysis challenging. Therefore, ATR-FTIR was found to be a superior method for elucidating the GAG composition of crude samples prior to further purification. The composition of the crude GAG extracts from clupeocephala and crustacea were found to be in accordance with the literature, containing predominantly CS/DS and HS/heparin, respectively (Table 5, Table 7).

Table 16: Percentage BACE-1 inhibitory activities and approximate composition of crude GAG extracts.

Species	HS/heparin (%)	CS (%)	DS (%)	% BACE-1 inhibitory activity
<i>P. pelagicus</i>	70	30	<1	93
<i>L. vannamei</i>	60	40	<5	-21
<i>S. pilchardus</i>	10	78	12	-16
<i>M. aeglefinus</i>	<2	58	42	38
<i>M. merluccius</i>	25	63	12	49
<i>C. batrachus</i>	<5	90	<5	42
<i>P. hypophthalmus</i>	10	30	60	28
<i>O. gorbuscha</i>	10	60	30	38

4.3.2. Determination of BACE-1 inhibitory activity of crude glycosaminoglycans extracts from aquatic species.

Following the extraction and characterisation of the composition of the crude GAGs extracts obtained from *P. pelagicus*, *M. merluccius*, *C. batrachus*, *G. morhua*, *M. aeglefinus*, *O. gorbuscha*, *P. hypophthalmus*, *S. pilchardus* and *L. vannamei*, they were screened for BACE-1 inhibitory activity in comparison to mammalian heparin.

Porcine intestinal mucosa heparin exhibited at IC_{50} of $2.4 \mu\text{g.mL}^{-1}$, this is in close accordance with previous reports which state an IC_{50} for heparin between $1\text{--}10 \mu\text{g.mL}^{-1}$ (Scholefield *et al.*, 2003; Hadfield, 2018); with the exception of Patey *et al.*, (2006) who observed an IC_{50} of $\sim 28 \text{ ng.mL}^{-1}$. This observed difference may be attributed to different experimental conditions and FRET pairs utilised. In addition, Beckman *et al.*, (2006) reported that BACE-1 activity was stimulated in the presence of $1 \mu\text{g.mL}^{-1}$ of heparin during the initial phase of the reaction, which was subsequently succeeded by enzyme inhibition. This promotion effect induced by low concentrations of heparin was suggested to be dependent upon interactions with the prodomain of BACE-1, with the mature enzyme lacking this ability (Beckman, Holsinger and Small, 2006; Klaver *et al.*, 2010). Furthermore, Beckman *et al.*, 2006 proposed that binding of the prodomain of BACE-1 induced an increase in autocatalytic cleavage of BACE-1 resulting in a corresponding increase in activity. Similarly, a promontory phase was also observed at low concentrations of heparin in this study ($1250.0\text{--}312.5 \text{ ng.mL}^{-1}$). When the time course reaction was monitored, a similar duple promontory and inhibitory phase was also observed in the presence of low concentrations of heparin. In contrast to this no

promontory affect was reported by Scholefield et al., 2003 or Patey et al., 2006, 2008. As the zymogen form of BACE-1 (Thr²²-Thr⁴⁵⁷) was utilised in this study, this possibly accounts for the promontory effect observed in the presence of low concentrations of heparin and supports the findings presented by Beckman et al., 2006 (Figure 40, Appendix 1).

The concentration at which heparin was found to exert maximum inhibition was observed to be 5 $\mu\text{g.mL}^{-1}$ (~92%), therefore this concentration was selected for screening of the crude GAG extracts. The extract obtained from *P. pelagicus*, comprised of 70% heparin/HS and 30% CS, exhibited the highest BACE-1 inhibitory activity at ~93%. This is in line with previous reports by Schofield et al., 2003, who only observed BACE-1 inhibition of by heparin, while CS and DS were reported possess negligible activity. All other crude extracts were observed to possess <50% BACE-1 inhibition at 5 $\mu\text{g.mL}^{-1}$. The extracts obtained from clupeocephala exhibited BACE-1 inhibition of between -16-49%. In particular the extract obtained from *C. batrachus*, containing approximately >90% CS, was observed to possess a BACE-1 inhibitory activity of ~42%. In addition, the extract obtained from *P. hypothalamus*, which primarily contained DS, exhibited BACE-1 inhibitory activity at ~28%. When the BACE-1 inhibitory activity of galactosaminoglycan standards was compared to that of heparin, under matched conditions, all samples possessed BACE-1 inhibitory activity of > 50% when tested at 5 $\mu\text{g.mL}^{-1}$ (PMH>CSC>CSD>CSA>CSD>CSE). This indicates that while reduced in comparison to heparin, galactosaminoglycans may exhibit greater BACE-1 inhibitory activity than previously reported by Scholefield et al., (2003). Furthermore, the BACE-1 inhibitory activity of galactosaminoglycans is likely to be dependent on the fine structure, akin to

that of HS/heparin, reported by Patey *et al.* 2006. This difference may therefore, be accounted for by the fine structure of the galactosaminoglycans utilised by Scholefield *et al.*, 2003, which was not reported. Furthermore, the different experimental conditions utilised by Scholefield *et al.*, 2006, also likely contributes to the observed difference in BACE-1 inhibition by galactosaminoglycans as a lower maximal inhibition was also observed for heparin at 60%.

The extracts obtained from *L. vannamei* and *S. pilchardus* containing predominantly HS and CS, respectively were observed to promote BACE-1 activity at the concentration tested. Although extracts obtained from both *L. vannamei* and *S. pilchardus* exhibited negative inhibitory values, this may be a result of the active component of the extract being present in low quantities. This is supported by the time-course of BACE-1 activity, which indicates dual promontory and inhibitory phases; alike to that observed in the presence of low concentrations of heparin (Appendix 2). Therefore, further purification of the eight crude extracts, which are composed of a mixture of GAG species, may result in isolation of fractions possessing increased BACE-1 inhibitory activity.

4.3.3. Fractionation of glycosaminoglycans extracts from aquatic species with potent BACE-1 inhibitory activity.

With the aim of further purifying the active components within the crude GAG extracts, each sample was subjected to weak anion exchange DEAE-Sephacel chromatography, in order to separate the components based upon charge, and the BACE-1 activity of the resulting fractions was subsequently determined.

Table 17: Percentage BACE-1 inhibition by fractionated GAG extracts determined using FRET. * In comparison to the respective crude sample.

Species	Fraction	% BACE-1 inhibition	Increase in % BACE-1 inhibition *
<i>P. pelagicus</i>	5	96	3
<i>L. vannamei</i>	3	6	15
	4	91	112
	5	71	92
<i>S. pilchardus</i>	4	75	91
<i>M. aeglefinus</i>	3	57	19
	4	56	18
	5	64	26
<i>M. merluccius</i>	4	55	6
	5	45	-4
<i>C. batrachus</i>	3	50	8
	4	40	-2
	5	64	8
	6	14	-26
<i>P. hypophthalmus</i>	4	45	17
	5	45	17
<i>O. gorbuscha</i>	4	-5	-43
	5	20	-18

With the exception of the extracts obtained from *O. gorbuscha*, fractionation resulted in an increase of BACE-1 activity. The highest percentage increase in BACE-1 activity was observed for the samples obtained from *L. vannamei* and *S. pilchardus*, in which the crude samples exhibited negative inhibition. For *L. vannamei* the sample eluted obtained by elution at 0.8 (F4) and 1 M NaCl (F5) displayed 91% and 71% BACE-1 inhibitory activity, respectfully. The fraction eluted at a lower NaCl concentration displayed greater activity, this may suggest that BACE-1 inhibition by GAGs is not solely

dependent on total anionic strength. This supports the work presented by Patey *et al.*, 2006, who demonstrated that over sulphation of heparin resulted in a loss in BACE-1 inhibitory activity. Furthermore, De-N-sulphation of was observed to increase the BACE-1 inhibitory activity of heparin (Patey *et al.*, 2006). The *L. vannamei* sample eluted at 0.5 M NaCl (F3), however displayed negligible BACE-1 inhibitory activity. This supports that the crude sample contained a mixture of active and inactive species and resulted in the observation of BACE-1 promotion for the crude sample, as the former was present at lower concentrations. This is also likely, for the extract obtained for *S. pilchardus*, in which the fraction eluted at 0.8 M NaCl (F4) displayed a BACE-1 inhibitory activity of 75%, in comparison to the crude sample at -16%. The extracts obtained from *M. aeglefinus*, *M. merluccius*, *C. batrachus* and *P. hypophthalmus* displayed negligible increases in BACE-1 inhibitory activity of no greater than 25%. Of these the fractions displaying the highest BACE-1 activity were *M. aeglefinus* and *C. batrachus* fraction 5 (0.8 M NaCl) at 64% (Table 17). Therefore, the fractionated samples obtained from *P. pelagicus* (F5), *L. vannamei* (F4 and F5) and *S. pilchardus* (F4), possessed the greatest BACE-1 inhibitory activity at 96%, 91%, 71% and 75%, respectively (Table 17). As a result, these compounds were selected for further characterisation.

Chapter 5: A glycosaminoglycan extract isolated from *Portunus pelagicus*, inhibits the Alzheimer's beta-secretase, BACE-1, with attenuated off target activities.

5.1. Introduction

Portunus pelagicus, commonly referred to as the blue swimming crab, belongs to the crustacea class and predominantly inhabits coastal regions of Southeast and Eastern Asia (Azra and Ikhwanuddin, 2015). Presently, *P. pelagicus* is acquired primarily from wild caught stocks, however as a result of increasing demands efforts are being directed towards the development of more sustainable and effective aquaculture methodologies for this economically important species (*idem*). Capture of *P. pelagicus* from wild stocks accounted for approximately 5% of the total crustaceans captured globally in 2018 at 298 thousand tonnes (FAO, 2020), whereas aquaculture accounted for 29 tonnes as of 2016 (*idem*). The number of *P. pelagicus* acquired from aquaculture has however, risen by 26 tonnes, from 3 tonnes in 2005, indicating the increasing utilisation of farming of this species.

P. pelagicus is primarily sold whole (alive or frozen) or utilised for industrial canning of the flesh obtained from the leg, claw, body and/or shoulder, following cooking and removal of the shell (Featherstone, 2016; FAO, 2020). The principal waste product obtained from industrial processing of *P. pelagicus* is therefore the shell, which is composed primarily of protein, chitin and mineral salts (Vázquez *et al.*, 2013). As such, crab shells have been suggested to be a valuable source of chitin; a polysaccharide composed of repeating GlcNAc, which possesses various bioactivities (Ravi Kumar, 2000; Kurita, 2006). In addition to the shell, a smaller proportion of cartilage and muscle is often present among waste obtained from the crab flesh canning industry (Vázquez *et al.*, 2013). The presence of GAGs within crab shells has yet to be described, however

several reports have identified CS and heparin/HS within the flesh and cartilage of various crab species (Yamada, Sugahara and Özbek, 2011)(Table 5, Table 7)

Such GAGs have been reported to possess a diverse array of biological activities, while presenting an attenuated ability to perturb the coagulation cascade (Medeiros *et al.*, 2000; Andrade *et al.*, 2013). Thus, each heparin/heparin-like compound from crab tissues tends to be a hitherto unknown compound with unique structural features and a potential novel therapeutic agent. As a result, the flesh of *P. pelagicus* obtained from the canning industry was evaluated as a potential source of GAGs, which possess the ability to inhibit BACE-1.

5.1.2 Chapter aims

The crude extract isolated from *P. pelagicus* was fractionated utilising DEAE anion exchange chromatography, produced a primary eluant at 1 M NaCl (termed *P. pelagicus* F5). The resulting sample was observed to possess a BACE-1 inhibitory activity of 96% at 5 $\mu\text{g}.\text{ml}^{-1}$, which is equivalent to that of mammalian heparin (Section 4.2). The crude sample of *P. pelagicus* was determined to be composed primarily of a heparin/HS, with a minor CS component. The aim of this chapter is therefore, to characterise the fractionated *P. pelagicus* F5 sample and to further elucidate the BACE-1 inhibitory activity of this extract. Additionally, the interaction between the *P. pelagicus* F5 extract and BACE-1 will be examined utilising differential scanning fluorimetry (DSF) and circular dichroism. This will enable the examination of the conformation and thermal stability of BACE-1, upon binding to *P. pelagicus* or mammalian heparin, in order to elucidate whether the mechanism of inhibition is similar to that of known peptide

inhibitors (Lo *et al.*, 2004). Furthermore, *P. pelagicus* F5 will be evaluated for the known potential off-target activities of heparin; anticoagulant activity and inhibition of the aspartic protease renin. Finally, the effect of *P. pelagicus* F5 on cell viability will be evaluated.

5.2. Results

5.2.1. Characterisation of the glycosaminoglycan extract from *Portunus pelagicus*, fraction 5.

The extract obtained from *P. pelagicus* (F5) was observed to possess electrophoretic mobility in line with that of mammalian HS/heparin, when subjected to agarose electrophoresis in 1,3-diaminopropane buffer (pH 9.0). No bands were observed that corresponded to chondroitin sulphate or dermatan sulphate (DS) (Figure 46) suggesting glucosaminoglycans are the primary constituent of the sample.

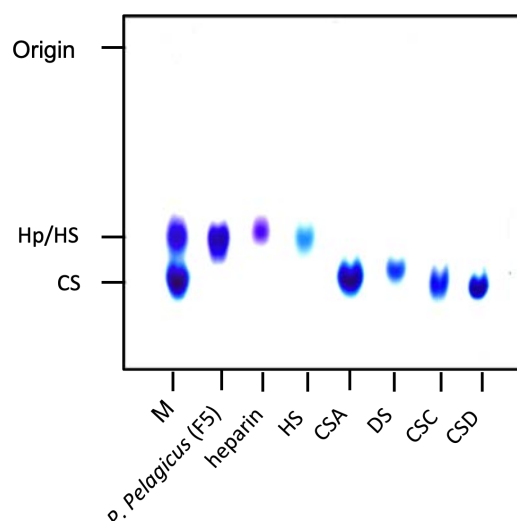


Figure 46: Agarose gel electrophoresis of *P. pelagicus* F5. The electrophoretic mobility of *P. pelagicus* F5 was compared to that of bone fide glycosaminoglycan standards, heparin (Hp), heparan sulphate (HS), dermatan sulphate (DS) and chondroitin sulphate A, C and D (CSA, CSC and CSD, respectively). M: CSA, Hp and HS mixture.

In order to corroborate that the *P. pelagicus* (F5) sample is composed primarily of heparin/HS, ATR-FTIR and CD spectroscopy coupled with PCA was employed. The ATR-FTIR spectra of *P. pelagicus* F5 exhibited similar spectral features to that of heparin, including bands attributed to sulphated uronic acid containing GAGs, at 1230 cm^{-1} , 1430 cm^{-1} and 1635 cm^{-1} , which are associated with S=O stretches, symmetric carbonyl stretching and asymmetric stretches, respectively. Furthermore, bands can also be observed at 990 cm^{-1} and 1025 cm^{-1} , which are indicative of HS/ heparin and CS respectively, within the *P. pelagicus* F5 sample, with the former band being higher in intensity. Several bands were also detected in the region of 750-880 cm^{-1} , which is commonly associated with the presence of sulphation. Additional peaks were also observed in the *P. pelagicus* F5 sample located at ~ 1750 , ~ 1370 cm^{-1} and 770 cm^{-1} that were absent in heparin (Figure 47).

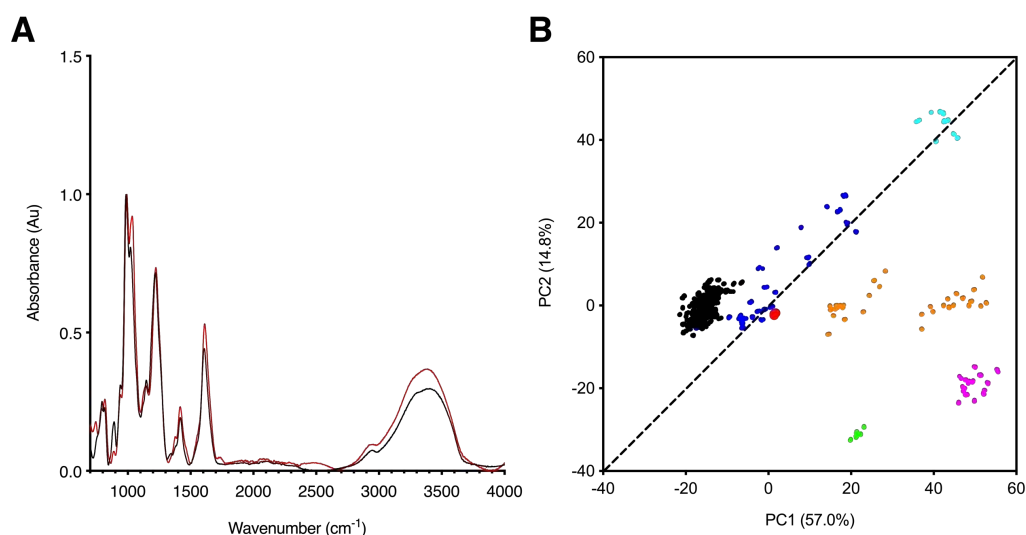


Figure 47: ATR-FTIR spectra of *P. pelagicus* F5. (A) ATR-FTIR spectra of porcine mucosal heparin (black) and *P. pelagicus* F5; (red), $n = 5$. (B) Principal component analysis (PCA) score plot for PC1 vs. PC2 of *P. pelagicus* F5 against a bone fide GAG library. Heparin, black; HS, blue; CS, orange; DS, magenta; hyaluronic acid (HA), cyan; oversulphated-CS, green and *P. pelagicus* F5, red (filled circle).

The ATR-FTIR spectrum of *P. pelagicus* F5 was subsequently subjected to PCA against the previously described library of GAGs. When PC1 and PC2 were compared the *P. pelagicus* F5 sample located within the region associated with HS, although the former component (covering ~57% of the total variance) separated the sample marginally towards the CS region (Figure 47). This location has previously been associated with heparin/HS samples containing minor CS components (Devlin, Mycroft-West, *et al.*, 2019). Principal component 2, covering ~15% of the total variance, separated *P. pelagicus* F5 towards the region indicative of HS/ heparin possessing a higher DoS.

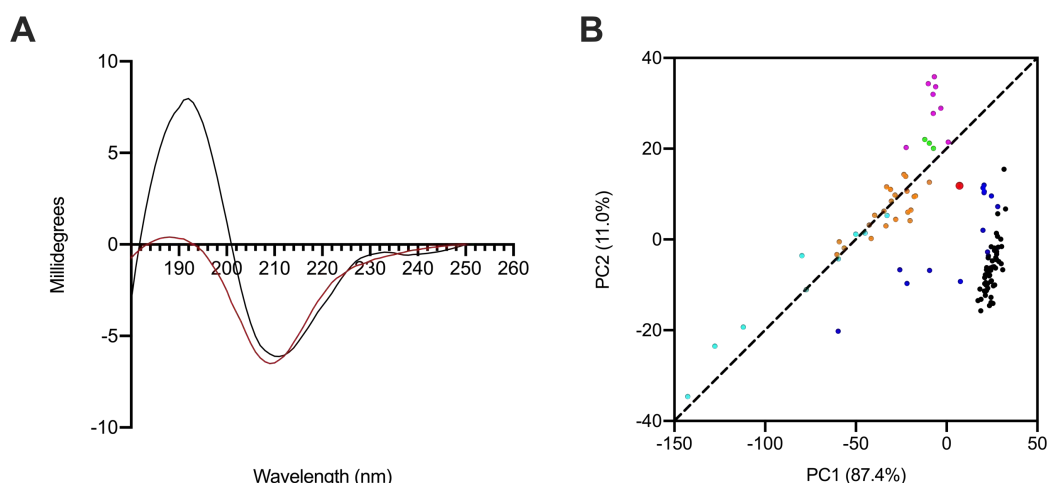


Figure 48: CD spectra of *P. pelagicus* F5. (A) CD spectra of porcine mucosal heparin (black) and *P. pelagicus* F5; (red), $n = 5$. (B) Principal component analysis (PCA) score plot for PC1 vs. PC2 of *P. pelagicus* F5 against a bone fide GAG library. Heparin, black; HS, blue; CS, orange; DS, magenta; hyaluronic acid (HA), cyan; oversulphated-CS, green and *P. pelagicus* F5, red (filled circle).

The CD spectrum of *P. pelagicus* F5 exhibited spectral features typical of GAGs with a negative CD band centring at ~210 nm and a positive CD band at ~190 nm. The intensity of the band observed at ~190 nm was however, greatly reduced in comparison to mammalian heparin, while that at ~210 nm was comparable (Figure 48). The CD spectrum of *P. pelagicus* F5 was subsequently interrogated against the previously described library of GAG standards, the sample. When PC1 and PC2 were compared

(covering ~98% of the total variance) the *P. pelagicus* F5 sample was located between the regions associated with CS and HS. Principal component 1, covering ~87% of the total variance however, separated the sample closer towards HS than CS (Figure 48). The ATR-FTIR and CS spectra of *P. pelagicus* F5, therefore suggest that the sample is primarily comprised of HS, with a minor CS component.

In order to further elucidate the fine structure of *P. pelagicus* F5 the sample was subjected disaccharide composition analysis following being exhaustively digested with *Flavobacterium heparinum* lyases I, II and III. The resulting products obtained following the digestion of *P. pelagicus* F5, heparin and HS control samples were analysed using SAX chromatography and the retention times compared to those of the eight common Δ -disaccharide standards present within both heparin and HS (Figure 49, Figure 50, Figure 51, Table 18).

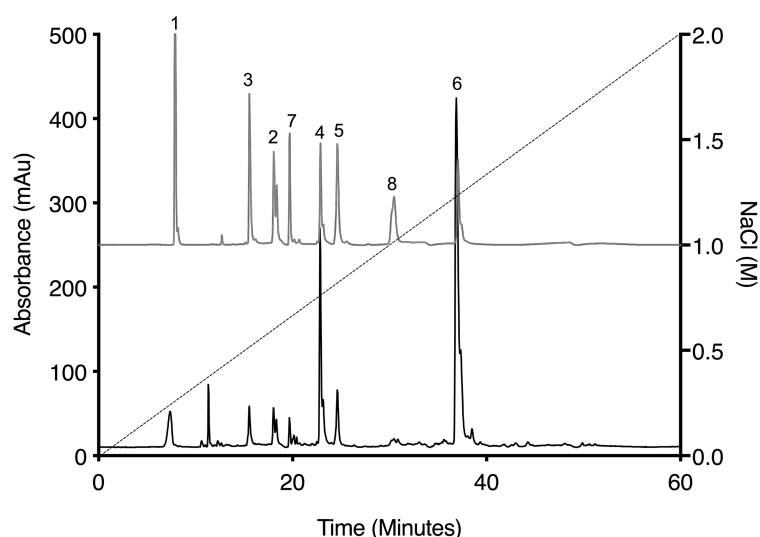


Figure 49: UV-SAX HPLC disaccharide composition analysis performed on the bacterial lyase digest of PIMH in reference to the eight common Δ -disaccharide standards. PMH (black), Δ -disaccharide standards (grey), 1; Δ UA-GlcNAc, 2; Δ UA-GlcNAc(6S), 3; Δ UA-GlcNS, 4; Δ UA-GlcNS(6S), 5; Δ UA(2S)-GlcNS, 6; Δ UA(2S)-GlcNS(6S), 7; Δ UA-(2S)-GlcNAc, 8; Δ UA(2S)-GlcNAc(6S). Elution was achieved with a linear gradient of 0–2 M NaCl (dashed line). Elution of Δ -disaccharides was monitored at $\lambda_{\text{Abs}} = 232$ nm.

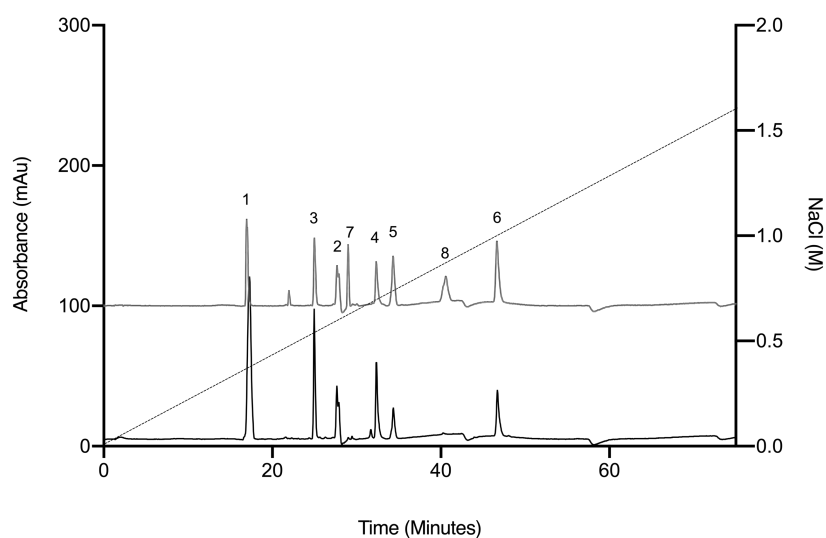


Figure 50: UV-SAX HPLC disaccharide composition analysis performed on the bacterial lyase digest of HS in reference to the eight common Δ -disaccharide standards. HS (black), Δ -disaccharide standards (grey), 1; Δ UA-GlcNAc, 2; Δ UA-GlcNAc(6S), 3; Δ UA-GlcNS, 4; Δ UA-GlcNS(6S), 5; Δ UA(2S)-GlcNS, 6; Δ UA(2S)-GlcNS(6S), 7; Δ UA-(2S)-GlcNAc, 8; Δ UA(2S)-GlcNAc(6S). Elution was achieved with a linear gradient of 0–2 M NaCl (dashed line). Elution of Δ -disaccharides was monitored at $\lambda_{\text{Abs}} = 232$ nm.

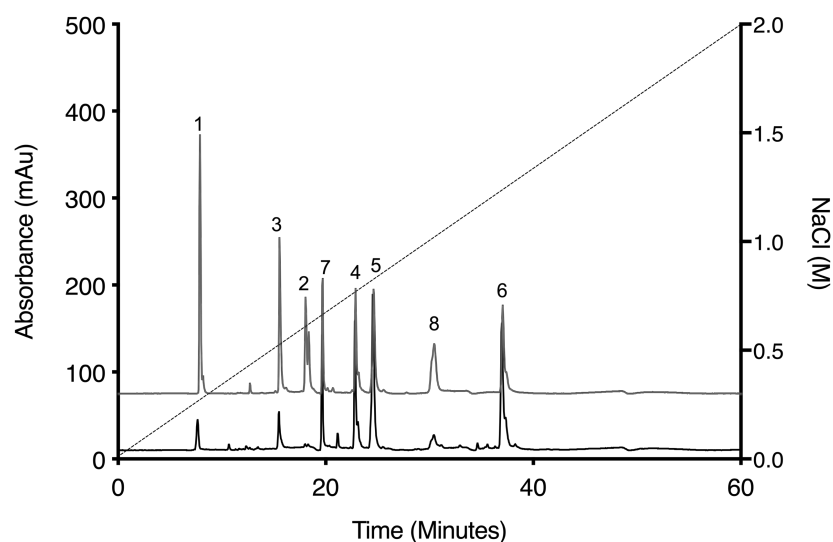


Figure 51: UV-SAX HPLC disaccharide composition analysis performed on the bacterial lyase digest of *P. pelagicus* F5 in reference to the eight common Δ -disaccharide standards. *P. pelagicus* F5 (black), Δ -disaccharide standards (grey), 1; Δ UA-GlcNAc, 2; Δ UA-GlcNAc(6S), 3; Δ UA-GlcNS, 4; Δ UA-GlcNS(6S), 5; Δ UA(2S)-GlcNS, 6; Δ UA(2S)-GlcNS(6S), 7; Δ UA-(2S)-GlcNAc, 8; Δ UA(2S)-GlcNAc(6S). Elution was achieved with a linear gradient of 0–2 M NaCl (dashed line). Elution of Δ -disaccharides was monitored at $\lambda_{\text{Abs}} = 232$ nm.

The digest products detected for PIMH were in close accordance with the previously reported disaccharide profile of heparin (Skidmore *et al.*, 2006), with 51.5% and 22.9 %of the total products being attributable to trisulphated Δ -UA(2S)-GlcNS(6S) and Δ -UA-GlcNS(6S) disaccharides, respectively. Mono- (12.3%) or unsulphated disaccharides (4.3%,) were also observed for PIMH in low abundance. A more disperse sulphation profile was observed for the *P. pelagicus* F5 sample (Table 18), with a relatively lower proportion of trisulphated disaccharides in comparison to PIMH at 23.1%. The *P. pelagicus* F5 sample also contained a higher proportion of monosulphated disaccharides (24.4%), of which 16.5% was attributed to Δ -UA(2S)-GlcNAc. Furthermore, a higher proportion of Δ -UA(2S)-GlcNS (23.5%) was detected in the *P. pelagicus* F5 sample, in comparison to PIMH (5.9%), indicating that the former compound displays distinct structural characteristics. Such features also contrast with that of mammalian HS, where approximately 50–70% of the total disaccharide composition can be attributed to Δ -UA-GlcNAc/ Δ -UA-GlcNS (Dietrich *et al.*, 1998; Skidmore *et al.*, 2006; Zhang *et al.*, 2009; Andrade *et al.*, 2013) (Table 18). In addition, the disaccharide profile of *P. pelagicus* F5 presents a greater proportion of trisulphated disaccharides (Δ -UA(2S)-GlcNS(6S); 23.1%) than commonly present in mammalian HS (7%) (Table 18).

Table 18: Corrected disaccharide composition analysis of *P. pelagicus* F5, heparin and HS.

Δ-Disaccharide	<i>P. pelagicus</i> F5 (%)	Heparin (%)	HS (%)
Δ -UA-GlcNAc	2.8	4.3	37.7
Δ -UA-GlcNS	5.6	4.2	17.8
Δ -UA-GlcNAc(6S)	2.3	5.0	12.8
Δ -UA(2S)-GlcNAc	16.5	3.1	0.4
Δ -UA-GlcNS(6S)	20.2	22.9	18.0
Δ -UA(2S)-GlcNS	23.5	5.9	6.0
Δ -UA(2S)-GlcNAc(6S)	6.0	3.1	0.4
Δ -UAs(2S)-GlcNS(6S)	23.1	51.5	7.0

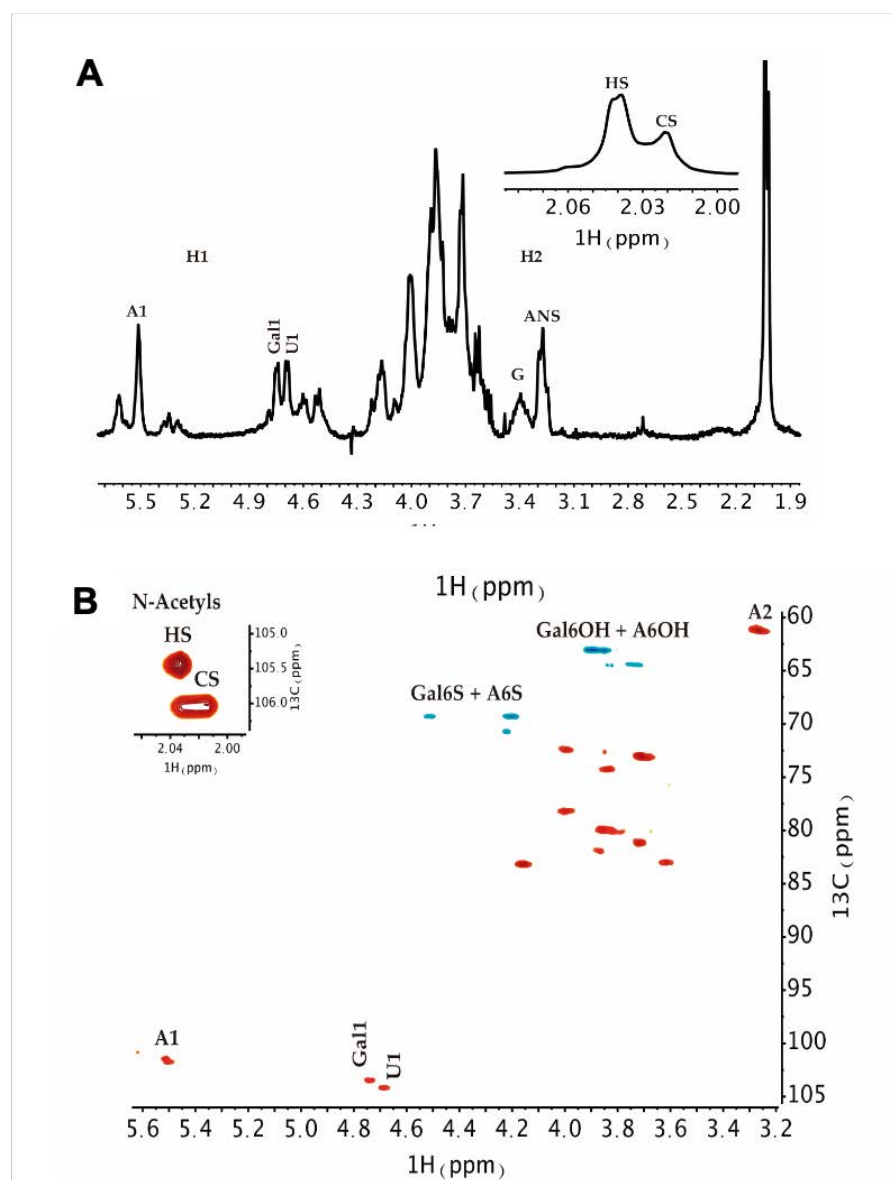


Figure 52: NMR spectra of *P. pelagicus* F5. (A) ^1H and (B) ^1H - ^{13}C HSQC NMR spectra of *P. pelagicus* F5 performed at 343 K. Major signals associated with HS and CS are indicated. Spectral integration was performed on the HSQC using labelled signals. Key: glucosamine, A; uronic acid, U; N-Acetyl, Nac and galactosamine, Gal.

Subsequently, ^1H and ^1H - ^{13}C Heteronuclear Single-Quantum Correlation (HSQC) NMR was employed to confirm the GAG composition of the *P. pelagicus* F5 sample. Both HS and CS (Figure 52) can easily identified within the ^1H spectrum of *P. pelagicus* F5 by the two N-acetyl signals at 2.04 ppm and 2.02 ppm, respectively. Negligible signals associated with the N-acetyl signal of DS were observed at approximately, 2.06 ppm

(Figure 50A, insert). Further signals associated with HS/heparin could be observed at ~5.5 ppm and ~3.3 ppm, corresponding to A2 and I1, respectively (Figure 52). Peaks corresponding to U2, Gal1 and U1 of CS can also be observed within the ^1H spectrum of *P. pelagicus* F5 at ~3.4 ppm, ~4.5 ppm and ~4.6 ppm (Figure 52). Integration of acetyl and A2 signals present within the ^1H spectrum of *P. pelagicus* F5 indicated that the sample was composed of approximately 75% HS and 25% CS. ^1H – ^{13}C HSQC NMR was utilised to further resolve the overlapping signals and to confirm the estimated polysaccharide composition using peak volume integration. Integration of N-acetyl and A2 signals was in agreement with the ^1H spectrum in that the extract is composed of approximately 75% HS and 25% CS (Figure 52). The combined integration of the N-acetyl and A2 signals indicated that the *P. pelagicus* F5 sample possesses a high proportion of N-sulphated residues, at approximately 76%. This supports the HPLC-based empirical disaccharide analysis, which indicated a total NS content of 72.4% (Figure 52, Table 18). Integration of signals associated with the presence, or absence, of sulphate modifications at position 6 of glucosamine, within the ^1H – ^{13}C HSQC spectrum, revealed that the *P. pelagicus* F5 sample was composed of approximately 60% of residues bearing this modification. Together, this data establishes that the HS of *P. pelagicus* F5 is considerably more sulphated than HS commonly extracted from mammalian sources (Table 18). In regard to the CS element of the *P. pelagicus* F5 sample, signals associated with the sulphation are present, however at low proportions, with galactosamine 6-O-sulphation occurring in approximately 35% of all CS residues (Figure 52). The absence of non-overlapping signals associated with galactosamine 4-O-sulphation suggests that this modification is present at negligible levels within the CS component.

5.2.2. *P. pelagicus* F5 inhibits the Alzheimer's Disease-Relevant β -Secretase

The BACE-1 inhibitory activity of the *P. pelagicus* F5 sample was subsequently evaluated, utilizing the fluorogenic peptide cleavage FRET assay at pH 4.0 (Figure 53). *P. pelagicus* F5 was determined to possess of IC_{50} value of BACE-1 inhibition at $1.9 \mu\text{g mL}^{-1}$ ($R^2 = 0.94$), with maximal inhibition occurring at $5 \mu\text{g.mL}^{-1}$ ($90.7 \pm 2.9\%$) . This was comparable to heparin, which displayed a maximal level of BACE-1 inhibition of $92.5 \pm 1.5\%$ ($n = 3$) at $5 \mu\text{g mL}^{-1}$, with an IC_{50} of $2.4 \mu\text{g mL}^{-1}$ ($R^2 = 0.93$) (Figure 53).

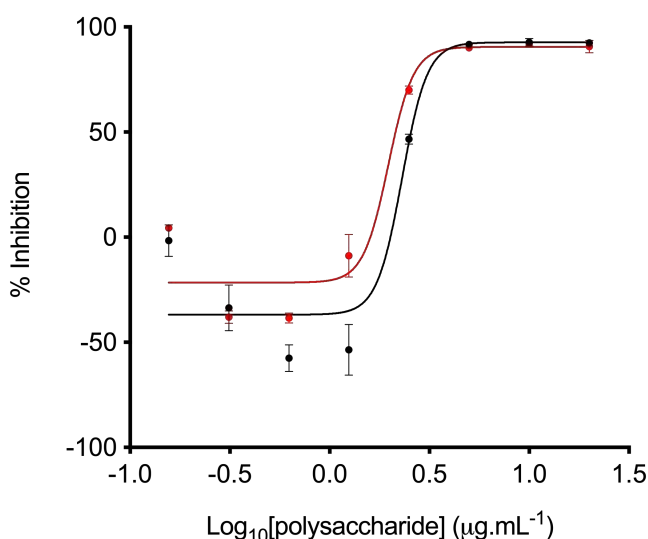


Figure 53: Inhibition of human BACE1 by heparin or *P. pelagicus* F5. Dose response of heparin (black) or *P. pelagicus* F5 (red) as determined using FRET. *P. pelagicus* F5, $IC_{50} = 1.9 \mu\text{g mL}^{-1}$ ($R^2 = 0.94$); heparin, $IC_{50} = 2.4 \mu\text{g mL}^{-1}$ ($R^2 = 0.93$); $n = 3$.

At low concentrations of heparin, an increase in BACE-1 activity was detected between $1250\text{-}312.5 \text{ ng.mL}^{-1}$ (Figure 53) with maximal promotion occurring at 625 ng mL^{-1} ($57.5 \pm 3.7\%$, $n = 3$). A maximum increase in BACE-1 activity was also observed in the presence of 625 ng. mL^{-1} of the *P. pelagicus* F5 sample ($38.5 \pm 1.4\%$, $n = 3$), although this was significantly reduced in comparison to the promontory activity displayed by the equivalent concentration of heparin ($57.5 \pm 3.7\%$, $n = 3$; $t(4) = 4.859$, $p = 0.0083$) . This,

therefore, indicates that the *P. pelagicus* F5 sample exhibits promontory activity, although significantly reduced in comparison to heparin. The percent activity level returned to that of the negative control value at concentrations lower than 312.5 ng.mL⁻¹, for both heparin and *P. pelagicus* F5 indicating that both inhibitory and promontory effects are dose dependent (Figure 53). The period of BACE-1 promotion observed in the presence of low concentrations of both For both heparin and *P. pelagicus* F5, was succeeded by enzyme inhibition, as previously reported (Figure 53, Figure 54) (Beckman, Holsinger and Small, 2006). The rate of BACE-1 activity between 60 and 90 min was significantly different from controls lacking either heparin (n = 3–6; t(4) = 7, $p < 0.003$) or *P. pelagicus* F5 (n = 3–6; t(6) = 7, $p < 0.004$), in which the reaction was within the linear range, suggesting that inhibition was not due to limitation of the substrate.

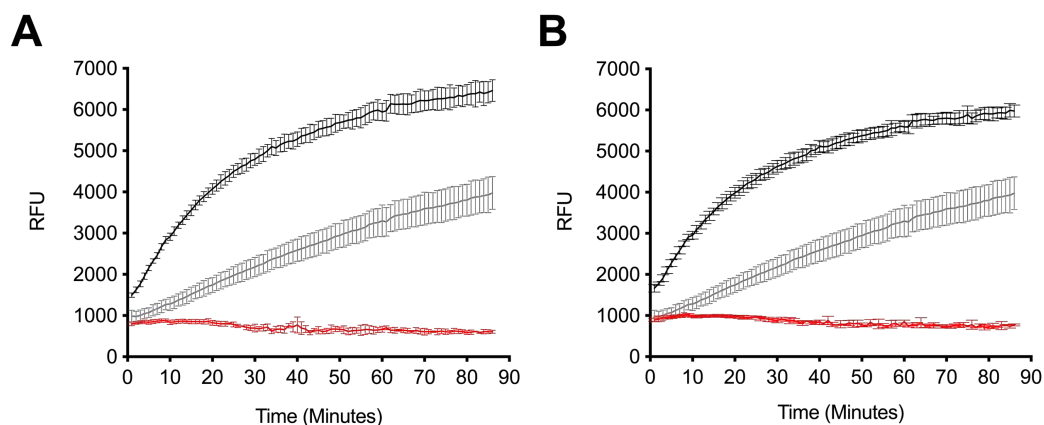


Figure 54: Inhibition of human BACE1 by heparin or *P. pelagicus* F5. (A) Time-course activation or inhibition of BACE1 by 5 µg mL⁻¹ (red) or 625 ng mL⁻¹ (black) heparin, compared to water control (grey). (B) The same as (A) for *P. pelagicus* F5.

5.2.3. Heparin and *P. pelagicus* F5 induce a conformational change in the Alzheimer's Disease-Relevant β -Secretase.

In light of the dual bioactivities of displayed by GAGs, when acting upon BACE-1 at differing concentrations, the ability of heparin and *P. pelagicus* F5 to induce structural changes in BACE1 was investigated utilising circular dichroism (CD) spectroscopy at a range of w/w ratios. The CD spectra of BACE-1 (9 μ g) in 50 mM sodium acetate buffer (pH 4.0) exhibited a positive CD band at wavelengths <200 nm; this region has previously been attributed to a sum of α -helical and β - sheet structures (Figure 55, Figure 56)(Greenfield, 2006). A broad negative CD band can also be observed between 240 nm and 200 nm, containing a split peak centring at approximately 218 nm and 208 nm, which is a common feature indicative of antiparallel β -sheets and α -helical structures, respectively (*idem*) (Figure 55, Figure 56). The CD spectra of BACE-1 (9 μ g; 50 mM sodium acetate buffer, pH 4.0) was estimated to be comprised of a secondary structural composition of 9% α -helix, 31% antiparallel β -sheet, 16% turn and 44% other (NRMSD < 0.1) when fitted against a library of representative proteins using BeStSel (Micsonai *et al* 2015). This was in close accordance with the BestSel secondary structure prediction of the x-ray crystal structure of BACE-1 at pH 4.0 (PDB accession no 2ZHS) (Shimizu *et al.*, 2008) of 7% α -helix, 30% antiparallel, 4% parallel, 12% turn and 47% other.

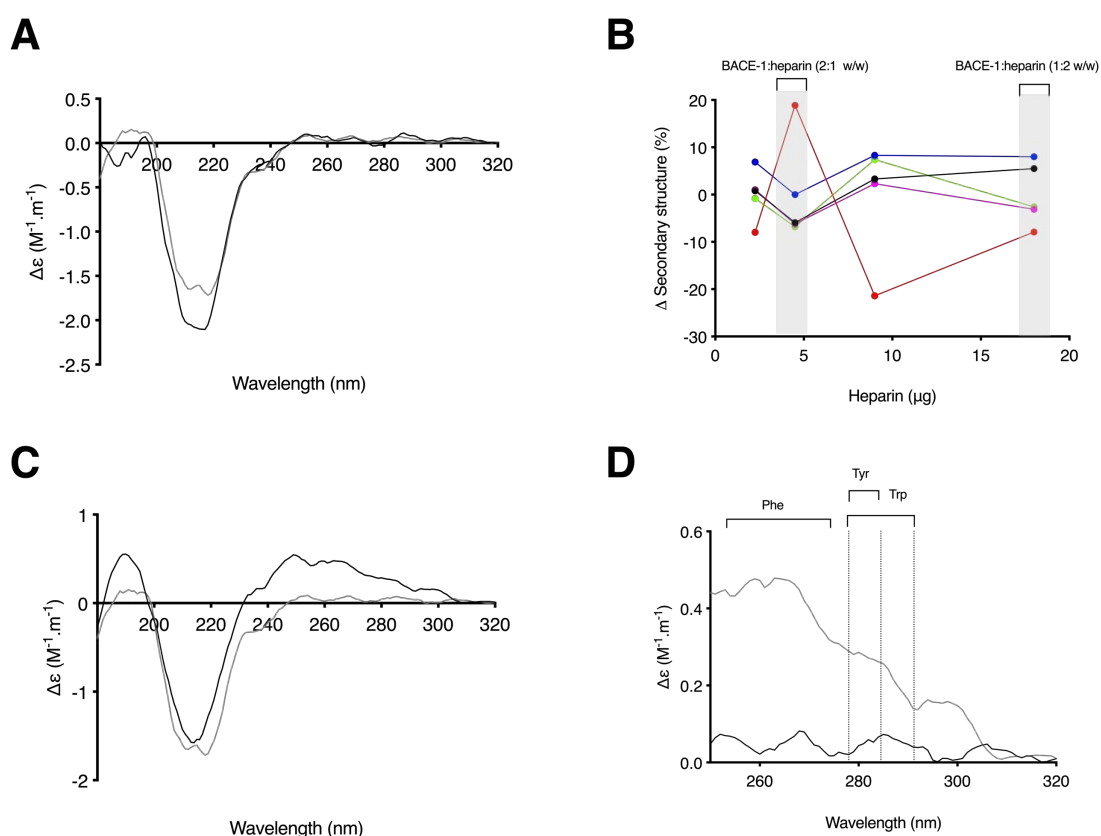


Figure 55: The structural change of BACE-1 observed in the presence of heparin by CD spectroscopy. (A) CD spectra of BACE-1 alone (grey) with heparin (black; ratio of 1:2 w/w; BACE-1:heparin); **(B)** Δ secondary structure (%) of BACE-1 upon the addition of increasing amounts of heparin; α -helix (black), antiparallel (red), parallel (blue), turn (magenta) and others (green) determined by BeStSel analysis server (Micsonai et al., 2015). % structural change of BACE-1:heparin; 1:2 (w/w) or 2:1 (w/w) ratio are highlighted in grey. **(C)** CD spectra of BACE1 alone (grey) or with heparin (black; ratio of 2:1 w/w); **(D)** Near-UV CD spectra of **(C)**; respective absorption regions of aromatic amino acids are indicated (Gasymov et al., 2014). Spectra were recorded in 50 mM sodium acetate buffer at pH 4.0 in all panels.

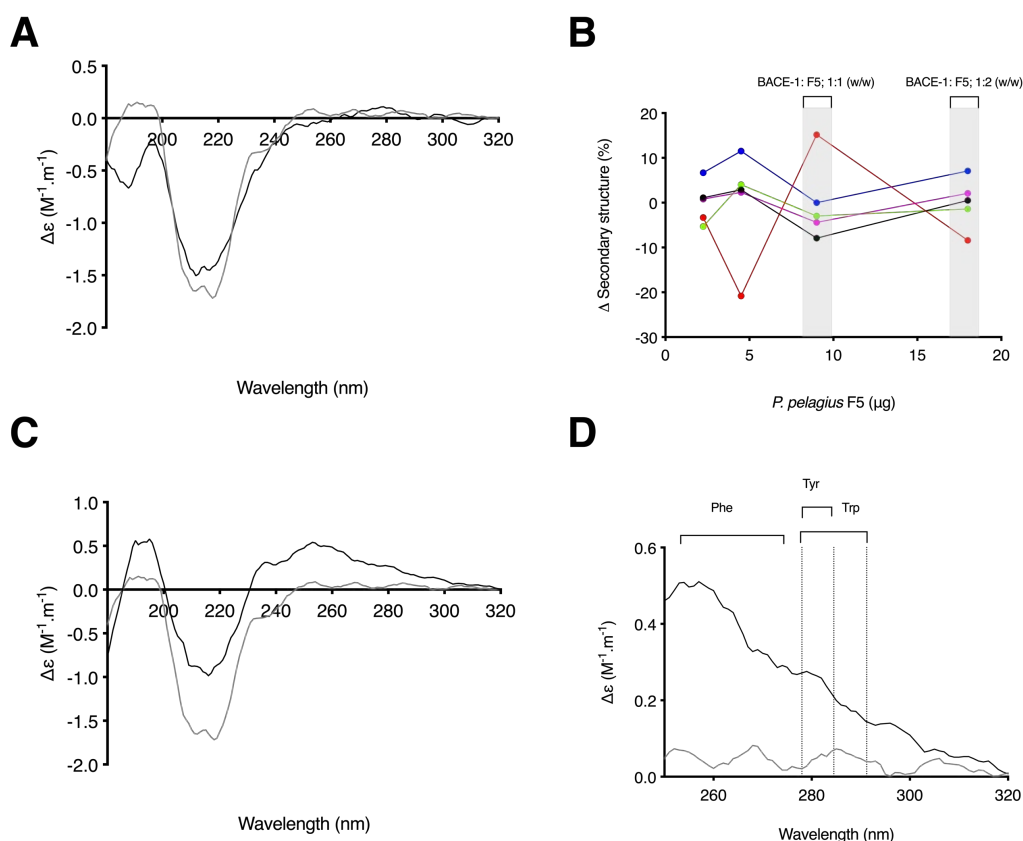


Figure 56: The structural change of BACE1 observed in the presence of *P. pelagicus* F5 by CD spectroscopy. (A) CD spectra of BACE-1 alone (grey) with *P. pelagicus* F5 (black; ratio of 1:2 w/w; BACE-1:F5); (B) Δ secondary structure (%) of BACE1 upon the addition of increasing amounts of *P. pelagicus* F5; α -helix (black), antiparallel (red), parallel (blue), turn (magenta) and others (green) determined by BeStSel analysis server (Micsonai *et al.*, 2015) % structural change of BACE-1:F5; 1:2 (w/w) or 1:1 (w/w) ratio are highlighted in grey. (C) CD spectra of BACE-1 alone (solid line) or with *P. pelagicus* F5 (dashed line; ratio of 1:1 w/w); (D) Near-UV CD spectra of (C); respective absorption regions of aromatic amino acids are indicated (Gasymov *et al.*, 2014). Spectra were recorded in 50 mM sodium acetate buffer at pH 4.0 in all panels.

At the approximate BACE-1:heparin ratio where maximal inhibition was observed in FRET assays (1:2, w/w), the CD spectrum of BACE-1 exhibited an increase in negative ellipticity <222 nm, in comparison to BACE-1 alone. This resulted in increase in the estimated α -helix (+6%) content and a reduction in antiparallel β -sheet content (-8%) (NRMSD < 0.1) (Micsonai *et al.*, 2015) (Figure 55, Figure 56). In comparison to heparin, BACE-1 in the presence of *P. pelagicus* F5 (BACE-1:F5), at the same ratio (1:2, w/w), exhibited a minor increase in the positive ellipticity of the CD band present between

222–200 nm and reduction in the ellipticity of the band present at $\lambda < 200$ nm. This resulted in an estimated change of +1% and - 8% for α -helical and antiparallel β -sheet content, respectively (Figure 55, Figure 56).

The conformational change of BACE-1 upon binding to heparin and *P. pelagicus* F5 was evaluated over a range of w/w ratios (Figure 55, Figure 56). At the approximate BACE-1:heparin ratio where promontory activity could be observed in FRET assays (2:1 w/w), a change in the CD spectrum of BACE-1 in the far-UV region ($\lambda < 250$ nm; Figure 8 C) was observed. This change was identified to correspond to an increase in antiparallel β -sheet structures by 19% and a reduction in α -helix by 6% (NRMSD < 0.1) (Micsonai *et al.*, 2015). In addition, an increase in positive ellipticity was observed in the near-UV region ($\lambda = 250$ –300 nm; Figure 53 C and D) following the addition of heparin, in contrast to BACE-1 alone, which may be attributed to a change in the structure of BACE-1 involving aromatic amino acids (Sreerama and Woody, 2004; Gasymov, Abduragimov and Glasgow, 2014). In contrast, BACE-1:F5 at the same ratio of 2:1 (w/w), exhibited a decrease in ellipticity in the near- and far- UV region ($\lambda < 300$ nm). An increase in positive ellipticity in the near-UV region was however, observed in the CD spectra of BACE-1 at a ratio of 1:1 (BACE-1:F5, w/w) (Figure 56). The secondary structural change in the far-UV region of the CD spectrum ($\lambda = 250$ –190 nm) of BACE-1 at a BACE-1:F5 ratio of 1:1 (w/w) was attributed to change in α -helix by -8% and in antiparallel β -sheet structures by +15% (Figure 56).

5.2.4. Heparin and *P. pelagicus* F5 destabilise the Alzheimer's Disease-Relevant β -Secretase.

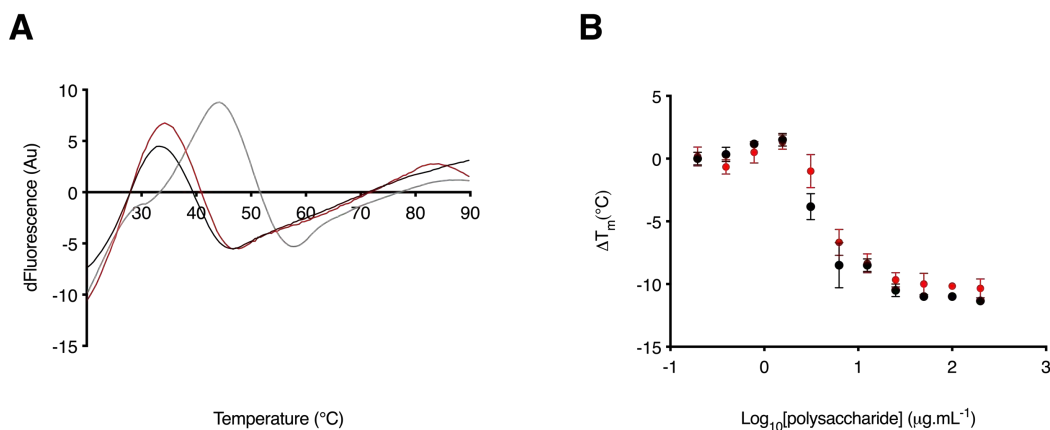


Figure 57: Differential scanning fluorimetry of BACE-1 in the presence of heparin or *P. pelagicus* F5. (A) First differential of the DSF thermal stability profile of BACE-1 alone (1 μg; grey), and with heparin (2 μg; black) or *P. pelagicus* F5 (2 μg; red) in 50 mM sodium acetate, pH 4.0; (B) ΔT_m of BACE-1 with increasing [heparin] or [*P. pelagicus* F5] (open or closed circles, respectively).

Both heparin and *P. pelagicus* F5 were shown to induce a conformational change in BACE-1 by CD, this is in contrast to previous CD studies of BACE-1 in the presence of peptide inhibitors (De Simone *et al.*, 2013). Therefore, in order to explore whether the binding of heparin or *P. pelagicus* F5 to BACE-1 also alters the thermal stability in a mechanism similar to known inhibitors, DSF was employed. In the presence of a BACE1:heparin or *P. pelagicus* F5 at a ratio of 1:2 (w/w), a decrease in the T_m of BACE-1 was observed, by 11°C and 10°C, respectively (Figure 55A). The change in T_m of BACE-1 as a result of binding of either heparin or *P. pelagicus* F5 was not significantly different, ($p = 0.1161$ $t = 2$ $df = 4$). In addition, the destabilisation of BACE-1 in the presence of both heparin and *P. pelagicus* F5 was concentration dependent (Figure 57).

5.2.5. Attenuated Anticoagulant Activities of the *P. pelagicus* F5 extract

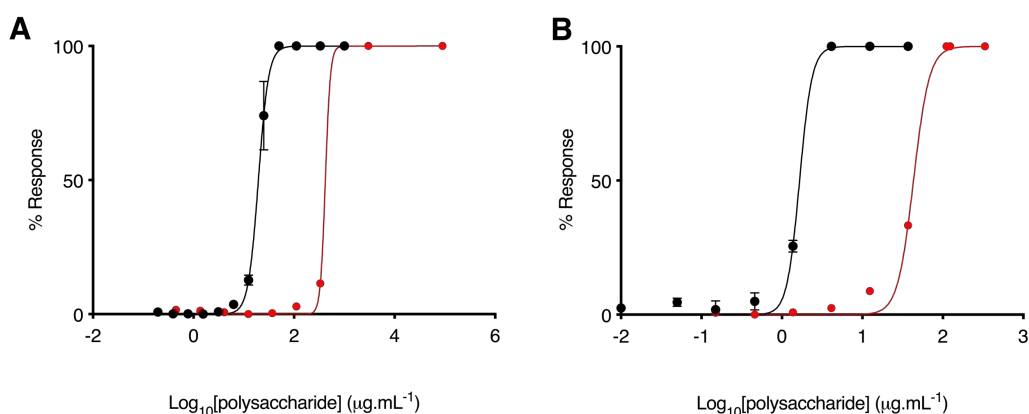


Figure 58: anticoagulant activity of heparin and *P. pelagicus* F5. (A) Prothrombin time (PT) and (B) activated partial thromboplastin time (aPTT) inhibitory response (x⁻%, ± SD, n = 3) for heparin (black) and *P. pelagicus* F5 (red); PT: heparin EC₅₀ = 19.53 μg mL⁻¹; *P. pelagicus* F5, EC₅₀ = 420.2 μg mL⁻¹. aPTT: heparin EC₅₀ = 1.66 μg mL⁻¹; *P. pelagicus* F5, EC₅₀ = 43.21 μg mL⁻¹.

The prothrombin time (PT) and activated partial thromboplastin time (aPTT) of *P. pelagicus* F5 were measured in comparison to heparin (193 IU.mg⁻¹), to elucidate the effect of the former sample on the extrinsic and intrinsic coagulation pathways, respectively (both assays also include the common coagulation pathway). In comparison to heparin, *P. pelagicus* F5 exhibited a 20 and 40 fold reduction in anticoagulant activity in the PT (Figure 56 A; EC₅₀ = 420.2 μg mL⁻¹ compared to 19.53 μg mL⁻¹, respectively) and aPTT (Figure 56B; EC₅₀ = 43.21 μg mL⁻¹ compared to 1.66 μg mL⁻¹, respectively) coagulation assays, respectively (Figure 58). This indicates that the extract obtained from *P. pelagicus* presents a negligible anticoagulant activity.

5.3. Discussion

The GAG extract isolated from *P. pelagicus*, fractionated by DEAE- anion-exchange chromatography, with elution at 1 M NaCl (designated *P. pelagicus* F5) displayed similar electrophoretic mobility to mammalian HS and heparin in 1-2 diaminopropane buffer. No bands were identified that corresponded to CS or DS standards, when *P. pelagicus* F5 was analysed by agarose gel electrophoresis. This is in accordance with the electrophoretic characteristics of the crude *P. pelagicus* extract discussed in 3.3. In contrast, the ATR-FTIR and CD spectrum *P. pelagicus* F5 identified features characteristic of both HS and CS saccharides within the extract, when analysed by PCA.

The results obtained from analysis of the ATR-FTIR and CD spectrum of *P. pelagicus* F5 were subsequently confirmed by ^1H - ^{13}C HSQC NMR, which indicated the presence of resonances associated with the N-acetyl peaks of both CS and HS/heparin. The absence of an IdoA signal from the NMR spectra suggests that *P. pelagicus* F5 more closely resembles HS than heparin, in that the predominant uronic acid constituent is GlcA (Table 10). It is however of note that the resolution of the spectrum ^1H - ^{13}C is not sufficient to distinguish between responses associated with GlcA linked to either hexosamine sugars, therefore additional NMR techniques, such as COSY, TOCSY and NOESY experiments, would be required to confirm that the predominant uronic acid within the glucosaminoglycan constituent of *P. pelagicus* F5 is GlcA. The HS component of the *P. pelagicus* F5 sample was also found to possess >70% N-sulphated glucosamine, which is greater than typically found within mammalian HS, but is not as heavily N-sulphated as mammalian heparins. Furthermore, the level of N-sulphation of the *P.*

pelagicus F5 extract was greater than that reported from a HS/heparin extract obtained from the crab *Goniopsis cruentata* (Andrade *et al.*, 2013). Approximately 50-60% of the *P. pelagicus* F5 sample was also found to possess 6S modifications on the glucosamine residue, which is also greater than mammalian HS and the compound isolated from *G. cruentata* (*idem*), however reduced in comparison to heparin. An intermediate level of trisulphated Δ -disaccharides (Δ UA(2S)-GlcNS(6S)) was also identified following bacterial lyase digestion of *P. pelagicus* F5, when compared to mammalian HS and heparin samples at approximately 23%, 52% and 7%, respectively. This was also comparatively higher than the reported level of trisulphated Δ -disaccharides present within the HS/heparin compound isolated from *G. cruentata* (12%, *idem*). Furthermore, the *P. pelagicus* F5 extract contained a low proportion of Δ -UA-GlcNAc/ Δ -UA-GlcNS, which is typical of more heparin-like structures. This suggests that the HS/heparin component of *P. pelagicus* F5 consists of a structure which lacks the domain structure of HS and exhibits a greater degree of sulphation, more commonly indicative of mammalian heparin, albeit with a lower proportion of trisulphated regions than the latter GAG. Such a hybrid HS/heparin structure was also reported by Andrade *et al.*, (2013) from *G. cruentata*, however this compound also displays distinct structural characteristics from the extract isolated in the present work. Regarding the CS component of the extract, peaks corresponding to Gal-6S and 6-OH were identified by NMR analysis, with no detectable 4-O-sulphation, indicating that the CS component of *P. pelagicus* F5 resembles CSC saccharides.

Subsequent to the approximate determination of the composition of the *P. pelagicus* F5 extract, the fractionated compound was evaluated for BACE-1 inhibitory activity. The *P.*

pelagicus F5 sample exhibited comparable BACE-1 inhibitory activity to that of mammalian heparin, as demonstrated by the observation of equivalent IC₅₀ concentrations via FRET based assays. This was despite the slightly diminished level of sulphate modifications at position 6 of the glucosamine residue within the *P. pelagicus* F5 extract, in comparison to mammalian heparin; this modification has previously been reported to be important for BACE-1 inhibitory activity (Patey *et al.*, 2006). Additionally, the presence of 2-sulphated uronic acid residues have also been suggested to be important for BACE-1 inhibitory activity, irrespective of the epimer (Patey *et al.*, 2006; Schwörer *et al.*, 2013). Therefore, the presence of slightly increased 2-sulphated uronic acid residues (determined by HPLC disaccharide analysis) within the *P. pelagicus* F5 extract, in comparison to mammalian heparin, may account for the observation of comparable BACE-1 inhibitory activities. The capability of *P. pelagicus* F5 to stimulate BACE-1 activity at low concentrations, as a result of the presence of the BACE-1 pro-domain (Beckman *et al.*, 2009; Klaver *et al.*, 2010), was diminished in comparison to mammalian heparin. Previously, Klaver *et al.*, (2010) reported that the promontory activity of BACE-1 was dependent upon the degree of sulphation of the polysaccharide chain. Therefore, the diminished level of sulphate modifications present within the HS/heparin component of the *P. pelagicus* F5 sample may account for the reduction in BACE-1 promontory activity in comparison to mammalian heparin. This suggests that the structural differences between these GAGs affects the nature of their interactions with human BACE-1. This was exemplified by the observed secondary structural changes in BACE-1 (by CD spectroscopy) in the presence of heparin or *P. pelagicus* F5, over a variety of concentrations.

Previously the secondary structure of BACE-1, measured by CD spectroscopy, has been predicted to contain increased levels of beta-sheet and a reduction in alpha-helical structures at pH 4.0; where catalytic activity is increased in comparison to higher pH values (De Simone *et al.*, 2013). When the secondary structure of BACE-1 was examined by CD spectroscopy in the presence of high concentrations of heparin (BACE-1:heparin ratio of 1:2 w/w), the structural features observed for BACE-1 were more closely aligned with those observed for BACE-1 alone at pH 7.4 by De Simone *et al* (2013), with increased alpha-helical and reduced beta-sheet structures. At high concentrations, the *P. pelagicus* F5 extract (BACE-1:F5 ratio of 1:2 w/w) induced similar, but not equal, changes to the secondary structure of BACE-1, in comparison to those of heparin at the same ratio.

In contrast, the CD spectra observed for BACE-1:heparin complexes under conditions in which BACE-1 promotion is facilitated (low heparin concentrations) indicated an estimated increase in beta-sheet and reduction in alpha-helical structures. Furthermore, the CD spectra of BACE-1: heparin at a 2:1 ratio demonstrated evidence that binding influenced the orientation of aromatic amino acids (near UV CD). This suggests that a conformational change in BACE-1 structure may occur upon heparin binding, which enables increased access to the active site as indicated by previous reports (Klaver *et al.*, 2010).

At lower concentrations, differences in BACE-1 change in secondary structure were observed between the equivalent ratios of BACE-1:heparin and BACE-1:F5 complexes. A similar change in the near UV CD spectra of BACE-1 was however observed with

increased amounts of *P. pelagicus* F5, in comparison to heparin (1:1 and 2:1 BACE:GAG ratio, respectively). This difference is likely accounted for by the reduced potency of *P. pelagicus* F5 regarding activating BACE-1 or could be suggestive of an alternative interaction. The conformational change induced in the near-UV CD spectra of BACE1 is likely attributed to the HS/heparin-like component of the *P. pelagicus* F5 extract, as CS has previously been shown to possess relatively lower BACE-1 promontory activity (Klaver *et al.*, 2010).

The decrease in the melting temperature (T_m) of BACE-1 in the presence of both heparin or the *P. pelagicus* F5 extract, when compared to human BACE-1 alone, suggests that the mechanism of BACE-1 inhibition by GAGs may also involve structural destabilisation. The reduction in the thermal stability of BACE-1 in the presence of heparin occurs in a concentration dependent manner, akin to that of the inhibitory potential observed in FRET assays. As observed for the BACE-1 FRET inhibition assays, *P. pelagicus* F5 also displayed comparable dose-dependent destabilisation of BACE-1 and exhibited similar T_m values to heparin at all concentrations tested. This is in contrast to previously identified non-GAG BACE-1 inhibitors, which were observed to stabilise BACE-1 by employing DSF (Lo *et al.*, 2004). This, coupled with the observed changes in BACE-1 conformation in the presence of GAG which were not observed in the presence of peptide inhibitions, suggests that GAGs act by modes of inhibition distinct to that of previously identified inhibitors.

One of the foremost obstacles precluding the potential therapeutic use of mammalian heparin compounds as BACE-1 inhibitors is the significant anticoagulant activities of this

biomolecule. The anticoagulant potential of heparin is afforded by the propensity of this polysaccharide to interact with antithrombin, thereby inhibiting the human coagulation pathway and ultimately preventing fibrin clot formation. The anticoagulant potential of *P. pelagicus* F5 was identified to be highly diminished in contrast to mammalian heparin, when evaluated by the aPTT and PT clotting assays. These coagulation assays are employed routinely in clinical settings in order to screen for the common pathway in combination with either the intrinsic (aPTT) or extrinsic pathways (PT).

Chapter 6: Glycosaminoglycan extracts with attenuated off target activities, isolated from *Litopenaeus vannamei*, inhibits the Alzheimer's beta-secretase, BACE1.

6.1. Introduction

Litopenaeus vannamei, also known as the whiteleg shrimp, is part of the class crustacea and is native to the Pacific coast of Latin America, where it can tolerate regions of varying salinity (southern Mexico to north Peru) (Liao and Chien, 2011). Shrimp and prawns are one of the most heavily traded aquatic products globally and are now largely produced via aquaculture as opposed to fishery production. In 2018, *L. vannamei* accounted for 52.9% of the major species of crustacea produced by aquaculture making *L. vannamei* the most farmed species of shrimp globally (FAO, 2020). The major producer countries of *L. vannamei* include those of Latin America and Asia, such as Brazil, China, Thailand, Indonesia, Malaysia and Viet Nam (Liao and Chien, 2011; FAO, 2020). Overall, Asia accounts for approximately one third of the total *L. vannamei* cultured globally (*idem*).

The farming and production of *L. vannamei* is continuing to grow year on year. Approximately only 50% of the shrimp being utilised for foodstuff, with the remainder, including the cephalothorax, carapace and tail, are being generated as waste products of the shrimp processing industry (Cahú *et al.*, 2012). These tissues are largely utilised as a source of proteins, essential amino acids and carotenoids for aquatic animal, livestock and poultry feeds (*idem*). In addition, the carapace can also be utilised as a source of chitin, which may hold various potential therapeutic applications (*idem*). The waste products obtained from the shrimp industry have also been explored as a potential source of bioactive GAGs (C. P. Dietrich *et al.*, 1999; Chavante *et al.*, 2000, 2014; Brito *et al.*, 2008; Cahú *et al.*, 2012; Cavalcante *et al.*, 2018). Heparin and HS like

GAGs have been identified in the heads of a variety of shrimp species including, *L. vannamei*, *A. franciscana* and *P. brasiliensis*, which all display novel and variable structural features in contrast to the mammalian counterparts. For instance, a heparin like compound isolated from the heads of *L. vannamei* was identified to contain high levels of trisulphated glucosamine residues, which were present in an unusual sequence (Chavante *et al.*, 2014). This compound was found to contain relatively high levels of glucuronic acid units in comparison to 2-S iduronic acid and therefore, appeared to possess structural features characteristic of both heparin and HS (*idem*). Similarly GAGs displaying structural characteristics of both heparin and HS, isolated from shrimp species, were described by Chavante *et al* (2000) and Dietrich *et al* (1999). Although, these compounds were also distinct from that isolated by Chavante *et al* (2014). In addition, CS with unique structural feature have also been isolated from the heads of *L. vannamei*. Such compounds were found to contain varying levels of 2 and 3-sulphate modifications on the glucuronic acid residue, which are typically rare (Cavalcante *et al.*, 2018; Palhares *et al.*, 2019). The aforementioned shrimp HS/heparin compounds have also been reported to possess various bioactivities including anti-inflammatory and anti-angiogenic properties (Brito *et al.*, 2008). Furthermore, such compounds have been shown to possess reduced anticoagulant activity (Table 6). *L. vannamei* therefore, appears to be a valuable source of novel GAG that possess a wide range of favourable bioactivities, which could potentially be exploited for therapeutic purposes. In light of this, GAGs were extracted from *L. vannamei* tissue and the resulting extracts were evaluated for the ability to inhibit BACE-1.

6.1.2. Aims

The crude GAG extracts obtained from *L.vannamei* by proteolysis were fractionated by DEAE-Sephacel anion-exchange chromatography, the resulting fractions were screened for the ability to inhibit recombinant human BACE-1 as reported in section 3.2. Fractions eluted with 800 mM (*L.vannamei* F4) and 1 M NaCl (*L.vannamei* F5), both possessed >70% BACE1 inhibitory at 70.8% and 90.5% respectively, when screened at 5 $\mu\text{g.mL}^{-1}$. The aim of this chapter was therefore, to further characterise the biological and structural properties of *L.vannamei* GAG extracts F4 and F5.

6.2. Results

6.2.1. Characterisation of glycosaminoglycan extracts from *Litopenaeus vannamei*

The electrophoretic mobility of *L. vannamei* F4 and F5, in 1,3-diaminopropane buffer (pH 9.0) was compared to that of heparin/HS and CS standards (Figure 62). Both fraction 4 and 5 separated into two distinct bands corresponding to HS and CS, revealing that the fractions are composed of a heterogeneous mixture of GAGs. The primary constituent of both fractions was observed to possess similar electrophoretic mobility to mammalian HS, migrating a marginally greater distance than porcine heparin. A further minor band was also present in both fractions, which migrated approximately the same distance as mono- and di-sulphated CS standards (Figure 59).

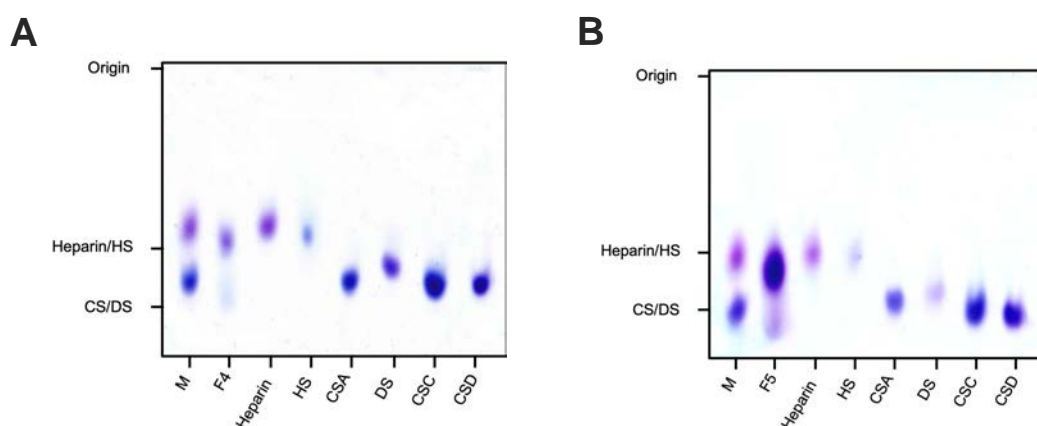


Figure 59: Electrophoretic mobility of *L.vannamei* F4 and F5 compared that of bona fide glycosaminoglycans. *L.vannamei* F4 (A) and F5 (B); heparin, heparan sulphate (HS), dermatan sulphate (DS) and chondroitin sulphate A, C and D (CSA, CSC and CSD, respectively), using agarose gel electrophoresis performed in 50 mM 1,3-diaminopropane buffer. M = mixture of CSA and heparin.

In order to further examine the structural characteristics of *L.vannamei* F4 and F5 FTIR and CD spectroscopy, coupled with PCA, was employed. As bands were present in both fractions corresponding to HS and CS, when analysed by agarose gel electrophoresis,

the ATR-FTIR and CD spectra of *L. vannamei* F4 and F5 was compared to that of CS and HS (Figure 60).

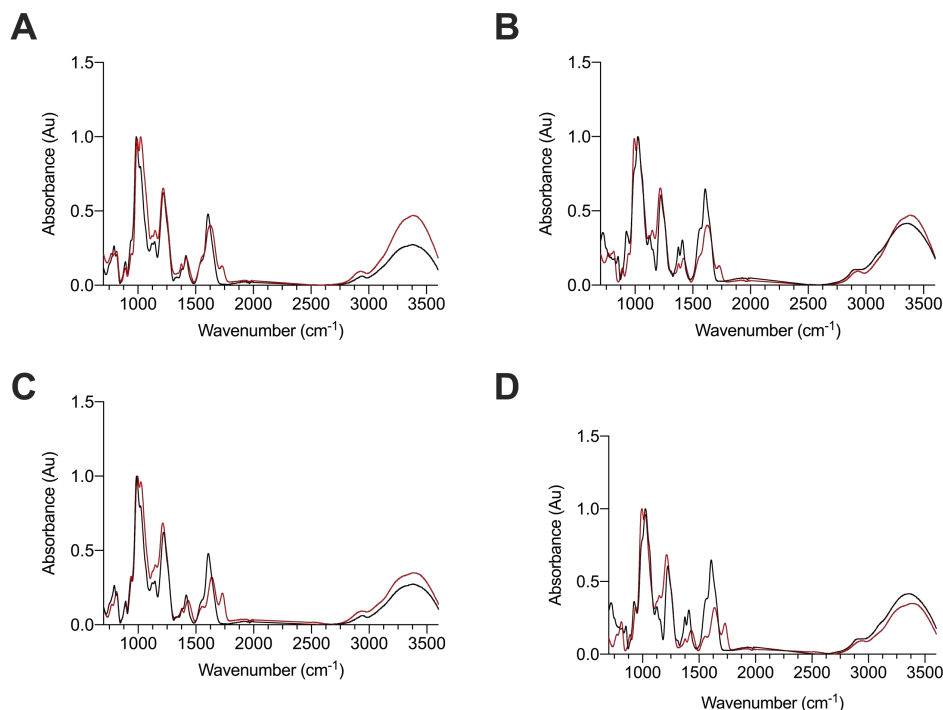


Figure 60: ATR-FTIR spectra of *L. vannamei* F4 and F5. (A) *L. vannamei* F4 (red) and HS (black) or (B) CS (black) (C) *L. vannamei* F5 (red) and HS (black) or (D) CS (black). n = 5.

Both *L. vannamei* F4 and F5 contained features representative of GAGs within the ATR-FTIR spectra, including peaks corresponding to the common motifs; amide II bond corresponding to the C-N vibrations of N-acetyl groups, S=O, symmetric carbonyl stretching and asymmetric stretching at 1559, 1230, 1430 and 1635 cm^{-1} , respectively (Figure 63). Notably, *L. vannamei* F4 contained a split peak at 990 cm^{-1} and 1025 cm^{-1} , which are indicative of HS/heparin and CS, respectively (Devlin, Mauri, *et al.*, 2019; Devlin, Mycroft-West, *et al.*, 2019). In contrast the peak at 990 cm^{-1} was more prominent in *L. vannamei* F5, in comparison to that which is present at 1025 cm^{-1} . This suggests that *L. vannamei* F5 contains a higher proportion of HS than *L. vannamei* F4.

The peak at 1025 cm^{-1} is also present in greater proportions in crude heparin preparations containing galactosaminoglycan contaminants, when compared to pharmaceutical heparin preparations (*idem*). In addition, differences between HS and CS samples have also been detected at $\lambda = \sim 1450\text{ cm}^{-1}$ and 1600 cm^{-1} . Both *L. vannamei* F4 and F5 more closely resembled HS in these regions (Figure 60). Furthermore, the peak shoulder present at $\sim 1370\text{ cm}^{-1}$ in both *L. vannamei* F4 and F5, has also previously been reported to be suggestive of a HS/CS mixture (*idem*). This further supports that both *L. vannamei* fractions are composed of a mixture of these GAG. An additional peak, which was absent in both HS and CS, at was observed at $\sim 1725\text{ cm}^{-1}$ in both *L. vannamei* F4 and F5 (Figure 60), suggesting that the *L. vannamei* GAG extracts may possess a novel structural feature. The ATR-FTIR spectra of *P. vannamei* F4 and F5 were subjected to post acquisition PCA in comparison to the previously described library of known GAGs, in order to further elucidate the composition of the extracts (Figure 61).

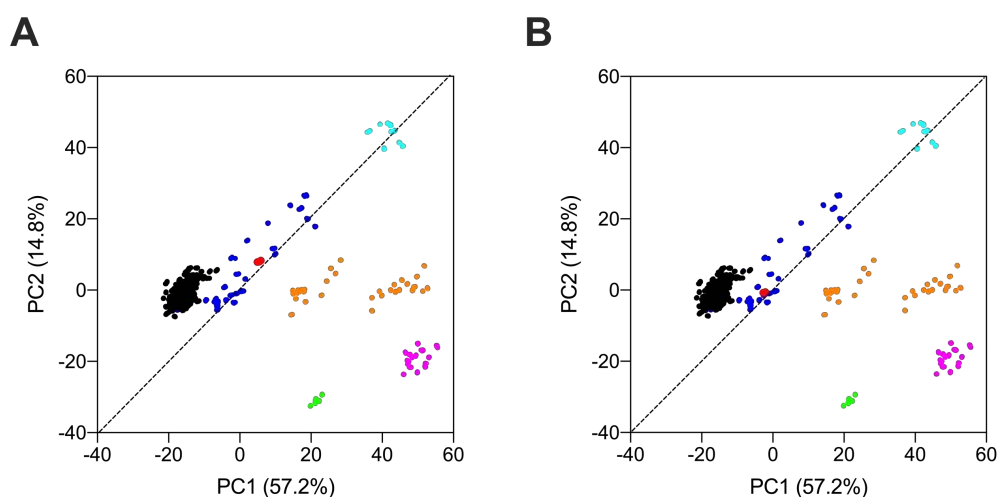


Figure 61: Principle component analysis Score Plot for PC1 vs. PC2 of the ATR-FTIR spectra *L. vannamei* F4 and F5 against a *bone fide* GAG library. *L. vannamei* F4 (A) and F5 (B); Heparin (black), HS (dark blue), CS (orange), DS (magenta), hyaluronic acid (cyan), oversulphated-CS (light green) and *L. vannamei* fractions (red).

Comparison of PC1 and PC2 (covering >70% of the total variance) revealed that both *L. vannamei* F4 and F5 are located within the region containing mammalian HS. 57% of the total variance was covered by PC1, which separated both *L. vannamei* F4 and F5 towards the region containing CS, however both extracts still overlapped with mammalian HS samples. The separation towards this region was more pronounced for *L. vannamei* F4 than *L. vannamei* F5, possibly indicating a greater level of CS within the former sample (Figure 61). Principal component 2, covering approximately 15% of the variance separated *L. vannamei* F5 closer towards the region associated with heparin than *L. vannamei* F4. This may indicate that the *L. vannamei* F5 sample contains a higher degree of sulphation (Figure 61).

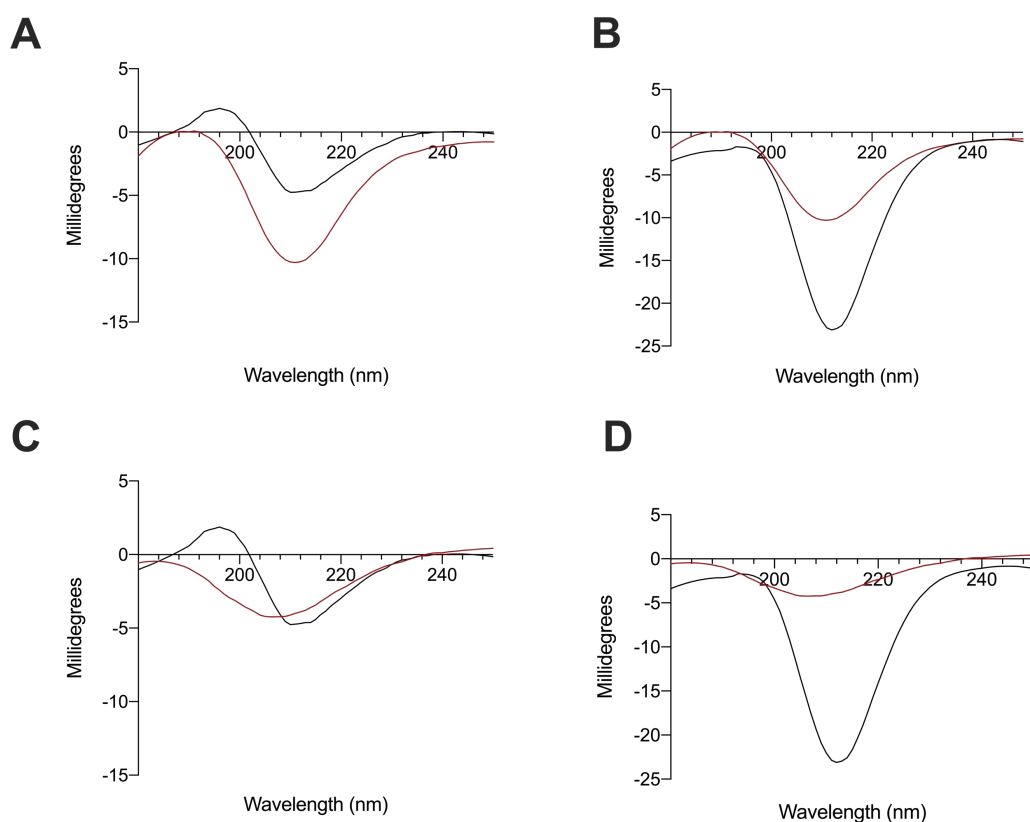


Figure 62. Circular dichroism spectra of *L. vannamei* F4 and F5. (A) *L. vannamei* F4 (ref) and HS (black) or (B) CS (black) (C) *L. vannamei* F5 (red) and HS (black) or (D) CS (black).

Circular dichroism has also previously been employed to aid the structural characterization of GAGs. As mentioned in prior chapters, the CD spectra of GAGs is sensitive to the conformation of the uronic acid, orientation of the glycosidic linkage and degree/position of sulphation (Rudd, Skidmore, Guimond, Cosentino, *et al.*, 2009; Rudd, Yates and Hricovini, 2009). In particular heparin, which higher levels of IdoA epimerisation and total sulphation in comparison to HS (Meneghetti *et al.*, 2015), displays a distinct CD to other GAGs. This is predominantly evident in the far UV region where an increase in positive ellipticity can be seen at ~190 nm in heparin. In addition, a negative peak at ~205-220 nm is present in the CD spectra of all GAGs to varying intensities.

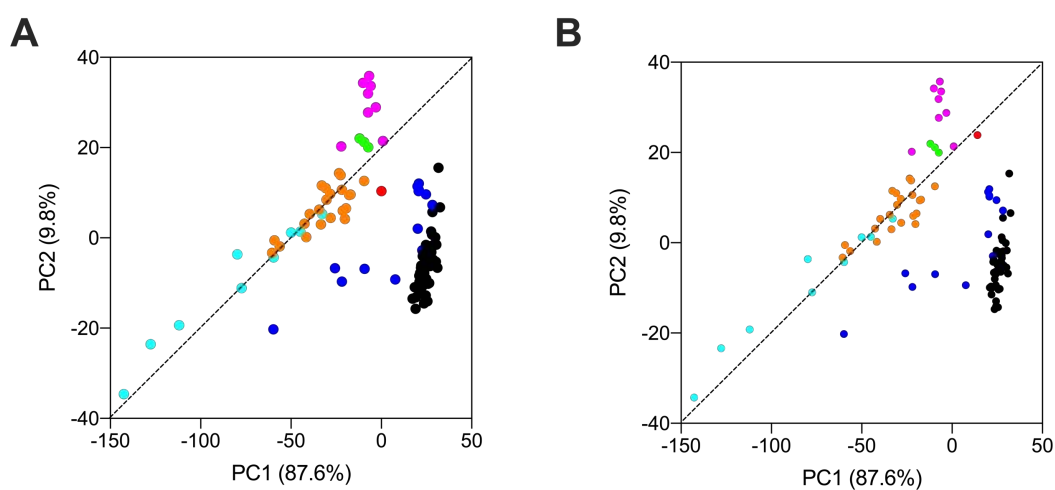


Figure 63: Principle component analysis (PCA) score Plot for PC1 vs. PC2 of the circular dichroism spectra *P.vannamei* F4 and F5 against a *bone fide* GAG library. *L. vannamei* F4 (A) and F5 (B) Heparin (black), HS (dark blue), CS (orange), DS (magenta), hyaluronic acid (cyan), over-sulphated-CS (light green) and *L. vannamei* fractions (red).

The CD spectra of *L. vannamei* F4 and F5 more closely resembled that of CS than HS, with no positive peak being present at ~190 nm (Figure 62). The peak present at ~210 nm in the CD spectrum of *L. vannamei* F4 exhibited an increased negative ellipticity

compared to HS, but not to the same extent as CS (Figure 65). However, this was not the case for *L. vannamei* F5 where the spectra more closely resembled that of HS between 200-220 nm; albeit with a slight blue shift in comparison to both HS, CS and *L. vannamei* F4 (Figure 62). To further analyse the CD spectrum of *L. vannamei* F4 and F5, the spectra were compared to that of known GAGs; heparin, HS, CS, DS, HA and OSCS, using PCA. Comparison of PC1 and PC2 (covering 97% of the total variance) separated both *L. vannamei* F4 and F5 into a region between heparin/HS and CS/DS (Table 11). Principle component 2, which covered ~10% of the total variants, located the *L. vannamei* F5 sample closer to the region containing DS and OSCS than *L. vannamei* F4, which separated closer towards the region containing mono-sulphated CS. Furthermore PC1, which contained ~90% of the total variance, positioned *L. vannamei* F5 closer to HS/heparin region than *L. vannamei* F4, which again was separated towards the CS region (Table 11). The PCA of the CD spectrum of *L. vannamei* F4 and F5 was therefore in agreement with that of the ATR-FTIR, suggesting that both fractions contain a mixture of GAGs with *L. vannamei* F4 containing a higher proportion of CS than F5.

Subsequently *L. vannamei* F4 and F5 were subjected to exhaustive enzymatic cleavage with *Flavobacterium heparinum* lyases I, II and III or chondroitinase ABC and the digestion products were examined using SAX-HPLC disaccharide composition analysis by comparing the retention times to those of the common HS/heparin Δ -disaccharide or CS/DS standards, respectively (Skidmore *et al.*, 2006). Heparin, HS, CSA and CSC standards were also extensively digested as controls to ensure enzymatic activity resulted in the expected digestion products.

The digestion products for both mammalian heparin and HS were in agreement with previously published disaccharide profiles and those reported in chapter 4, which were performed on a separate occasion (*idem*). The trisulphated Δ -UA(2S)-GlcNS(6S) accounted for the primary disaccharide present in heparin at 51.4%, in comparison to HS, where this disaccharide accounted for ~7% of the total chain. The second most prevalent disaccharide present in mammalian heparin was found to be Δ -UA-GlcNS(6S) (18.2%), as reported elsewhere (*idem*). As previously identified, mammalian HS was composed primary of di- and mono- sulphated disaccharide standards; Δ -UA-GlcNS (17.8%), Δ -UA-GlcNAc(6S) (12.8%), Δ -UA-GlcNS(6S) and (18.0%), which accounted for ~ 50% of the total disaccharide composition. This is likely attributable to the transition and S-domains present within HS. The most prevalent disaccharide detected in the mammalian HS sample was the un-sulphated, Δ -UA-GlcNAc (37.7%) which accounts for the NAc-domains of HS (Table 19).

Table 19: Corrected disaccharide composition analysis of *P. vannamei* F4, F5, heparin and HS.

Δ-Disaccharide	<i>L. vannamei</i> F4 (%)	<i>L. vannamei</i> F5 (%)	Heparin (%)	HS (%)
Δ -UA-GlcNAc	14.8	9.4	8.5	37.7
Δ -UA-GlcNS	9.6	7.6	3.5	17.8
Δ -UA-GlcNAc(6S)	3.7	5.7	5.5	12.8
Δ -UA(2S)-GlcNAc	1.1	0.8	2.8	0.4
Δ -UA-GlcNS(6S)	31.7	47.9	18.2	18.0
Δ -UA(2S)-GlcNS	23.7	12.9	7.6	6.0
Δ -UA(2S)-GlcNAc(6S)	0.5	0.6	2.5	0.4
Δ -UA(2S)-GlcNS(6S)	14.9	15.0	51.4	7.0

The digest products of *L. vannamei* F4 and F5 exhibited a more disperse sulphation profile than mammalian heparin and HS. Both *L. vannamei* F4 and F5 contained a lower proportion of the trisulphated disaccharide, Δ -UA(2S)-GlcNS(6S), when compared to heparin at ~15%, however this is approximately double than that typically present in mammalian HS (Table 19, Figure 65, Figure 64). *L. vannamei* F4 exhibited a slightly higher proportion of unsulphated disaccharides (Δ -UA-GlcNAc) when compared to mammalian heparin at 14.8%. However, this is substantially lower than typically reported for HS (Dietrich *et al.*, 1998; Skidmore *et al.*, 2006; Zhang *et al.*, 2009; Andrade *et al.*, 2013). In comparison *L. vannamei* F5 contained approximately the same proportion of Δ -UA-GlcNAc as mammalian heparin at 9.4%. Both fractions therefore, contained a low proportion of both the trisulphated disaccharide, Δ -UA(2S)-GlcNS(6S) and unsulphated disaccharide, Δ -UA-GlcNAc which are characteristic of heparin and HS respectively (Table 19, Figure 65, Figure 64). indicating that the *L. vannamei* fractions contain a heparin-HS like GAG with distinct structural characteristics than the mammalian counterparts.

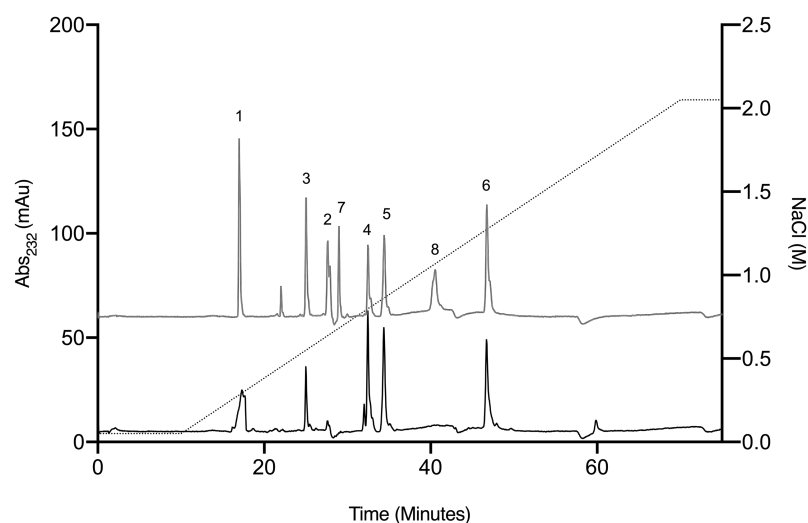


Figure 65: UV-SAX HPLC disaccharide composition analysis was performed on the bacterial lyase digest of *L. vannamei* F4 ($\lambda = 232$ nm) eluting with a linear gradient of 0-2 M NaCl (dashed line). Eluted Δ -disaccharides were referenced against the eight common standards present with heparin and HS (grey); 1; Δ UA-GlcNAc, 2; Δ UA-GlcNAc(6S), 3; Δ UA-GlcNS, 4; Δ UA-GlcNS(6S), 5; Δ UA(2S)-GlcNS, 6; Δ UA(2S)-GlcNS(6S), 7; Δ UA-(2S)-GlcNAc, 8; Δ UA(2S)-GlcNAc(6S).

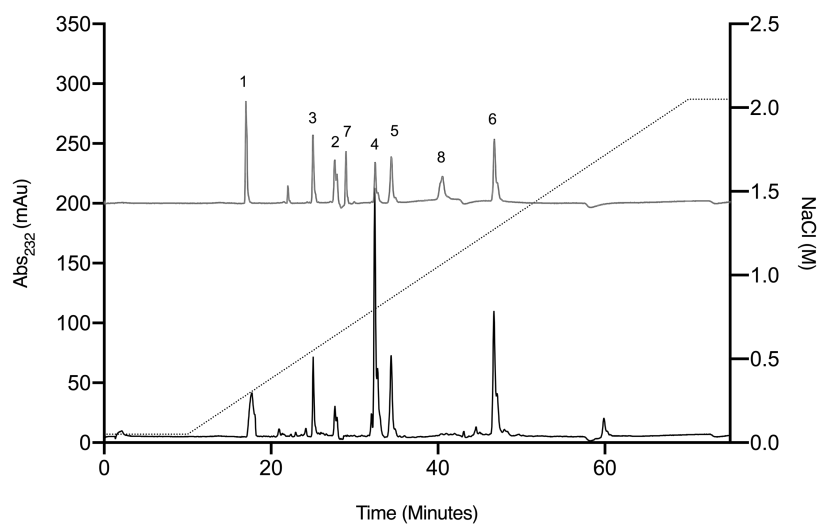


Figure 64: UV-SAX HPLC disaccharide composition analysis was performed on the bacterial lyase digest of *L. vannamei* F5 ($\lambda = 232$ nm) eluting with a linear gradient of 0-2 M NaCl (dashed line). Eluted Δ -disaccharides were referenced against the eight common standards present with heparin and HS (grey); 1; Δ UA-GlcNAc, 2; Δ UA-GlcNAc(6S), 3; Δ UA-GlcNS, 4; Δ UA-GlcNS(6S), 5; Δ UA(2S)-GlcNS, 6; Δ UA(2S)-GlcNS(6S), 7; Δ UA-(2S)-GlcNAc, 8; Δ UA(2S)-GlcNAc(6S). Elution was achieved with a linear gradient of 0–2 M NaCl (dashed line). Elution of Δ -disaccharides was monitored at $\lambda_{Abs} = 232$ nm.

Both *L. vannamei* F4 and F5 were largely composed of di-sulphated disaccharides which accounted for ~56% and 61% of the chain respectively, with the most prevalent disaccharide being Δ -UA-GlcNS(6S) for both fractions. Δ -UA-GlcNS(6S) is also the most prevalent di-sulphated disaccharide present in mammalian heparin and HS. *L. vannamei* F4 and F5 also contained ~ 14% mono-sulphated disaccharides, of which the majority was attributed to Δ -UA-GlcNS in both fractions, however this was to a greater extent in *L. vannamei* F4 than F5. *L. vannamei* F5 also contained a higher proportion of the disaccharide Δ -UA-GlcAc(6S) when compared to F4 at 5.7% and 3.7% respectively. The percentage of mono-sulphated disaccharides in the *L. vannamei* fractions, more closely resembled heparin than HS which contained ~12% and 31% respectively. The majority of the HS component of the *L. vannamei* fractions therefore contained sulphation at position C6 of glucosamine (F4; 51% and F5; 69%) and were N-sulphated (F4; 80% and F5; 83%) as opposed to N-acetylated (Table 19, Figure 65, Figure 64).

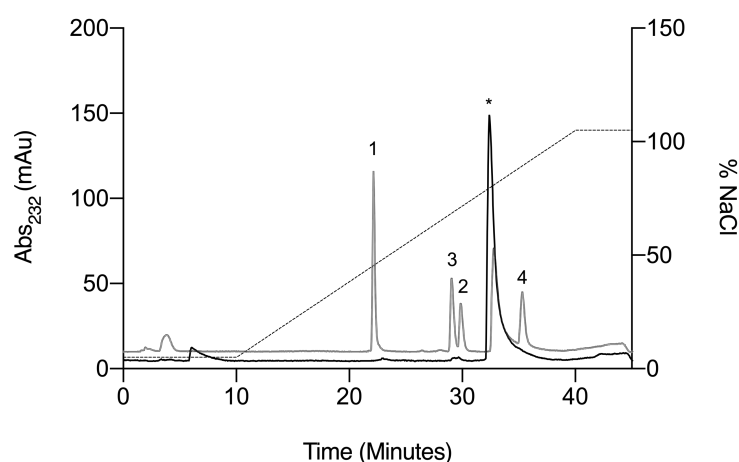


Figure 66: UV-SAX HPLC disaccharide composition analysis was performed on the ABC chondroitinase digest of *L. vannamei* F4 ($\lambda = 232$ nm) eluting with a linear gradient of 0-2 M NaCl (dashed line), pH 3.5. Eluted Δ -disaccharides were referenced against four common standards present with CS (grey). 1; Δ UA-GalNAc, 2; Δ UA-GalNAc(4S), 3; Δ UA-GalNAc(6S), 4 Δ UA-GalNAc(4,6S).

In regard to the CS component within the *L. vannamei* samples, only minimal digestion by chondroitinase ABC was observed for both fractions, as evidenced by the low intensity of the HPLC chromatogram at 232 nm (Figure 66, Figure 67), suggesting that CS is low in abundance. Matched chondroitinase ABC digestions of CSA and CSC standards were also employed to ensure that the enzymes were active (Appendix 3, Appendix 4). Digestion of both CSA and CSC generated disaccharide profiles typical of the respective CS-type bearing predominantly 4S or 6S modifications (Appendix 3, Appendix 4). The profile obtained from the matched CSA and CSC controls were high in intensity at 232 nm, in comparison to both *L. vannamei* fractions, indicating that a lack of enzymatic activity could not account for the minimal digestion of the latter samples. Of the detected digest products the CS disaccharide composition analysis indicated that *L. vannamei* F4 possess mainly CSC (~50%) and CSA (~30%) units while, *L. vannamei* F5 possess mainly CSC (~40%) and CSE units (~45%) (Table 20).

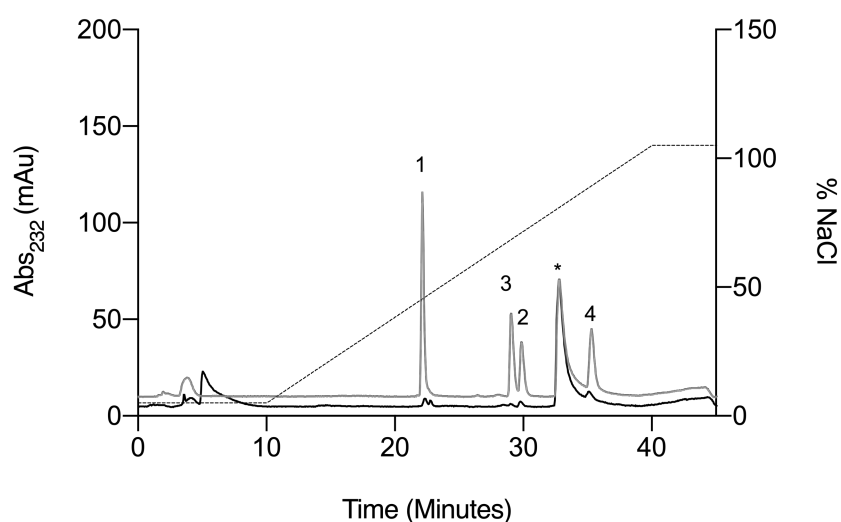


Figure 67: UV-SAX HPLC disaccharide composition analysis was performed on the ABC chondroitinase digest of *L. vannamei* F5 ($\lambda = 232$ nm) eluting with a linear gradient of 0-2 M NaCl (dashed line), pH 3.5. Eluted Δ -disaccharides were referenced against four common standards present with CS (grey). 1; Δ UA-GalNAc, 2; Δ UA-GalNAc(4S), 3; Δ UA-GalNAc(6S), 4 Δ UA-GalNAc(4,6S).

Table 20: Corrected disaccharide composition analysis of *L. vannamei* F4, F5, CSA and CSC.

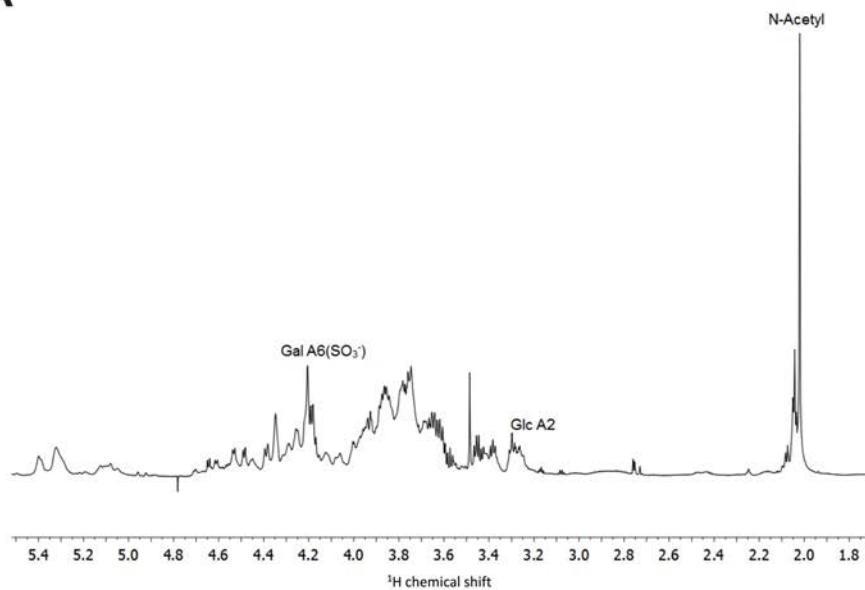
Δ-Disaccharide	<i>L. vannamei</i> F4 (%)	<i>L. vannamei</i> F5 (%)	CSC (%)	CSA (%)
Δ -UA-GalNAc	18.3	8.8	3.7	2.4
Δ -UA-GalNAc(6S)	53.0	43.0	72.0	4.3
Δ -UA-GalNAc(4S)	34.0	3.4	18.2	93.2
Δ -UA-GalNAc(4S,6S)	<i>N. D</i>	44.9	6.0	<i>N.D</i>

Subsequently ^1H and ^1H - ^{13}C HSQC NMR was employed to confirm the GAG composition of *L. vannamei* F4 and F5. ^1H NMR revealed signals indicative of the *N*-acetyl of CS (~2.02 ppm), DS (~2.07 ppm) and HS (~2.04 ppm) within both *L. vannamei* F4 and F5 (Figure 68, Figure 69). The major *N*-acetyl signal in both fractions was present at 2.02 ppm and 2.04 ppm, with the former being in higher intensity, suggesting that the fractions are composed of primarily of CS. Integration of the resonances attributed to the *N*-acetyl and A2 peaks however indicated that *L. vannamei* F4 was composed of approximately 59% HS, 38% CS and <5% DS (Figure 68). *L. vannamei* F5 was also estimated to be composed of 67% HS/heparin, 34% CS and <5% DS, through integration of the *N*-acetyl and A2 peaks (Figure 69). Peak volume integration of the signals attributed to *N*-acetyl and A2 signals present within the ^1H - ^{13}C HSQC also indicated that *L. vannamei* F4 is composed of approximately 52% CS, 48% HS and <5% DS (Figure 68) and that *L. vannamei* F5 is composed of approximately CS 45%, 55% HS and <5% DS (Figure 69).

The anomeric region can also be utilized to distinguish between GAGs classes, with the signal attributed to the anomeric carbon of glucosamine occurring downfield to that of galactosamine. A signal can be observed at approximately 4.5-6/103 ppm and 5.4/100

ppm in the ^1H - ^{13}C HSQC of *L. vannamei* F4 and F5, which is indicative of the presence of galactosamine and glucosamine, respectively. By definition CS and DS are distinguishable by the epimerisation of the uronic acid residue from GlcA to IdoA. The anomeric peak of IdoA linked to galactosamine is typically located downfield to GlcA at 5.0/105 ppm and 4.5-4.7/106 ppm, respectively. A peak can be observed which likely corresponds to the anomeric carbon of GlcA within the ^1H - ^{13}C HSQC of *L. vannamei* F4 and F5, however signals attributed to IdoA were not identified. This supports that the major galactosaminoglycan component within *L. vannamei* F4 and F5 is CS (Figure 68, Figure 69). Within the ^1H - ^{13}C HSQC of *L. vannamei* F4 several signals can be identified that have previously been attributed to the anomeric carbon of GlcA, within CS, at 4.45/106, 4.48/106.5ppm, 4.65/106.5 and 4.7/106.5 ppm (Figure 68). As for *L. vannamei* F5 a single peak present at 4.7/106.5 ppm is observed (Figure 69). A similar downfield shift has previously been identified to result from varying extents of 2-and 3-O sulphation of the GlcA residue within CS (Cavalcante *et al.*, 2018; Palhares *et al.*, 2019). This may therefore, indicate that CS component of *L. vannamei* F4 could harbor rare sulphation patterns, which have previously been observed within GAG extracts obtained from *L. vannamei* heads.

A



B

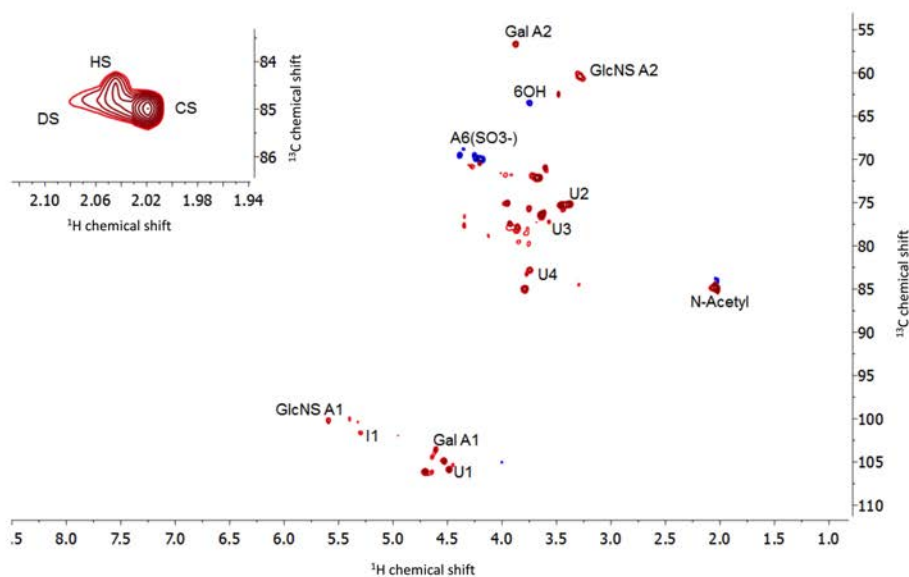
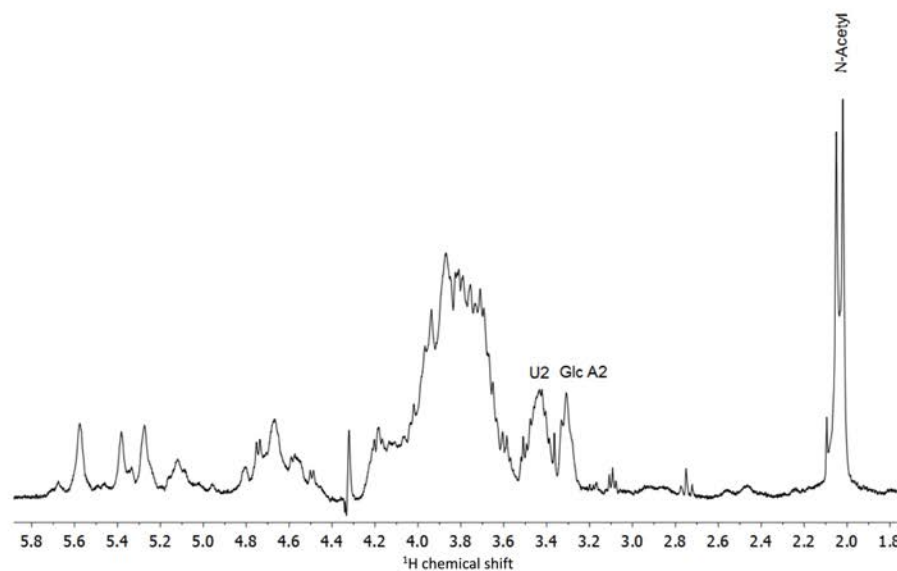


Figure 68: NMR spectra of *L. vannamei* F4. (A) ¹H and (B) ¹H-¹³C HSQC NMR spectra of *L. vannamei* F4. Major signals associated with CS and HS are indicated. Spectral integration was performed on the HSQC using labelled signals. Glucosamine, Glc; galactosamine, Gal; uronic acid, U; iduronic acid, I.

A



B

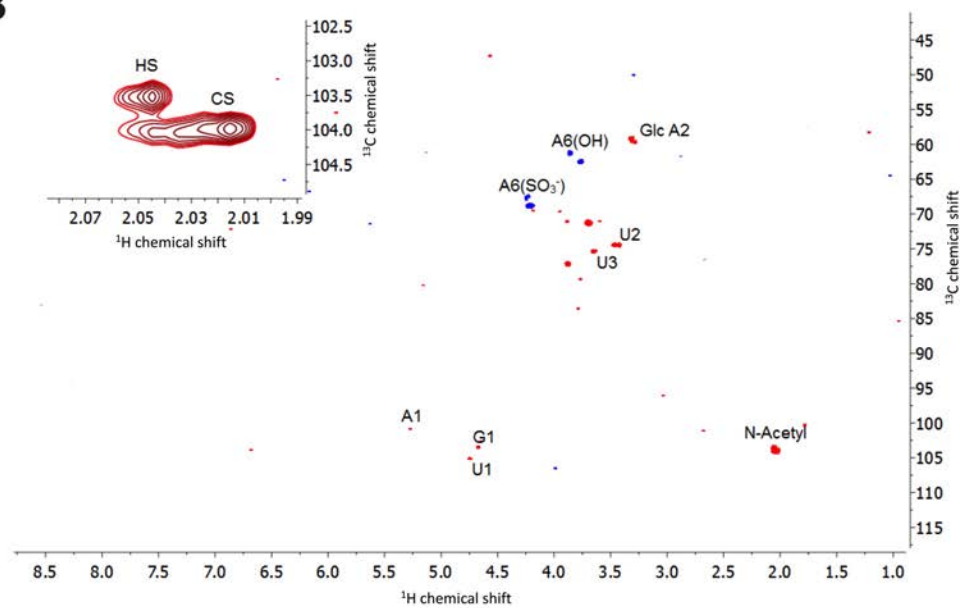


Figure 69: NMR spectra of *L. vannamei* F5. (A) ^1H and (B) ^1H - ^{13}C HSQC NMR spectra of *L. vannamei* F5. Major signals associated with CS and HS are indicated. Spectral integration was performed on the HSQC using labelled signals. Glucosamine, Glc; galactosamine, Gal; uronic acid, U.

In regard to the heparin component present within the *L. vannamei* extracts, a low intensity peak corresponding to a iduronic acid can be observed at 5.2/101 ppm in *L. vannamei* F4, whereas this signal was not detected for *L.vannamei* F5 (Figure 68, Figure 69). Having said this the signal present at approximately 5.4/100 ppm within both samples, which is attributed to the anomeric carbon of glucosamine. This therefore, further indicates the presence of HS/heparin within both fractions. Additionally, signals associated with position 2 of N-sulphated glucosamine (A2) can be identified within the ^1H - ^{13}C HSQC of both fractions. Integration of the A2 and N-acetyl peak indicated that the HS component within both *L. vannamei* F4 and F5 ~70% N-sulphated (Figure 68, Figure 69). This is in close agreement with the HPLC based disaccharide compositional analysis.

The peaks present at ~3.8-3.7/62-62 ppm and ~4.2/68-67 can be assigned to position 6 of the amide sugar which possesses OH or SO_3^- , respectively. Differentiation of the signals attributed to galactosamine, and glucosamine was however, prohibited due to the over lapping resonances. Despite this the signal intensity indicates that both the CS and HS component of *L. vannamei* fractions contain a greater proportion of sulphate modifications at position 6 of the amine residue, in comparison to hydroxyl groups (Figure 68, Figure 69).

6.2.2. *L. vannamei* F4 and F5 inhibits the Alzheimer's Disease-Relevant β -Secretase

Subsequent to the determination of the GAG composition of *L. vannamei* fraction 4 and 5, BACE1 inhibitory activity was evaluated by the previously described FRET-based fluorogenic peptide assay. In accordance with previous reports, the IC_{50} of BACE-1

inhibition by heparin was found to be $\sim 2 \mu\text{g.mL}^{-1}$. Furthermore, maximal BACE-1 inhibition was achieved at $>5 \mu\text{g.mL}^{-1}$ of heparin. In comparison maximal BACE-1 inhibition was observed at $10 \mu\text{g.mL}^{-1}$ of *L. vannamei* F4 and F5; double the concentration of heparin required to achieve an equivalent level of inhibition. The IC_{50} of BACE-1 inhibition by *L. vannamei* F4 and F5 was found to be 4.6 and $5.9 \mu\text{g.mL}^{-1}$ respectively, further indicating that both fractions exhibit moderately reduced BACE-1 inhibitory activity in comparison to mammalian heparin. *L. vannamei* F4, was however found to be more potent than *L. vannamei* F5 (Figure 70).

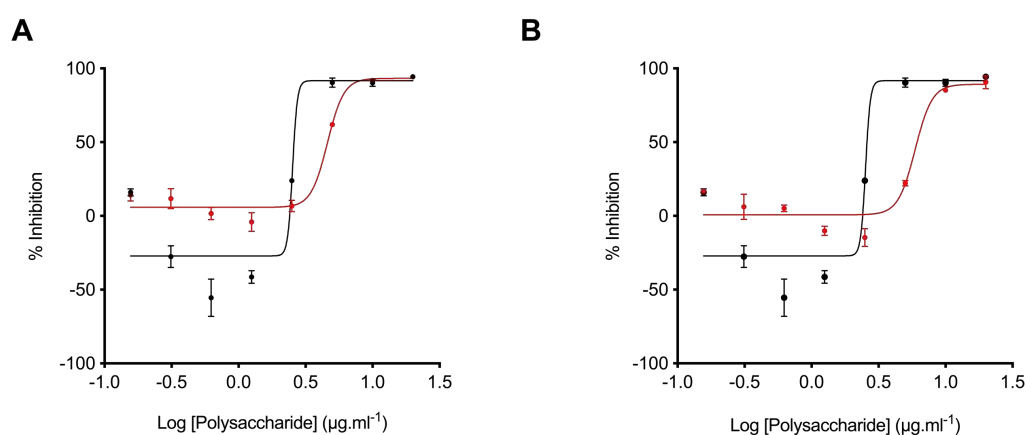


Figure 70: Inhibition of the human beta-secretase, BACE-1, *L. vannamei* F4 and F5 determined by FRET. The IC_{50} of *L. vannamei* F4 (A; red) and F5 (B; red) was determined to be $4.61 \mu\text{g.mL}^{-1}$ ($R^2 = 0.97$) and $5.93 \mu\text{g.mL}^{-1}$ ($R^2 = 0.93$) respectively. In contrast the IC_{50} heparin (A and B black) was $\sim 2.43 \mu\text{g.mL}^{-1}$ ($R^2 = 0.93$).

As previously described, at low concentrations of heparin (1.3 - $0.3 \mu\text{g.mL}^{-1}$) promotion of BACE-1 activity was observed (Figure 70, Figure 71, Figure 72). A slight increase in BACE-1 activity was also observed in the presence of low concentrations of *L. vannamei* F4 and F5, this was however reduced in comparison to the heparin at all concentrations tested, in particular in regards to the former fraction (Figure 70, Figure 71, Figure 72).

At 625 ng.mL^{-1} , the concentration in which heparin exhibits maximal BACE-1 promotor activity, BACE-1 exhibited only a marginal increase in activity in the presence of *L. vannamei* F4 and F5. In contrast at $5 \mu\text{g.mL}^{-1}$, where complete inhibition of BACE-1 is observed in the presence of heparin, *L. vannamei* F4 and F5 were found to initially stimulate BACE-1 activity prior to inhibiting the enzyme (Figure 71, Figure 72). This again indicates that both *L. vannamei* F4 and F5 display reduced BACE-1 inhibitory activity in comparison to mammalian heparin.

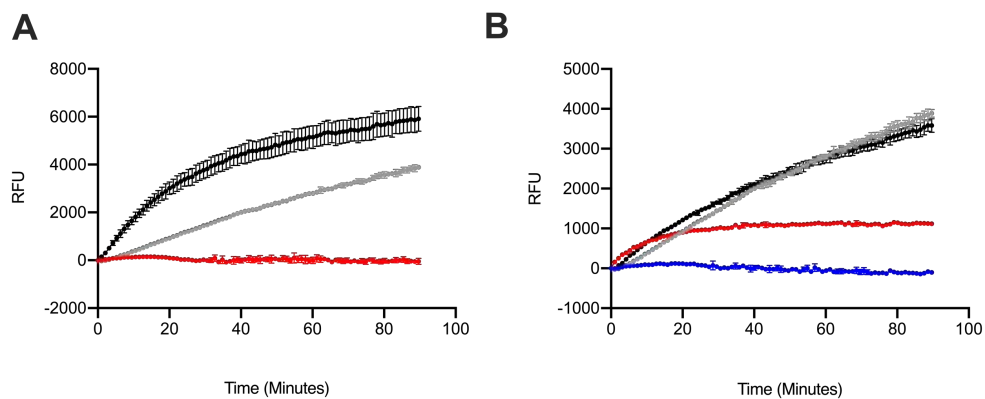


Figure 71: Inhibition of human BACE1 by heparin, *L. vannamei* F4. Time-course activation or inhibition of BACE1 by 10 (blue), $5 \mu\text{g mL}^{-1}$ (red) or 625 ng mL^{-1} (black) compared to water control (grey) heparin (A) or *L. vannamei* F4 (B).

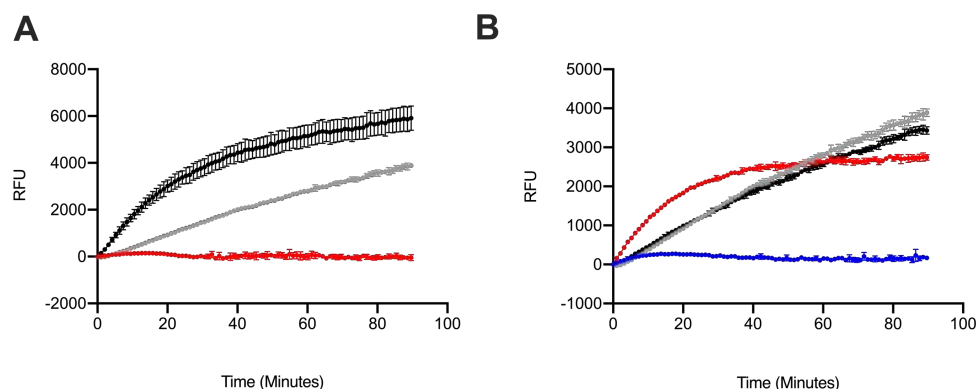


Figure 72: Inhibition of human BACE1 by heparin, *L. vannamei* F5. Time-course activation or inhibition of BACE1 by 10 (blue), $5 \mu\text{g mL}^{-1}$ (red) or 625 ng mL^{-1} (black) compared to water control (grey) heparin (A) or *L. vannamei* F5 (B).

6.2.3. Attenuated Anticoagulant Activities of the *L. vannamei* F4 and F5 extracts

Despite *L. vannamei* F4 and F5 displaying reduced BACE-1 inhibitory activity in comparison to mammalian heparin, the anticoagulant activities were determined, using the prothrombin time (PT) and activated partial thromboplastin time (aPTT) assays, in order to evaluate whether the former compounds displayed diminished activity. As the anticoagulant activity of heparin precludes the repurposing of this clinically approved pharmaceutical as a drug targeting AD, the attenuation of this off-target activity would prove favourable the redeployment of GAG based therapeutics. In contrast to heparin (193 IU.mg⁻¹), *L. vannamei* F4 displayed negligible anticoagulant activity in both the PT and aPTT assays, which measure the extrinsic and intrinsic coagulation pathways, respectively. Where, *L. vannamei* F4 displayed an EC₅₀ of 1.28 mg.mL⁻¹ (PT) and 27.91 µg.mL⁻¹ (aPTT), compared to heparin at 19.53 µg.mL⁻¹ and 1.66 µg.mL⁻¹ (aPTT) (Figure 73). *L. vannamei* F5 also demonstrated a reduction in anticoagulant activity in the PT assay and aPTT assays in comparison to heparin at EC₅₀ = 138.80 µg.mL⁻¹ and 14.60 µg.mL⁻¹, respectively (Figure 74). Although the anticoagulant activity of *L. vannamei* F5 was greater than that of *L. vannamei* F4.

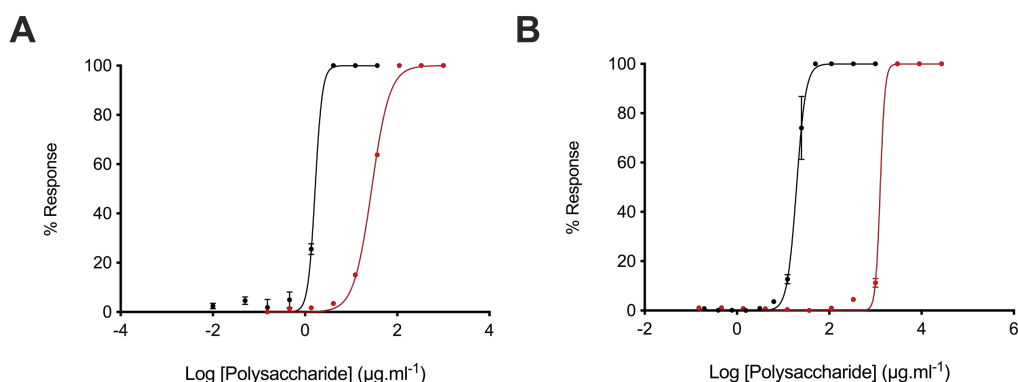


Figure 73. Anticoagulant activity of *L. vannamei* F4. (A) Activated partial thromboplastin time (aPTT) and (B) prothrombin time (PT) inhibitory response (\bar{x} %, \pm SD, $n=3$) for heparin (open circle, dashed line) and *L. vannamei* F4 (closed circle, solid line). aPTT: heparin EC₅₀ = 1.66 µg.mL⁻¹; *L. vannamei* F4 EC₅₀ = 27.91 µg.mL⁻¹. PT: heparin EC₅₀ = 19.53 µg.mL⁻¹; *L. vannamei* F4 EC₅₀ = 1.28 mg.mL⁻¹.

Therefore, despite *L. vannamei* F4 and F5 displaying reduced BACE-1 inhibitory activity in comparison to heparin, when anticoagulant activity is considered the GAG extracts demonstrated increased therapeutic ratios at 6.10, 2.46 and 0.68 respectively (FRET:aPTT) (Table 21). *L. vannamei* F4, was found to possess the most favourable therapeutic value out of the compounds tested, and as a result was employed for further experiments.

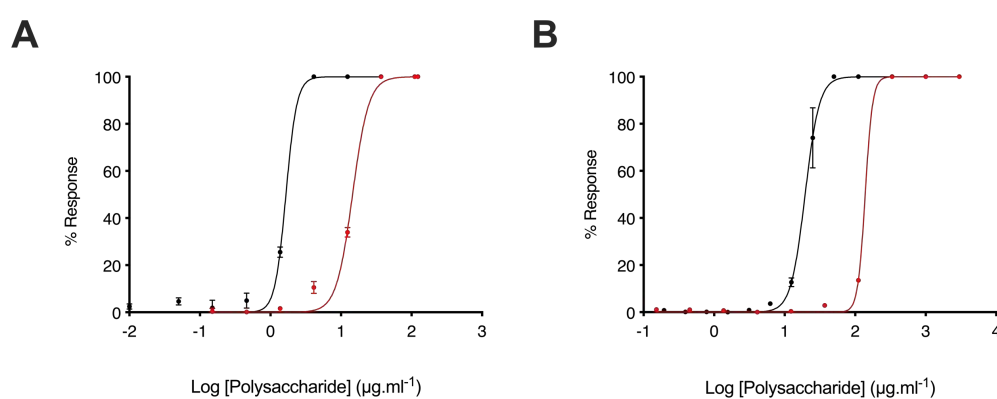


Figure 74: Anticoagulant activity of *L. vannamei* F5. (A) Activated partial thromboplastin time (aPTT) and (B) prothrombin time (PT) inhibitory response (\bar{x} %, \pm SD, $n=3$) for heparin (open circle, dashed line) and *L. vannamei* F5 (closed circle, solid line). aPTT: heparin EC₅₀ = 1.66 $\mu\text{g.mL}^{-1}$; *L. vannamei* F5 EC₅₀ = 14.60 $\mu\text{g.mL}^{-1}$. PT: heparin EC₅₀ = 19.53 $\mu\text{g.mL}^{-1}$; *L. vannamei* F5 EC₅₀ = 138.80 $\mu\text{g.mL}^{-1}$.

Table 21: Therapeutic ratio of *L. vannamei* F4 and F5 compared to heparin. The therapeutic ratio was calculated from the IC₅₀ of BACE1 inhibitory activity measures by FRET/ aPTT anticoagulant activity. GAG = glycosaminoglycan, aPTT = activated partial thromboplastin time, PT = prothrombin time.

GAG	aPTT ($\mu\text{g.mL}^{-1}$)	PT ($\mu\text{g.mL}^{-1}$)	BACE1 inhibitory activity ($\mu\text{g.mL}^{-1}$)	Therapeutic ratio
PMIH	1.66	19.53	2.43	0.68
<i>L. vannamei</i> (F4)	27.91	1276.00	4.61	6.10
<i>L. vannamei</i> (F5)	14.60	138.80	5.93	2.46

6.2.4. Heparin and *L. vannamei* F4 induce a conformational change in the Alzheimer's Disease-Relevant β -Secretase.

The secondary structure composition of BACE-1 at pH 4.0 was calculated by fitting the CD spectra to a library of representative proteins, as described in section 4.2 (Micsonai *et al.*, 2015). The CD spectrum of BACE-1 alone was predicted to possess a secondary structure composition of approximately 6% helix, 35% antiparallel, 0% parallel, 16% turn and 43% other. The CD spectrum of BACE-1 was subsequently recorded in the presence of a 1:4 (w/w) ratio of BACE-1:polysaccharide; the same ratio at which *L. vannamei* F4 exhibited maximal activity in FRET peptide inhibition assays. Under these conditions heparin exerted a conformational change in BACE-1 which was predicted to result in an increase in α -helix content (+ 8%) and a reduction in antiparallel β -sheet (- 35%). Similarly, in the presence of *L. vannamei* F4 (1:4 w/w; BACE-1: *L. vannamei* F4) BACE-1 the secondary structure of BACE-1 was predicted to exhibit an increase in α -helix (+2%) and reduction in antiparallel β -sheet (-6%) content (Figure 75). This suggests that a similar conformational change in BACE-1 structure may occur upon binding to GAGs.

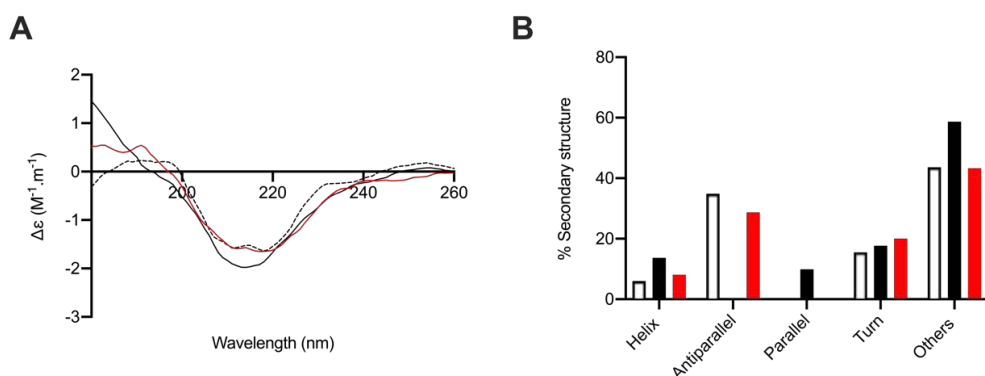


Figure 75. The secondary structural change of BACE-1 observed in the presence of heparin and *L. vannamei* F4. (A) CD spectra of BACE-1 alone (9 μg ; dashed line) and in the presence of 36 μg heparin (black solid line) or *L. vannamei* F4 (red) in 50 mM Sodium acetate buffer pH 4.0. (B) Secondary structure (%) of BACE-1 alone (white) and in the presence of heparin (black solid line) or *L. vannamei* F4 (red), estimated using BeStSel between 180-260 nm.

6.2.4. Heparin and *L. vannamei* F4 destabilise the Alzheimer's Disease-Relevant β -Secretase.

Previously, in section 4.2 GAGs were observed induce destabilisation of BACE-1; indicated by a decrease in the melting temperature (T_m) by DSF. The maximum level of BACE-1 destabilisation was observed in the presence of $50 \mu\text{g.mL}^{-1}$ heparin, where a change in T_m of $\sim -10^\circ\text{C}$ was recorded. At an equivalent concentration *L. vannamei* F4 was found to induce a reduction in the T_m of BACE-1 by approximately 5°C . This again indicates that GAG may induce BACE-1 inhibition in a similar manner, which is distinct from other known peptide inhibitors (Lo *et al.*, 2004). Destabilisation of BACE-1 by heparin and *L. vannamei* F4 was also found to be dose dependent (Figure 76).

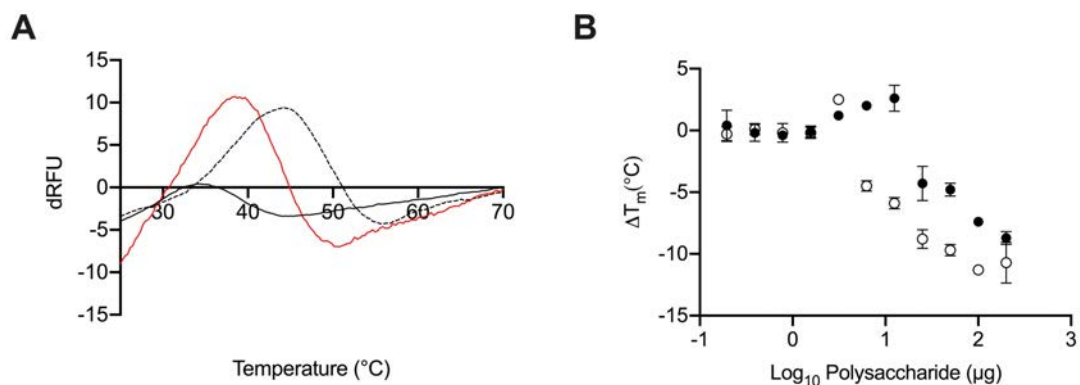


Figure 76: Differential scanning fluorimetry of BACE-1 in the presence of heparin or *L. vannamei* F4. (A) First derivative of the DSF thermal stability profile of BACE1 alone ($1 \mu\text{g}$; dashed line) and with heparin ($2 \mu\text{g}$ black line) or *L. vannamei* F4 ($2 \mu\text{g}$ red line) in 50 mM sodium acetate buffer pH 4.0. (B) ΔT_m of BACE1 with increasing heparin (open circles) or *L. vannamei* F4 (closed circles) concentration.

6.3. Discussion

The fractionated extracts obtained from *L. vannamei* were confirmed to be composed of a heterogeneous mixture of GAGs, including HS, CS and DS. ^1H - ^{13}C HSQC NMR revealed that *L. vannamei* F4 and F5, which were eluted from the DEAE-Sephacel anion exchange column with 0.8 M and 1M NaCl respectively, contained primarily HS and CS, with less than 5% DS being present within both fractions. *L. vannamei* F5 was found to contain a higher proportion of HS/heparin than F4 at ~70 and ~60%, respectively. Analysis utilising agarose gel electrophoresis indicated that both *L. vannamei* fractions contained a greater proportion of HS than CS, with the major and minor bands observed displaying migration distances corresponding to the former and latter compounds, respectively. Having said this the intensity of the band corresponding to CS was lower than what would be expected based upon the estimated GAG composition determined by NMR spectroscopy. Previous reports of CS obtained from *L. vannamei* have been shown to possess similar electrophoretic mobility to HS (Cavalcante *et al.*, 2018; Palhares *et al.*, 2019). This observation was suggested to be attributable to the presence of rare sulphate modifications at positions 2 and 3 on the GlcA residue. The presence of sulphated glucuronic acid residues within the *L. vannamei* fractions would therefore, account for the relatively low intensity of the band corresponding to CS when analysed by agarose gel electrophoresis. Furthermore, this may also account for why analysis of the ATR-FTIR spectroscopy of both *L. vannamei* fractions indicated the presence of disproportionately high levels of HS. In support of this, the ^1H - ^{13}C HSQC NMR of both *L. vannamei* fractions indicated the presence of a peak at approximately 4.7/106 ppm, which was previously assigned to the anomeric position of GlcA residues bearing 2-

and/or 3-sulphation within CS extracts obtained from *L. vannamei* (*idem*). Additionally, analysis of *L. vannamei* F4 and F5 by CD spectroscopy suggested that both fractions contained a higher proportion of CS than originally indicated by analysis of the ATR-FTIR spectra and by agarose gel electrophoresis. In further support of the presence of 2 and/or 3-sulphated GlcA modifications within the CS component of the *L. vannamei* GAG extracts, digestion utilising chondroitinase ABC resulted in negligible detectable disaccharide products via SAX-HPLC. Previously it has been observed that CS samples containing GlcA residues bearing sulphate modifications are largely resistant to chondroitinase ABC digestion (Sugahara *et al.*, 1996) and that GlcA-Gal disaccharides possessing 3-O sulphate modifications are not detectable by HPLC analysis (Kinoshita-toyoda *et al.*, 2004). The presence of sulphated GlcA residues within the *L. vannamei* fractions could therefore, account for the higher proportion of CS detected through NMR spectroscopy, in comparison to ATR-FTIR spectroscopy and agarose electrophoresis, in addition to the resistance to digestion by chondroitinase ABC. It should, however, be noted that neutral sugars present within the tetrasaccharide linkage region (galactose and xylose) also exhibit NMR resonances within the region of 4.4-4.7/105-106 ppm. As such, further analysis utilising NMR correlation spectroscopy techniques, for instance COSY and TOCSY, should be employed to confirm the presence of sulphated glucuronic acid residues within the *L. vannamei* fractions.

In addition to sulphated GlcA residues, NMR analysis suggested that the CS component within the *L. vannamei* F4 and F5 contains predominantly sulphate modifications at position 6 of the galactosamine residue. The higher level of sulphation at position 6 of galactosamine in both *L. vannamei* 4 and 5 was also detected through SAX-HPLC

disaccharide composition analysis. In addition to Gal6S, SAX-HPLC disaccharide analysis indicated the presence of CSA units in *L. vannamei* F4 and CSE units in *L. vannamei* F5, albeit to a lesser extent. This contrasts with the NMR analysis, which did not detect the presence of sulphation at position 4 of galactosamine in either fraction. As minimal digestion products of *L. vannamei* F4 and F5 were detected from the action of chondroitinase ABC yielded, the absence of disaccharides bearing 4-sulphated modifications on the galactosamine residue in ^1H - ^{13}C HSQC NMR analysis may be accounted for by the low abundance of this modification within the extracts. Additionally, the ^1H - ^{13}C HSQC NMR spectra should be recorded utilising a greater number of scans and at higher temperature, in order to improve the resolution. This would also increase the likelihood of detecting the presence of Gal(4S) modifications by preventing suppression as a result of overlapping resonances with H_2O when spectra are recorded at lower temperatures. Despite this, both the constitutional analysis by ^1H - ^{13}C HSQC NMR and SAX-HPLC indicated that the sulphation pattern of the CS component of the *L. vannamei* fractions is complex, although further analysis should be conducted in order to further elucidated the fine structure of the CS contained within this extract.

In regard to the HS component of *L. vannamei* F4 and F5 both fractions exhibited a fine structure intermediate to that typically observed for mammalian HS and heparin. The absence of an IdoA signal in the ^1H - ^{13}C HSQC spectrum of *L. vannamei* F5 suggests that the predominant uronic acid within this fraction is GlcA, a feature more typical of HS than heparin. A minor signal attributable to anomeric carbon of IdoA was however, present within *L. vannamei* F4 suggesting that this sample may contain a higher level of

epimerised uronic acid residues in comparison to *L. vannamei* F5. The HS/heparin component of both *L. vannamei* fractions was determined to possess approximately 70-80% N-sulphated glucosamine residues, which is more typical of heparin than HS. Furthermore, *L. vannamei* F4 and F5 were found to possess approximately 50% and 69% 6-sulphated glucosamine modifications, respectively. This is approximately double typically reported for mammalian HS but slightly reduced in comparison to mammalian heparin. In addition, a lower proportion of trisulphated disaccharides (Δ UA(2S)-GlcNS(6S)) were identified following bacterial lyase digestion of *L. vannamei* F4 and F5 at ~15%, in comparison to mammalian heparin. Conversely, *L. vannamei* F4 and F5 were found to possess a lower proportion of unsulphated disaccharides (-UA-GlcNAc) in comparison to mammalian HS, which is more typical of heparin samples. Therefore, the HS/heparin component of *L. vannamei* F4 and F5 is composed of a fine structure which is an intermediate of that typical of mammalian heparin and HS. Heparin/HS like compounds displaying similar features have previously been isolated from shrimp species (Dietrich *et al.*, 1999; Chavante *et al.*, 2000, 2014), however these also displayed some structural features which were distinct from the extracts presented in this work. For instance, the heparin/HS like compound isolated from *L. vannamei* by Chavante *et al.*, (2014) was found to contain a high content of trisulphated glucosamine monosaccharides (GlcNS(3S,6S)). Similar to the extracts presented within this study, the heparin/HS like compound isolated from the shrimp *Artemia franciscana* by Chavante *et al* (2000), was found to contain a high level of NS sulphated glucosamine residues, however the level of 6-sulphated glucosamine was lower than that of the *L. vannamei* GAG samples described here. This highlights the diverse and heterogeneous fine sequences displayed by heparin/HS samples obtained from shrimp species.

Subsequently the BACE-1 inhibitory activity of *L. vannamei* F4 and F5 were evaluated in comparison to mammalian heparin, using the previously described FRET-fluorogenic peptide assay. *L. vannamei* F4 and F5 were found to inhibit BACE-1, albeit at a slightly diminished level in comparison to heparin. *L. vannamei* F4 was observed to possess an increased BACE-1 inhibitory activity in contrast to *L. vannamei* F5, with IC₅₀ values of 4.6 µg·mL⁻¹ and 5.9 µg·mL⁻¹, respectively. Despite both *L. vannamei* fractions being predominantly composed of a mixture of CS and HS, with F4 containing a higher proportion of CS, the ability of CS to inhibit BACE-1 was observed in section 3.2.2 This was in contrast to previous reports which indicated that CS displayed negligible BACE-1 inhibitory activity (Scholefield *et al.*, 2003). It therefore, cannot be assumed that the HS/heparin component of the *L. vannamei* fractions is the sole active species and it is likely that specific sulphation sequences within CS chains are also able to elicit BACE-1 inhibition; in a manner akin to that previously described for heparin (Patey *et al.*, 2006). Having said this the majority of the HS component of the *L. vannamei* fractions was found to contain sulphation at position C6 of the glucosamine residue (F4; 51% and F5; 69%). Previously 6-O sulphation of glucosamine was reported to be essential for potent BACE-1 inhibitory activity. Furthermore, the presence of 2-sulphated uronic acid residues have also been identified to be important for BACE-1 inhibitory activity, irrespective of the epimer (Patey *et al.*, 2006; Schwörer *et al.*, 2013). *L. vannamei* F4 was found to display an increased proportion of 2S uronic acid residues, in comparison to *L. vannamei* F5 at ~40% and 30%, respectively. Despite both fractions containing a lower level of 2 sulphated uronic acid residues than heparin, this may therefore, account for the higher BACE-1 inhibitory activity observed for *L. vannamei* F4 in comparison to F5. The extracts isolated from *L. vannamei* provide further evidence

that 6-O and 2-O- sulphation of HS/heparin is important for BACE-1 inhibitory activity (Patey *et al.*, 2006). The ability of the *L. vannamei* extract to promote proBACE-1 at low concentrations was extensively reduced in comparison to heparin, suggesting that this source of GAGs may be more favourable for therapeutic applications against AD.

Due to the anticoagulant activity of heparin-based drugs largely precluding the repurposing of this clinically approved pharmaceutical for the treatment of AD, the ability of *L. vannamei* F4 and F5 to perturb the intrinsic, extrinsic and common coagulation pathways was evaluated. Both *L. vannamei* fractions were demonstrated to possess negligible anticoagulant activities in both the PT and aPTT assays. As such, despite the reduced BACE-1 inhibitory activity displayed by *L. vannamei* F4 and F5, in comparison to mammalian heparin, the therapeutic value is greater when the off-target activity of anticoagulation is also considered. *L. vannamei* F4 demonstrated a higher therapeutic value than both heparin and *L. vannamei* F5 and was, therefore utilised for further evaluation of the interaction of this extract with BACE-1.

To determine whether *L. vannamei* F4 inhibits BACE-1 through a mechanism comparable to that displayed by heparin, the interaction with BACE-1 was evaluated using CD spectroscopy and DSF. The CD spectrum of BACE-1 in the presence of heparin was previously identified to induce a change in the secondary structure of BACE-1 (chapter 5.2). This was in contrast to peptide inhibitors, where previously no change in BACE-1 conformation was observed (De Simone *et al.*, 2013). In addition, DSF measurements were also previously shown to observe a decrease in the melting temperature (T_m) of BACE-1 in the presence of heparin (chapter 4.3), again this was in

contrast to other inhibitors which exerted a stabilising effect upon BACE-1 (Lo et al., 2004). In the presence of *L. vannamei* F4 a concentration dependent destabilisation of BACE-1 was also observed; exemplified by a decreased T_m , measured via DSF. The reduction in the T_m of BACE-1 in the presence of *L. vannamei* F4 was comparable to the IC_{50} of *L. vannamei* F4 in FRET-based assays, in that the change in T_m was two-fold lower than elicited by heparin. This provides further support that a decrease in the T_m of BACE-1 in the presence of GAG-like polysaccharides, when measured using DSF, can reduce the potential inhibitory activity of the compound. The conformational change of BACE-1 in the presence of heparin observed by CD experiments, was shown to result in an increase in α -helix content and reduction in antiparallel β -sheet (Chapter 4.2). This change in secondary structure was found to be in-line with the conformational changes observed between BACE-1 in active (pH 4.0) and inactive (pH 7.4) conformations, when measured by CD spectroscopy (*idem*). The CD spectra of BACE-1 in the presence of *L. vannamei* F4 was also observed to elicit a reduction in antiparallel β -sheet and an increase in α -helix content. This further suggests that BACE-1 inhibition by GAGs occurs via inducing a conformational change, rendering BACE-1 inactive, and that this mechanism is distinct from the effects of known inhibitors.

Chapter 7: Glycosaminoglycan extracts with attenuated off target activities, isolated from *Sardinia pilchardus*, inhibit the Alzheimer's beta-secretase, BACE1.

7.1 Introduction

Sardinia pilchardus belongs to the genus *clupeocephala* (bony fishes) and mainly inhabits the coasts of eastern North Atlantic, from Iceland to Senegal, however *S. pilchardus* can also be found in the Mediterranean, Sea of Marmara and the Black Sea. *S. pilchardus* is an important fishery species, with 1, 281, 391 tonnes captured in 2016, this number has also been rising steadily since 2000 (FAO, 2020). *S. pilchardus* are principally caught in the waters of the aforementioned regions, although some attempts to establish an aquaculture industry have been made in Portugal. Following capture *S. pilchardus* are primarily utilised within the fish canning industry, to which they are supplied whole, and a small proportion also enters the market sold as either frozen or fresh whole fish (Archer, 2001). Following arrival at canning factories *S. pilchardus* are processed, resulting in the production of waste material including heads, viscera, lungs, flaps and in some cases skin (Archer, 2001; Carvalho *et al.*, 2018). The resulting waste products are currently largely utilised for fishmeal, however the income generated as a result is extremely low. Alternatively, within the UK processors are required to pay to dispose of waste products at landfill (Archer, 2001).

Of the total UK fish and shellfish industry it was reported that approximately 57% ends up as waste (*idem*). Similarly, within the EU 5.2 million tonnes of fish waste is generated per year, up to 65% of which is generated by the fish canning industry (Carvalho *et al.*, 2018). Furthermore, it has also been estimated that up to 39.5 million tonnes of whole fish catches, dead or alive, are discarded worldwide each year by commercial fisheries (Archer, 2001). Therefore, a growing interest in the utilisation of fish waste has arisen

with the aim of increasing sustainability, increasing the utilisation of resources, and generating increased revenues (Archer, 2001; Carvalho *et al.*, 2018). Several reports have indicated that fish, including the waste products generated from processing from the food industry, are a valuable source of GAGs (Table 5, Table 7). In particular, CS and DS have widely been isolated from various fish species (Table 7). In light of this, GAGs were extracted from *S. pilchardus* and the resulting extracts were evaluated for the ability to inhibit BACE-1.

7.1.2. Aims

The crude GAG extracts isolated from *S. pilchardus* by proteolysis were fractionated by DEAE-Sephacel anion-exchange chromatography in Chapter 4. The resulting fraction obtained via elution with 800 mM NaCl was subsequently screened for the ability to inhibit recombinant human BACE-1, where approximately 75% inhibition was observed at 5 $\mu\text{g}.\text{mL}^{-1}$ (section 4.2). The aim of this chapter is to further characterise the biological and structural properties of *S. pilchardus* F4.

7.2. Results

The *S. pilchardus* fraction obtained via DEAE-Sephacel anion-exchange chromatography, eluted with 8.0 M NaCl (designated fraction 4; F4), was analysed by agarose gel electrophoresis in 1-2-diaminopropane buffer (Figure 77). *S. pilchardus* F4 was observed to possess comparable electrophoretic migration to that of CS and DS. No bands were observed that not corresponded the migration of mammalian heparin or HS (Figure 77). A minor band with a migration rate slower to that of heparin and HS was observed within the *S. pilchardus* F4 sample (Figure 77).

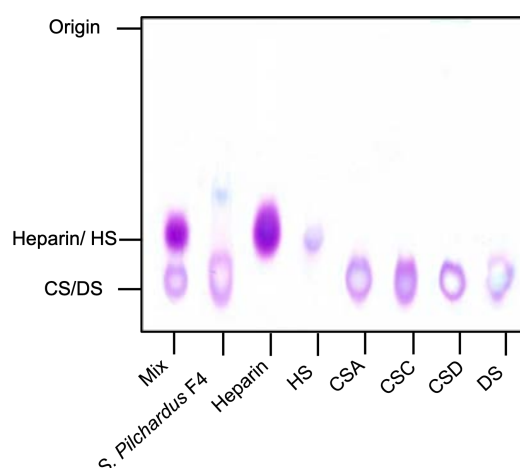


Figure 77: Agarose gel electrophoresis of *S. pilchardus* F4 in 1-2-diaminopropane buffer. The electrophoretic mobility of *S. pilchardus* F4 was compared to that of bona fide GAG standards; heparin, heparan sulphate (HS), chondroitin sulphate A (CSA), C (CSC) and D (CSD), and dermatan sulphate (DS). Mix = CSA, heparin and HS mixture.

In order to corroborate that the *S. pilchardus* F4 sample is composed primarily of CS/DS and to further elucidate the major galactosaminoglycan constituent of this extract, ATR-FTIR and CD spectroscopy were employed. The ATR-FTIR spectrum of *S. pilchardus* F4 exhibited spectral features characteristic of sulphated GAGs with bands observable at

1230 cm^{-1} , 1430 cm^{-1} and 1635 cm^{-1} , which are associated with S=O stretches, symmetric and asymmetric carbonyl stretching, respectively. In addition, a band can also be observed centering at 1025 cm^{-1} , which is indicative of CS. Bands in the region of 750-880 cm^{-1} , which are associated with the presence of sulphate modifications, were also observed to be similar to CSA. To further evaluate the composition of *S. pilchardus* F4 the ATR-FTIR spectrum was subjected to PCA against the previously described library of GAGs (Figure 78). When PC1 and PC2 were compared, which comprised 72% of the total variance, *S. pilchardus* F4 located within the region containing CS and was distinctly separated from all other GAGs (Figure 78).

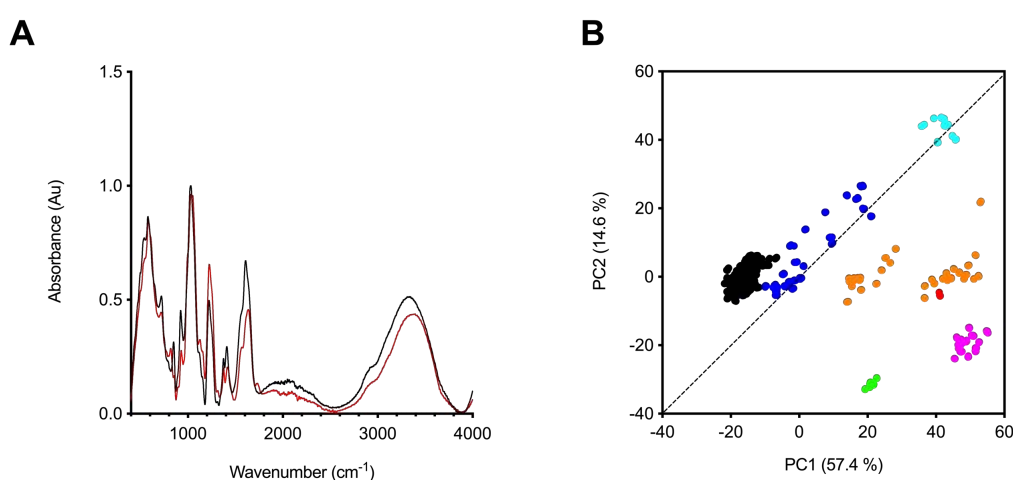


Figure 78: ATR-FTIR spectrum of *S. pilchardus* F4. (A) Attenuated total reflection Fourier-transform infrared spectra of chondroitin sulphate (black) and *S. pilchardus* F4 (red), $n = 5$. (B) Principal component analysis Score Plot (PC1 v. PC2) of *S. pilchardus* F4 compared against a bone fide glycosaminoglycan library. Heparan sulphate (blue), heparin (black), chondroitin sulphate (orange), dermatan sulphate (magenta), over-sulphated chondroitin sulphate (OCS; green), hyaluronic acid (cyan), *S. pilchardus* F4 (red).

The CS spectrum of *S. pilchardus* F4 also exhibited spectral features typical of CS, with a negative CD band centering at ~ 210 nm. The CD spectrum of the *S. pilchardus* F4 extract also exhibited negative ellipticity at wavelengths < 190 nm, which is typical of CS (Figure 79). Principal component analysis was subsequently employed in order to

compare the CD spectrum of *S. pilchardus* F4 against that of known GAG standards (Figure 79). Comparison of PC1, which covered approximately 88 % of the total variance, located the *S. pilchardus* F4 towards the region associated with CS/DS and away from that of heparin/HS samples. Further comparison of PC1 and PC2, comprising approximately 97 % of the total variance, separated *S. pilchardus* F4 closer towards CS from DS samples, with *S. pilchardus* F4 locating within the center of the CS region.

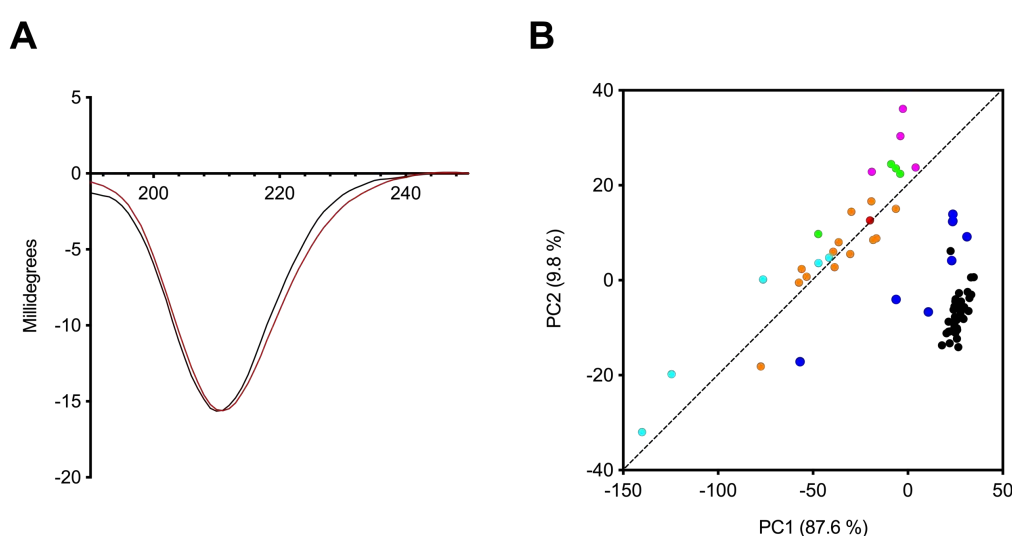


Figure 79: Circular dichroism spectrum of *S. pilchardus* F4. (A) Circular dichroism spectra of spectra of chondroitin sulphate (black) and *S. pilchardus* F4 (red). (B) Principal component analysis Score Plot (PC1 v. PC2) of *S. pilchardus* F4 against a bone fide glycosaminoglycan library. Heparan sulphate (blue), chondroitin sulphate (orange), heparin (black), DS (magenta), over sulphated chondroitin sulphate (green), hyaluronic acid (cyan), *S. pilchardus* glycosaminoglycan (red).

To further elucidate the fine structure of the *S. pilchardus* F4 extract, the sample was subjected to disaccharide compositional analysis utilizing SAX HPLC, following being exhaustively digested with chondroitinase ABC. The resulting chromatograms obtained for the digestion products of *S. pilchardus* F4, and matched CSA and CSC controls, were compared to those of the common Δ -disaccharides standards present within CS and DS (Figure 80, Appendix 3, Appendix 4).

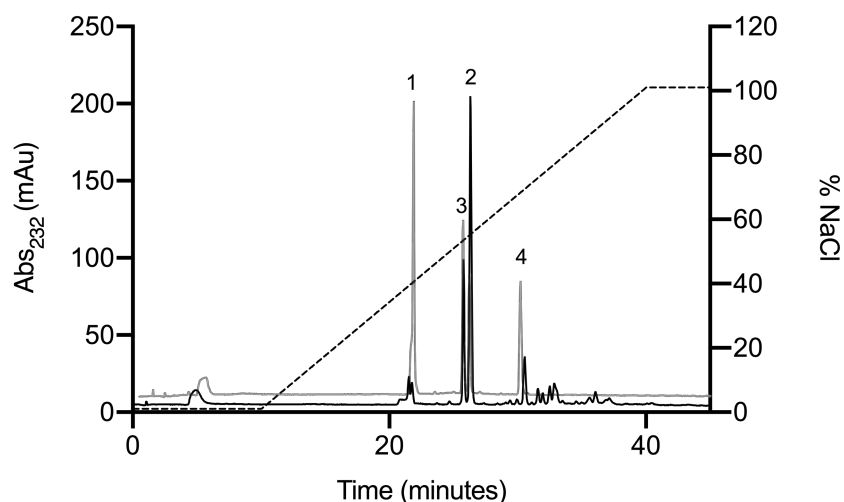


Figure 80: UV-SAX HPLC disaccharide composition analysis performed on the bacterial lyase digest products obtained from *S. pilchardus* F4 in reference to the most common Δ -disaccharides standards present within CS. *S. pilchardus* F4 (black), Δ -disaccharides standards (grey); 1, Δ -UA-GalNAc; 2, Δ -UA-GalNAc(4S); 3, Δ -UA-GalNAc(6S); 4, Δ -UA-GalNAc(4S,6S). Elution of Δ -disaccharides was performed with a linear gradient of NaCl and monitored at $\lambda_{\text{abs}} = 232$ nm.

The digest products detected for CSA were as expected, with the 93.2% of the total disaccharides present being Δ -UA-GalNAc(4S) (Table 22, Appendix 3, Appendix 4). Likewise, the major disaccharide present within the CSC standard was found to be Δ -UA-GalNAc(6S) at 72%, minor amount of Δ -UA-GalNAc(4S) and Δ -UA-GalNAc(4,6S) were also detected within this sample at 18.2% and 6.0%, respectively. Both CSC and CSA standards were observed to possess minimal unsulphated disaccharides (Δ -UA-GalNAc) (Table 22, Appendix 3, Appendix 4). A more disperse sulphation profile was observed for the *S. pilchardus* F4 sample, however the major disaccharide unit was observed to be Δ -UA-GalNAc(4S) at 58.1%. Approximately 27.6% and 10.3% of the disaccharides present within the *S. pilchardus* F4 sample were attributed to Δ -UA-GalNAc(6S) and Δ -UA-GalNAc(4,6S), respectively. Alike to both CSC and CSA standards the *S. pilchardus* F4 sample was also found to possess minimal unsulphated disaccharides at approximately

4%. In addition, several unidentified peaks were observed within the *S. pilchardus* F4 sample, with retention times greater than the Δ -UA-GalNAc(4,6S) di-sulphated standard. These peaks may be attributed to the presence of di-sulphated disaccharides bearing sulphated uronic acid residues or tri-sulphated disaccharides. The *S. pilchardus* F4 sample therefore, is composed predominantly of CSA units, however the total disaccharide composition is more disperse than that of CS standards.

Table 22: Corrected disaccharide composition analysis of *S. pilchardus* F4, CSA and CSC.

Δ -Disaccharide	<i>S. pilchardus</i> F4 (%)	CSC (%)	CSA (%)
Δ -UA-GalNAc	3.9	3.7	2.4
Δ -UA-GalNAc(6S)	27.6	72.0	4.3
Δ -UA-GalNAc(4S)	58.1	18.2	93.2
Δ -UA-GalNAc(4S,6S)	10.3	6.0	N.D

Subsequently, ^1H and ^1H - ^{13}C HSQC NMR was employed to confirm the GAG composition of the *S. pilchardus* F4 sample. Both ^1H and ^1H - ^{13}C HSQC indicated that the *S. pilchardus* F4 was composed predominantly of CSA. The ^1H spectra revealed that the principal GAG constituent of the *S. pilchardus* F4 samples was CS, as the predominant signal attributed to N-acetyl occurred at 2.02 ppm. Minor peaks at approximately 2.04 ppm and 2.08 ppm were also observed in the ^1H spectra, which is characteristic of HS and DS (Figure 81). Integration of the N-Acetyl peaks observed within the ^1H spectrum indicated that the *S. pilchardus* F4 sample was composed of ~90% CS, and <10% DS and HS (Figure 81). This was supported by the presence of signals at ~3.4 and 3.5 ppm corresponding to U2 and U3 of CS, respectively. Furthermore, minimal signals were observed at resonances > 5 ppm, which would be indicative of the presence of DS and HS/heparin (Figure 81).

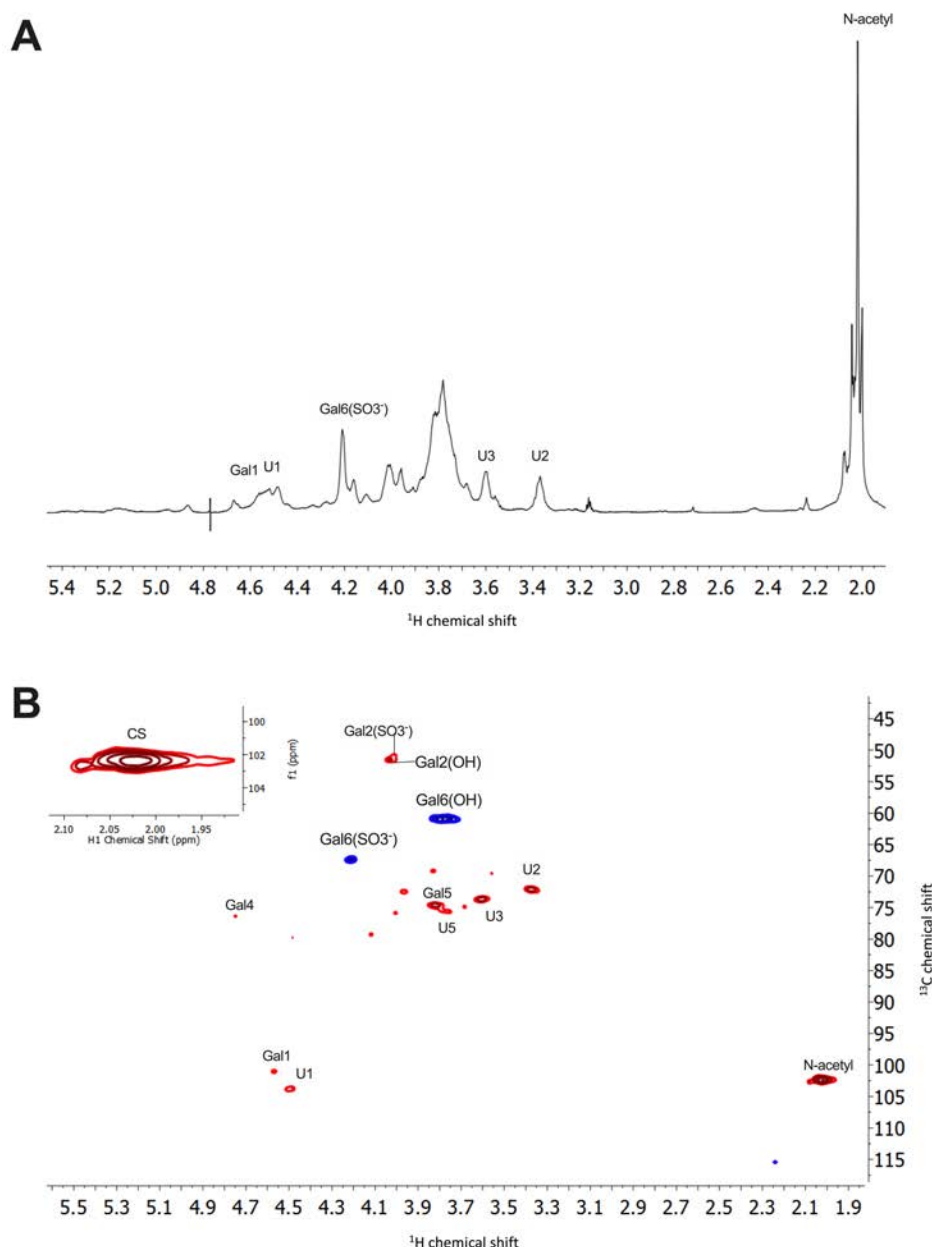


Figure 81: Nuclear magnetic resonance spectra for *S. pilchardus* F4. (A) ¹H and (B) ¹H-¹³C HSQC NMR spectra of *S. pilchardus* F4. Chondroitin sulphate-associated major signals are indicated. Spectral integration was carried out using labelled signals. A: galactosamine; U: uronic acid. Minor peaks are observed but with low intensity meaning that their abundance is lower than 5%. F1 and F2 are the indirect and direct dimensions, respectively.

¹H-¹³C HSQC NMR was subsequently employed to further resolve the composition of the *S. pilchardus* F4 extract. Through integration of the N-acetyl signals corresponding to each respective GAG the *S. pilchardus* F4 sample was found to be composed of > 95% CS. In addition, integration of the signals attributed to position 2 and 6 of

galactosamine indicated that the predominant site of sulphation is C₄. In agreement with the HPLC disaccharide composition analysis minor peaks that could be associated to other GAGs and/or different CS substitution patterns were also detected, however these are low in intensity (Figure 81). Overall, the combined data indicate that the *S. pilchardus* F4 sample is composed of a CSA-like polysaccharide.

7.2.2. *S. pilchardus* F4 inhibits the Alzheimer's Disease-Relevant β -Secretase

The BACE-1 inhibitory activity of the *S. pilchardus* F4 extract was evaluated in comparison to heparin utilizing the previously described FRET peptide assay. *S. pilchardus* F4 was observed to demonstrate maximal BACE-1 inhibition at concentrations greater than 10 $\mu\text{g.mL}^{-1}$, with an IC₅₀ value of 4.8 $\mu\text{g.mL}^{-1}$ (R^2 of 0.93) (Figure 82). This was found to be approximately 2-fold lower than that of PMH, which displayed an IC₅₀ value of 2.6 $\mu\text{g.mL}^{-1}$ ($R^2 = 0.97$) and maximal BACE-1 inhibition at concentrations > 5 $\mu\text{g.mL}^{-1}$ (Figure 82). These findings are in contrast to previous reports, which suggest that CS possess only weak BACE-1 inhibitory activity (Scholefield et al. 2003), the specific structural composition, in regards of the total sulphation level or pattern, of the CS utilized in this study was however, not reported. In addition, no difference was found observed in BACE-1 promontory activity was observed between the *S. pilchardus* F4 extract and heparin (Figure 82, Figure 83). The period of BACE-1 promotion induced by both *S. pilchardus* F4 and heparin was succeeded by enzyme inhibition as previously described (Figure 83).

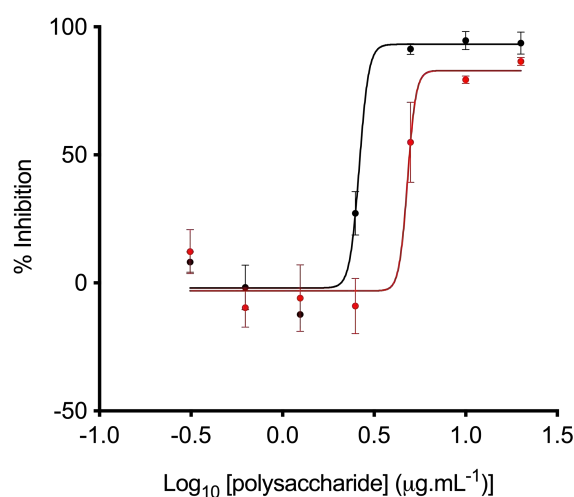


Figure 82: Inhibition of human BACE-1 by *S. pilchardus* F4 or heparin as determined by FRET. Porcine mucosal heparin (black) $IC_{50} = 2.6 \mu\text{g.mL}^{-1}$ with an R^2 of 0.97; *S. pilchardus* F4 (red) $C_{50} = 4.8 \mu\text{g.mL}^{-1}$ with an R^2 of 0.93.

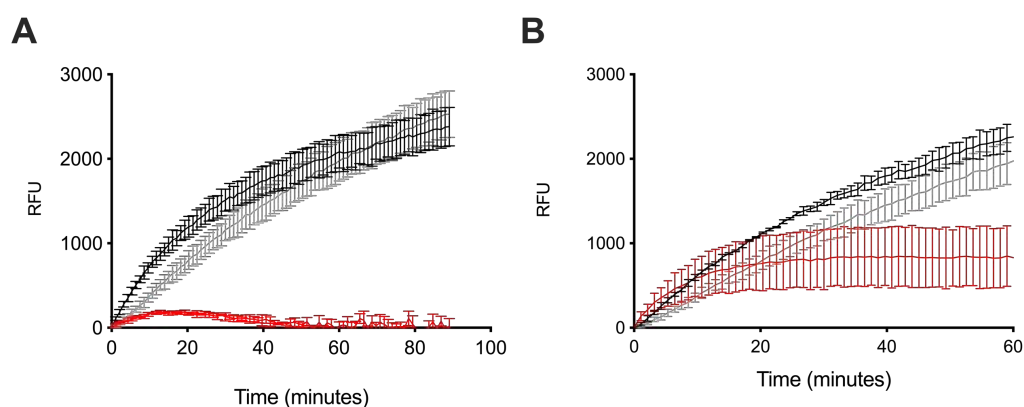


Figure 83: Inhibition of human BACE-1 by heparin or *S. pilchardus* F4. (A) time-course activation or inhibition of BACE-1 by $5 \mu\text{g.mL}^{-1}$ (red) or 625 ng.mL^{-1} (black) heparin, compared to water control. (B) The same as (A) for *S. pilchardus* F4.

7.2.3. Attenuated anticoagulant of the *S. pilchardus* F4 extract

As previously discussed, the anticoagulant activity of heparin largely precludes its use as a therapeutic against alternative diseases such as AD. With the omission of OSCS, native CS possess highly reduced anticoagulant activity in comparison to mammalian heparin (Hogwood *et al.*, 2018). In order to confirm this, the anticoagulant activities of

S. pilchardus F4 was evaluated in the aPTT (intrinsic pathway) and PT (extrinsic pathway) assays in comparison to pharmaceutical heparin (193 IU.mg⁻¹). *S. pilchardus* F4 displayed a >200-fold decrease in activity by the aPTT (Figure 84) with an EC₅₀ of 403.8 µg.mL⁻¹ compared to PMH (EC₅₀ = 1.6 µg.mL⁻¹). Furthermore, a greater than an 80-fold reduction in activity in the PT assay was observed for *S. pilchardus* F4 in comparison to heparin (Figure 84) with an EC₅₀ of 1.3 mg.mL⁻¹ and 14.8 µg.mL⁻¹, respectively. Both coagulation assays therefore, indicate that the *S. pilchardus* F4 sample exhibits negligible anticoagulant activity.

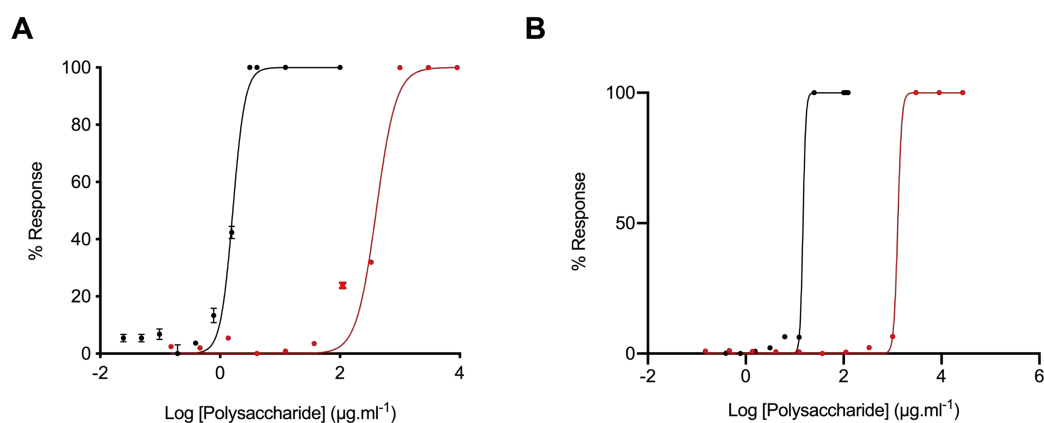


Figure 84: Anticoagulation activity of *S. pilchardus* F4 in comparison to heparin. Inhibitory response of heparin (black) or *S. pilchardus* F4 (red) (mean % response, n = 3; ± SD) of (A) activated partial thromboplastin time (heparin EC₅₀ = 1.6 µg.mL⁻¹, *S. pilchardus* F4 EC₅₀ = 403.8 µg.mL⁻¹) and (B) Prothrombin time (heparin EC₅₀ = 14.8 µg.mL⁻¹, *S. pilchardus* F4 EC₅₀ = 1.3 mg.mL⁻¹)

7.2.4. Heparin and *S. pilchardus* F4 induce a conformational change in the Alzheimer's Disease-Relevant β -Secretase.

The secondary structure composition of BACE-1 at pH 4.0 was calculated by comparing the CD spectra to that of a library of representative proteins, as described previously (Micsonai *et al.*, 2015). The CD spectrum of BACE-1 alone was estimated to possess a secondary structure composition of approximately, 4.1% helix, 33.6% antiparallel, 15.6% turn and 46.6% other. This was in close agreement with the predicted secondary structure of BACE-1 at pH 4.0 reported in section 4.2 and 5.2. The CD spectrum of BACE-1 was subsequently recorded in the presence of a 1:2 w/w ratio of BACE-1: *S. pilchardus* F4. In the presence of : *S. pilchardus* F4 under these conditions, BACE-1 exhibited a change in secondary structure of +3% helix, -2.1% antiparallel, +4.6% turn and -5.4% other (Figure 85). The change BACE-1 secondary structure was similar to that observed for heparin and other GAG samples, further suggesting that a upon binding to this class of polysaccharides BACE-1 adopts a conformation rendering the enzyme inactive.

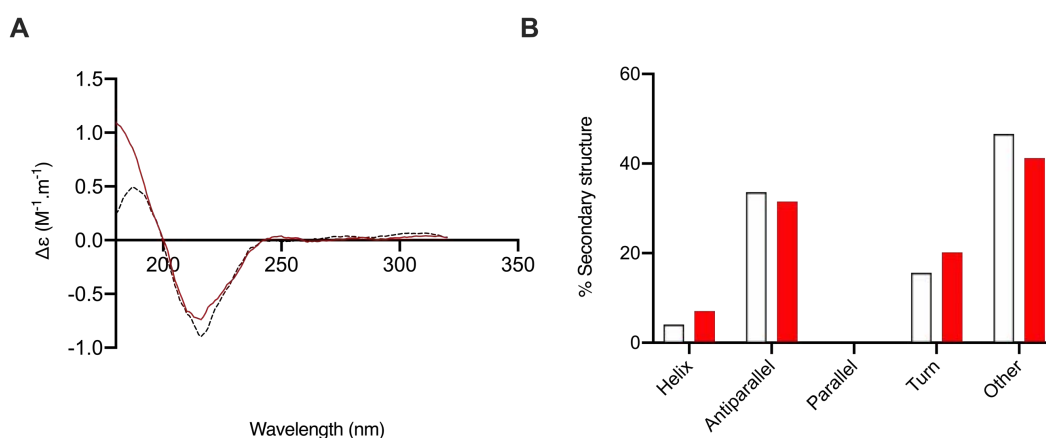


Figure 85: The secondary structural change of BACE-1 observed in the presence of *S. pilchardus* F4. (A) CD spectra of BACE-1 alone (9 μg ; dashed line) and in the presence of 18 μg *S. pilchardus* F4 (red). (B) Secondary structure (%) of BACE-1 alone (white) and in the presence of *S. pilchardus* F4, estimated using BeStSel between 180-260 nm.

7.2.5. Heparin and *S. pilchardus* F4 destabilise the Alzheimer's Disease-Relevant β -Secretase.

DSF was utilized to determine whether the *S. pilchardus* F4 sample induced BACE-1 destabilization in a similar manner to that observed for heparin. A 1:4 ratio (w/w) of BACE-1:heparin altered the thermal stability of BACE-1 by $\Delta T_m = -10.5^\circ\text{C}$ (± 0.5 SD, $n = 3$), in line with the findings presented in previous chapters (4.2 and 5.2). In contrast, in the presence of the *S. pilchardus* F4 at an equivalent w/w ratio (1:4, BACE-1:*S. pilchardus* F4) the ΔT_m of BACE-1 = -5°C (± 1.3 SD, $n = 3$), an approximate 2-fold reduction in the level of thermal destabilization compared to that of heparin. In addition, the destabilization of BACE-1 by both heparin and the *S. pilchardus* F4 sample demonstrated concentration dependence (Figure 86). This again suggests that GAGs may induce BACE-1 inhibition via a common mechanism, which is distinct from other known inhibitors (Lo *et al.*, 2004).

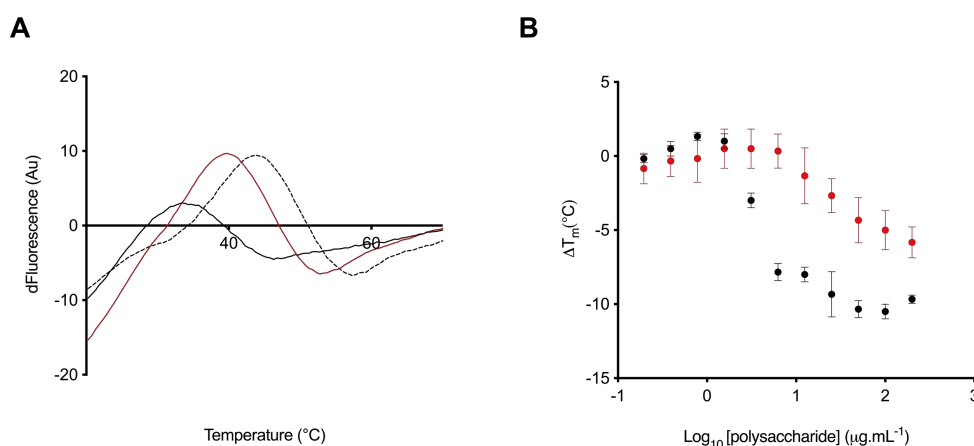


Figure 86: Differential scanning fluorimetry of BACE-1 in the presence of *S. pilchardus* F4 or heparin. (A) First derivative of the DSF profile of BACE-1 alone (1 μg ; dashed line) and with heparin (4 μg ; black) *S. pilchardus* F4. (4 μg ; red) in 50 mM sodium acetate buffer pH 4.0. (B) ΔT_m of BACE-1 in the presence of increasing concentrations of heparin or *S. pilchardus* F4.

7.3. Discussion

The extract obtained from *S. pilchardus* was observed to possess comparable electrophoretic migration to that of CS/DS when analyzed by agarose gel electrophoresis in 1,2-diaminopropane buffer. Further spectroscopic analysis, utilizing ATR-FTIR and CD coupled with PCA, of *S. pilchardus* F4 supported that the major GAG constituent of the extract is CS. 1D and 2D HSQC NMR, confirmed that major GAG component of *S. pilchardus* F4 was CS, with the majority of the units being comprised of 4-O-sulphated GalNAc residues. Minor spectral features were also observed however, these were low in intensity, suggesting they account for < 5% of the extract. In support of this the primary disaccharide constituent of the *S. pilchardus* F4 sample was found to be Δ -UA-GalNAc(4S) at 58%, by SAX-HPLC disaccharide composition analysis. The presence of minor amounts of Δ -UA-GalNAc(6S) and Δ -UA-GalNAc(4,6S) disaccharide were also detected, in addition to peaks possibly attributed to other di- or tri- sulphated disaccharides. This suggests that *S. pilchardus* F4 contains a more varied sulphation pattern that typically observed for CSA.

S. pilchardus F4 was observed to possess inhibitory activity against BACE-1 in a manner akin to heparin albeit at a slightly diminished level, as demonstrated by the IC₅₀ values obtained from FRET peptide assays. This contrasts from previous reports that CS displays BACE-1 inhibitory activity no greater than ~20%. The fine structure of the CS utilized in this study was however not reported (Scholefield *et al.*, 2003). The BACE-1 inhibitory activity of CS may therefore, require sulphation at defined positions, rather

inhibition being a result of total anionic charge, as previously identified for HS/heparin (Patey et al., 2006). In addition, when the BACE-1 inhibitory activity of CS standards were examined under the same conditions utilized in this work, inhibition of >50% was observed for all standard samples tested, albeit to different extents (Figure 42). This also indicates that the difference in experimental conditions utilized for FRET peptide BACE-1 activity assays may affect the overall level of inhibition observed when screening test compounds using this assay system. The ability of *S. pilchardus* F4 to promote proBACE-1 activity at low concentrations was not observed to be different to that of heparin. This is in contrast to previous reports that indicated that CS displayed reduced BACE-1 promontory activity in comparison to heparin (Klaver *et al.*, 2010). The study by Klaver *et al.*, (2010) did however, only examine the activity mono-sulphated CS samples, whereas the *S. pilchardus* F4 reported here exhibits a more diverse sulphation profile.

The interaction of BACE-1 with *S. pilchardus* F4 was probed utilizing CD spectroscopy and DSF to elucidate whether this compound exhibits a similar mechanism of BACE-1 inhibition to that observed for other GAG samples. The CD spectrum of BACE-1 in the presence of *S. pilchardus* F4 was identified to induce a similar change in protein secondary structure to that evoked by heparin with an increase in α -helical and a reduction in β -sheet content. This indicates that GAGs may share a common mode of BACE-1 inhibition, which results from a conformational change that renders the enzyme inactive. This is in contrast to other known peptide inhibitions where no change in BACE-1 secondary structure was observed (De Simone *et al.*, 2013). A decrease in the thermal

stability of BACE-1, was also observed by DSF in the presence of heparin and *S. pilchardus* F4, exemplified by a reduction in the T_m value of BACE-1. The ability of heparin and *S. pilchardus* F4 extract to induce thermal destabilization of BACE-1 occurred within a concentration-dependent manner similar to that observed for the inhibitory potential evaluated by FRET peptide activity assays. A comparable two-fold decrease in the IC_{50} required for BACE-1 inhibition (FRET) and in ΔT_m (DSF) was observed in the presence of *S. pilchardus* F4 compared to heparin. This provides further support that the mode of BACE-1 inhibition by the GAGs may involve structural a conformational change, which results in destabilization. This is in contrast to other known BACE-1 inhibitors, for which no conformational change was observed and stabilization of BACE-1 has been reported using DSF (Lo *et al.*, 2004).

The repurposing of heparin pharmaceuticals as potential BACE-1 inhibitors, or for other alternative therapeutics, is largely prohibited by the significant side effect of heparins potent anticoagulant activity. With the exception of OSGs, which does not occur naturally, CS exhibits reduced anticoagulant activity in comparison to mammalian heparin (Hogwood *et al.*, 2018). The anticoagulant activity of *S. pilchardus* F4 was therefore examined using the aPTT (intrinsic) and PT (extrinsic) coagulation assays, which both incorporates the common pathway. *S. pilchardus* F4 was observed to possess highly attenuated activity compared to heparin in both the aPTT and PT assays. Despite the approximately two-fold reduction in potency observed for BACE-1 inhibitory activity by *S. pilchardus* F4, in comparison to unmodified heparin, the therapeutic value of the former compound is therefore, greater when anticoagulation

activity is taken into account. In addition to heparin, CS is also widely available as a over the counter nutraceutical (USA) or and as a prescribed drug under the European Medical Agency (EMA) for the treatment of osteoarthritis (Henrotin *et al.*, 2010). This is due to the lack of significant side effects observed for CS (*idem*), in contrast to heparin, which possesses the well-known side effect of heparin-induced thrombocytopenia (HIT). Furthermore, CS has been suggested to be bioavailable through oral and subcutaneous routes (*idem*), whereas heparin is not absorbed following oral administration without the requirement of additional formulations (Mousa *et al.*, 2007). The development of a CS based therapeutic for AD may therefore offer additional advantages over other GAGs, and small peptide inhibitors, which have unfavorable pharmacokinetic properties (Vassar, 2016).

Chapter 8: Discussion and future directions

The search for effective AD treatments is still on-going, as such inhibition of BACE-1, a key drug target against AD, has arisen as a potential mechanism to prevent the production of toxic $\alpha\beta$ fragments. Heparin, a GAG obtained from mammalian sources (usually porcine or bovine intestinal tissue), has long been known to possess potent BACE-1 inhibitory activity (Scholefield *et al.*, 2003; Patey *et al.*, 2006). Furthermore, heparin surmounts the challenge presented by the large substrate-binding cleft of the enzyme, the unfavourable pharmacokinetics of peptide-based inhibitors and financial constraints of monoclonal antibody therapeutics. Despite this, the undesirable anticoagulation activity of heparin has largely precluded further exploitation of this polysaccharide as an AD therapeutic. Many heparin/HS like GAGs have been isolated from the tissue of aquatic species that display attenuated anticoagulation activities in comparison to mammalian derived heparin pharmaceuticals (Table 6). As such, sourcing bioactive GAGs from aquatic species offers an attractive source of novel BACE-1 inhibitors, which largely lack the undesired off target effect of perturbing the coagulation cascade. Moreover, GAG obtained from a variety of aquatic species largely display increased structural diversity compared to their mammalian counterparts (Table 5, Table 7) and in turn display a vast array of biological activities. The augmented reservoir of structural modifications presented by GAGs isolated from aquatic species, therefore offers an attractive source of complex bioactive carbohydrates for therapeutic exploitation, the like of which has yet to be explored for potential BACE-1 inhibition. Furthermore, sourcing pharmaceutical grade GAGs from aquatic species, in particular aquaculture waste products, would offer increased sustainability, be

financially viable and reduce the concerns regarding transmissible pathogens and religious mores, which are currently associated with heparin obtained from mammalian origins. Finally, the increased structural diversity displayed by GAGs obtained from aquatic species allows for further exploration of structure-function analysis, enabling further insight which, could potentially be exploited the development of synthetic or semi-synthetic drug candidates.

In light of this eight aquatic species were selected based upon the ability to obtain a tissue from aquatic species which, are commonly caught or farmed, for the food industry. These included *P. pelagicus*, *M. merluccius*, *C. batrachus*, *G. morhua*, *M. aeglefinus*, *O. gorbuschua*, *P. hypothalmus*, *S. pilchardus* and *L. vannamei*. Crude GAG extracts were obtained via the method discussed in section 3.3.1. Briefly, GAGs were liberated from their constituent protein cores via proteolytic digestion of the dried defatted tissue. Subsequently, free GAG chains were captured by the addition of strong anion exchange chromatography resin (Amberlite IRA-900) to the digestate. Bound GAGs were eluted by incubation of the resin with 3 M NaCl, which was subjected to prior washes with 1 M NaCl and H₂O. Precipitation of GAGs was then conducted by the addition of methanol to the resin eluant. Following desalination, the crude samples obtained from all eight aquatic tissues were subjected to analysis to determine the presence of GAGs and screened for the ability to inhibit BACE-1.

The presence of GAGs within the crude samples was determined through the combined use of agarose gel electrophoresis, ATR-FTIR, CD and NMR spectroscopy. The results obtained via each of the aforementioned techniques were in agreement, indicating that

all crude extracts were composed of a mixture of GAGs (Table 15). The extracts obtained from *P. pelagicus* and *L. vannamei* were found to contain predominantly HS/heparin, at 70% and 60% respectively. The extract obtained from *P. hypophthalmus* was observed to contain predominantly DS (60%), whereas all other extracts were primarily comprised of CS (between 60-90%). Screening of the compounds for inhibition of BACE-1, utilising the previously described FRET peptide assay, indicated that the crude extract obtained from *P. pelagicus* possesses the greatest activity at 93%. All remaining extracts possessed BACE-1 inhibitory activities of between -21 and 49% (Table 16). The extracts obtained from *L. vannamei* and *S. pilchardus* were the only samples observed to induce promotion of BACE-1 activity. As discussed in section 3.3.2 and 3.3.3, this was likely a result of the active component of these extracts comprising a low percentage of the total sample. Subsequent to the determination that the majority of extracts possessed BACE-1 inhibitory activity further purification was conducted utilising DEAE-Sephacel chromatography. This was with the aim of isolating the active components contained within each crude sample to enable further characterisation to be conducted. With the exception of the extract obtained from *O. gorbuscha*, fractionation resulted in an increase in BACE-1 inhibitory activity. Of the eight species selected, the fractions obtained from *P. pelagicus* (F5; 96%), *L. vannamei* (F4;91% and F5;71%) and *S. pilchardus* (F4;75%), exhibited the most potent BACE-1 inhibitory activity when initially screened at $5\mu\text{g.mL}^{-1}$; where F4 and F5 refer to the sample eluted from the DEAE-Sephacel column with 0.8 M NaCl or 1 M NaCl, respectively. These compounds were, therefore selected for further structural and biological activity analysis.

The fractionated sample obtained from *P. pelagicus* (F5) was found to possess an estimated GAG composition of 75% HS/heparin and 25% CS. This translates to an approximate change in composition of +5% HS/heparin, -5% CS and -1% DS, in comparison to the crude *P. pelagicus* sample. The samples obtained following fractionation of the crude *L. vannamei* were found to be composed of 59% HS/heparin, 38% CS and <5% DS and 67% HS/heparin, 38% CS and <5% DS, for F4 and F5, respectively. This translated into an approximate change in composition of -1% HS and -2% CS for *L. vannamei* F4, in comparison to the crude sample. In contrast the change in composition, for *L. vannamei* F5 was found to be approximately, +7% HS/heparin and -2% CS in comparison to the crude sample. *S. pilchardus* F4 was found to be composed of ~ 90% CS, <10% HS/heparin and <10% DS. This resulted in a change in composition of approximately +12% CS and -2% DS. As a result, fractions eluted from the DEAE-Sephacel column with 1 M NaCl were observed to contain an increase in the percentage of HS/heparin, and a decrease in CS, present within the sample. Presumably this is a result of heparin/HS typically possessing a higher degree of sulphation than CS, which would be eluted from the column at lower NaCl concentrations. In agreement with this, a negligible change in percentage GAG composition was observed for the *L. vannamei* F4 and an increase in the percentage of CS present within *S. pilchardus* F4 was observed (eluted with 0.8 M NaCl) (Table 23).

Table 23: Approximate change in GAG composition following fractionation utilising DEAE-Sephacel anion exchange chromatography.

Species	HS/heparin (%)	CS (%)	DS (%)
<i>P. pelagicus</i> F5	+5	-5	-1
<i>L. vannamei</i> F4	-1	-2	0
<i>L. vannamei</i> F5	+7	-2	0
<i>S. pilchardus</i> F4	0	+12	-2

Besides for *S. pilchardus* F4, fractionation did not result in adequate purification of a primary GAG species (>90% purity). This may have resulted from the CS constituent of both the *L.vannamei* and *P. pelagicus* samples containing a higher degree of sulphation than typically reported. In particular the fractions obtained from *L. vannamei* were observed to possess resonances within the ^1H - ^{13}C HSQC NMR spectra which have previously been assigned to the presence of 2 and/or 3-sulphated glucuronic acid residues (Cavalcante *et al.*, 2018; Palhares *et al.*, 2019). Furthermore, the CS present within *L. vannamei* F5 was also found to possess ~45% Δ -UA-GalNAc(4,6S) and Δ -UA-GalNAc(6S) disaccharides (determined by SAX-HPLC) (Table 24). The *P.pelagicus* F5 sample was only observed to possess minimal sulphate modifications upon the CS component of the extract, when analysed by ^1H - ^{13}C HSQC NMR. SAX-HPLC disaccharide composition analysis was however, not performed on the CS component within this sample and therefore, should be conducted to further elucidate the fine structure of the CS composed within *P. pelagicus* F5.

Table 24: Approximate GAG composition. Determined by HPLC disaccharide composition analysis and ^1H - ^{13}C NMR spectroscopy. * contains additional minor modifications.

Species	HS/heparin				CS	
	NS (%)	6S (%)	2S (%)	4S (4%)	6S (%)	4,6S (%)
<i>P. pelagicus</i> F5	75	60	70		35	
<i>L. vannamei</i> F4*	70	50	40	34	53	
<i>L. vannamei</i> F5 *	70	70	30		43	44.9
<i>S. pilchardus</i> F4*				60	30	10

In order to obtain fractions containing a higher purity of one GAG species (in particular for those containing primarily HS), fractionation utilising organic solvent precipitation (ethanol and acetone) could have been performed prior to DEAE-Sepharcel chromatography. Fractionation with increasing volumes ethanol/methanol (0.1 v/v) has

previously been described to successfully fractionate heparin, DS and CS with precipitation of heparin occurring at ~1 volume followed by DS and then CS (Volpi, 1996, Silva, 2006, van der Meer, Kellenbach and van den Boss, 2017). Differential precipitation of GAGs has also been reported using the sequential addition of acetone; heparin (<0.6 v/v), DS (0.6-0.7 v/v) and CS (>0.7 v/v) (Volpi 1994, Silva, 2006). In addition, selective enzymatic degradation, utilising the respective polysaccharide lyase could have been employed. This, however, would likely not have resulted in the complete removal of CS, in particular for *L. vannamei* fractions, which were observed to be largely resistance to degradation by chondroitinase ABC.

The approximate fine structure of the primary GAGs present within the samples obtained from *P. pelagicus*, *L. vannamei* and *S. pilchardus* is summarised in (Table 24). Of the fractions analysed, which contained HS/heparin, an intermediate level of sulphation was observed compared that which is typically identified for mammalian heparin and HS. All fractions possess a high degree of N-sulphated glucosamine residues at >70%, which is marginally reduced in contrast to mammalian heparin (~80%) but is substantial in comparison to mammalian HS (~50%). Likewise, each fraction also contained greater than 50% 6-sulphated glucosamine residues, which is intermediate between the typically reported values for mammalian heparin (~80%) and HS (~40%). In addition, the levels of 2-sulphahted uronic acids observed within each fraction was increased in comparison to mammalian HS (~15%). For fractions obtained from *L. vannamei* the level of 2-sulphated uronic acids were below that typically reported for mammalian heparin (~65%), however *P. pelagicus* F5 was observed to contain comparatively increased levels of this modification. It important to note however that

the further analysis utilising NMR techniques such as COSY, NOSEY and TOSEY, should be performed to further elucidate the identity of the uronic acid bearing this modification within the *P. pelagicus* F5 sample.

When the BACE-1 inhibitory activity of *P. pelagicus* (F5), *L. vannamei* (F4 and F5) and *S. pilchardus* (F4) was evaluated further, the IC₅₀ values of inhibition were found to be between ~2-6 $\mu\text{g}.\text{mL}^{-1}$. The sample found to possess the highest BACE-1 inhibitory activity was *P. pelagicus* F5 with an IC₅₀ of $\mu\text{g}.\text{mL}^{-1}$. This sample also contained HS with the highest degree of sulphation out of the GAG extracts examined. The fraction with the lowest BACE-1 inhibitory activity was found to be *L. vannamei* F5 at 5.9 $\mu\text{g}.\text{mL}^{-1}$. *L. vannamei* F5 was also observed to contain the lowest proportion of 2-sulphated uronic acid residues within HS component of the extract. Previously, the presence of 2-sulphated uronic acid residues have been described to be important for the BACE-1 inhibitory activity of heparin/HS, irrespective of the epimer (Patey *et al.*, 2006; Schwörer *et al.*, 2013). The inhibitory activities displayed by the extracts analysed in this study, therefore provide further support for the importance of this modification for the potency of inhibition by heparin/HS polysaccharides against BACE-1. Sulphation at position 6 of glucosamine within heparin has also been described to be important for the BACE-1 inhibitory activity of heparin (Patey *et al.*, 2006). Despite this no clear correlation between the level of 6-O- sulphated HS, within the extracts reported in this work, was identified. Having said this each extract possessed >50% 6-sulphation, which may be sufficient for maximal BACE-1 inhibition. Therefore, in order to support the work conducted by Patey *et al.*, (2008) selective sulphation of the polysaccharides obtained within this study could be performed to determine whether a reduction in BACE-1

inhibitory activity is observed. This would also include selective sulphation/re-acetylation, which was reported to not affect the inhibitor activity of heparin against BACE-1 (*idem*).

In regard to the BACE-1 promontory activity induced by heparin at low concentrations, as reported by Beckman *et al.*, (2006), the fractionated compounds obtained from *P. pelagicus* and *L. vannamei* displayed reduced stimulatory activity in comparison to mammalian heparin. This may be accounted for by the diminished level of total sulphate modifications within the HS/heparin component of these extracts, as it has been reported that promontory activity of BACE-1 is dependent upon the degree of sulphation (Klaver *et al.*, 2010). Klaver *et al.*, (2010) described that selective sulphation of NS and/or 2S modifications present within heparin resulted in slightly diminished BACE-1 promontory activity. In contrast complete sulphation of mammalian heparin resulted in a near complete loss of stimulatory activity (*idem*). Despite this, chemically modified heparins which have undergone selective sulphation/re-acetylation at all possible positions of heparin were not evaluated within this study and as such, should be determined to further elucidate the nature of this activity. The *S. pilchardus* F4 displayed almost comparable BACE-1 promontory activity, in comparison to heparin. This was in contrast to previous reports that displayed reduced stimulatory activity in comparison to mammalian heparins (*idem*). The extract obtained from *S. pilchardus* was however, found to contain a more diverse sulphation pattern than typical of CSA and CSC polysaccharides. Therefore, as only the latter compounds were evaluated for BACE-1 stimulatory activity samples composed of alternative CS units, for examples CSE and CSD, should be evaluated for the ability to promote BACE-1 activity. Overall, this

supports previous reports that the fine structural of GAGs affects the nature of their interactions with human BACE-1.

In order to further elucidate the nature of the interaction between GAGs and BACE-1, CD spectroscopy and DSF was employed. The secondary structure of BACE-1, when measured by CD spectroscopy, was in agreement with previous reports, which indicated that at pH 4.0 BACE-1 was found to contain a greater proportion of beta-sheet and reduced alpha-helical structures (De Simone *et al.*, 2013). The estimated secondary structure of BACE-1 in the presence of inhibitory concentrations of heparin, was closer aligned with the structural features observed for BACE-1 alone at pH 7.4 (*idem*), where increased alpha-helical and reduced beta-sheet structures were observed. A similar change to the secondary structure of BACE-1, in comparison to those of observed for heparin, was observed for all GAG fractions evaluated within this study when assessed at inhibitory concentrations. This suggests that a common mechanism of BACE-1 inhibition by GAGs is to induce a conformational change that renders the enzyme in an inactive conformation.

In contrast, the CD spectra observed for BACE-1:heparin complexes under conditions in which BACE-1 promotion is facilitated (low heparin concentrations) indicated an estimated increase in beta-sheet and reduction in alpha-helical structures. Furthermore, the CD spectra of BACE-1 under these conditions demonstrated evidence that binding influenced the orientation of aromatic amino acids (near UV CD). Previously, Tyr-71, located within the BACE-1 flap, has been suggested to be involved in modulating conformational changes between the flap-open and flap-closed states,

which in turn are involved in regulating substrate access to the active site of BACE-1 (Spronk and Carlson, 2011). Therefore, the presence of CD bands attributed to aromatic amino acids, solely under conditions where proBACE-1 stimulatory activity can be observed, may be indicative of the flap region being in a more open orientation. This supports previous reports that suggest a conformational change in BACE-1 structure may occur upon heparin binding, which enables increased access to the active site (Klaver *et al.*, 2010). In addition, it was suggested that movement of a loop spanning residues 46-65, which partially covers the active site, would be required for enhanced substrate entry to the active site of proBACE-1 and that binding of heparin to an adjacent region may facilitate this necessary conformational change (*idem*). Binding of heparin to the propeptide domain, which contains several basic amino acids, as suggested by Beckman *et al.*, (2006), may therefore providing an explanation for the observation of BACE-1 promotion of proBACE-1 in contrast to mature enzyme forms (Beckman, Holsinger and Small, 2006). Furthermore, modelling of BACE-1 omitting the aforementioned loop region, indicated a patch of high electropositivity close to the active site, which potentially contains multiple heparin binding sites. The increase in proBACE-1 activity by heparin has been shown to be followed by a period of inhibition in the current work for all extracts evaluated and by Beckman *et al.*, 2006. This may suggest that arrangement of the loop spanning residues 46-65 is required to grant access to the underlying region of dense electropositivity, in which heparin can then bind and inhibit BACE-1 activity by preventing substrate access to the active site. This also supports the work by Schofield *et al.* (2003) who proposed that the mode of inhibition is non-competitive and that heparin acts by preventing access of the substrate to the active site. Similar changes in the conformation of BACE-1 under

conditions in which, promotion was observed, were also observed for the extract isolated from *P. pelagicus* (F5), supporting that this may be a common interaction among GAGs.

The effect of GAGs on the thermal stability of BACE-1 was also evaluated utilising DSF as previously this technique has been reported to demonstrate stabilisation of BACE-1 in the presence of known inhibitors (Lo *et al.*, 2004). In contrast, decrease in the melting temperature (T_m) of BACE-1 in the presence of both heparin or the extracts obtained from *P. pelagicus*, *L. vannamei* and *S. pilchardus*, was observed when compared to human BACE-1 alone. This suggests that the mechanism of BACE-1 inhibition by GAGs may involve structural destabilisation as opposed to stabilisation. The reduction in the thermal stability of BACE-1 in the presence of heparin or the aforementioned extracts occurred in a concentration dependent manner, akin to that of the inhibitory potential observed in FRET assays. In addition, the extent of destabilisation of BACE-1 induced by GAGs was also observed to be indicative of potency of inhibition. For instance, compounds which displayed a greater reduction in the T_m of BACE-1 were found to possess lower IC_{50} inhibitory concentrations by FRET peptide assays. Therefore, when coupled with the observed changes in BACE-1 conformation in the presence of GAGs, this suggests that this class of polysaccharides may act by inducing a conformational change that renders the enzyme in an inactive and destabilised conformation.

Table 25: Therapeutic ratio of fractionated extracts compared to heparin to heparin. The therapeutic ratio was calculated from the IC₅₀ of BACE-1 inhibitory activity measures by aPTT/FRET anticoagulant activity. GAG = glycosaminoglycan, aPTT = activated partial thromboplastin time, PT = prothrombin time.

GAG	aPTT (μg.mL ⁻¹)	PT (μg.mL ⁻¹)	BACE1 inhibitory activity (μg.mL ⁻¹)	Therapeutic ratio
PMIH	1.7	19.5	2.4	0.7
<i>P. pelagicus</i> (F5)	43.2	420.2	1.9	22.7
<i>L. vannamei</i> (F4)	27.9	1276.0	4.6	6.1
<i>L. vannamei</i> (F5)	14.6	138.8	5.9	2.5
<i>S. pilchardus</i> (F4)	403.8	1300.0	4.8	84.1

One obstacle precluding the therapeutic use of heparin as an BACE-1 inhibitor is the significant anticoagulant activity of this polysaccharide. The anticoagulant activity of heparin is afforded by the propensity of this molecule to interact with antithrombin, thereby inhibiting the human coagulation pathway and ultimately preventing fibrin clot formation. The anticoagulation activity of each fraction was therefore, determined in comparison to mammalian heparin through the use of the aPTT and PT assays. All fractions obtained from *P.pelagicus*, *L. vannamei* and *S. pilchardus* were observed to possess attenuated activities in both the aPTT and PT assays, in comparison to mammalian heparin. Therefore, in order to determine the compound which possessed the greatest therapeutic ratio, activities observed for the aPTT and FRET peptide BACE-1 inhibitory assays were compared (Table 25). All fractions analysed exhibited greater therapeutic ratios in comparison to heparin. The extract isolated from *S. pilchardus*,

composed primarily of CS, however possessed the most favourable therapeutic ratio (Table 25). This was a result of the negligible anticoagulant activity displayed by this sample. Therefore, for future considerations the ability of CS to inhibit BACE-1 should be explored.

Overall, the utilization of GAGs derived from aquatic species for the discovery of novel bioactive compounds has been demonstrated to be advantageous over other mammalian sources currently being explored (for both heparin and CS therapeutics). Many aquatic species such as, *P. pelagicus*, *L. vannamei* and *S. pilchardus*, have been demonstrated to be novel sources of GAGs, which possess a wide array of bioactivities, such as potent BACE-1 inhibition. The attenuated anticoagulant activities displayed by these GAGs, in contrast to mammalian heparins, offers increases therapeutic value for alternative pharmaceutical applications of these polysaccharide, where anticoagulation would be considered a severe side effect. Furthermore, many aquatic species overcome the religious mores associated with the use of heparins (bovine and porcine origins) and are free from mammalian pathogens (e.g., spongiform encephalopathies, swine viruses). Glycosaminoglycans can also be obtained readily from marine aquaculture waste material and in some cases can be farmed in a controlled aquaculture environment, making their exploitation economically and environmentally favorable. The exploitation of marine species as a novel source of bioactive GAGs is therefore an attractive alternative to the mammalian sources that are currently utilized to obtain GAGs for therapeutic use.

Chapter 9: References

Abdi, H. and Williams, L. J. (2010) 'Principal component analysis', *Wiley Interdisciplinary Reviews: Computational Statistics*. John Wiley & Sons, Ltd, pp. 433–459. doi: 10.1002/wics.101.

Adams, R. L. C. and Bird, R. J. (2009) 'Review article: Coagulation cascade and therapeutics update: Relevance to nephrology. Part 1: Overview of coagulation, thrombophilias and history of anticoagulants', *Nephrology*. John Wiley & Sons, Ltd, pp. 462–470. doi: 10.1111/j.1440-1797.2009.01128.x.

Algar, W. R. *et al.* (2019) 'FRET as a biomolecular research tool — understanding its potential while avoiding pitfalls', *Nature Methods*. Springer US, 16(9), pp. 815–829. doi: 10.1038/s41592-019-0530-8.

Almond, J. W. (1998) 'Bovine spongiform encephalopathy and new variant Creutzfeldt-Jakob disease', *British Medical Bulletin*. Royal Society of Medicine Press Ltd, pp. 749–759. doi: 10.1093/oxfordjournals.bmb.a011724.

Alquwaizani, M. *et al.* (2013) 'Anticoagulants: A Review of the Pharmacology, Dosing, and Complications', *Current Emergency and Hospital Medicine Reports*. Springer Science and Business Media LLC, 1(2), pp. 83–97. doi: 10.1007/s40138-013-0014-6.

Andrade, P. V. G. *et al.* (2013) 'A heparin-like compound isolated from a marine crab rich in glucuronic acid 2-O-sulfate presents low anticoagulant activity', *Carbohydrate Polymers*, 94(1), pp. 647–654.

Appeltans, W. *et al.* (2012) 'The Magnitude of Global Marine Species Diversity', *Current Biology*. Cell Press, 22(23), pp. 2189–2202. doi: 10.1016/J.CUB.2012.09.036.

Archer, M. (2001) 'Fish Waste Production in the United Kingdom', *Sea fish Industry Authority*, (November), pp. 1–63.

Arima, K. *et al.* (2013) 'Amounts and compositional analysis of glycosaminoglycans in the tissue of fish', *Carbohydrate Research*. Elsevier Ltd, 366, pp. 25–32. doi: 10.1016/j.carres.2012.11.010.

Azra, M. N. and Ikhwanuddin, M. (2015) 'Larval culture and rearing techniques of

commercially important crab, *Portunus pelagicus* (Linnaeus, 1758): Present status and future prospects', *Songklanakarin Journal of Science and Technology*, 37(2), pp. 135–145.

Bastos, F. M. *et al.* (2014) 'Fucosylated Chondroitin Sulphate Inhibits *Plasmodium Falciparum* Cytoadhesion and Merozoite Invasion', *Antimicrobial Agents and Chemotherapy*, 58(4), pp. 1862–1871.

Beckman, M. *et al.* (2009) 'Activation of cathepsin D by glycosaminoglycans', *FEBS Journal*, 276(24), pp. 7343–7352. doi: 10.1111/j.1742-4658.2009.07444.x.

Beckman, M., Holsinger, R. M. D. and Small, D. H. (2006) 'Heparin activates β -secretase (BACE1) of Alzheimer's disease and increases autocatalysis of the enzyme', *Biochemistry*, 45(21), pp. 6703–6714. doi: 10.1021/bi052498t.

Bianchini, P. *et al.* (1997) 'Heterogeneity of unfractionated heparins studied in connection with species, source, and production processes', *Seminars in Thrombosis and Hemostasis*, 23(1), pp. 3–10. doi: 10.1055/s-2007-996063.

Blum, M. M. and John, H. (2012) 'Historical perspective and modern applications of Attenuated Total Reflectance - Fourier Transform Infrared Spectroscopy (ATR-FTIR)', *Drug Testing and Analysis*, 4(3–4), pp. 298–302. doi: 10.1002/dta.374.

Brito, A. S. *et al.* (2008) 'Anti-inflammatory properties of a heparin-like glycosaminoglycan with reduced anti-coagulant activity isolated from a marine shrimp', *Bioorganic & Medicinal Chemistry*. Elsevier Ltd, 16(21), pp. 9588–9595. doi: 10.1016/j.bmc.2008.09.020.

Brito, A. S. *et al.* (2014) 'A non-hemorrhagic hybrid heparin / heparan sulfate with anticoagulant potential', *Carbohydrate Polymers*. Elsevier Ltd., 99, pp. 372–378. doi: 10.1016/j.carbpol.2013.08.063.

Cahú, T. B. *et al.* (2012) 'Recovery of protein , chitin , carotenoids and glycosaminoglycans from Pacific white shrimp (*Litopenaeus vannamei*) processing waste', *Process Biochemistry*. Elsevier Ltd, 47(4), pp. 570–577. doi: 10.1016/j.procbio.2011.12.012.

Cai, H. *et al.* (2001) 'BACE1 is the major β -secretase for generation of A β peptides by neurons', *Nature Neuroscience*. Nature Publishing Group, 4(3), pp. 233–234. doi: 10.1038/85064.

Cappelletti, R., Del Rosso, M. and Chiarugi, V. P. (1979) 'A new electrophoretic method for the complete separation of all known animal glycosaminoglycans in a monodimensional run', *Analytical Biochemistry*, 99(2), pp. 311–315. doi: 10.1016/S0003-2697(79)80012-3.

Cardilo-Reis (2006) 'In vivo antithrombotic properties of a heparin from the oocyte test cells of the sea squirt *Styela plicata*', 39, pp. 1409–1415.

Carvalho, A. P. *et al.* (2018) 'Sardine Canning Byproducts as Sources of Functional Ingredients', *ACS Sustainable Chemistry and Engineering*, 6(11), pp. 15447–15454. doi: 10.1021/acssuschemeng.8b03897.

Casey, D. A., Antimisiaris, D. and O'Brien, J. (2010) 'Drugs for Alzheimer's disease: Are they effective?', *P and T. Medi Media USA Inc*, pp. 208–211.

Casu, B. *et al.* (1987) 'High Haemorrhagic Potential', *The Lancet*, pp. 1088–1089.

Casu, B. *et al.* (1994) 'Heparin-like compounds prepared by chemical modification of capsular polysaccharide from *E. coli* K5.', *Carbohydrate research*, 263(2), pp. 271–84.

Casu, B. *et al.* (1996) 'Characterization of sulfation patterns of beef and pig mucosal heparins by nuclear magnetic resonance spectroscopy.', *Arzneimittel-Forschung*, 46(5), pp. 472–7.

Cavalcante, M. C. M. *et al.* (2000) 'Occurrence of heparin in the invertebrate *Styela plicata* (Tunicata) is restricted to cell layers facing the outside environment: An ancient role in defense?', *Journal of Biological Chemistry*, 275(46), pp. 36189–36196. doi: 10.1074/jbc.M005830200.

Cavalcante, R. S. *et al.* (2018) '2, 3-Di- O -sulfo glucuronic acid : An unmodified and unusual residue in a highly sulfated chondroitin sulfate from *Litopenaeus vannamei*', *Carbohydrate Polymers*. Elsevier, 183(December 2017), pp. 192–200. doi: 10.1016/j.carbpol.2017.12.018.

Chavante, S. F. *et al.* (2000) 'A novel heparan sulphate with high degree of N -sulphation and high heparin cofactor-II activity from the brine shrimp *Artemia franciscana*', 27, pp. 49–57.

Chavante, S. F. *et al.* (2014) 'A heparin-like glycosaminoglycan from shrimp containing high levels of 3-O-sulfated D -glucosamine groups in an unusual trisaccharide sequence',

Carbohydrate Research. Elsevier Ltd, 390, pp. 59–66. doi: 10.1016/j.carres.2014.03.002.

Chen, S. *et al.* (2011) 'Comparison of structures and anticoagulant activities of fucosylated chondroitin sulfates from different sea cucumbers', *Carbohydrate Polymers*. Elsevier Ltd., 83(2), pp. 688–696. doi: 10.1016/j.carbpol.2010.08.040.

Collins, S. J., Lawson, V. A. and Masters, C. L. (2004) 'Transmissible spongiform encephalopathies', in *Lancet*. Elsevier B.V., pp. 51–61. doi: 10.1016/S0140-6736(03)15171-9.

Conrad, H. E. (1995) 'β-Elimination for Release of O -Linked Glycosaminoglycans from Proteoglycans ', *Current Protocols in Molecular Biology*, 31(1), pp. 15–17. doi: 10.1002/0471142727.mb1715as31.

Cruts, M., Theuns, J. and Van Broeckhoven, C. (2012a) 'Locus-specific mutation databases for neurodegenerative brain diseases', *Human Mutation*. John Wiley & Sons, Ltd, 33(9), pp. 1340–1344. doi: 10.1002/humu.22117.

Cruts, M., Theuns, J. and Van Broeckhoven, C. (2012b) 'Locus-specific mutation databases for neurodegenerative brain diseases', *Human Mutation*. John Wiley & Sons, Ltd, 33(9), pp. 1340–1344. doi: 10.1002/humu.22117.

Dahlbäck, B. (2000) 'Blood coagulation', *Lancet*. Elsevier B.V., pp. 1627–1632. doi: 10.1016/S0140-6736(00)02225-X.

Davie, W. E., Fujikawa, K. and Kisiel, W. (1991) 'The Coagulation Cascade: Initiation, Maintenance, and Regulation?', *Biochemistry*, 30(43), pp. 10363–10370.

Devlin, A., Mycroft-West, C., *et al.* (2019) 'Analysis of solid-state heparin samples by ATR-FTIR spectroscopy', *bioRxiv*, p. 538074. doi: 10.1101/538074.

Devlin, A., Mycroft-west, C. J., *et al.* (2019) 'Analysis of solid-state heparin samples by ATR-FTIR spectroscopy .

Devlin, A., Mauri, L., *et al.* (2019) 'The use of ATR-FTIR spectroscopy to characterise crude heparin samples by composition and structural features', *bioRxiv*. doi: 10.1101/744532.

Dietrich, C. P. *et al.* (1985) 'Isolation and characterization of a heparin with high anticoagulant activity from *Anomalocardia brasiliensis*', *BBA - General Subjects*. Elsevier,

843(1–2), pp. 1–7. doi: 10.1016/0304-4165(85)90041-8.

Dietrich, C. P. *et al.* (1989) 'Heparin in molluscs: chemical, enzymatic degradation and ¹³C and ¹H n.m.r. spectroscopical evidence for the maintenance of the structure through evolution', *International Journal of Biological Macromolecules*. Elsevier, 11(6), pp. 361–366. doi: 10.1016/0141-8130(89)90008-1.

Dietrich, C. P. *et al.* (1998) 'Structure of heparan sulfate: identification of variable and constant oligosaccharide domains in eight heparan sulfates of different origins.', *Cellular and molecular biology (Noisy-le-Grand, France)*, 44(3), pp. 417–29.

Dietrich, C. P. *et al.* (1999) 'Structural features and anticoagulant activities of a novel natural low molecular weight heparin from the shrimp *Penaeus brasiliensis*', *Biochimica et Biophysica Acta (BBA) - General Subjects*. Elsevier, 1428(2–3), pp. 273–283. doi: 10.1016/S0304-4165(99)00087-2.

Dietrich, C. P. and Dietrich, S. M. C. (1976) 'Electrophoretic behaviour of acidic mucopolysaccharides in diamine buffers', *Analytical Biochemistry*, 70(2), pp. 645–647. doi: 10.1016/0003-2697(76)90496-6.

Dietrich, C. P., McDuffie, N. M. and Sampaio, L. O. (1977) 'Identification of acidic mucopolysaccharides by agarose gel electrophoresis', *Journal of Chromatography A*, 130(C), pp. 299–304. doi: 10.1016/S0021-9673(00)89809-X.

Dietrich, P. C. *et al.* (1999) 'Structural features and anticoagulant activities of a novel natural low molecular weight heparin from the shrimp *Penaeus brasiliensis*', 1428, pp. 273–283.

Ekins, J. *et al.* (2012) 'Development of a multiplex real-Time pcr assay for the detection of ruminant dna', *Journal of Food Protection*, 75(6), pp. 1107–1112. doi: 10.4315/0362-028X.JFP-11-415.

Eriksson, A., Burcharth, J. and Rosenberg, J. (2013) 'Animal derived products may conflict with religious patients' beliefs', *BMC Medical Ethics*. BMC Med Ethics, 14(1). doi: 10.1186/1472-6939-14-48.

Esko, J. D. (1993) 'Special Considerations for Proteoglycans and Glycosaminoglycans and Their Purification', *Current Protocols in Molecular Biology*, 22(1), pp. 1–9. doi: 10.1002/0471142727.mb1702s22.

FAO (2020) *The State of World Fisheries and Aquaculture 2020. Sustainability in action*. Rome. doi: <https://doi.org/10.4060/ca9229en>.

FDA (2012) 'Guidance for Industry Heparin for Drug and Medical Device Use : Monitoring Crude Heparin for Quality Guidance for Industry Heparin for Drug and Medical Device Use : Monitoring Crude Heparin for Quality', (February 2012), pp. 1–9.

Featherstone, s (2016) *A Complete Course in Canning and Related Processes, A Complete Course in Canning and Related Processes*. Elsevier. doi: 10.1016/c2013-0-16340-4.

Feta, A. *et al.* (2009) 'Molecular analysis of heparan sulfate biosynthetic enzyme machinery and characterization of heparan sulfate structure in *Nematostella vectensis*', 593, pp. 585–593. doi: 10.1042/BJ20082081.

Frazier, S. B. *et al.* (2008) 'The Quantification of Glycosaminoglycans: A Comparison of HPLC, Carbazole, and Alcian Blue Methods.', *Open glycoscience*. NIH Public Access, 1, pp. 31–39. doi: 10.2174/1875398100801010031.

Fukumoto, H. *et al.* (2002) 'β-secretase protein and activity are increased in the neocortex in Alzheimer disease', *Archives of Neurology*. Arch Neurol, 59(9), pp. 1381–1389. doi: 10.1001/archneur.59.9.1381.

Gailani, D. and Renné, T. (2007) 'Intrinsic pathway of coagulation and arterial thrombosis', *Arteriosclerosis, Thrombosis, and Vascular Biology*. Lippincott Williams & Wilkins, pp. 2507–2513. doi: 10.1161/ATVBAHA.107.155952.

Gallagher, J. T. and Walker, A. (1985) 'Molecular distinctions between heparan sulphate and heparin', *Biochemical Journal*, 230(3), pp. 665–674.

Gandhi, N. S. and Mancera, R. L. (2008) 'The Structure of Glycosaminoglycans and their Interactions with Proteins', *Chemical Biology & Drug Design*, 72(6), pp. 455–82. doi: 10.1111/j.1747-0285.2008.00741.x.

Garg, H. G., Linhardt, R. J. and Hales, C. A. (2005) *Chemistry and Biology of Heparin and Heparan Sulfate, Chemistry and Biology of Heparin and Heparan Sulfate*. Elsevier. doi: 10.1016/B978-0-08-044859-6.X5000-X.

Garnjanagoonchorn, W., Wongekalak, L. and Engkagul, A. (2007) 'Determination of chondroitin sulfate from different sources of cartilage', *Chemical Engineering and*

Processing: Process Intensification, 46(5), pp. 465–471. doi: 10.1016/j.cep.2006.05.019.

Gasymov, O. K., Abduragimov, A. R. and Glasgow, B. J. (2014) 'Probing tertiary structure of proteins using single Trp mutations with circular dichroism at low temperature', *Journal of Physical Chemistry B*, 118(4), pp. 986–995. doi: 10.1021/jp4120145.

Gavva, C. *et al.* (2020) 'Glycosaminoglycans from fresh water fish processing discard - Isolation, structural characterization, and osteogenic activity', *International Journal of Biological Macromolecules*. Elsevier B.V., 145, pp. 558–567. doi: 10.1016/j.ijbiomac.2019.12.189.

Ghosh, A. K. and Osswald, H. L. (2014) 'BACE1 (β -secretase) inhibitors for the treatment of Alzheimer's disease.', *Chemical Society reviews*. NIH Public Access, 43(19), pp. 6765–813. doi: 10.1039/c3cs60460h.

Glassford, S. E., Byrne, B. and Kazarian, S. G. (2013) 'Recent applications of ATR FTIR spectroscopy and imaging to proteins', *Biochimica et Biophysica Acta - Proteins and Proteomics*. Elsevier B.V., 1834(12), pp. 2849–2858. doi: 10.1016/j.bbapap.2013.07.015.

Goate, A. *et al.* (1991) 'Segregation of a missense mutation in the amyloid precursor protein gene with familial Alzheimer's disease', *Nature*. Nature, 349(6311), pp. 704–706. doi: 10.1038/349704a0.

Gomes (2010) 'Unique Extracellular Matrix Heparan Sulfate from the Bivalve *Nodipecten nodosus* (Linnaeus , 1758) Safely Inhibits Arterial Thrombosis after Photochemically Induced Endothelial Lesion *', 285(10), pp. 7312–7323. doi: 10.1074/jbc.M109.091546.

Gomes, A. M. *et al.* (2015) 'Antitumor properties of a new non-anticoagulant heparin analog from the mollusk *Nodipecten nodosus* : Effect on P-selectin , heparanase , metastasis and cellular recruitment', 25(4), pp. 386–393. doi: 10.1093/glycob/cwu119.

Gomes, P. B. and Dietrich, C. P. (1982) 'Distribution of heparin and other sulfated glycosaminoglycans in vertebrates', *Comparative Biochemistry and Physiology -- Part B: Biochemistry and Comp Biochem Physiol B*, 73(4), pp. 857–863. doi: 10.1016/0305-0491(82)90329-7.

Grant, D. *et al.* (1989) 'Infrared spectroscopy of chemically modified heparins', *Biochemical Journal*, 261(3), pp. 1035–1038. doi: 10.1042/bj2611035.

Grant, D. *et al.* (1991) 'Infrared spectroscopy of heparins suggests that the region 750-950 cm⁻¹ is sensitive to changes in iduronate residue ring conformation', *Biochemical Journal*. Biochem J, 275(1), pp. 193–197. doi: 10.1042/bj2750193.

Gray, E., Mulloy, B. and Barrowcliffe, T. W. (2008) 'Heparin and low-molecular-weight heparin', *Thrombosis and Haemostasis*. Thromb Haemost, pp. 807–818. doi: 10.1160/TH08-01-0032.

Greenfield, N. J. (2006) 'Using circular dichroism spectra to estimate protein secondary structure', *Nature protocols*. NIH Public Access, 1(6), p. 2876. doi: 10.1038/NPROT.2006.202.

Greiling, H. (1974) 'C. Glycosaminoglycans', in Curtius, H. C. (ed.). Berlin, Boston: De Gruyter, pp. 944–971.

Grüninger-Leitch, F. *et al.* (2002) 'Substrate and inhibitor profile of BACE (β -secretase) and comparison with other mammalian aspartic proteases', *Journal of Biological Chemistry*. Elsevier, 277(7), pp. 4687–4693. doi: 10.1074/jbc.M109266200.

Guerrini, M. *et al.* (2008) 'Oversulfated chondroitin sulfate is a contaminant in heparin associated with adverse clinical events', *Nature Biotechnology*. Nature Publishing Group, 26(6), pp. 669–675. doi: 10.1038/nbt1407.

Guerrini, M., Bisio, A. and Torri, G. (2001) 'Combined quantitative ¹H and ¹³C nuclear magnetic resonance spectroscopy for characterization of heparin preparations', *Seminars in Thrombosis and Hemostasis*, 27(5), pp. 473–482. doi: 10.1055/s-2001-17958.

Guimond, S. E. *et al.* (2009) 'Rapid purification and high sensitivity analysis of heparan sulfate from cells and tissues. Toward glycomics profiling', *Journal of Biological Chemistry*. © 2009 ASBMB. Currently published by Elsevier Inc; originally published by American Society for Biochemistry and Molecular Biology., 284(38), pp. 25714–25722. doi: 10.1074/jbc.M109.032755.

Hadfield, L. (2018) 'Heparin and heparin-like molecules inhibit the Alzheimer's β -secretase (BACE1): considerations for biological assay and future therapeutic development', *Keele University*.

Hardingham, T. E. and Fosang, A. J. (1992) 'Proteoglycans: many forms and many functions', *The FASEB Journal*. Wiley, 6(3), pp. 861–870. doi: 10.1096/fasebj.6.3.1740236.

Hedlund, K. D. *et al.* (2013) 'The heparin recall of 2008', *Perfusion (United Kingdom)*, 28(1), pp. 61–65. doi: 10.1177/0267659112462274.

Hemming, M. L. *et al.* (2009) 'Identification of β -secretase (BACE1) substrates using quantitative proteomics', *PLoS ONE*, 4(12). doi: 10.1371/journal.pone.0008477.

Henrotin, Y. *et al.* (2010) 'Chondroitin sulfate in the treatment of osteoarthritis: from in vitro studies to clinical recommendations.', *Therapeutic advances in musculoskeletal disease*. SAGE Publications, 2(6), pp. 335–48. doi: 10.1177/1759720X10383076.

Hermann, K., Frank, G. and Ring, J. (1994) 'Contamination of heparin by histamine: measurement and characterization by high-performance liquid chromatography and radioimmunoassay', *Allergy*. *Allergy*, 49(7), pp. 569–572. doi: 10.1111/j.1398-9995.1994.tb01131.x.

Higashi, K., Takeuchi, Y., *et al.* (2015) 'Composition of Glycosaminoglycans in Elasmobranchs including Several Deep-Sea Sharks: Identification of Chondroitin/Dermatan Sulfate from the Dried Fins of *Isurus oxyrinchus* and *Prionace glauca*', *PLoS one*. doi: <https://doi.org/10.1371/journal.pone.0120860>.

Higashi, K., Okamoto, Y., *et al.* (2015) 'Functional chondroitin sulfate from *Enteroctopus dofleini* containing a 3-O-sulfo glucuronic acid residue', *Carbohydrate Polymers*. Elsevier Ltd., 134, pp. 557–565. doi: 10.1016/j.carbpol.2015.07.082.

Hirsh, J. *et al.* (2001) 'Heparin and low-molecular-weight heparin: Mechanisms of action, pharmacokinetics, dosing, monitoring, efficacy, and safety', in *Chest*. American College of Chest Physicians, pp. 64S-94S. doi: 10.1378/chest.119.1_suppl.64S.

Hogwood, J. *et al.* (2018) 'The effect of increasing the sulfation level of chondroitin sulfate on anticoagulant specific activity and activation of the kinin system', *PLOS ONE*. Edited by P. Garcia de Frutos. Public Library of Science, 13(3), p. e0193482. doi: 10.1371/journal.pone.0193482.

Holland, S. M. (2019) 'Principal Component Analysis (PCA)'.

Holme, K. and Perlin, A. (1989) 'Nuclear Magnetic Resonance Spectra of Heparin in A Mixture with Dermatan Sulfate and Other Glycosaminoglycans. 2-D Spectra of the Chondroitin Sulphates', *Carbohydrate research*, 186, pp. 301–312.

Hong, L. *et al.* (2000) 'Structure of the protease domain of memapsin 2 (β -secretase)

complexed with inhibitor', *Science*. American Association for the Advancement of Science, 290(5489), pp. 150–153. doi: 10.1126/science.290.5489.150.

Hong, L. *et al.* (2002) 'Crystal structure of memapsin 2 (β -secretase) in complex with an inhibitor OM00-3', *Biochemistry*. American Chemical Society, 41(36), pp. 10963–10967. doi: 10.1021/bi026232n.

Hook, M. *et al.* (1984) 'Cell-Surface Glycosaminoglycans', *Annual Review of Biochemistry*, 53, pp. 847–869.

Hovingh, P. and Linker, A. (1982) 'An unusual heparan sulfate isolated from lobsters (*Homarus americanus*).', *Journal of Biological Chemistry*. Elsevier, 257(16), pp. 9840–9844. doi: 10.1016/s0021-9258(18)34147-4.

Hsieh, P. H. *et al.* (2016) 'Uncovering the Relationship between Sulphation Patterns and Conformation of Iduronic Acid in Heparan Sulphate', *Scientific Reports*, 6. doi: 10.1038/srep29602.

Huang, N. *et al.* (2013) 'The depolymerized fucosylated chondroitin sulfate from sea cucumber potently inhibits HIV replication via interfering with virus entry', *Carbohydrate Research*. Elsevier Ltd, 380, pp. 64–69. doi: 10.1016/j.carres.2013.07.010.

Imbimbo, B. P. *et al.* (2007) '1-(3',4'-Dichloro-2-fluoro[1,1'-biphenyl]-4-yl) - cyclopropanecarboxylic acid (CHF5074), a novel γ -secretase modulator, reduces brain β -amyloid pathology in a transgenic mouse model of Alzheimer's disease without causing peripheral toxicity', *Journal of Pharmacology and Experimental Therapeutics*. American Society for Pharmacology and Experimental Therapeutics, 323(3), pp. 822–830. doi: 10.1124/jpet.107.129007.

Iozzo, R. V. and Schaefer, L. (2015) 'Proteoglycan form and function: A comprehensive nomenclature of proteoglycans', *Matrix Biology*. Elsevier, pp. 11–55. doi: 10.1016/j.matbio.2015.02.003.

Jeremy Johnson, R. *et al.* (2014) 'Rapid and adaptable measurement of protein thermal stability by differential scanning fluorimetry: Updating a common biochemical laboratory experiment', *Journal of Chemical Education*, 91(7), pp. 1077–1080. doi: 10.1021/ed400783e.

Jia, Q., Deng, Y. and Qing, H. (2014) 'Potential therapeutic strategies for Alzheimer's disease targeting or beyond β -Amyloid: Insights from clinical trials', *BioMed Research International*. Hindawi Publishing Corporation. doi: 10.1155/2014/837157.

Johnson, W. C. (1988) 'Secondary structure of proteins through circular dichroism spectroscopy.', *Annual review of biophysics and biophysical chemistry*. Annu Rev Biophys Biophys Chem, pp. 145–166. doi: 10.1146/annurev.bb.17.060188.001045.

Jolliffe, I. T. and Cadima, J. (2016) 'Principal component analysis: A review and recent developments', *Philosophical Transactions of the Royal Society A: Mathematical, Physical and Engineering Sciences*. Royal Society of London. doi: 10.1098/rsta.2015.0202.

Jones, G. A. and Bradshaw, D. S. (2019) 'Resonance Energy Transfer: From Fundamental Theory to Recent Applications INTRODUCTION AND THE EARLY YEARS OF RET', *Frontiers in Physics* / www.frontiersin.org, 1. doi: 10.3389/fphy.2019.00100.

Karimzadeh, K. (2018) 'Anticoagulant Effects of Glycosaminoglycan Extracted from Fish Scales', *International Journal of Basic Science in Medicine*, 3(2), pp. 72–77. doi: 10.15171/ijbsm.2018.13.

Karran, E., Mercken, M. and Strooper, B. De (2011) 'The amyloid cascade hypothesis for Alzheimer's disease: An appraisal for the development of therapeutics', *Nature Reviews Drug Discovery*. Nat Rev Drug Discov, pp. 698–712. doi: 10.1038/nrd3505.

Keire, D. *et al.* (2010) 'Analysis of crude heparin by (1)H NMR, capillary electrophoresis, and strong-anion-exchange-HPLC for contamination by over sulfated chondroitin sulfate.', *J Pharm Biomed Anal*, 51.

Kennedy, M. E. *et al.* (2003) 'Measuring human β -secretase (BACE1) activity using homogeneous time-resolved fluorescence', *Analytical Biochemistry*. Academic Press Inc., 319(1), pp. 49–55. doi: 10.1016/S0003-2697(03)00253-7.

Kinoshita-toyoda, A. *et al.* (2004) 'Structural Determination of Five Novel Tetrasaccharides Containing 3- O -Sulfated D -Glucuronic Acid and Two Rare Oligosaccharides Containing a - D -Glucose Branch Isolated from Squid Cartilage Chondroitin Sulfate E ⁺', pp. 11063–11074.

Kitagawa, H., Kinoshita, A. and Sugahara, K. (1995) 'Microanalysis of glycosaminoglycan-derived disaccharides labeled with the fluorophore 2-aminoacridone by capillary electrophoresis and high-performance liquid chromatography', *Analytical Biochemistry*, 232(1), pp. 114–121. doi: 10.1006/abio.1995.9952.

Klaver, D. W. *et al.* (2010) 'Glycosaminoglycan-induced activation of the β -secretase (BACE1) of Alzheimer's disease', *Journal of Neurochemistry*, 112, pp. 1552–1561. doi:

doi: 10.1111/j.1471-4159.2010.06571.x.

Kreuger, J. and Kjellén, L. (2012) 'Heparan Sulfate Biosynthesis: Regulation and Variability', *Journal of Histochemistry and Cytochemistry*. SAGE PublicationsSage CA: Los Angeles, CA, 60(12), pp. 898–907. doi: 10.1369/0022155412464972.

Krichen, F. *et al.* (2018) 'Purification and structural elucidation of chondroitin sulfate/dermatan sulfate from Atlantic bluefin tuna (*Thunnus thynnus*) skins and their anticoagulant and ACE inhibitory activities', *RSC Advances*. Royal Society of Chemistry, 8(66), pp. 37965–37975. doi: 10.1039/C8RA06704J.

Kumar, A., Singh, A. and Ekavali (2015) 'A review on Alzheimer's disease pathophysiology and its management: An update', *Pharmacological Reports*. Elsevier, pp. 195–203. doi: 10.1016/j.pharep.2014.09.004.

Kurita, K. (2006) 'Mini-Review Chitin and Chitosan: Functional Biopolymers from Marine Crustaceans', *Marine Biotechnology*, 8, pp. 203–226. doi: 10.1007/s10126-005-0097-5.

Lauder, R. M. (2015) *Proteoglycans and Acidic Polysaccharides Analysis, Encyclopedia of Analytical Chemistry*. doi: 10.1002/9780470027318.a0310.pub2.

Van de Lest, C. H. A. *et al.* (1994) 'Quantification and characterization of glycosaminoglycans at the nanogram level by a combined azure A-silver staining in agarose gels', *Analytical Biochemistry*, pp. 356–361. doi: 10.1006/abio.1994.1425.

Leveugle, B. *et al.* (1998) 'Heparin oligosaccharides that pass the blood-brain barrier inhibit beta-amyloid precursor protein secretion and heparin binding to beta-amyloid peptide.', *Journal of neurochemistry*, 70(2), pp. 736–44.

Leveugle, B. and Fillit, H. (1994) 'Proteoglycans and the acute-phase response in Alzheimer's disease brain', *Molecular Neurobiology*, 9(1–3), pp. 25–32. doi: 10.1007/BF02816102.

Levieux, A., Rivera, V. and Levieux, D. (2001) 'A sensitive ELISA for the detection of bovine crude heparin in porcine heparin.', *J Immunoassay Immunochem*, 22.

Levieux, A., Rivera, V. and Levieux, D. (2002) 'Immunochemical control of the species origin of porcine crude heparin and detection of ovine and caprine materials', *Journal of Pharmaceutical and Biomedical Analysis*, 27(1–2), pp. 305–313. doi: 10.1016/S0731-7085(01)00544-1.

Li, L., Ly, M. and Linhardt, R. J. (2012) 'Proteoglycan sequence', *Molecular BioSystems*, 8(6), pp. 1613–1625. doi: 10.1039/c2mb25021g.

Li, W. *et al.* (2004) 'Structure of the antithrombin-thrombin-heparin ternary complex reveals the antithrombotic mechanism of heparin', *Nature Structural and Molecular Biology*. Nature Publishing Group, 11(9), pp. 857–862. doi: 10.1038/nsmb811.

Liao, I. C. and Chien, Y. (2011) *In the Wrong Place - Alien Marine Crustaceans: Distribution, Biology and Impacts*, *In the Wrong Place - Alien Marine Crustaceans: Distribution, Biology and Impacts*. doi: 10.1007/978-94-007-0591-3.

Lima, M. A. *et al.* (2011) 'A New Approach for Heparin Standardization: Combination of Scanning UV Spectroscopy, Nuclear Magnetic Resonance and Principal Component Analysis', *PLoS ONE*. Edited by P. L. Ho. Public Library of Science, 6(1), p. e15970. doi: 10.1371/journal.pone.0015970.

Linhardt, R. J. and Sibel Gunay, N. U. R. (1999) 'Production and chemical processing of low molecular weight heparins', *Seminars in Thrombosis and Hemostasis*, 25(SUPPL. 3), pp. 5–16.

Liu, C. C. *et al.* (2013) 'Apolipoprotein e and Alzheimer disease: Risk, mechanisms and therapy', *Nature Reviews Neurology*. Nature Publishing Group, 9(2), pp. 106–118. doi: 10.1038/nrneurol.2012.263.

Liverani, L., Mascellani, G. and Spelta, F. (2009) 'Heparins: Process-related physico-chemical and compositional characteristics, fingerprints and impurities', in *Thrombosis and Haemostasis*. Thromb Haemost, pp. 846–853. doi: 10.1160/TH09-01-0064.

Lo, M.-C. *et al.* (2004) 'Evaluation of fluorescence-based thermal shift assays for hit identification in drug discovery', *Analytical Biochemistry*. Academic Press, 332(1), pp. 153–159. doi: 10.1016/J.AB.2004.04.031.

Luppi, E., Cesaretti, M. and Volpi, N. (2005) 'Purification and Characterization of Heparin from the Italian Clam *Callista chione* +', pp. 1672–1678. doi: 10.1021/bm049196b.

Maccari, F., Ferrarini, F. and Volpi, N. (2010) 'Structural characterization of chondroitin sulfate from sturgeon bone', *Carbohydrate Research*. Elsevier Ltd, 345(11), pp. 1575–1580. doi: 10.1016/j.carres.2010.05.016.

Maccari, F., Galeotti, F. and Volpi, N. (2015) 'Isolation and structural characterization of

chondroitin sulfate from bony fishes', *Carbohydrate Polymers*. Elsevier, 129, pp. 143–147. doi: 10.1016/J.CARBPOL.2015.04.059.

Mackman, N., Tilley, R. E. and Key, N. S. (2007) 'Role of the extrinsic pathway of blood coagulation in hemostasis and thrombosis', *Arteriosclerosis, Thrombosis, and Vascular Biology*. Lippincott Williams & Wilkins, pp. 1687–1693. doi: 10.1161/ATVBAHA.107.141911.

Macleod, R. *et al.* (2015) 'The role and therapeutic targeting of α -, β - and γ -secretase in Alzheimer's disease', *Future Science OA*. Future Medicine Ltd. doi: 10.4155/fso.15.9.

Mahajan, S. and Mehta, A. A. (2006) *R RE EV VI IE EW W A AR RT TI IC CL LE E Role of Cytokines in Pathophysiology of Asthma, IRANIAN JOURNAL OF PHARMACOLOGY & THERAPEUTICS*.

Mahley, R. W., Weisgraber, K. H. and Huang, Y. (2006) 'Apolipoprotein E4: A causative factor and therapeutic target in neuropathology, including Alzheimer's disease', *Proceedings of the National Academy of Sciences of the United States of America*. Proc Natl Acad Sci U S A, pp. 5644–5651. doi: 10.1073/pnas.0600549103.

Mainreck, N. *et al.* (2011) 'Rapid characterization of glycosaminoglycans using a combined approach by infrared and Raman microspectroscopies', *Journal of Pharmaceutical Sciences*. John Wiley and Sons Inc., 100(2), pp. 441–450. doi: 10.1002/jps.22288.

Ben Mansour, M. *et al.* (2009) 'Characterization of a novel dermatan sulfate with high antithrombin activity from ray skin (*Raja radula*)', *Thrombosis Research*, 123(6), pp. 887–894. doi: 10.1016/j.thromres.2008.09.009.

Marques, J. *et al.* (2016) 'Marine organism sulfated polysaccharides exhibiting significant antimalarial activity and inhibition of red blood cell invasion by *Plasmodium*', *Scientific Reports*. The Author(s), 6, p. 24368.

Mattson, M. P. (2004) 'Pathways towards and away from Alzheimer's disease', *Nature*. NIH Public Access, pp. 631–639. doi: 10.1038/nature02621.

Mauri, L. *et al.* (2019) '1D and 2D-HSQC NMR: Two Methods to Distinguish and Characterize Heparin From Different Animal and Tissue Sources', *Frontiers in Medicine*, 6(June), pp. 1–9. doi: 10.3389/fmed.2019.00142.

McGeown, M. G., Martin, E. and Neill, D. W. (1955) 'Phosphate contamination of commercial heparin', *Journal of clinical pathology*, 8(3), pp. 247–248. doi: 10.1136/jcp.8.3.247.

Medeiros, G. F. *et al.* (2000) 'Distribution of sulfated glycosaminoglycans in the animal kingdom: widespread occurrence of heparin-like compounds in invertebrates', *Biochimica et Biophysica Acta (BBA) - General Subjects*. Elsevier, 1475(3), pp. 287–294. doi: 10.1016/S0304-4165(00)00079-9.

van der Meer, J.-Y., Kellenbach, E. and van den Bos, L. J. (2017) 'From Farm to Pharma: An Overview of Industrial Heparin Manufacturing Methods.', *Molecules (Basel, Switzerland)*. Multidisciplinary Digital Publishing Institute (MDPI), 22(6). doi: 10.3390/molecules22061025.

Meneghetti, M. C. Z. *et al.* (2015) 'Heparan sulfate and heparin interactions with proteins', *Journal of The Royal Society Interface*, 12(110), p. 20150589. doi: 10.1098/rsif.2015.0589.

Micsonai, A. *et al.* (2015) 'Accurate secondary structure prediction and fold recognition for circular dichroism spectroscopy', *Proceedings of the National Academy of Sciences*, 112(24), pp. E3095–E3103. doi: 10.1073/pnas.1500851112.

Monroe, D. M. and Hoffman, M. (2009) 'The Coagulation Cascade in Cirrhosis', *Clinics in Liver Disease*, 13(1), pp. 1–9. doi: 10.1016/j.cld.2008.09.014.

Mousa, S. A. *et al.* (2007) 'Pharmacokinetics and pharmacodynamics of oral heparin solid dosage form in healthy human subjects.', *Journal of clinical pharmacology*. NIH Public Access, 47(12), pp. 1508–20. doi: 10.1177/0091270007307242.

Mucci, A., Schenetti, L. and Volpi, N. (2000) 'H and ¹³ C nuclear magnetic resonance identification and characterization of components of chondroitin sulfates of various origin', 41, pp. 37–45.

Muir, H. M. (1962) 'Uranic T . BITTER Acid Carbazole The reaction of uranic acids with carbazole (I-2) is the most satisfactory method of estimating uranic acids in chromatographic tions but requires 2 hr for the full development of color and , with certain compounds , the', 334, pp. 330–334.

Muratore, C. R. *et al.* (2014) 'The familial alzheimer's disease APPV717I mutation alters APP processing and Tau expression in iPSC-derived neurons', *Human Molecular Genetics*. Oxford University Press, 23(13), pp. 3523–3536. doi: 10.1093/hmg/ddu064.

Nader, H. B. *et al.* (1983) 'A correlation between the sulfated glycosaminoglycan concentration and degree of salinity of the "habitat" in fifteen species of the classes Crustacea, Pelecypoda and Gastropoda', *Comparative Biochemistry and Physiology -- Part B: Biochemistry and*, 76(3), pp. 433–436. doi: 10.1016/0305-0491(83)90271-7.

Nader, H. B., Ferreira, T. M. P. C. and Paiva, J. F. (1984) 'Isolation and structural studies of heparan sulfates and chondroitin sulfates from three species of molluscs', *Journal of Biological Chemistry*. Elsevier, 259(3), pp. 1431–1435. doi: 10.1016/s0021-9258(17)43424-7.

Nakano, T., Betti, M. and Pietrasik, Z. (2010) 'Extraction, Isolation and Analysis of Chondroitin Sulfate Glycosaminoglycans', *Recent Patents on Food, Nutrition & Agriculture*, 2(1), pp. 61–74. doi: 10.2174/1876142911002010061.

Nakano, T., Betti, M. and Pietrasik, Z. (2012) 'Extraction, Isolation and Analysis of Chondroitin Sulfate Glycosaminoglycans', *Recent Patents on Food, Nutrition & Agriculture*, 2(1), pp. 61–74. doi: 10.2174/2212798411002010061.

Nakano, T., Nakano, K. and Sim, J. S. (1998) 'Extraction of Glycosaminoglycan Peptide from Bovine Nasal Cartilage with 0.1 M Sodium Acetate', *Journal of Agricultural and Food Chemistry*, 46(2), pp. 772–778. doi: 10.1021/jf970387y.

NEELY, W. (1957) 'Infrared spectra of carbohydrates.', *Adv Carbohydr Chem.*, (12), pp. 13–33.

Niesen, F. H., Berglund, H. and Vedadi, M. (2007) 'The use of differential scanning fluorimetry to detect ligand interactions that promote protein stability', *Nature Protocols*. Nat Protoc, 2(9), pp. 2212–2221. doi: 10.1038/nprot.2007.321.

Olson, S. T. and Chuang, Y. J. (2002) 'Heparin activates antithrombin anticoagulant function by generating new interaction sites (exosites) for blood clotting proteinases', *Trends in Cardiovascular Medicine*. Elsevier Ltd, pp. 331–338. doi: 10.1016/S1050-1738(02)00183-4.

Palhares, L. C. G. F. *et al.* (2019) 'A Further Unique Chondroitin Sulfate from the shrimp *Litopenaeus vannamei* with Antithrombin Activity that Modulates Acute Inflammation', *Carbohydrate Polymers*. Elsevier, 222(April), p. 115031. doi: 10.1016/j.carbpol.2019.115031.

Palta, S., Saroa, R. and Palta, A. (2014) 'Overview of the coagulation system', *Indian Journal of Anaesthesia*. Indian Society of Anaesthetists, pp. 515–523. doi:

10.4103/0019-5049.144643.

Pan, J. *et al.* (2010) 'Oversulfated chondroitin sulfate is not the sole contaminant in heparin', *Nature Biotechnology*, 28(3), pp. 203–207. doi: 10.1038/nbt0310-203.

Park, J. W. and Chakrabarti, B. (1978) 'Conformational transition of hyaluronic acid carboxylic group participation and thermal effect', *BBA - General Subjects*. Elsevier, 541(2), pp. 263–269. doi: 10.1016/0304-4165(78)90399-9.

Patel, S. *et al.* (2004) 'Apo and inhibitor complex structures of BACE (β -secretase)', *Journal of Molecular Biology*. Academic Press, 343(2), pp. 407–416. doi: 10.1016/j.jmb.2004.08.018.

Patey, S. J. *et al.* (2006) 'Heparin derivatives as inhibitors of BACE-1, the Alzheimer's β -secretase, with reduced activity against factor Xa and other proteases', *Journal of Medicinal Chemistry*, 49(20), pp. 6129–6132. doi: 10.1021/jm051221o.

Patey, S. J. *et al.* (2008) 'Engineered heparins: novel beta-secretase inhibitors as potential Alzheimer's disease therapeutics.', *Neuro-degenerative diseases*. Karger Publishers, 5(3–4), pp. 197–9. doi: 10.1159/000113701.

Pavão, M. S. G. (2014) 'Glycosaminoglycans analogs from marine invertebrates: structure, biological effects, and potential as new therapeutics.', *Frontiers in cellular and infection microbiology*. Frontiers Media SA, 4, p. 123. doi: 10.3389/fcimb.2014.00123.

Pejler, G. *et al.* (1987) 'Structure and antithrombin-binding properties of heparin isolated from the clams *Anomalocardia brasiliana* and *Tivela mactroides*.', *Journal of Biological Chemistry*. Elsevier, 262(24), pp. 11413–11421. doi: 10.1016/s0021-9258(18)60822-1.

Pomin, V. H. (2014) 'NMR chemical shifts in structural biology of glycosaminoglycans', *Analytical Chemistry*, 86(1), pp. 65–94. doi: 10.1021/ac401791h.

Postina, R. *et al.* (2004) 'A disintegrin-metalloproteinase prevents amyloid plaque formation and hippocampal defects in an Alzheimer disease mouse model', *Journal of Clinical Investigation*. The American Society for Clinical Investigation, 113(10), pp. 1456–1464. doi: 10.1172/JCI20864.

Prabhakar, V., Capila, I. and Sasisekharan, R. (2009) *The Structural Elucidation of*

Glycosaminoglycans. In: Packer N.H., Karlsson N.G. (eds) Glycomics. Methods in Molecular Biology (Methods and Protocols). Totowa, NJ: Humana Press. doi: 10.1007/978-1-59745-022-5.

Prydz, K. (2015) 'Determinants of glycosaminoglycan (GAG) structure', *Biomolecules*, 5(3), pp. 2003–2022. doi: 10.3390/biom5032003.

Prydz, K. and Dalen, K. T. (2000) 'Synthesis and sorting of proteoglycans.', *Journal of cell science*, 113 Pt 2, pp. 193–205.

Querfurth, H. W. and LaFerla, F. M. (2010) 'Alzheimer's Disease', *New England Journal of Medicine*, 362(4), pp. 329–344. doi: 10.1056/NEJMra0909142.

Rabenstein, D. L. (2002) 'Heparin and heparan sulfate: structure and function', *Natural Product Reports*, 19(3), pp. 312–331. doi: 10.1039/b100916h.

Raghuraman, H. (2013) 'EXTRACTION OF SULFATED GLYCOSAMINOGLYCANS DEDICATION TO : My parents', (July).

Ranjbar, B. and Gill, P. (2009) 'Circular dichroism techniques: Biomolecular and nanostructural analyses- A review', *Chemical Biology and Drug Design*. John Wiley & Sons, Ltd, pp. 101–120. doi: 10.1111/j.1747-0285.2009.00847.x.

Ravi Kumar, M. N. V. (2000) 'A review of chitin and chitosan applications', *Reactive and Functional Polymers*. Elsevier, pp. 1–27. doi: 10.1016/S1381-5148(00)00038-9.

Roberds, S. L. *et al.* (2001) 'BACE knockout mice are healthy despite lacking the primary beta-secretase activity in brain: implications for Alzheimer's disease therapeutics.', *Human molecular genetics*, 10(12), pp. 1317–24.

Rudd, T. *et al.* (2007) 'Influence of substitution pattern and cation binding on conformation and activity in heparin derivatives.', *Glycobiology*, 17.

Rudd, T. *et al.* (2008) 'Site-specific interactions of copper(II) ions with heparin revealed with complementary (SRCD, NMR, FTIR and EPR) spectroscopic techniques', *Carbohydrate Research*, 343(12), pp. 2184–2193. doi: 10.1016/j.carres.2007.12.019.

Rudd, T., Skidmore, M., Guimond, S., Cosentino, C., *et al.* (2009) 'Glycosaminoglycan origin and structure revealed by multivariate analysis of NMR and CD spectra.', *Glycobiology*, 19.

Rudd, T., Skidmore, M., Guimond, S., Holman, J., *et al.* (2009) 'The potential for circular dichroism as an additional facile and sensitive method of monitoring low-molecular-weight heparins and heparinoids.', *Thromb Haemost*, 102.

Rudd, T. R. *et al.* (2007) 'Influence of substitution pattern and cation binding on conformation and activity in heparin derivatives', *Glycobiology*. Oxford University Press, 17(9), pp. 983–993. doi: 10.1093/glycob/cwm062.

Rudd, T., Yates, E. and Hricovini, M. (2009) 'Spectroscopic and Theoretical Approaches for the Determination of Heparin Saccharide Structure and the Study of Protein-Glycosaminoglycan Complexes in Solution', *Current Medicinal Chemistry*, 16(35), pp. 4750–4766. doi: 10.2174/092986709789878193.

Ruoslahti, E. (1988) 'Structure and biology of proteoglycans', *Annual Review of Cell Biology*, 4, pp. 229–255.

Sahoo, H. (2011) 'Förster resonance energy transfer - A spectroscopic nanoruler: Principle and applications', *Journal of Photochemistry and Photobiology C: Photochemistry Reviews*. Elsevier, pp. 20–30. doi: 10.1016/j.jphotochemrev.2011.05.001.

Santos, J. C. *et al.* (2007) 'Isolation and characterization of a heparin with low antithrombin activity from the body of *Styela plicata* (Chordata-Tunicata). Distinct effects on venous and arterial models of thrombosis', pp. 213–223. doi: 10.1016/j.thromres.2007.03.025.

Saravanan, R. and Shanmugam, A. (2010) 'Isolation and Characterization of Low Molecular Weight Glycosaminoglycans from Marine Mollusc *Amusium pleuronectus* (Linne) using Chromatography', pp. 791–799. doi: 10.1007/s12010-008-8498-3.

Sasisekharan, R. and Venkataraman, G. (2000) 'Heparin and heparan sulfate: Biosynthesis, structure and function', *Current Opinion in Chemical Biology*. Elsevier Ltd, pp. 626–631. doi: 10.1016/S1367-5931(00)00145-9.

Schaefer, L. and Schaefer, R. M. (2010) 'Proteoglycans: From structural compounds to signaling molecules', *Cell and Tissue Research*, 339(1), pp. 237–246. doi: 10.1007/s00441-009-0821-y.

Schneider, C. A., Rasband, W. S. and Eliceiri, K. W. (2012) 'NIH Image to ImageJ: 25 years of image analysis', *Nature Methods*. NIH Public Access, pp. 671–675. doi: 10.1038/nmeth.2089.

Scholefield, Z. *et al.* (2003) 'Heparan sulfate regulates amyloid precursor protein processing by BACE1, the Alzheimer's beta-secretase.', *The Journal of cell biology*. Rockefeller University Press, 163(1), pp. 97–107. doi: 10.1083/jcb.200303059.

Schuchman, E. H. and Desnick, R. J. (1981) 'A new continuous, monodimensional electrophoretic system for the separation and quantitation of individual glycosaminoglycans', *Analytical Biochemistry*, 117(2), pp. 419–426. doi: 10.1016/0003-2697(81)90801-0.

Schwörer, R. *et al.* (2013) 'Synthesis of a targeted library of heparan sulfate hexa- to dodecasaccharides as inhibitors of β -secretase: Potential therapeutics for Alzheimer's disease', *Chemistry - A European Journal*, 19(21), pp. 6817–6823. doi: 10.1002/chem.201204519.

Shastri, M. D. *et al.* (2015) 'In-vitro suppression of IL-6 and IL-8 release from human pulmonary epithelial cells by non-anticoagulant fraction of enoxaparin', *PLoS ONE*. Public Library of Science, 10(5). doi: 10.1371/journal.pone.0126763.

Shen, J. *et al.* (1997) 'Skeletal and CNS defects in Presenilin-1-deficient mice', *Cell*. Elsevier B.V., 89(4), pp. 629–639. doi: 10.1016/S0092-8674(00)80244-5.

Shen, J. and Kelleher, R. J. (2007) 'The presenilin hypothesis of Alzheimer's disease: Evidence for a loss-of-function pathogenic mechanism', *Proceedings of the National Academy of Sciences of the United States of America*. National Academy of Sciences, pp. 403–409. doi: 10.1073/pnas.0608332104.

Shimizu, H. *et al.* (2008) 'Crystal structure of an active form of BACE1, an enzyme responsible for amyloid beta protein production.', *Molecular and cellular biology*. American Society for Microbiology Journals, 28(11), pp. 3663–71. doi: 10.1128/MCB.02185-07.

Silva, L. C. F. (2006) 'Isolation and Purification of Chondroitin Sulfate', *Advances in Pharmacology*, 53(05), pp. 21–31. doi: 10.1016/S1054-3589(05)53002-3.

De Simone, A. *et al.* (2013) 'Surface plasmon resonance, fluorescence, and circular dichroism studies for the characterization of the binding of BACE-1 inhibitors', *Analytical and Bioanalytical Chemistry*, 405(2), pp. 827–835. doi: 10.1007/s00216-012-6312-0.

Skidmore, A. M. *et al.* (2008) 'Disruption of Rosetting in Plasmodium falciparum Malaria with chemically modified Heparin and Low Molecular Weight Derivatives Possessing

Reduced Anticoagulant and Other Serine Protease Inhibition Activities.', *Journal of Medicinal Chemistry*, 51(5), pp. 1453–1458.

Skidmore, M. A. *et al.* (2006) 'High sensitivity separation and detection of heparan sulfate disaccharides', *Journal of Chromatography A*, 1135(1), pp. 52–56. doi: 10.1016/j.chroma.2006.09.064.

Skidmore, M. A. *et al.* (2010) 'Disaccharide compositional analysis of heparan sulfate and heparin polysaccharides using UV or high-sensitivity fluorescence (BODIPY) detection', *Nature Protocols*. Nature Publishing Group, 5(12), pp. 1983–1992. doi: 10.1038/nprot.2010.145.

Small, D. H. *et al.* (1994) 'A heparin-binding domain in the amyloid protein precursor of Alzheimer's disease is involved in the regulation of neurite outgrowth', *Journal of Neuroscience*. Society for Neuroscience, 14(4), pp. 2117–2127. doi: 10.1523/jneurosci.14-04-02117.1994.

Song, Y., Zhang, F. and Linhardt, R. J. (2021) 'Analysis of the Glycosaminoglycan Chains of Proteoglycans', *Journal of Histochemistry and Cytochemistry*. SAGE Publications Ltd, pp. 121–135. doi: 10.1369/0022155420937154.

Spronk, S. A. and Carlson, H. A. (2011) 'The role of tyrosine 71 in modulating the flap conformations of BACE1', *Proteins: Structure, Function, and Bioinformatics*, 79(7), pp. 2247–2259. doi: 10.1002/prot.23050.

Sreerama, N. and Woody, R. W. (2004) 'On the analysis of membrane protein circular dichroism spectra', *Protein Science*, 13(1), pp. 100–112. doi: 10.1110/ps.03258404.

Stanley, F. E. and Stalcup, A. M. (2011) 'The use of circular dichroism as a simple heparin-screening strategy', *Analytical and Bioanalytical Chemistry*. Springer, 399(2), pp. 701–706. doi: 10.1007/s00216-010-4272-9.

Stelling, M. P. *et al.* (2019) 'Methods for isolation and characterization of sulfated glycosaminoglycans from marine invertebrates', *Methods in Molecular Biology*, 1952, pp. 55–70. doi: 10.1007/978-1-4939-9133-4_5.

Stone, A. L. (1971) 'Optical rotary dispersion of mucopolysaccharides III. Ultraviolet circular dichroism and conformational specificity in amide groups', *Biopolymers*. John Wiley & Sons, Ltd, 10(4), pp. 739–751. doi: 10.1002/bip.360100411.

De Strooper, B. *et al.* (1999) 'A presenilin-1-dependent γ -secretase-like protease mediates release of notch intracellular domain', *Nature*. Nature, 398(6727), pp. 518–522. doi: 10.1038/19083.

De Strooper, B., Iwatsubo, T. and Wolfe, M. S. (2012) 'Presenilins and γ -secretase: Structure, function, and role in Alzheimer disease', *Cold Spring Harbor Perspectives in Medicine*. Cold Spring Harbor Laboratory Press, 2(1). doi: 10.1101/cshperspect.a006304.

Sugahara, K. *et al.* (1996) 'Structural analysis of unsaturated hexasaccharides isolated from shark cartilage chondroitin sulfate D that are substrates for the exolytic action of chondroitin ABC lyase', 880, pp. 871–880.

Suleria, H. A. R. *et al.* (2015) 'Marine-Based Nutraceuticals: An Innovative Trend in the Food and Supplement Industries.', *Marine drugs*. Multidisciplinary Digital Publishing Institute (MDPI), 13(10), pp. 6336–51. doi: 10.3390/md13106336.

Suleria, H. A. R. *et al.* (2016) 'Marine bioactive compounds and health promoting perspectives; innovation pathways for drug discovery', *Trends in Food Science & Technology*. Elsevier, 50, pp. 44–55. doi: 10.1016/J.TIFS.2016.01.019.

Suleria, Hafiz Ansar Rasul, Masci, P. P., *et al.* (2017) 'Anti-coagulant & anti-thrombotic properties of blacklip abalone (*Haliotis rubra*): In vitro & animal studies', *Marine Drugs*. Multidisciplinary Digital Publishing Institute (MDPI), 15(8). doi: 10.3390/md15080240.

Suleria, Hafiz Ansar Rasul, Addepalli, R., *et al.* (2017) 'In vitro anti-inflammatory activities of blacklip abalone (*Haliotis rubra*) in RAW 264.7 macrophages', *Food and Agricultural Immunology*. Taylor & Francis, 28(4), pp. 711–724. doi: 10.1080/09540105.2017.1310186.

Suleria, H. A. R. *et al.* (2017) 'Therapeutic potential of abalone and status of bioactive molecules: A comprehensive review', *Critical Reviews in Food Science and Nutrition*. Taylor & Francis, 57(8), pp. 1742–1748. doi: 10.1080/10408398.2015.1031726.

Susannah J. Patey *et al.* (2006) 'Heparin Derivatives as Inhibitors of BACE-1, the Alzheimer's β -Secretase, with Reduced Activity against Factor Xa and Other Proteases'. American Chemical Society . doi: 10.1021/JM051221O.

Tacias-Pascacio, V. G. *et al.* (2020) 'Use of Alcalase in the production of bioactive peptides: A review', *International Journal of Biological Macromolecules*. Elsevier B.V, 165, pp. 2143–2196. doi: 10.1016/j.ijbiomac.2020.10.060.

Takahashi, H. K., Nader, H. B. and Dietrich, C. P. (1981) 'A method for rapid quantitation and preparation of antithrombin III-high-affinity heparin fractions', *Analytical Biochemistry*, 116(2), pp. 456–461. doi: 10.1016/0003-2697(81)90388-2.

Talmoudi, N., Ghariani, N. and Sadok, S. (2020) 'Glycosaminoglycans from Co-Products of «scyliorhinus canicula»: Extraction and Purification in Reference to the European Pharmacopoeia Requirement', *Biological Procedures Online*. BioMed Central Ltd., 22(1), p. 1. doi: 10.1186/s12575-019-0113-1.

Tan, J. Z. A. and Gleeson, P. A. (2019) *The role of membrane trafficking in the processing of amyloid precursor protein and production of amyloid peptides in Alzheimer's disease*, *Biochimica et Biophysica Acta - Biomembranes*. Elsevier B.V. doi: 10.1016/j.bbamem.2018.11.013.

Templeton, D. M. (1988) 'The basis and applicability of the dimethylmethylene blue binding assay for sulfated glycosaminoglycans', *Connective Tissue Research*, 17(1), pp. 23–32. doi: 10.3109/03008208808992791.

Thinakaran, G. and Koo, E. H. (2008) 'Amyloid precursor protein trafficking, processing, and function.', *The Journal of biological chemistry*. American Society for Biochemistry and Molecular Biology, 283(44), pp. 29615–9. doi: 10.1074/jbc.R800019200.

Tipson, R. S. (1968) 'Infrared Spectroscopy Of Carbohydrates A Review DEPARTMENT OF COMMERCE NATIONAL BUREAU OF STANDARDS'.

Turnbull, J. E. (2001) 'Analytical and Preparative Strong Anion-Exchange HPLC of Heparan Sulfate and Heparin Saccharides', in *Proteoglycan Protocols (Methods in Molecular Biology, vol.171)*, pp. 141–148.

Turnbull, J., Powell, A. and Guimond, S. (2001) 'Heparan sulfate: Decoding a dynamic multifunctional cell regulator', *Trends in Cell Biology*, 11(2), pp. 75–82. doi: 10.1016/S0962-8924(00)01897-3.

Turner, R. T. *et al.* (2005) 'Structural locations and functional roles of new subsites S5, S6, and S7 in memapsin 2 (β -secretase)', *Biochemistry*. American Chemical Society , 44(1), pp. 105–112. doi: 10.1021/bi048106k.

Uniewicz, K. a *et al.* (2010) 'Differential Scanning Fluorimetry measurement of protein stability changes upon binding to glycosaminoglycans : a rapid screening test for binding specificity Figure S-1 Sequence data for tested FGF-s Figure S-2 Sulfation pattern of the major repeating di', 82(9), pp. 1–3.

Vassar, R. (2004) 'BACE1: The β -secretase enzyme in Alzheimer's disease', *Journal of Molecular Neuroscience*. J Mol Neurosci, pp. 105–113. doi: 10.1385/JMN:23:1-2:105.

Vassar, R. (2014) 'BACE1 inhibitor drugs in clinical trials for Alzheimer's disease.', *Alzheimer's research & therapy*. BioMed Central, 6(9), p. 89. doi: 10.1186/s13195-014-0089-7.

Vassar, R. (2016) 'BACE1 inhibition as a therapeutic strategy for Alzheimer's disease.', *Journal of sport and health science*. Shanghai University of Sport, 5(4), pp. 388–390. doi: 10.1016/j.jshs.2016.10.004.

Vassar, R. and Kandalepas, P. C. (2011) 'The β -secretase enzyme BACE1 as a therapeutic target for Alzheimer's disease', *Alzheimer's Research and Therapy*. Alzheimers Res Ther. doi: 10.1186/alzrt82.

Vázquez, J. A. *et al.* (2013) 'Chondroitin sulfate, hyaluronic acid and chitin/chitosan production using marine waste sources: Characteristics, applications and eco-friendly processes: A review', *Marine Drugs*. MDPI AG, pp. 747–774. doi: 10.3390/md11030747.

Versteeg, H. H. *et al.* (2013) 'New Fundamentals in Hemostasis', *Physiological Reviews*, 93(1), pp. 327–358. doi: 10.1152/physrev.00016.2011.

Vivoli, M. *et al.* (2014) 'Determination of Protein-ligand Interactions Using Differential Scanning Fluorimetry', *Journal of Visualized Experiments*, (91), pp. 1–13. doi: 10.3791/51809.

Volpi, N. (1994) 'Fractionation of heparin, dermatan sulfate, and chondroitin sulfate by sequential precipitation: A method to purify a single glycosaminoglycan species from a mixture', *Analytical Biochemistry*, pp. 382–391. doi: 10.1006/abio.1994.1196.

Volpi, N. (1996a) 'Electrophoresis separation of glycosaminoglycans on nitrocellulose membranes', *Analytical Biochemistry*, 240(1), pp. 114–118. doi: 10.1006/abio.1996.0337.

Volpi, N. (1996b) 'Purification of heparin, dermatan sulfate and chondroitin sulfate from mixtures by sequential precipitation with various organic solvents', *Journal of Chromatography B: Biomedical Applications*, 685(1), pp. 27–34. doi: 10.1016/0378-4347(96)00154-5.

Volpi, N. and Maccari, F. (2002) 'Detection of submicrogram quantities of

glycosaminoglycans on agarose gels by sequential staining with toluidine blue and Stains-All', *Electrophoresis*, 23(24), pp. 4060–4066. doi: 10.1002/elps.200290021.

Volpi, N. and Maccari, F. (2006) 'Electrophoretic approaches to the analysis of complex polysaccharides', *Journal of Chromatography B: Analytical Technologies in the Biomedical and Life Sciences*, 834(1–2), pp. 1–13. doi: 10.1016/j.jchromb.2006.02.049.

Walsh, D. M. and Selkoe, D. J. (2007) 'A? Oligomers ? a decade of discovery', *Journal of Neurochemistry*. John Wiley & Sons, Ltd (10.1111), 101(5), pp. 1172–1184. doi: 10.1111/j.1471-4159.2006.04426.x.

Wang, G. T. *et al.* (1993) 'A continuous fluorescence assay of renin activity', *Analytical Biochemistry*. Academic Press, 210(2), pp. 351–359. doi: 10.1006/abio.1993.1207.

Wolfe, M. S. (2012) 'Processive proteolysis by γ -secretase and the mechanism of Alzheimer's disease', in *Biological Chemistry*. De Gruyter, pp. 899–905. doi: 10.1515/hsz-2012-0140.

Wong, P. C. *et al.* (1997) 'Presenilin 1 is required for Notch 1 and Dll1 expression in the paraxial mesoderm', *Nature*. Nature Publishing Group, 387(6630), pp. 288–292. doi: 10.1038/387288a0.

Woody, R. W. (1996) *Theory of circular dichroism of proteins*. In: Fasman, G.D., Ed., *Circular Dichroism and the Conformational Analysis of Biomolecules*. New York: Plenum Press.

Xu, Y. *et al.* (2012) 'Flexibility of the flap in the active site of BACE1 as revealed by crystal structures and molecular dynamics simulations', *Acta Crystallographica Section D: Biological Crystallography*, 68(1), pp. 13–25. doi: 10.1107/S0907444911047251.

Yamada, S., Sugahara, K. and Özbek, S. (2011) 'Evolution of glycosaminoglycans: Comparative biochemical study', *Communicative and Integrative Biology*, 4(2), pp. 150–158. doi: 10.4161/cib.4.2.14547.

Yan, R. and Vassar, R. (2014) 'Targeting the β secretase BACE1 for Alzheimer's disease therapy', *The Lancet Neurology*. Lancet Neurol, pp. 319–329. doi: 10.1016/S1474-4422(13)70276-X.

Yates, E. A. *et al.* (1996) '1H and 13C NMR spectral assignments of the major sequences of twelve systematically modified heparin derivatives.', *Carbohydrate research*, 294, pp.

15–27.

Yates, E. A. and Rudd, T. R. (2016) 'Recent innovations in the structural analysis of heparin', *International Journal of Cardiology*. Elsevier Ireland Ltd, 212, pp. S5–S9. doi: 10.1016/S0167-5273(16)12002-9.

Zhang, F., Xie, J. and Linhardt, R. J. (2014) 'Isolation and structural characterization of glycosaminoglycans from heads of red salmon (*Oncorhynchus nerka*).', *Jacobs journal of biotechnology and bioengineering*. NIH Public Access, 1(1), p. 002.

Zhang, F., Zhang, Z. and Linhardt, R. J. (2010) 'Glycosaminoglycans', *Handbook of Glycomics*, pp. 59–80. doi: 10.1016/B978-0-12-373600-0.00003-2.

Zhang, G. *et al.* (2014) 'Towards understanding the roles of heparan sulfate proteoglycans in Alzheimer's disease.', *BioMed research international*. Hindawi, 2014, p. 516028. doi: 10.1155/2014/516028.

Zhang, X. and Song, W. (2013) 'The role of APP and BACE1 trafficking in APP processing and amyloid- β generation', *Alzheimer's Research and Therapy*. Alzheimers Res Ther. doi: 10.1186/alzrt211.

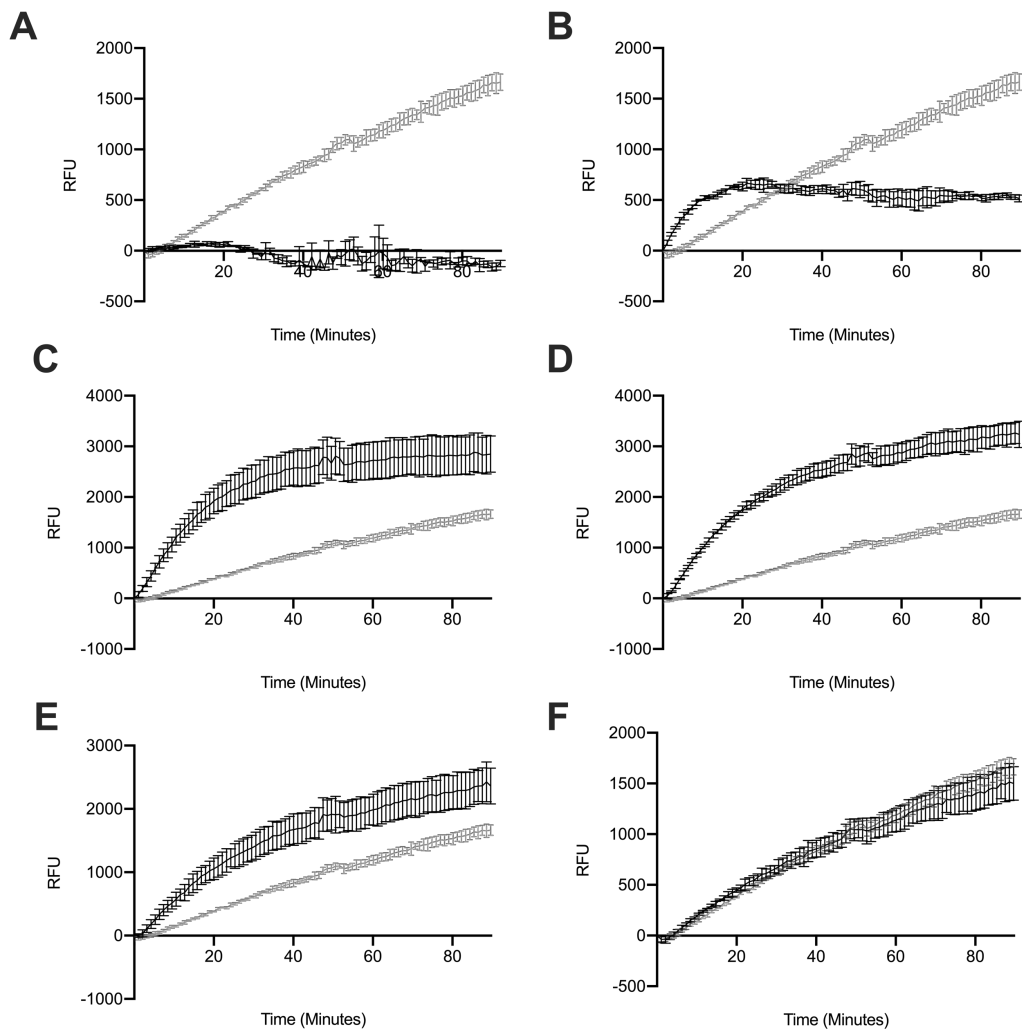
Zhang, Y. W. *et al.* (2011) 'APP processing in Alzheimer's disease', *Molecular Brain*. Mol Brain. doi: 10.1186/1756-6606-4-3.

Zhang, Z. *et al.* (2009) 'Quantification of heparan sulfate disaccharides using ion-pairing reversed-phase microflow high-performance liquid chromatography with electrospray ionization trap mass spectrometry.', *Analytical chemistry*, 81(11), pp. 4349–55. doi: 10.1021/ac9001707.

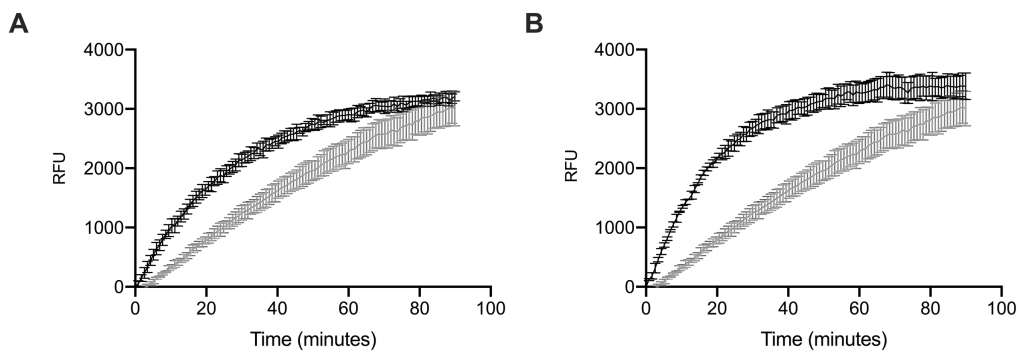
Zhao, T. *et al.* (2013) 'Extraction , purification and characterisation of chondroitin sulfate in Chinese sturgeon cartilage', (September 2012). doi: 10.1002/jsfa.5937.

Zou, Z. *et al.* (2014) 'Clinical genetics of Alzheimer's disease', *BioMed Research International*. Hindawi Publishing Corporation. doi: 10.1155/2014/291862.

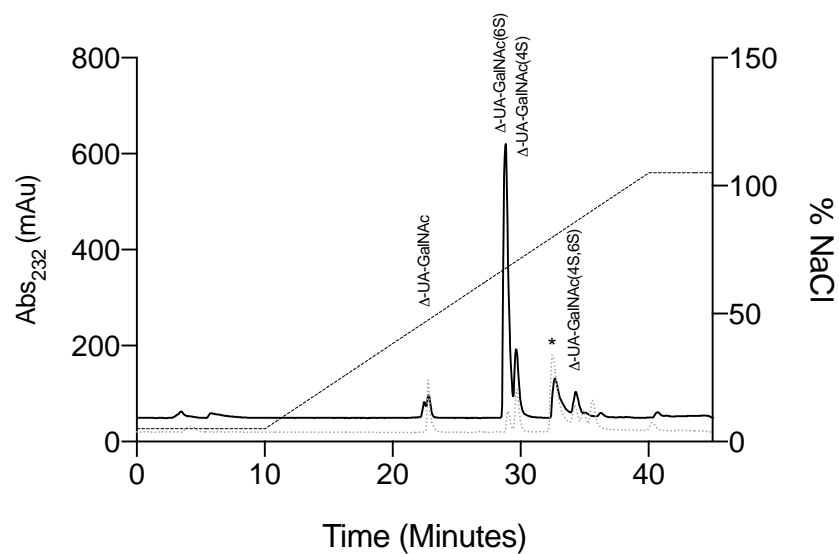
Chapter 10: Appendix



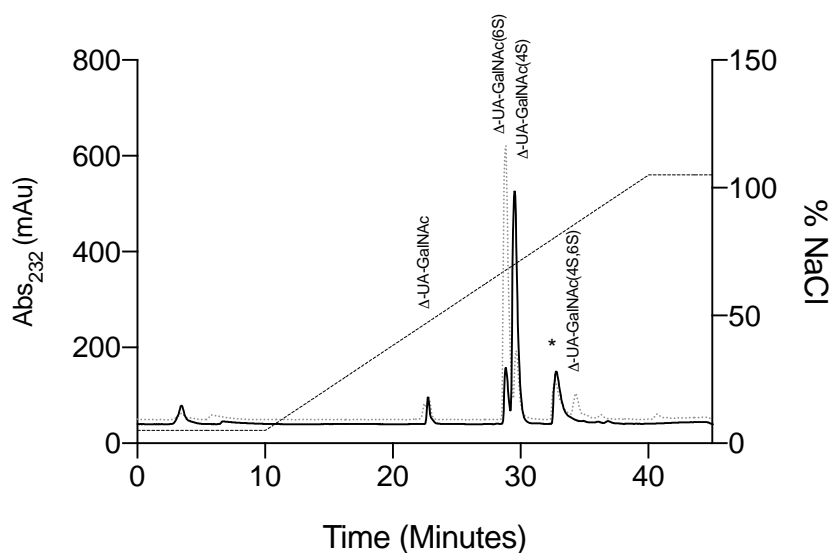
Appendix 1: FRET BACE1 with heparin. A- 5 ug B 2.5, c1.25 d- 0.625 e – 0.3125 f – 0.156. Black with heparin grey h₂o control.



Appendix 2: FRET (A) crude *S. pilchardus* (B) Crude *L. vannamei*.



Appendix 3: UV-SAX HPLC disaccharide composition analysis was performed on the ABC chondroitinase digest of CSC ($\lambda = 232$ nm) eluting with a linear gradient of 0-2 M NaCl (dashed line), pH 3.5. Eluted Δ -disaccharides were referenced against four common standards present with CS (grey). 1; Δ UA-GalNAc, 2; Δ UA-GalNAc(4S), 3; Δ UA-GalNAc(6S), 4 Δ UA-GalNAc(4,6S).



Appendix 4: UV-SAX HPLC disaccharide composition analysis was performed on the ABC chondroitinase digest of CSA ($\lambda = 232$ nm) eluting with a linear gradient of 0-2 M NaCl (dashed line), pH 3.5. Eluted Δ -disaccharides were referenced against four common standards present with CS (grey). 1; Δ UA-GalNAc, 2; Δ UA-GalNAc(4S), 3; Δ UA-GalNAc(6S), 4 Δ UA-GalNAc(4,6S).